

UCLA

UCLA Electronic Theses and Dissertations

Title

Strategies for Modulating Stabilities of Soft and Hard Hybrid Materials with Boron Clusters

Permalink

<https://escholarship.org/uc/item/6j64k8gm>

Author

Grumbles, Mary Waddington

Publication Date

2021

Peer reviewed|Thesis/dissertation

UNIVERSITY OF CALIFORNIA

Los Angeles

Strategies for Modulating Stabilities of
Soft and Hard Hybrid Materials with Boron Clusters

A dissertation submitted in partial satisfaction

of the requirements for the degree Doctor of Philosophy in Chemistry

by

Mary Waddington Grumbles

2021

© Copyright by

Mary Waddington Grumbles

2021

ABSTRACT OF THE DISSERTATION

Strategies for Modulating Stabilities of Soft and Hard Hybrid Materials with Boron Clusters

by

Mary Waddington Grumbles

Doctor of Philosophy in Chemistry and Biochemistry

University of California, Los Angeles, 2021

Professor Alexander M. Spokoyny, Chair

Selective tuning of molecular properties such as solubility, melting point and crystallinity remains a crucial and unmet challenge towards unlocking new functionalities of molecular species. A common strategy towards engendering new properties of hybrid materials relies upon the mixing of traditionally hard inorganic fragments with softer organic components. Herein we disclose efforts made towards modulating the properties of hybrid materials using boron clusters. First, we demonstrate the capacity of monocarborane weakly coordinating anions $[\text{HCB}_{11}\text{H}_{11}]^-$ to overcome the classical moisture and oxygen instability exhibited by many anions employed in ionic liquid mixtures. After, we present a library of partially halogenated, dodecaborate-based weakly coordinating anions ($[\text{B}_{12}\text{X}_9(\text{OR})_3]^{2-}$ where $\text{X} = \text{Cl}, \text{Br}$ and $\text{R} = \text{H}, \text{CH}_3$) as alternatives to perhalogenated analogues which suffer low solubility in a variety of solvents. Overall, these materials augment the utility of weakly coordinating anions by providing highly stable and

modular substrates capable of addressing challenges in many electrodeposition, battery, and ionic liquid applications. Next, we report the grafting of unprotected peptides and model protein with *m*-carborane using an organometallic approach to chemoselectively borylate cysteine (Cys) residues. Cys-borylated peptides show no additional toxicity compared to their Cys alkyl-based congeners and exhibited an enhanced resistance to proteolytic degradation. Finally, we describe developments in non-traditional teaching methods to engage mostly humanities and social science audiences in discussion of basic chemical principles in the pilot chemistry general elective course Material World.

DEDICATION

*For my parents
and my husband, Jonathan,
who have walked every step of this journey with me*

TABLE OF CONTENTS

Chapter 1. Background: Boron Cluster Materials

Article

Boron Cluster Introduction.....	1
Boron Cluster Weakly Coordinating Anions.....	1-3
Boron Cluster Bioconjugation.....	4-5
Advances in Teaching.....	5-6
References.....	6-10

Chapter 2. Reversible Electrodeposition from Boron Cluster Ionic Liquid (BCIL)

Electrolytes

Abstract.....	11
Introduction.....	11-15
Results and Discussion.....	15-22
Conclusion and Outlook.....	22-24
References.....	25-28
Supporting Information.....	29-42
SI References.....	43

Chapter 3. Mixed Halogenation Strategy for Tuning Properties of a Dodecaborate Anion

Abstract.....	44
Introduction.....	44-48
Results and Discussion.....	49-55
Conclusion and Outlook.....	56
References.....	57-60

Supporting Information.....	61-105
Chapter 4. An Organometallic Strategy for Cysteine Borylation	
Abstract.....	106
Introduction.....	106-109
Results and Discussion.....	109-122
Conclusion and Outlook.....	122
References.....	122-130
Supporting Information.....	131-202
SI References.....	203-206
Chapter 5. Narratives of Undergraduate Research, Mentorship, and Teaching at UCLA	
Abstract.....	207
Introduction.....	207-209
Narratives of Undergraduate Research.....	209-224
Improving Chemistry Appreciation Among STEM and non-STEM Students.....	224-230
References.....	230-234

LIST OF FIGURES

Chapter 1. Background: Boron Cluster Materials

Figure 1.1: Structures of **A:** dodecaborate ($[\text{B}_{12}\text{H}_{12}]^{2-}$), **B:** monocarborane ($[\text{HCB}_{11}\text{H}_{11}]^-$) and **C:** *meta*-carborane ($m\text{-C}_2\text{B}_{10}\text{H}_{12}$).....1

Figure 1.2: Schematic of electrochemical sandwich device incorporating boron cluster ionic liquid demonstrating the capacity of deposition to modulate incident radiation.....3

Figure 1.3: Schematic demonstrating Cys-borylation of unprotected peptide using a Pt(II) precursor.....4

Chapter 2. Reversible Electrodeposition from Boron Cluster Ionic Liquid (BCIL) Electrolytes

Figure 2.1 A: some decomposition products of commonly used ionic liquid anions. **B:** monocarborane anion used in this work.....12

Figure 2.2 A: Formation of **BCIL-1** by mixing $[\text{BMIM}]\text{Br}$ with $\text{Ag}[\text{HCB}_{11}\text{H}_{11}]$. Inset shows the elementary steps associated with silver electrodeposition in **BCIL-1**. **B:** Representative cyclic voltammogram (100 mV/s) of **BCIL-2**, Red and blue arrows indicate forward (deposition) and reverse (dissolution) potential sweep direction, respectively.....14

Figure 2.3: Two-electrode cyclic voltammograms (100 mV/s) of **BCIL-1** without CuBr_2 additive. Increasing the $\text{Br}^-:\text{Cl}^-$ ratio increases the electrodeposition current. Red and blue arrows indicate cathodic and anodic sweep direction respectively. Green areas indicate the composition dependent FTO | $[\text{AgX}_2]^-$, X_3^- | Ag^0 | FTO process, red dashed lines indicate the maximum electrodeposition current density at -2.3 V vs. FTO counter electrode.....16-17

Figure 2.4 A: Two-electrode cyclic voltammograms (100 mV/s) of **BCIL-2** after equilibrating at ambient conditions overnight and after heating the equilibrated cell to 60 °C, top and bottom

respectively. **B:** Two-electrode cyclic voltammograms (100 mV/s) of **BCIL-3** after equilibrating at ambient conditions overnight and after heating the equilibrated cell to 60 °C, top and bottom respectively. Red and blue arrows indicate cathodic and anodic sweep direction respectively. **C:** Change in reflectivity ($\Delta\rho$) at 633 nm of **BCIL-3** electrochemical cell during extended “freeze-thaw” cycling and during a single deposition-dissolution cycle, top and bottom respectively. The electrochemical cell was regenerated every 40 cycles by heating to 60 °C.....18-19

Figure 2.5 A: Scanning electron micrographs and EDX elemental mapping of **BCIL-3** working electrode after deposition of a silver film. **B:** Magnified scanning electron micrographs and EDX elemental mapping showing a silver film beneath AgBr deposits.....21

Figure 2.6 A: schematic of IR transparent electrochemical cell. **B:** FTIR transmission spectrum of **BCIL-3** IR transparent cell before and after silver film electrodeposition.....22

Chapter 3. Mixed Halogenation Strategy for Tuning Properties of a Dodecaborate Anion

Abstract

Figure 3.1: Structures of **A:** the perfluoroalkoxyaluminate anion $[Al\{OC(CF_3)_3\}_4]^-$ **B:** partially halogenated monocaborane anion $[HCB_{11}H_5X_6]^-$ and **C:** the dodecaborate anion $[B_{12}H_{12}]^{2-}$46

Figure 3.2: Schematic detailing the facile generation of $Na_2B_{12}H_{12}$ from the pyrolysis of NaB_3H_848

Figure 3.3: Schematic detailing the hydroxylation, halogenation and alkoxylation of $[B_{12}X_{12}]^{2-}$49

Figure 3.4 A: thermogravimetric analysis of $Li_2B_{12}Cl_{12}$, $Li_2B_{12}Cl_9(OH)_3$ and $Li_2B_{12}Cl_9(OCH_3)_3$ and **B:** thermogravimetric analysis of $Li_2B_{12}Br_{12}$, $Li_2B_{12}Br_9(OH)_3$ and $Li_2B_{12}Br_9(OCH_3)_3$. Samples were heated at a rate of 10 °C/min under a constant flow of argon (200 mL/min).....53

Chapter 4. An Organometallic Strategy for Cysteine Borylation

Figure 4.1 A: Summary of selective C-S bond forming reactions for bioconjugation of unprotected peptides and proteins. Metal-mediated strategies result in thiol arylation with the transferred group highlighted in blue. **B:** Summary of selective S-B bond forming reactions.....108

Figure 4.2A: Representative LC trace collected after **1** (1.2 equiv) and H₂N-VKGALGVCG-CONH₂ (5 mM) were allowed to react for 1.5 h at 25 °C in the presence of Tris•HCl buffer (30 mM) in dimethylformamide (DMF). Internal standard was produced through alkylation of H₂N-VKGALGVCG-CONH₂ (see SI section I). **B:** Proposed reaction scheme between **1** and cysteine-containing peptide **C:** Peptide substrate scope with isolated yields (%) and conversion (%).....111

Figure 4.3: LC-MS traces of **7b** incubated with 100 excess **A:** hydrochloric acid **B:** potassium carbonate and **C:** **7a** after 24 hrs at r.t. followed by 48 and 72 hrs at 37 °C (See SI Section VII for full details). **D:** The % cell viability assessed after four-hour incubation of **7b** and **7c** with Chinese Hamster Ovarian (CHO) cells at 5 μM, 10 μM and 50 μM concentration of analyte (See SI Section IX for full details).....114

Figure 4.4 A: Representation of the inclusion complex formed between *m*-carborane and β-cyclodextrin.^{53,54} **B:** ITC binding plot for carboranylated glutathione and β-cyclodextrin to yield an association constant ($K_a = 1.47 \times 10^4 \pm 500 \text{ M}^{-1}$) and binding stoichiometry ($N = 1$). **C:** ITC binding plot for phenyl-glutathione and β-cyclodextrin. **D:** ITC binding plot for unmodified glutathione and β-cyclodextrin.....115

Figure 4.5: Molecular dynamics simulations of **A:** the secondary binding pocket identified as an important docking site **B:** **2b** binding with Proteinase K, **C:** **2a** binding with Proteinase K and **D:** **2c** binding with Proteinase K at 120 ns of equilibration. Proteinase K is represented using QuickSurf representation in VMD.....121

LIST OF TABLES

Table 4.1: The reaction schemes and the observed corresponding degradation of 2a , 2b and 2c with Proteinase K under various conditions.....	119
--	-----

ACKNOWLEDGEMENTS

First and foremost, I would like to thank Prof. Alexander M. Spokoyny for exceptional guidance, creativity and support over the last 5 years. Beyond research interests, Prof. Spokoyny invested in various professional development pursuits that were invaluable. As a young mentor to a young group of mentees, we all grew and learned together.

Further, I would like to thank the members of the Spokoyny lab who gave invaluable advice. In particular, I would like to thank Dr. Rafal M. Dziezic who served as a research mentor when I joined the group. I would also like to thank Kierstyn P. Anderson and Azin Saebi who offered endless and flawless friendship. Thank you also to Mr. Nicholas A. Bernier and Mr. Harrison A. Mills who tackled each stage of this program in parallel with myself.

I am grateful for the time and advice of my thesis committee members: Prof. Paula L. Diaconescu, Dr. Chong Liu and Dr. Andrea M. Kasko. Thank you for agreeing to aid my development as a scientist.

Importantly, I would like to thank the following people who shed light during dark times: Ms. Kristen Camputaro, Mr. Kegan Lovelace, Ms. Rachel Binagia, Mr. Brian Bogdan, Mrs. Sara Bogdan, Mr. Zachary Hern, Mr. Ben Natinsky, Mr. Ben Hoar and Ms. Roselyn Rodriguez. I am especially grateful to Mr. Henry X. Dao who generously gave me a new laptop at the start of my tenure at UCLA, aided many excursions and never failed to be there when needed. To Dr. Dane A. Stanfield, Mrs. Allison L. Stanfield and Mr. Oppenheimer Stanfield, your endless support and friendship will be cherished indefinitely.

I am inexpressibly grateful to my family. Mrs. Elizabeth A. Schoblocher, you were my first and forever friend. Mr. Matthew A. Grumbles and Mr. Nick S. Grumbles, thank you for accepting me as family and supporting my tenure at UCLA. Thank you, Mr. Robert W. Waddington and

Mrs. Norma J. Waddington, for offering endless support and love as I continue to grow and navigate the next stages of life. Thank you to Mrs. Marie T. Hill and Mr. Stephen D. Hill who emotionally supported the transition between multiple summer internships and also suffered through filing taxes in 3 different states. Your love and support has defined this stage of life, augmenting my personal happiness and capacity to achieve. Mr. Guy E. Grumbles, your enthusiasm and love is indispensable and uniquely encouraging. Thank you for cheerleading various aspects of my life. Mrs. Julie A. Jamieson and Mr. William L. Jamieson, you are the single greatest influences upon my success as a scientist and as a person. You patiently quizzed me with flashcards and read every paper I wrote in early education. This indelible support extends to every aspect of my adulthood and underlies my continued joy for life.

Finally, thank you to my husband, Mr. Jonathan W. Grumbles. Every aspect of this program was experienced also by you. Patiently you supported me, cheered for me, cried with me, reasoned with me- you loved me. I cannot articulate the gratitude I feel to you except to say the most significant title I will ever carry is your wife.

PREVIOUS PUBLICATION AND CONTRIBUTION OF CO-AUTHORS

Chapter 2. This chapter is a version of Dzedzic, R. M.; Waddington, M. A.; Lee, S. E.; Kleinsasser, J.; Plumley, J. B.; Ewing, W. C.; Bosley, B. D.; Lavallo, V.; Peng, T. L.; Spokoyny, A. M. "Reversible Silver Electrodeposition from Boron Cluster Ionic Liquid (BCIL) Electrolytes", *ACS Appl. Mater. Interfaces* **2018**, *10*, 6825-6830. The manuscript was co-written by D.R.M. and M.A.W. Synthesis of compounds was completed by W.C.E., B.D.B., V.L., J.K. and S.E.L. Device construction, electrochemical characterization and IR transmission measurements were carried out by D.R.M. and M.A.W. Scanning electron microscopy was conducted by J.B.P. The project was conceived by T.L.P., W.C.E., B.D.B., V.L. and A.M.S.

Chapter 3. This unpublished chapter was co-authored by Waddington, M. A.; Ganley, E.; Dzedzic, R. M.; Nelson, Y. A.; Pathuri, R.S.; Ewing, W. C.; Bosley, B. D.; Spokoyny, A. M. The manuscript was written by M.A.W. Syntheses were conceived by M.A.W., R.M.D. and A.M.S. and executed by Y.A.N., R.S.P., E.G., D.R.M and M.A.W. Large-scale synthesis was conducted by W.C.E. and B.D.B. Thermogravimetric and solubility analysis was completed by M.A.W.

Chapter 4. This chapter is a version of Waddington, M. A.; Zheng, X.; Stauber, J. M.; Hakin Moully, E.; Montgomery, H. R.; Saleh, L. M. A.; Král, P.; Spokoyny, A. "An Organometallic Strategy for Cysteine Borylation." *J. Am. Chem. Soc.* **2021**, *in press*. The manuscript was written by M.A.W. with contribution from J.M.S. DARPin expression was completed by H.R.M. The project was conceived by A.M.S., E. H.-M. and L.M.A.S. Computational modeling was completed by P.K. and X.Z. All other experiments were executed by M.A.W.

Chapter 5. This chapter is a version of Stevens, S. L.; Phung, A. C.; Gonzalez, A.; Shao, Y.; Moully, E. H.; Nguyen, V. T.; Martin, J. L.; Mao, C.; Saebi, A.; Mosallaei, A.; Kirillos, M.; Chong, P.; Umanzor, A.; Qian, K.; Marin, G.; Ebrahim, O. M.; Pathuri, R. S.; Hopp, M.;

Ramachandran, R.; Waddington, M. A.; Spokoyny, A. M. "Narratives of Undergraduate Research, Mentorship, and Teaching at UCLA", *Pure & Appl. Chem.* **2021**, *93*, 207-221. M.A.W, R.R. and A.M.S. compiled perspectives of all authors and co-authored the remainder of the publication.

VITA

EDUCATION

- Current University of California Los Angeles
Ph.D. Candidate, Cum. GPA 3.814
Advisor: Prof. Alexander Spokoyny
Research Focus: I developed synthetic methods incorporating boron-based building blocks to generate hybrid materials for therapeutics, battery and metal deposition applications. After synthesis, I completed extensive characterizations and purifications to fully investigate structure-function relationships.
- May 2016 Kent State University
B.S. Chemistry (ACS Certified), Cum. GPA 3.938
Chemistry Major; Chemistry Concentration
Advisors: Prof. Nicola Brasch and Prof. Jacob Shelley

PATENT APPLICATIONS

1. Spokoyny, **Grumbles**, Dzedzic, Wixtrom, Ganley, Bosley, Ewing, "Boron Cluster Weakly-Coordinating Anions and Related Materials" UCLA Provisional Patent Application (November 23, 2020).

PUBLICATIONS

1. **Waddington, M. A.**; Zheng, A.; Stauber, J. M.; Mouly, E. H.; Saleh, L. M. A.; Kral, P.; Spokoyny, A. M. "Cysteine Borylation in Unprotected Peptides", *submitted*. Preprint: <https://doi.org/10.26434/chemrxiv.13553030.v1>.
2. Stevens, S. L.; Phung, A. C.; Gonzalez, A.; Shao, Y.; Mouly, E. H.; Nguyen, V. T.; Martin, J. L.; Mao, C.; Saebi, A.; Mosallaei, A.; Kirollos, M.; Chong, P.; Umanzor, A.; Qian, K.; Marin, G.; Ebrahim, O. M.; Pathuri, R. S.; Hopp, M.; Ramachandran, R.*; **Waddington, M. A.***; Spokoyny, A. M.* "Narratives of Undergraduate Research, Mentorship, and Teaching at UCLA", *Pure & Appl. Chem.*, *in press*.
3. Mu, X.; Hopp, M.; Dzedzic, R. M.; **Waddington, M. A.**; Rheingold, A. L.; Sletten, E. M.; Axtell, J. C.*; Spokoyny, A. M.* "Expanding the Scope of Pd-Catalyzed B-N Cross-Coupling Chemistry in Carboranes", *Organometallics* **2020**, *39*, 4380–4386.
4. Anderson, K. P.; **Waddington, M.A.**; Balaich, G. J.; Stauber, J. M.; Caram, J. R.*; Djurovich, P. I.*; Spokoyny, A. M.* "A Molecular Boron Cluster-Based Chromophore with Dual Emission", *Dalton Trans.* **2020**, *49*, 16245-16251 New Talent: Americas, Special.
5. Messina, M. S.; Stauber, J. M.; **Waddington, M. A.**; Rheingold, A. L.; Maynard, H. D.*; Spokoyny, A. M.* "Organometallic Gold(III) Reagents for Cysteine Arylation", *J. Am. Chem. Soc.* **2018**, *140*, 7065-7069.
6. Ramachandran, R.; Jung, D.; Bernier, N. A.; Logan, J. K.; **Waddington, M. A.**; Spokoyny, A. M.* "Sonochemical Synthesis of Small Boron Oxide Nanoparticles", *Inorg. Chem.* **2018**, *57*, 8037-8041.
7. Dzedzic, R. M. +; **Waddington, M. A. +**; Lee, S. E.; Kleinsasser, J.; Plumley, J. B.; Ewing, W. C.; Bosley, B. D.*; Lavallo, V.*; Peng, T. L.*; Spokoyny, A. M.* "Reversible Silver Electrodeposition from Boron Cluster Ionic Liquid (BCIL) Electrolytes", *ACS Appl. Mater. Interfaces* **2018**, *10*, 6825-6830.

+ These authors contributed equally

* corresponding author

WORK EXPERIENCE

- 2019- 2021 Technology Development Group
Paid Graduate Intern
Hands-on experience in marketing and business development leading to technology commercialization.
- 2019-2019 Cabot Microelectronics
Graduate Student Intern
Advisor: Dr. Charles Hamilton
Optimized procedure for high throughput analysis of polishing slurries. Using this newly developed method, I was able to stabilize a classically unstable slurry which lead to **two internal innovation awards**. Extensive use of **isothermal titration calorimetry and dynamic light scattering** instrumentation.
- 2017- 2017 Advanced Materials Laboratory
Graduate Summer Research Scholar
Advisor: Dr. Thomas L. Peng
Fabrication of electrochemical devices for thermal regulation onboard spacecraft and satellites. Extensive use of **scanning electron microscopy, thermogravimetric analysis, differential scanning calorimetry and electrochemical analysis tools** like cyclic voltammetry and impedance measurement.
- 2016-
Present UCLA
Graduate Researcher
Advisor: Prof. Alexander M. Spokoyny
My doctoral work involved comprehensive use of **LCMS-based analysis, HPLC purification and isothermal titration calorimetry**. Proficient in cellular assay techniques.
- 2014- 2015 Kent State University
Assistant to Lab Coordinator and Instrumentation Manager
Prepared solutions and assembled materials to aid academic laboratory instruction.
- 2015 Hexion (Formerly Momentive) Specialty Chemicals
Society of Chemical Industry 2015 Intern
Advisors: Drs. Michael C. Smith and Warefta Hasan
Improved synthetic method for a proprietary epoxy resin polymer, enhancing reproducibility in final adhesive performance. Extensive use of rheology and Karl Fischer titration.
- 2014-2015 Kent State University — Analytical Research Lab
Student Researcher
Advisor: Prof. Jacob T. Shelley
Proteomics of bioconjugates using **LCMS analysis**.
- 2014 Eglin Air Force Base — High Explosives Research and Development
Summer Research Scholar
Advisor: Dr. Stacy M. Grant
Synthesized mesoporous, polymeric materials. Developed **solid state syntheses**.
- 2012-2014 Kent State University — Biological Inorganic Research Lab
Research Experience for Undergraduates (REU) Participant (Summer 2013)
Student Researcher
Advisor: Prof. Nicola E. Brasch
Investigation of reactive oxygen species using **UV-Vis, nuclear magnetic resonance and infrared spectroscopies**. Expertise in **air-free techniques**.

CHAPTER 1

Background: Boron Cluster Materials

Article

Boron Cluster Introduction

Boron clusters are hierarchical boranes with a central, three-dimensional aromaticity and terminal sigma bonds to hydrogen.^{1,2} Due to this bonding structure, boron clusters are often conceptualized as three-dimensional analogues of benzene^{1,2}; however, unlike benzene, polyhedral boranes exhibit 3-center, 2-electron bonding interactions.³ Despite the electron deficiency of this bonding interaction, polyhedral boranes exhibit exceptional stability profiles. For example, dodecaborate ($[\text{B}_{12}\text{H}_{12}]^{2-}$) survives strongly acidic (2M HCl for 1 month), basic (2M NaOH for 1 month) and oxidizing conditions (reflux in 30% peroxide) as well as temperatures reaching 600 °C in air.² While boron clusters range in size (i.e. $[\text{B}_6\text{H}_6]^{2-}$, $[\text{B}_{10}\text{H}_{10}]^{2-}$, $[\text{B}_{12}\text{H}_{12}]^{2-}$) and can exist as intact *closo*- compounds or open-caged *nido*- species^{2,4,5}, the scope of this thesis is limited to the following icosahedrons: $[\text{B}_{12}\text{H}_{12}]^{2-}$, $[\text{HCB}_{11}\text{H}_{11}]^-$ and *meta*-carborane (*m*- $\text{C}_2\text{B}_{10}\text{H}_{12}$) (Figure 1.1).

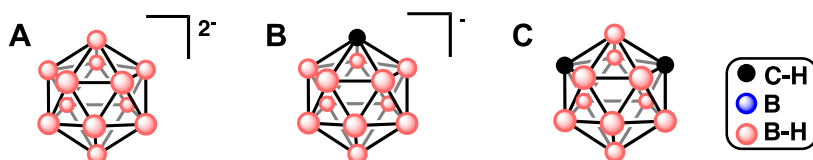


Figure 1.1: Structures of **A:** dodecaborate ($[\text{B}_{12}\text{H}_{12}]^{2-}$), **B:** monocarborane ($[\text{HCB}_{11}\text{H}_{11}]^-$) and **C:** *meta*-carborane (*m*- $\text{C}_2\text{B}_{10}\text{H}_{12}$).

Boron Cluster Weakly Coordinating Anions

Weakly coordinating anions enable various industries such as battery materials, catalysis and electronics development.⁶ Despite widespread application of weakly coordinating anions, generation of new constructs is complicated by multifaceted requirements including low nucleophilicity, solubility in a variety of solvents, large degree of electron delocalization, scalable

and inexpensive preparation as well as high kinetic and thermal stability.⁶⁻⁸ Decades of development have resulted in weakly coordinating anions capable of meeting many of these specifications. Major classes of such anions include halogenated alkyl- and arylborates,^{9,10} teflate-based anions,¹¹ poly- or perfluorinated alkoxy- and aryloxymetallates¹²⁻¹⁴ and boron cluster-based anions.^{4,5} Of these, boron cluster-based anions have emerged as particularly interesting substrates owing to the exceptional stability profiles, large degree of electron delocalization, weak cation coordination and synthetic modularity associated with these species.² In fact, [HCB₁₁H₁₁]⁻ exhibited the shortest bond distance to Fe(TPP)⁺ ever reported, resulting in the claim that monocarborane is “the least coordinating anion.”¹⁵ Herein we augment the body of research surrounding boron cluster-based weakly coordinating anions, highlighting the capacity of sequential synthetic tuning to alter molecular properties such as melting point, solubility and thermal stability.

In particular, we present a series of AgHCB₁₁H₁₁-based room temperature ionic liquids that circumvent known moisture and oxygen-mediated degradative pathways of commonly utilized anions.¹⁶ We hypothesize that modification of the cluster core can be used to tune physical properties of the ionic liquid such as viscosity and solidification temperature, negating the need for tedious electrolyte reformulation. After, we construct electrochemical sandwich devices incorporating boron cluster ionic liquids to reversibly electrodeposit silver and modulate incident radiation (Figure 1.2).¹⁶ These results suggest the potential utility of boron cluster ionic liquids to enhance lifetimes of reconfigurable electronics while allowing for operational in a variety of environments.

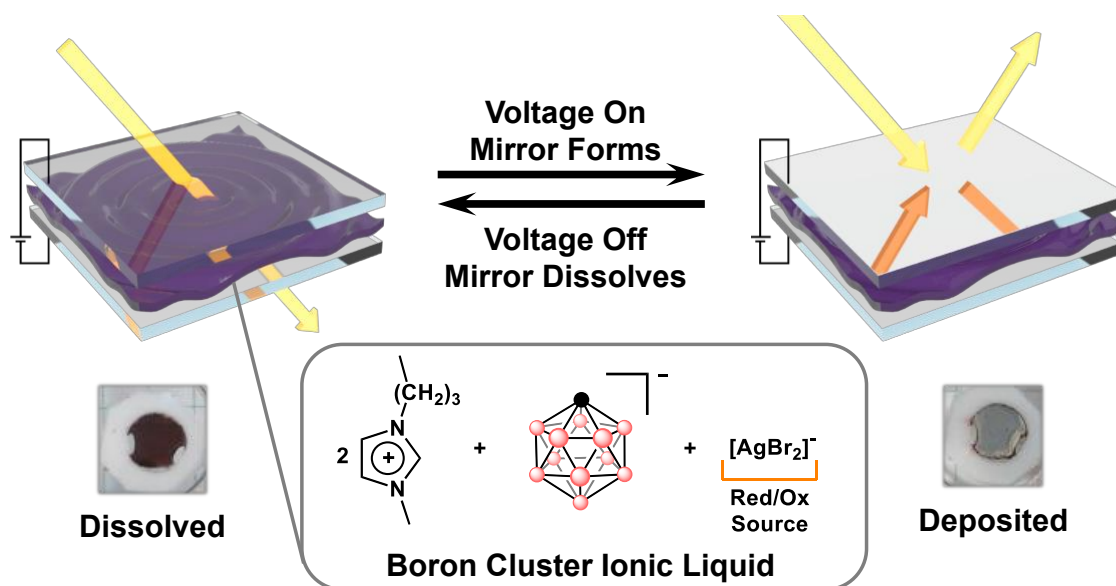


Figure 1.2: Schematic of electrochemical sandwich device incorporating boron cluster ionic liquid demonstrating the capacity of deposition to modulate incident radiation.¹⁶

We also expand the scope of $[\text{B}_{12}\text{H}_{12}]^{2-}$ weakly coordinating anions which offer similar chemical stability profiles as $[\text{HCB}_{11}\text{H}_{11}]^{-}$ but can be produced from a single-step, scalable reaction. As the B-H bonds are susceptible to electrophilic substitution, dodecaborate-based weakly coordinating anions are often perhalogenated to yield $[\text{B}_{12}\text{X}_{12}]^{2-}$ where X= Cl, Br, I, F.¹⁷ Unfortunately, these species are known to have low solubility in a variety of solvents, limiting widespread application.^{18a} We have developed a mixed halogenation strategy to generate $[\text{B}_{12}\text{X}_9(\text{OR})_3]^{2-}$ (X= Cl, Br and R= H, CH₃) anions that offer the ability to tune steric bulk, stability and solubility of the resulting anions. We report chlorination using sodium hypochlorite in acid to generate Cl₂ *in situ* to enhancing the safety of the reaction by eliminating the need for chlorine gas tanks or highly corrosive chemicals.^{18b,c} Further, we describe trends in both solubility and stability as the cluster is modified. This library of compounds augments the usability of dodecaborate-based anions while retaining facile and scalable preparation.

Boron Cluster Bioconjugation

Cys arylation has become a powerful tool in bioconjugation. A multitude of substrates including drug molecules, affinity tags, fluorescent probes and polymers can be covalently linked to peptides and proteins producing bioconjugates with unique chemical properties.¹⁹⁻²¹ Organometallic-mediated routes towards Cys arylation have become particularly attractive owing to the fast kinetics, aqueous compatibility and chemoselectivity associated with these reactions.²² Specifically, metal complexes incorporating Ni(II)^{23,24}, Pd(II)^{19,25,26} and Au(III)^{20,21,27} have achieved chemoselective C-S bond formation within unprotected biomolecule substrates. Comparatively, reactions capable of forging a B-S bonding modality are scarce. While both catalytic and heat-mediated borylation of simple thiol-containing substrates has been reported, these methods lack thiol selectivity and could not be applied to complex biomolecules which contain many nucleophilic and basic side chain functional groups.²⁸⁻³¹ We envisioned an organometallic-mediated route towards chemoselective Cys borylation via reductive elimination of boron-bound *m*-C₂B₁₀H₁₂ from a Pt(II) metal complex (Figure 1.3).³²

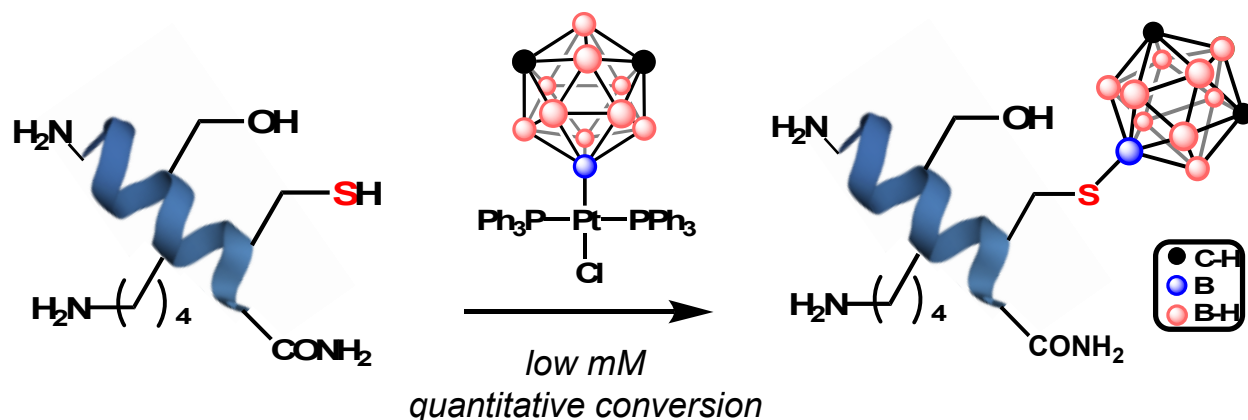


Figure 1.3: Schematic demonstrating Cys-borylation of unprotected peptide using a Pt(II) precursor.

We report the reactivity of this complex with many peptide substrates containing a variety of side-chain functional groups as well as a model protein, DARPin (designed ankyrin repeat protein).³² The stability of the resultant bioconjugates in the presence of acid, base and external thiol is evaluated and the toxicity compared to Cys alkyl-based congeners is reported. Finally, we explore the capacity of Cys-borylation to produce hybrid peptide bioconjugates that resist proteolytic degradation while maintaining binding affinity to a target protein.³² This work expands the toolbox of accessible bioconjugations and further demonstrates the importance of organometallic-based approaches in designing chemoselective transformations in complex substrates.

Advances in Teaching

Throughout the duration of my graduate career, I had the opportunity to aid in the development of alternative approaches to undergraduate chemical education. Specifically, I assisted in the generation of the first chemistry general elective course offered at UCLA. Previously, students from non-science majors would satisfy this requirement by enrolling in the general chemistry course also taken by students in the major (14A General Chemistry for Life Scientists I). While 14A represents a fundamentally important survey of the underlying concepts of basic chemistry, the highly mathematical nature of the course alienates many from appreciating the broader impacts of a chemical education. Further, feelings of incapability are often betrayed by the apparent north vs south campus divide within UCLA student culture. We observed these events and together Prof. Spokoyny and I developed CHEM 3, a course designed to showcase materials throughout history and how the properties of these materials have shaped our society. The pilot course was administered in spring of 2018 and was well received. One point of improvement was the quarter-long project which required students to write a mock press release of a recently published research journal article. While educational, the assignment felt antiquated with little tangible outcome. Through the assignment, we hoped students would visualize how warped information can become through media interpretation. Was there a way to achieve this goal with a modern and accessible platform? To answer this question, we looked to the mass spreading of misinformation on Twitter. We asked students to both find

and respond, politely and with referenced sources, to some scientific inaccuracy they saw being propagated. The students were asked to then present the tweets and responses to the class, articulating what falsehoods were being posted. The “Twitter Throwdown” assignment was incredibly well received and when multiple tweets were noticed by Alchemie’s blogger Julia Winter, she asked both Alex and I to interview so we could better inform others on this unique teaching tool. We later published the concepts of our new course alongside a series of excerpts describing student perspectives.³³ This work highlights the multidisciplinary nature of effective education and offers insights for future course development.

References

1. Hawthorne, M. F.; Farha, O. K.; Julius, R.; Ma, L.; Jalisatgi, S. S.; Li, T.; Bayer, M. J. Polyhedral Boranes in the Nanoworld. *ACS Symp. Ser.* **917**, **2005**, 312-324.
2. Grimes, R. N. *Carboranes*, 3rd ed.; Academic Press, **2016**.
3. Lipscomb, W. N. The Boranes and Their Relatives. *Science* **1977**, *196*, 1047-1055.
4. Pitochelli, A. R. & Hawthorne, M. F. The Isolation of the Icosahedral $B_{12}H_{12}^{2-}$ Ion. *J. Am. Chem. Soc.* **1960**, *82*, 3228-3229.
5. Knoth, W. H. $1-B_9H_9CH^-$ and $B_{11}H_{11}CH^-$. *J. Am. Chem. Soc.* **1967**, *89*, 1274-1275.
6. Krossing, I. & Raabe, I. Noncoordinating Anions- Fact or Fiction? A Survey of Likely Candidates. *Angew. Chem. Int. Ed.* **2004**, *43*, 2066-2090.
7. Riddlestone, I. M.; Kraft, A.; Schaefer, J.; Krossing, I. Taming the Cationic Beast: Novel Developments in the Synthesis and Application of Weakly Coordinating Anions. *Angew. Chem. Int. Ed.* **2018**, *57*, 13982-14024.
8. Strauss, S. H. The Search for Larger and More Weakly Coordinating Anions. *Chem. Rev.* **1993**, *93*, 927-942.

9. Golden, J. H.; Mutolo, P. F.; Lobkovsky, E. B.; DiSalvo, F. J. Lithium-Mediated Organofluorine Hydrogen Bonding: Structure of Lithium Tetrakis(3,5-bis(trifluoromethyl)phenyl)borate Tetrahydrate. *Inorg. Chem.* **1994**, *33*, 5374–5375.
10. Seppelt, K. “Noncoordinating” Anions, II. *Angew. Chem. Int. Ed.* **1993**, *32*, 1025-1027.
11. Van Seggen, D. M.; Hurlburt, P. K.; Noirot, M. D.; Anderson, O. P.; Strauss, S. H. Tetrakis(pentafluorooxotellurato)borate(1-): coordinating ability and reactivity of a very large weakly coordinating anion. *Inorg. Chem.* **1992**, *31*, 1423-1430.
12. Rupp, A. B. A. & Krossing, I. Ionic Liquids with Weakly Coordinating $[M^{III}(OR^F)_4]^-$ Anions. *Acc. Chem. Res.* **2015**, *48*, 2537-2546.
13. Metz, M. V.; Sun, Y.; Stern, C. L.; Marks, T. J. Weakly Coordinating Al-, Nb-, Ta-, Y-, and La-Based Perfluoroaryloxymetalate Anions as Cocatalyst Components for Single-Site Olefin Polymerization. *Organomet.* **2002**, *21*, 3691-3702.
14. Sun, Y.; Metz, M. V.; Stern, C. L.; Marks, T. J. Perfluoroaryloxy Anions as Cocatalysts for Metallocene-Mediated Ziegler–Natta Olefin Polymerization. *Organomet.* **2000**, *19*, 1625-1627.
15. Shelly, K.; Lee, Y. J.; Scheidt, W. R.; Reed, C. A. The least coordinating anion. *J. Am. Chem. Soc.* **1986**, *108*, 3117–3118.
16. Dziedzic, R.; Waddington, M. A.; Lee, S. E.; Kleinsasser, J.; Plumley, J. B.; Ewing, W. C.; Bosley, B. D.; Lavallo, V.; Peng, T. L.; Spokoyny, A. M. Reversible Silver Electrodeposition from Boron Cluster Ionic Liquid (BCIL) Electrolytes. *ACS Appl. Mater. Interfaces* **2018**, *10*, 6825.

17. Ivanov, S. V.; Miller, S. M.; Anderson, O. P.; Solntsev, K.A; Strauss, S. H. Synthesis and Stability of Reactive Salts of Dodecafluoro-*closo*-dodecaborate(2-). *J. Am. Chem. Soc.* **2003**, *125*, 4694-4695.
18. (a) Avelar, A.; Tham, F. S.; Reed, C. A. Superacidity of Boron Acids H₂(B₁₂X₁₂) (X= Cl, Br). *Angew. Chem. Int. Ed.* **2009**, *48*, 3491-3493. (b) Geis, V.; Guttische, K.; Knapp, C.; Scherer, H.; Uzun, R. Synthesis and Characterization of Synthetically Useful Salts of the Weakly-Coordinating Dianion [B₁₂Cl₁₂]²⁻. *Dalton Trans.* **2009**, *15*, 2649-2884. (c) Gu, W. & Ozerov, O. V. Exhaustive Chlorination of [B₁₂H₁₂]²⁻ without Chlorine Gas and the Use of [B₁₂Cl₁₂]²⁻ as a Supporting Anion in Catalytic Hydrodefluorination of Aliphatic C-F Bonds *Inorg. Chem.* **2011**, *50*, 2726-2728.
19. Vinogradova, E. V.; Zhang, C.; Spokoyny, A. M.; Pentelute, B. L.; Buchwald, S. L. Organometallic Palladium Reagents for Cysteine Bioconjugation. *Nature* **2015**, *526*, 687-691.
20. Kung, K. K.-Y.; Ko, H.-M.; Cui, J.-F.; Chong, H.-C.; Leung, Y.-C.; Wong, M.-K. Cyclometalated Gold(III) Complexes for Chemoselective Cysteine Modification *via* Ligand Controlled C-S Bond-forming Reductive Elimination. *Chem. Commun.* **2014**, *50*, 11899-11902.
21. Messina, M. S.; Stauber, J. M.; Waddington, M. A.; Rheingold, A. L.; Maynard, H. D.; Spokoyny, A. M. Organometallic Gold(III) Reagents for Cysteine Arylation. *J. Am. Chem. Soc.* **2018**, *140*, 7065-7069.
22. Vinogradova, E. V. Organometallic Chemical Biology: An Organometallic Approach to Bioconjugation. *Pure & Appl. Chem.* **2017**, *89*, 1619-1640.

23. Vara, B. A.; Li, X.; Berritt, S.; Walters, C. R.; Petersson, E. J.; Molander, G. A. Scalable Thioarylation of Unprotected Peptides and Biomolecules Under Ni/Photoredox Catalysis. *Chem. Sci.* **2018**, *9*, 336-344.
24. Hanaya, K.; Ohata, J.; Miller, M. K.; Mangubat-Medina, A. E.; Swierczynski, M. J.; Yang, D. C.; Rosenthal, R. M.; Popp, B. V.; Ball, Z. T. Rapid Nickel(II)-Promoted Cysteine S-Arylation with Arylboronic Acids. *Chem. Commun.* **2019**, *55*, 2841-2844.
25. Al-Shuaeeb, R. A. A.; Kolodych, S.; Koniev, O.; Delacroix, S.; Erb, S.; Nicolăy, S.; Cintrat, J.-C.; Brion, J.; Cianféroni, S.; Alami, M.; Wagner, A.; Messaoudi, S. Palladium-Catalyzed Chemoselective and Biocompatible Functionalization of Cysteine-Containing Molecules at Room Temperature. *Chem. Eur. J.* **2016**, *22*, 11365-11370.
26. Willwacher, J.; Raj, R.; Mohammed, S.; Davis, B. G. Selective Metal-Site-Guided Arylation of Proteins. *J. Am. Chem. Soc.* **2016**, *138*, 8678-8681.
27. Chan, A. O.-Y.; Tsai, J. L.-L.; Lo, V. K.-Y.; Li, L.-G.; Wong, M.-K.; Che, C.-M. Gold-mediated Selective Cysteine Modification of Peptides Using Allenes. *Chem. Commun.* **2013**, *49*, 1428-1430.
28. Yang, Z.; Zhong, M.; Ma, X.; Nijesh, K.; De, S.; Parameswaran, P.; Roesky, H. W. An Aluminum Dihydride Working as a Catalyst in Hydroboration and Dehydrocoupling. *J. Am. Chem. Soc.* **2016**, *138*, 2548-2551.
29. Fernández-Salas, J. A.; Manzini, S.; Nolan, S. P. Efficient Ruthenium-Catalysed S-S, S-Si and S-B Bond Forming Reactions. *Chem. Commun.* **2013**, *49*, 5829-5831.
30. Romero, E. A.; Peltier, J. L.; Jazzar, R.; Bertrand, G. Catalyst-free Dehydrocoupling of Amines, Alcohols, and Thiols with Pinacol Borane and 9-Borabicyclononane (9-BBN). *Chem. Commun.* **2016**, *52*, 10563-10565.

31. Yang, A.; Ha, S.; Ahn, J.; Kim, R.; Kim, S.; Lee, Y.; Kim, J.; Söll, D.; Lee, H.-Y.; Park, H.-S. A Chemical Biology Route to Site-Specific Authentic Protein Modifications. *Science* **2016**, *354*, 623-626.
32. Waddington, M. A.; Zheng, A.; Stauber, J. M.; Mouilly, E. H.; Montgomery, H. E.; Saleh, L. M. A.; Kral, P.; Spokoyny, A. M. An Organometallic Strategy for Cysteine Borylation. *J. Am. Chem. Soc.* **2021**, *in press*.
33. Stevens, S. L.; Phung, A. C.; Gonzalez, A.; Shao, Y.; Mouilly, E. H.; Nguyen, V. T.; Martin, J. L.; Mao, C.; Saebi, A.; Mosallaei, A.; Kirolos, M.; Chong, P.; Umanzor, A.; Qian, K.; Marin, G.; Ebrahim, O. M.; Pathuri, R. S.; Hopp, M.; Ramachandran, R.; Waddington, M. A.; Spokoyny, A. M. Narratives of Undergraduate Research, Mentorship, and Teaching at UCLA. *Pure & Appl. Chem.* **2021**, *93*, 207-221.

CHAPTER 2

Reversible Silver Electrodeposition from Boron Cluster Ionic Liquid (BCIL) Electrolytes

This chapter is a version of Dziedzic, R. M.; Waddington, M. A.; Lee, S. E.; Kleinsasser, J.; Plumley, J. B.; Ewing, W. C.; Bosley, B. D.; Lavallo, V.; Peng, T. L.; Spokoyny, A. M. "Reversible Silver Electrodeposition from Boron Cluster Ionic Liquid (BCIL) Electrolytes", *ACS Appl. Mater. Interfaces* **2018**, *10*, 6825-6830.

Abstract

Electrochemical systems offer a versatile means for creating adaptive devices. However, the utility of electrochemical deposition is inherently limited by the properties of the electrolyte. The development of ionic liquids enables electrodeposition in high-vacuum environments and presents opportunities for creating electrochemically adaptive and regenerative spacecraft components. In this work we developed a silver-rich, boron cluster ionic liquid (BCIL) for reversible electrodeposition of silver films. This air and moisture stable electrolyte was used to deposit metallic films in an electrochemical cell to tune the emissivity of the cell *in situ*, demonstrating a proof-of-concept design for spacecraft thermal control.

Introduction

Electrodeposited metallic structures are ubiquitous in modern technologies (e. g. batteries, protective coatings, displays, and microchips) and emerging technologies such as resistive memory and reconfigurable electronics.^{1,2} The broad utility of electrochemically deposited structures grows as new electrolytes enable electrodeposition in increasingly challenging environments. Controlled reversible electrodeposition of metallic structures offers tunable optical properties and electrical conductivity along with the ability to adapt the electrochemical system to changing application

needs. This adaptability is appealing in the context of reconfigurable electronic components which could extend a device's lifetime through *in situ* restructuring.

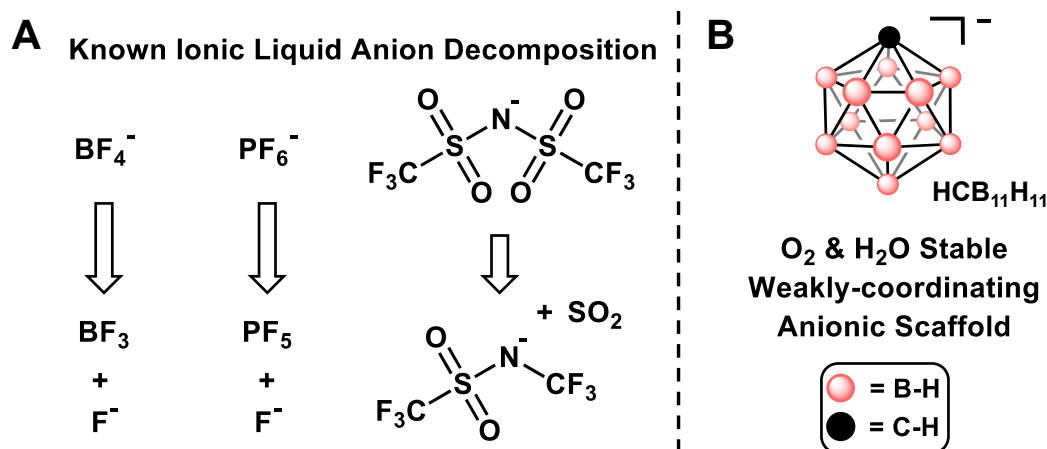


Figure 2.1 **A:** some decomposition products of commonly used ionic liquid anions. **B:** monocarborane anion used in this work.

Early electrodeposition methods used aqueous electrolytes due to the solubility of common metal ions.¹ The development of non-aqueous electrolytes has enabled safe electrodeposition of water sensitive metals for new electrochemical applications such as high-density energy storage.³ Additionally, electrodeposition from ionic liquids has emerged as a potential alternative to organic solvent electrolytes and presented new opportunities for electrodeposition in high vacuum and hostile environments such as electron microscopes and plasma chambers.⁴

Ionic liquids (ILs), salts with low melting points (typically <100 °C), combine the high ion solubility of aqueous media, the chemical flexibility of organic solvents, and low volatility and wide electrochemical windows achievable with molten salts.⁷ The versatility of ILs is increased by tailoring the cation-anion pairs for individual applications.⁵ Yet, despite the numerous cation-anion pairs that can form ionic liquids, much of ionic liquid tunability is achieved by modifying the cationic component.^{5,6} This disparity is largely due to the synthetic availability of cationic

molecular scaffolds such as ammonium, phosphonium, and heterocyclic motifs. Conversely, ionic liquids in which the anionic component engenders the IL properties are scarce and the anions are seldom amenable to additional functionalization.⁷⁻¹⁰ Furthermore, the relative instability of commonly used IL anions limits the longevity of IL-based electrochemical devices (Figure 2.1A). This becomes especially problematic when designing systems which require prolonged operation time. Therefore, we sought to develop an ionic liquid that contains a highly stable and easily tunable anionic core. Such “anion-based” ILs could use the metal of interest as the cation and enable high metal loadings suitable for rapid electrodeposition. Anionic polyhedral boranes represent a class of modular molecular building blocks suitable for designing “anion-based” boron cluster ionic liquids (BCILs).^{11,12} Their robust boron-cluster framework provides an anionic scaffold amenable to tuning of melting point, solubility, and redox potential.^{13,14} In this work, we set out to develop an all-ionic electrolyte suitable for reversible deposition of silver films. Specifically, we describe an all-ionic electrolyte to reversibly deposit silver films for the purpose of controlling infrared (IR) emission from an electrochemical cell as a means of actively regulating thermal emission. This technology complements existing approaches to controlling thermal emission from spacecraft surfaces.¹⁵⁻¹⁸ Importantly, BCILs represent a critical component allowing these devices to perform reliably without having to exclude air and moisture; common contaminants that are introduced during electrochemical device assembly that are difficult to remove.

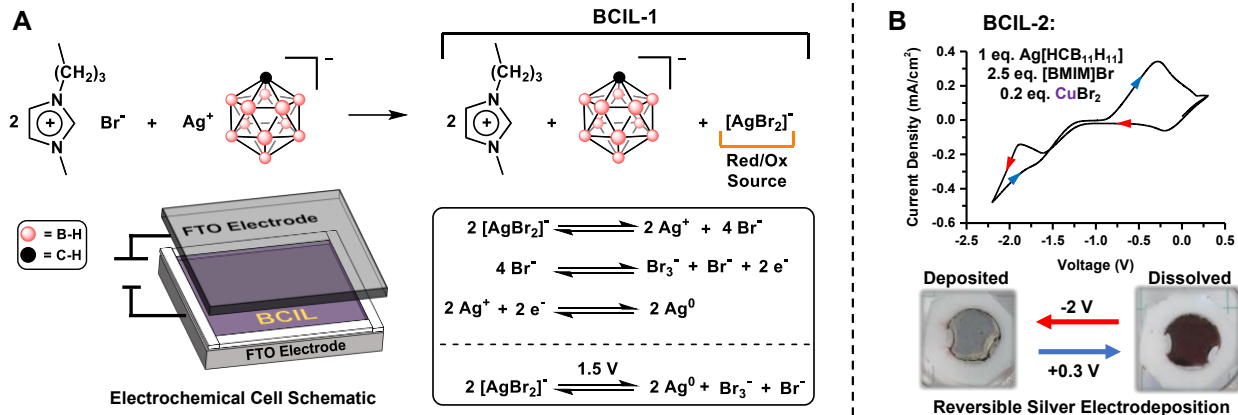


Figure 2.2 A: Formation of **BCIL-1** by mixing $[\text{BMIM}]\text{Br}$ with $\text{Ag}[\text{HC}(\text{B}_{11}\text{H}_{11})]$. Inset shows the elementary steps associated with silver electrodeposition in **BCIL-1**. **B:** Representative cyclic voltammogram (100 mV/s) of **BCIL-2**, Red and blue arrows indicate forward (deposition) and reverse (dissolution) potential sweep direction, respectively.

Silver films play an important technological role as electrical conductors and optical coatings. Silver offers unique advantages over other transition metals because of its high spectral reflectivity, high electrical conductivity and corrosion resistance.¹⁹ These qualities make silver an attractive metal for tuning the properties of spacecraft surfaces. Additionally, the low volatility of IL electrolytes offers a means of performing electrodeposition in high vacuum environments. Due to its positive reduction potential, only small voltages are required to electrodeposit silver from ionic salt precursors.¹ Electrodeposition of silver was historically performed using cyanide-based electrolytes due to the formation of stable $\text{Ag}(\text{CN})_x^{1-x}$ complexes.¹ However the toxicity of aqueous cyanide baths lead to the development of silver electrodeposition from ILs and organic solvents.^{5,20} These non-aqueous electrolytes were suitable for reversible silver electrodeposition and served as proof-of-concept works for electrochemically modulated optical films.²¹⁻²³ The

reversibility in these systems is attained from the halide-trihalide redox couples (X^-/X_3^- , $X = \text{Cl}, \text{Br}, \text{or I}$),^{24,25} and stable $[\text{AgX}_2]^-$ complexes.²⁶ Despite these advances, reversibility in all-ionic electrolytes was limited only to a handful of ILs. The majority of these, however, still generate unstable, volatile, or corrosive decomposition products (Figure 2.1A).^{27,28} In this report, we detail our work on creating an electrolyte for silver deposition containing a stable anion amenable to additional functionalization.

Results and Discussion

We developed a salt metathesis reaction between 1-butyl-3-methyl-imidazolium bromide, $[\text{BMIM}]\text{Br}$, and silver monocarborane, $\text{Ag}[\text{HCB}_{11}\text{H}_{11}]$, to generate a boron cluster ionic liquid, **BCIL-1**, with high silver content (Figure 2A). The parent carborane salt can be easily synthesized via a salt metathesis reaction between $\text{Cs}[\text{HCB}_{11}\text{H}_{11}]$ and AgNO_3 with an 82% yield (see SI) This ionic liquid, features an inert ionic matrix of $[\text{BMIM}]^+$ and $[\text{HCB}_{11}\text{H}_{11}]^-$ ions with $[\text{AgBr}_2]^-$ ions acting as the primary redox species (Figure 2.2A). Dialkylimidazolium cations and monocarborane anions were selected due to their electrochemical stability and weakly-coordinating characteristics suitable for designing an inert ionic matrix.²⁹ The BCILs were enclosed between two FTO electrodes to form transparent, two-electrode electrodeposition cell (Figure 2.2A). One FTO electrode was set as the working electrode while the other was set as both the counter and reference electrode. Cyclic voltammograms (CVs) show a reduction peak corresponding to reduction of silver complexes to form silver deposits at the working electrode (Figure 2.2B and 2.3). Electrodeposition begins at -1.5 V vs. FTO with a distinct current loop occurring in the cathodic region, which indicates a nucleation-limited deposition.²⁰ Reversing the polarity of the electrochemical cell toward $+0.3 \text{ V vs. FTO}$ leads to dissolution of the silver deposits at the working electrode back into the electrolyte. It was also observed that halide and metal ion additives

can affect the rate of the silver deposition and etching (Figure 2.2B and Figure 2.3). A general feature of these IL based electrolytes is an excess of halide, X^- ($X = \text{Br}$ or Cl) to Ag^+ . Typically, $X^-:\text{Ag}^+$ ion ratios of 2.5:1 were sufficient to fully dissolve the silver salts at room temperature. The excess halide promotes the formation of $\text{AgBr}_{x^{1-x}}$ species and provides additional halide ions to access the halide-trihalide (X^-/X_3^-) redox couple.

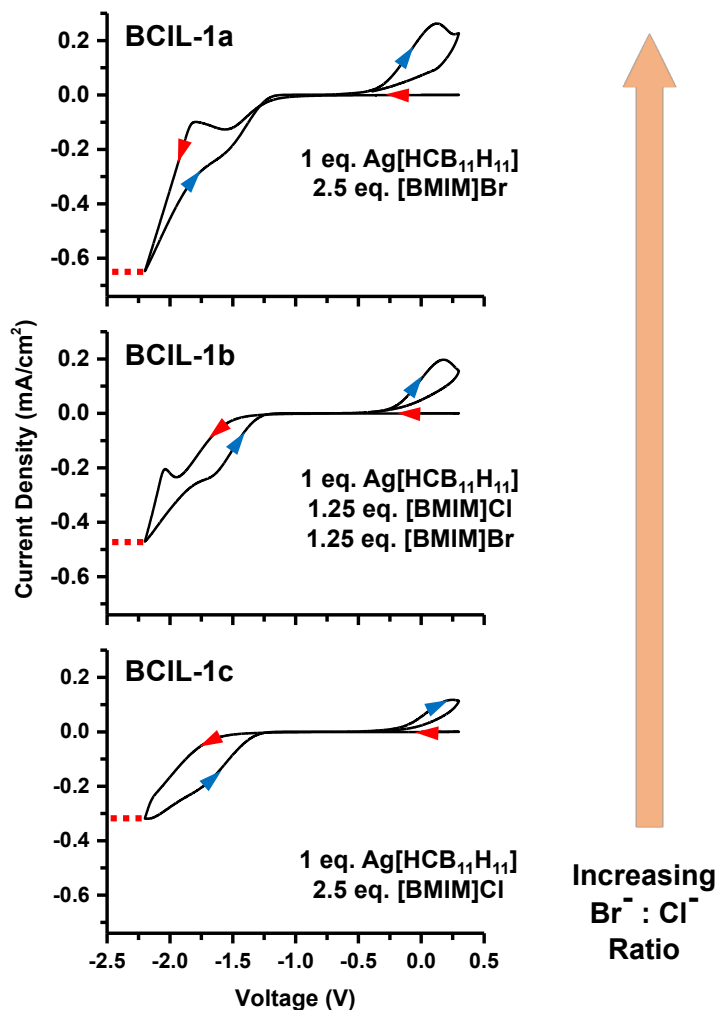


Figure 2.3: Two-electrode cyclic voltammograms (100 mV/s) of **BCIL-1** without CuBr_2 additive. Increasing the $\text{Br}^-:\text{Cl}^-$ ratio increases the electrodeposition current. Red and blue arrows indicate cathodic and anodic sweep direction respectively. Green areas indicate the composition dependent

FTO | [AgX₂]⁻, X₃⁻ | Ag⁰ | FTO process, red dashed lines indicate the maximum electrodeposition current density at -2.3 V vs. FTO counter electrode.

As the composition of the electrolyte, with a fixed halide concentration, is varied from chloride-rich to bromide-rich the potential for silver electrodeposition shifts to less cathodic potentials (Figure 2.3). This dependence on halide identity in the BCIL provides a simple method for tuning the onset of silver reduction and the current density of silver electrodeposition. Similar irreversible behavior in previously reported optical modulation devices were resolved by adding Cu(II) salts.^{20,22} Related studies on the effects of CuBr₂ in [BMIM]Br ionic liquids found that CuBr₂ complexes were effective at etching copper films.³⁰ Likewise, addition of 10 mol % CuBr₂ (relative to Ag⁺) to **BCIL-1** dramatically improved the reversibility of the ionic liquid formulation, generating **BCIL-2** (Figure 2.2B). Noteworthy was the change in film dissolution dynamics, wherein silver films deposited in the presence of Cu(II) were readily removed and exhibited larger oxidative currents (Figure 2.2B and Figure 2.3).

Previously, it has been shown that water content present in ILs during their ambient handling can alter the reversibility of silver deposition.³¹ Importantly, **BCIL-2** containing devices placed into a 98% humidity chamber did not experience alterations in device performance (Figure S2.2). CV experiments showed identical operating currents even after 4 days at these conditions. Such water tolerance enabled an easy benchtop assembly. Despite the electrochemical and moisture stability of **BCIL-2**, a gradual decrease in electrodeposition current was observed during electrochemical cycling of **BCIL-2** cells (Figure S2.4). After leaving the electrochemical cell overnight at room temperature, the electrodeposition current through the cell decayed and redox features became indistinguishable (Figure 2.4A). Visual inspection of the electrolyte showed

partial crystallization of the BCIL. Heating the cell to 60 °C for 1 hour dissolved the visible crystallites thereby restoring the cell to the original performance. This ultimately suggests that formation of small crystallites leads to reduced ion mobility and electrodeposition current.

Contrary to prevailing approaches of changing the physical properties of ILs by altering the cation, we sought to inhibit crystallite formation by functionalizing the monocarborane anion. A third electrolytic mixture, **BCIL-3**, was prepared using a monocarborane functionalized with a *sec*-butyl group appended on the carbon vertex of the boron-rich cluster (Figure 2.4B). After the electrochemical cell containing **BCIL-3** was kept at room temperature for 24 hours the deposition currents were comparable to those obtained from freshly prepared **BCIL-3** suggesting that, at this timescale, no observable crystallization occurs and hence the device performance remains unaffected. Heating of the **BCIL-3** cell to 60 °C for 1 hour further increased the electrodeposition current and eliminated the hysteresis current loop completely (Figure S2.4).

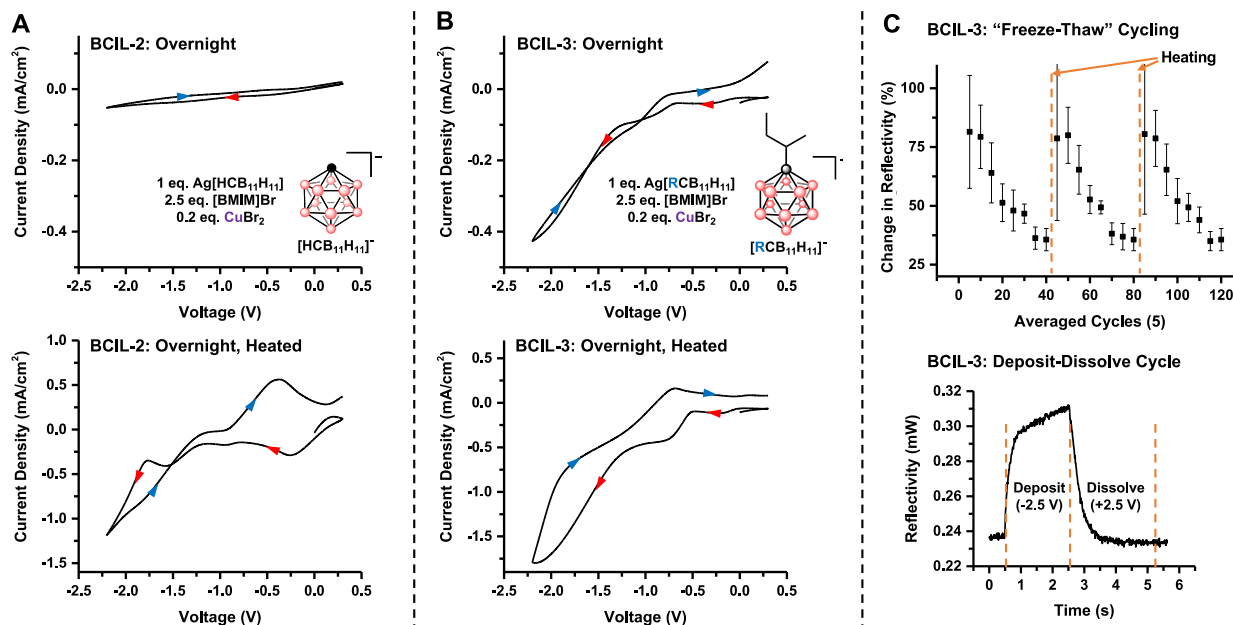


Figure 2.4 A: Two-electrode cyclic voltammograms (100 mV/s) of **BCIL-2** after equilibrating at ambient conditions overnight and after heating the equilibrated cell to 60 °C, top and bottom

respectively. **B:** Two-electrode cyclic voltammograms (100 mV/s) of **BCIL-3** after equilibrating at ambient conditions overnight and after heating the equilibrated cell to 60 °C, top and bottom respectively. Red and blue arrows indicate cathodic and anodic sweep direction respectively. **C:** Change in reflectivity ($\Delta\rho$) at 633 nm of **BCIL-3** electrochemical cell during extended “freeze-thaw” cycling and during a single deposition-dissolution cycle, top and bottom respectively. The electrochemical cell was regenerated every 40 cycles by heating to 60 °C.

The quality of the electrodeposited films was monitored using a 633 nm laser to correlate the film growth to the electrochemical behavior of the cells. Extended electrochemical cycling of a **BCIL-3** cell revealed a decay in reflectance change (Figure 2.4C), likely due to partial crystallization of **BCIL-3**. These effects were mitigated by heating the cell every 40 cycles (Figure 2.4C) to restore reflectance changes of up to 80%.

The silver film electrodeposition from **BCIL-3** can reach maximum reflectance within ~ 3 seconds when applying a -2.5 V cathodic potential, and it can be quickly removed by reversing the polarity of the electrochemical cell to +2.5 V (Figure 2.4C). Oxidative etching of the electrodeposited silver film is likely accelerated by electromigration of halides toward the working electrode and subsequent removal of electrodeposited silver as solvated silver halide anions.²⁰⁻²³ Applying a voltage (-1.8 V) for 450 seconds produced a thick film, which could be analyzed by scanning electron microscopy (SEM).³² Consistent with nucleation-limited deposition, the silver deposits grow as a film of silver crystallites approximately 500 nm in diameter (Figure 2.5). EDX elemental mapping shows two types of silver-containing deposits; an underlying Ag film with AgBr crystals on top of the film. The AgBr deposits likely formed during the washing of the working electrode, as described previously.²¹

Having identified a suitably resilient electrolyte capable of depositing silver films, we set out to control the IR transmission of the electrochemical cell by depositing a metallic film. From the law of conservation of energy, the sum of the absorption/emission (α/ε), transmission (τ), and reflection (ρ) interactions of an incident electromagnetic wave must sum to unity (Eq. 1).³³

$$\alpha + \rho + \tau = 1 = \varepsilon + \rho + \tau \text{ (Eq. 1)}$$

$$\alpha = \varepsilon$$

As such, a perfect blackbody radiator ($\alpha = \varepsilon = 1$) is not reflective ($\rho = 0$) because the absorption term dominates Eq. 1. Conversely, a perfectly reflective surface ($\rho = 1$) would not absorb/emit energy ($\alpha = \varepsilon = 0$). Thus, the emissivity (ε) of a fixed transparency object can be altered by changing the surface reflectivity (ρ) (Eq. 2).

$$\Delta \varepsilon = -\Delta \rho \text{ (Eq. 2)}$$

Similarly, electrodeposition of a reflective film onto an IR emitter would block the IR emission of the underlying IR sources (e.g. electrolyte and counter electrode), see SI for demonstration.^{15-18, 34} Such variable emissivity materials serve as the basis for adaptive surfaces for spacecraft thermal control. However, environmental instability and slow switching times limit their wide-spread application.

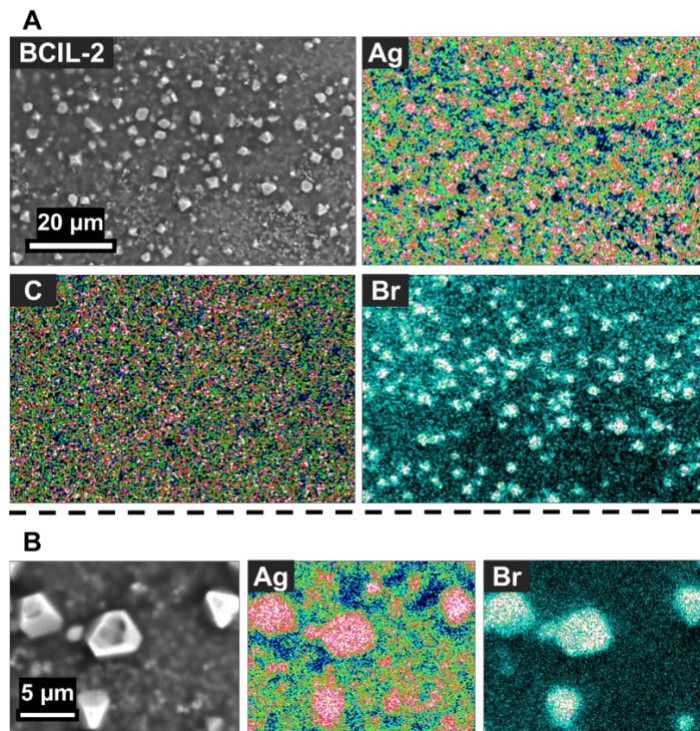


Figure 2.5 A: Scanning electron micrographs and EDX elemental mapping of **BCIL-3** working electrode after deposition of a silver film. **B:** Magnified scanning electron micrographs and EDX elemental mapping showing a silver film beneath AgBr deposits.

Metal-rich, all-ionic electrolytes can offer the vacuum stability of solid-state materials and rapid deposition rates of liquid electrolytes. A proof-of-concept IR transparent electrochemical cell was fabricated by enclosing **BCIL-3** between two IR transparent conductors composed of a 200 nm ITO film deposited onto a sapphire (Al_2O_3) window which is IR transparent up to $\sim 6 \mu\text{m}$ (1667 cm^{-1}). The electrochemical cell was mounted in an FTIR spectrometer with the working electrode facing the detector and IR transmission spectra were collected for the REM in the unplated and plated states (Figure 2.6). Electrodeposition of a metallic film reduced the IR energy transmission ($1500 - 4000 \text{ cm}^{-1}$) from 16% in the dissolved state to 8% in the deposited state, indicating that the deposition of a reflective film blocked the emission of the underlying IR sources (see SI for energy

transmission calculation). Strong absorption at ~ 3000 and ~ 2400 cm^{-1} is attributed to the imidazolium and carborane ions respectively. Although the longevity of the IR transparent cell was limited by the ITO electrode instability (Figure S2.3), it showcases the potential liquid-based technologies achievable with ionic liquids.

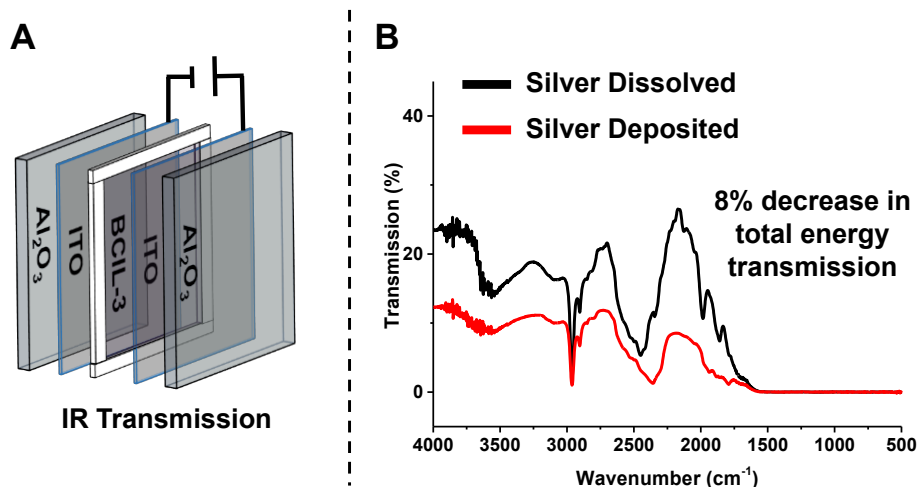


Figure 2.6 A: schematic of IR transparent electrochemical cell. **B:** FTIR transmission spectrum of **BCIL-3** IR transparent cell before and after silver film electrodeposition.

Conclusion and Outlook

In summary, we prepared a stable, all-ionic electrolyte designed around the weakly coordinating carborane framework for reversible electrodeposition of silver films. The metal-rich electrolyte enables rapid, reversible silver electrodeposition. Meanwhile, the ionic composition presents opportunities for electrodeposition in extreme environments (such as high temperature and low pressure). We demonstrate the utility of this electrolyte in electrochemically modulated optical devices.

Continued research efforts aim to further reduce the viscosity of BCIL formulations and inhibit solidification of the mixtures under repeated cycling. In particular, we have generated BCIL-4 which incorporates an identical salt formulation as BCIL-3 except the monocarborane *sec*-

butyl modifier was replaced with an isopentyl group to yield $\text{Ag}[(\text{CH}_3)_2\text{CHCH}_2\text{CH}_2\text{-CB}_{11}\text{H}_{11}]$ (Figure 2.7A). We envisioned an elongation of the alkyl chain could introduce more anisotropy to the system, limiting deleterious crystallization. To test this hypothesis, BCIL-4 was placed into an electrochemical sandwich device for further testing. As incorporation of a seed layer was previously shown to enhance deposition uniformity³⁵, BCIL-4 was sandwiched between FTO and an FTO slide with a Pt seed layer (100 nm) that had been vapor deposited (Figure 2.7B). After, the device was subjected to a “break-in” phase where the device was shuttled from 0.0 V to -1.6 V to 1.0 V to 0.0 V at a scan rate of 10 mV/sec for 50 consecutive cycles (Figure 2.7C). After this “break-in” phase, uniform current output was observed, and the optical reflectivity of the device was evaluated.

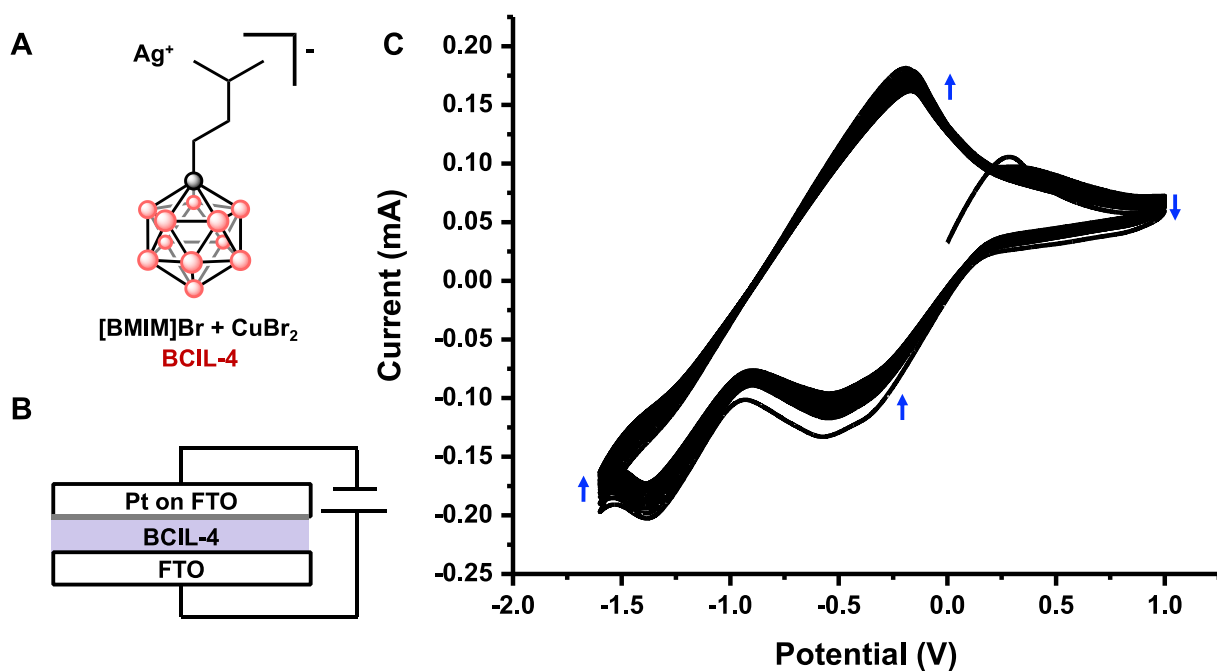


Figure 2.6 A: Formulation of BCIL-4 incorporating [BMIM]Br, CuBr_2 and $\text{Ag}[\text{isopentyl-CB}_{11}\text{H}_{11}]$ B: Schematic of electrochemical device C: Cyclic voltammograms of the first 50 cycles from 0.0 V to -1.6 V to 1.0 V to 0.0 V at a scan rate of 10 mV/sec.

Evaluation of the optical reflectivity was conducted using the experimental set-up and configuration established for devices incorporating BCIL-3. A BCIL-4 containing device was placed in front of a 633 nm HeNe laser and changes in the reflection of the incident laser were plotted against time (Figure 2.7A). Plating at -1.6 V for 15 seconds was followed by 10 seconds at 0.0 V and then 10 seconds at 1.0 V to redissolve the electrodeposited mirror (Figure 2.7B). Unlike devices incorporating BCIL-3, BCIL-4 electrochemical sandwiches resulted in consistently reversible changes in reflectance across 500 cycles (Figure 2.7A). Continued research efforts will repeat this experiment to establish error in degree of reflectance change and extend cycling to assess maximum device lifetime. These preliminary results further highlight the impact small synthetic changes to the monocarborane structure can impart on overall electrolyte properties, expanding the utility of these constructs for various weakly coordinating applications.

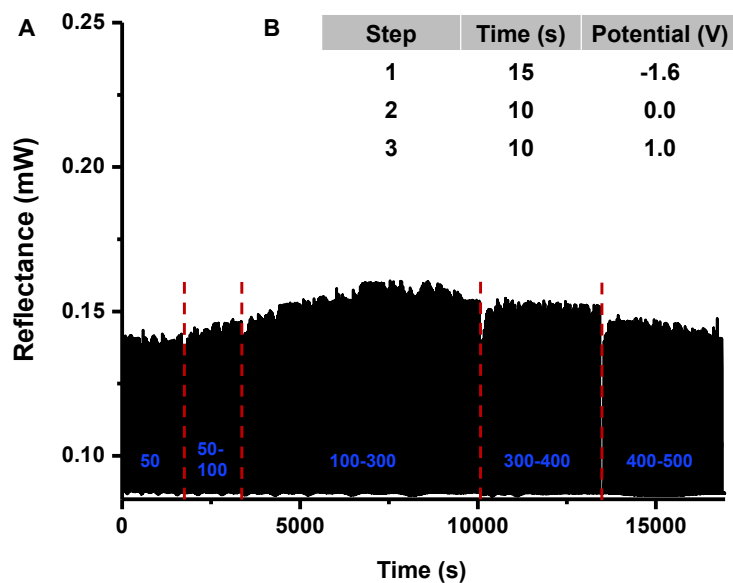


Figure 2.7 A: Changes in optical reflectivity of a BCIL-4 containing device across repeated electrochemical cycling. **B:** Summary of step-wise plating and de-plating with the times various voltages were applied.

References

1. Modern Electroplating, Schlesinger, M and Paunovic, M. 2014, John Wiley & Sons, Inc. Hoboken 2014.
2. Harada, A.; Yamaoka, H.; Watanabe, K.; Kinoshita, K.; Kishida, S.; Fukaya, Y.; Nokami, T.; Itoh, T. Copper Ion-containing Ionic Liquids Provide Improved Endurance and Switching Voltage Distributions of Conducting-bridge Random Access Memory *Chem. Lett.* **2015**, *44*, 1578-1580.
3. Watanabe, M.; Thomas, M. L.; Zhang, S.; Ueno, K.; Yasuda, T.; Dokko, K. Application of Ionic Liquids to Energy Storage and Conversion Devices *Chem. Rev.* **2017**, *117*, 7190-7239.
4. Kuwabata, S.; Tsuda, T.; Torimoto, T. Room-temperature Ionic Liquid. A New Medium for Material Production and Analyses under Vacuum Conditions *J. Phys. Chem. Lett.* **2010**, *1*, 3177-3188.
5. Simka, W.; Puszczuk, D.; Nawrat, G. Electrodeposition of Metals from Non-aqueous Solutions *Electrochim. Acta* **2009**, *54*, 5307-5319.
6. Baker, G. A.; Baker, S. N.; Pandey, S.; Bright, F. V. An Analytical View of Ionic Liquids *Analyst* **2005**, *130*, 800-808.
7. Zeng, Z.; Twamley, B.; Shreeve, J. Structure and Properties of Substituted Imidazolium, Triazolium, and Tetrazolium Poly(1,2,4-triazolyl)borate Salts *Organometallics* **2007**, *26*, 1782-1787
8. Türp, D.; Wagner, M.; Enkelmann, V.; Müllen, K. Synthesis of Nanometer-sized, Rigid, and Hydrophobic Anions *Angew. Chem. Int. Ed.* **2011**, *50*, 4962-4965.
9. Shkrob, I. A.; Marin, T. W.; Wishart, J. F. Ionic Liquids Based on Polynitrile Anions: Hydrophobicity, Low Proton Affinity, and High Radiolytic Resistance Combined *J. Phys. Chem. B* **2013**, *117*, 7084-7094.

10. Gelinas, B.; Das, D.; Rochefort, D. Air-stable, Self-bleaching Electrochromic Devices Based on Viologen- and Ferrocene-containing Triflimide Redox Ionic Liquids *ACS Appl. Mater. Interfaces* **2017**, *9*, 28726-28736.
11. Vöge, A.; Gabel, D. Boron in Weakly Coordinating Anions and Ionic Liquids. In *Boron Science: New Technologies and Applications*; Hosmane, N. S.; CRC Press, Boca Raton, FL, 2012; pp 807-826.
12. Reed, C. A. Carborane Acids. New “Strong Yet Gentle” Acids for Organic and Inorganic Chemistry *Chem. Commun.* **2005**, *0*, 1669-1677.
13. Zhu, Y.; Hosmane, N. S. Ionic Liquids: Recent Advances and Applications in Boron Chemistry *Eur. J. Inorg. Chem.* **2017**, 4369-4377.
14. Sivaev, I. B. Nitrogen Heterocyclic Salts of Polyhedral Borane Anions: from Ionic Liquids to Energetic Materials *Chem. Het. Comp.* **2017**, *53*, 638-658.
15. Shannon III, K. C.; Sheets, J.; Groger, H.; Williams, A. Thermal Management Integration using Plug-and-play Variable Emissivity Devices *Proc. of SPIE* **2009**, *7330*, 73300F.
16. Chandrasekhar, P.; Zay, B. J.; Lawrence, D.; Caldwell, E.; Sheth, R.; Stephan, R.; Cornwell, J. Variable-emittance Infrared Electrochromic Skins Combining Unique Conducting Polymers, Ionic Liquid Electrolytes, Microporous Polymer Membranes, and Semiconductor/Polymer Coatings, for Spacecraft Thermal Control *J. Appl. Polym. Sci.* **2014**, *131*, 40850.
17. Farrar, D.; Douglas, D. M.; Swanson, T.; Collins, C.; Darrin, A.; Osiander, R. MEMS Shutters for Thermal Control – Flight Validation and Lessons Learned *AIP Conf. Proc.* **2007**, *73*, 880.
18. Bergeron, B. V.; White, K. C.; Boehme, J. L.; Gelb, A. H.; Joshi, P. B. Variable Absorptance and Emittance Devices for Thermal Control *J. Phys. Chem. C* **2008**, *112*, 832-838.

19. CRC Handbook of Chemistry and Physics, 98th ed.; Rumble, J. R., Ed.; CRC Press/Taylor & Francis: Boca Raton, FL, (Internet Version 2018).
20. Reyna-González, J. M.; Reyes-López, J. C.; Aguilar-Martínez, M. Silver and Silver-copper Electrodeposition from a Pyridinium-based Ionic Liquid *Electrochim. Acta* **2013**, *94*, 344-352
21. Stocker, H. J.; Van Uiter, L. G.; Loomis, T. C.; Koch, F. B. An SEM Study of the Nature of the Electrochemical Deposit in Reversible Electrodeposition Displays *J. Electrochem. Soc.* **1981**, *128*, 746-748.
22. Mascaro, L. H.; Kaibara, E. K.; Bulhões, L. O. An Electrochemical System Based on the Reversible Electrodeposition of Lead *J. Electrochem. Soc.* **1997**, *144*, L273-L274.
23. Lu, W.; Fadeev, A. G.; Qi, B.; Mattes, B. R. Fabricating Conducting Polymer Electrochromic Devices Using Ionic Liquids *J. Electrochem. Soc.* **2004**, *151*, H33-H39.
24. Popov, A. I.; Geske, D. H. Studies on the Chemistry of Halogen and of Polyhalides. XVI. Voltammetry of Bromine and Interhalogen Species in Acetonitrile *J. Am. Chem. Soc.* **1958**, *80*, 5346-5349.
25. Allen, G. D.; Buzzeo, M. C.; Villagrán, C.; Hardacre, C.; Compton, R. G. A Mechanistic Study of the Electro-oxidation of Bromide in Acetonitrile and the Room Temperature Ionic Liquid, 1-butyl-3-methylimidazolium bis(trifluoromethylsulfonyl)imide at Platinum Electrodes *J. Electroanal. Chem.* **2005**, *575*, 311-320.
26. Luehrs, D. C.; Iwamoto, R. T.; Kleinberg, J. Solubility of Silver Halides and Stability of Silver Halide Complexes in Selected Nonaqueous Media *Inorg. Chem.* **1966**, *5*, 201-204.
27. Freire, M. G.; Neves, C. M. S. S.; Marrucho, I. M.; Coutinho, J. A. P.; Fernandes, A. M. Hydrolysis of Tetrafluoroborate and Hexafluorophosphate Counter Ions in Imidazolium-based Ionic Liquids *J. Phys. Chem. A* **2010**, *114*, 3744-3749.

28. Wang, B.; Qin, L.; Mu, T.; Xue, Z.; Gao, G. Are Ionic Liquids Chemically Stable? *Chem. Rev.* **2017**, *117*, 7113-7131.
29. Douvris, C.; Michl, J. Update 1 of: Chemistry of the Carba-*closo*-dodecaborate(-) Anion, $\text{CB}_{11}\text{H}_{12}^-$ *Chem. Rev.* **2013**, *113*, PR179-PR233.
30. Grishina, E. P.; Kudryakova, N. O.; Pimenova, A. M. Corrosion and Anodic Oxidation of Copper in 1-butyl-3-methylimidazolium Bromide-Copper(II) Bromide Ionic Liquid *Prot. Met. Phys. Chem. Surf.* **2017**, *53*, 663-669.
31. Basile, A.; Bhatt, A.I.; O'Mullane, A. P.; Bhargava, S. K. An Investigation of Silver Electrodeposition from Ionic Liquids: Influence of Atmospheric Water Uptake on the Silver Electrodeposition Mechanism and Film Morphology *Electrochim. Acta* **2011**, *56*, 2895-2905.
32. SEM studies required thicker Ag films due to etching of the films by solvent used to remove excess BCIL and expose the underlying Ag deposits.
33. G. B. Rybicki, A. P. Lightman, Fundamentals of Radiative Transfer, Radiative Processes in Astrophysics, Wiley-VCH, 2004.
34. J. F. Clawson, G. T. Tsuyuki, B. J. Anderson, C. G. Justus, W. Batts, D. Ferguson, D. G. Gilmore, Spacecraft Thermal Environments, pg 21-69, Spacecraft Thermal Control Handbook, Volume 1: Fundamental Technologies, 2nd Ed., The Aerospace Press, 2002.
35. Solanki, R. & Pathangey, B. Atomic Layer Deposition of Copper Seed Layers. *Electrochem. Solid-State Lett.* **2000**, *3*, 479-480.

Supporting Information

I. Materials and Methods

General Considerations:

Two-electrode symmetrical cells were used to study the electrochemical behavior of the ionic liquid during electrodeposition. The cells were composed of two fluorine-doped tin oxide glass (FTO) separated by a 0.25 mm thick PTFE spacer containing a 9/32" (7.14 mm) diameter hole. The PTFE spacer was coated with a thin layer of silicone grease, placed on the conductive side of the FTO electrode, the PTFE spacer cavity was filled with IL electrolyte, and sealed with a second FTO electrode. All electrochemical cell construction was done in ambient conditions. FTO glass was used instead of tin-doped indium oxide (ITO) because ITO electrodes degraded during electrochemical cycling as judged by the increased resistance of areas exposed to the ionic liquid. Copper (II) bromide and (CuBr_2) were Sigma Aldrich and used without further purification. Silver monocarborane salt and variants were synthesized as described in Section 3. Devices were heated by resting on a hot plate set to 60 °C for 1 hour. Devices were then cooled to room temperature for 1 hour before further testing.

Instrumentation:

NMR: ^1H , ^{11}B , $^{11}\text{B}\{^1\text{H}\}$ NMR spectra were recorded on DRX500, AVIII 500 and AV600 spectrometers in ambient conditions unless stated otherwise. Bruker Topspin V3.2 software was used to process the FID data and MestReNova V10.0.2-15465 software was used to visualize the spectra.

Electrochemistry: Electrochemical analysis was performed using a CH instruments CHI630D potentiostat.

SEM imaging: Scanning electron micrographs were obtained using a JEOL JSM-IT100 SEM. Energy-dispersive X-ray spectroscopy was obtained using a JEOL electron beam spectrometer.

Thermal Imaging: An FLIR E40 series camera from AZ technology was used for all emissivity imaging.

Reflectivity Measurements: Laser reflectivity measurements were performed using a 633 nm He-Ne laser and Thor Labs S120VC 50mW power meters interfaced with ThorLabs PM100 Multi-Power Meter Software. The experimental configuration consisted of the laser beam striking the center of the electrodeposition cavity from 23 cm away and the reflected beam was measured with the power meter 28 cm away.

IR Transmission Attenuation: A two-electrode cell was assembled as described above using sapphire substrates coated with a 200 nm thick ITO layer. The cell was mounted in an FT-IR spectrometer and IR transmission spectra were obtained before electrodeposition and after depositing a silver film by applying 2.5 V for 30 seconds. For all cycling measurements, a multi-potential stepping program was used. Specifically, the device was pulsed -1.8 V (15 seconds), 0.6 V (40 seconds), 0.8 V (5 seconds), 0.0 V (30 seconds). Total energy transmission was calculated relative to a 100% photon transmission in the 1500 – 4000 cm^{-1} region.

$$\frac{\int_{\nu=1500 \text{ cm}^{-1}}^{\nu=4000 \text{ cm}^{-1}} (T_{\nu} \times E_{\text{photon},\nu}) d\nu}{\int_{\nu=1500 \text{ cm}^{-1}}^{\nu=4000 \text{ cm}^{-1}} (E_{\text{photon},\nu}) d\nu}$$

Where T_{ν} is the percent transmission at a given frequency ν , and $E_{\text{photon},\nu}$ is the energy of a photon at frequency ν .

II. Precursor Synthesis

Silver Monocarbaborane ($\text{Ag}[\text{HCB}_{11}\text{H}_{11}]$)

This salt was made according to a literature procedure.¹

Cesium Monocarborane (Cs[HCB₁₁H₁₁])

This salt was made according to a literature procedure.²

S-Butyl Silver Monocarborane (Ag[*s*-butylCB₁₁H₁₂])

Li[*closo*-1-LiCB₁₁H₁₁] was prepared according to literature³: under an inert atmosphere, 5.0 grams of (CH₃)₃NH [HCB₁₁H₁₁] was dissolved in 10 mL THF in a 20 mL scintillation vial equipped with a stir bar. 2.2 equivalents of 2.5 M *n*-butyllithium in hexanes was added and the mixture was allowed to stir for 3 hours. The resulting solution was added dropwise to a 250 mL round bottom flask containing 70 mL hexanes while stirring, resulting in a white precipitate. The solvent was decanted and the remaining white precipitate dried under vacuum. The isolated white precipitate was dissolved in 10 mL THF. Two equivalents of 1-iodo-2-methylpropane were added to the reaction solution and stirred for 90 minutes. The solution was removed from inert conditions, organic solvents were removed *in vacuo*, and the crude product was added to 50 mL H₂O. The alkylated carborane product was purified using the following salt exchange procedure: (CH₃)₃NH HCl was added in excess to the aqueous solution, precipitating the (CH₃)₃NH alkyl carborane salt. The solution was filtered and the precipitate was redissolved in approximately 80 mL slightly basic H₂O with an excess of CsCl. The solution was concentrated down to 30-40 mL, and upon cooling to room temperature the Cs⁺ salt of the alkylated carborane product precipitated as a white crystalline solid. A concentrated solution of 1.3 grams of Cs⁺ 2-methylpropyl-1-carborane, Cs[(C₄H₉)CB₁₁H₁₁] was prepared by heating in 50 mL of slightly acidic DI water (3-5 drops of concentrated HNO₃). 1.1 equivalents of AgNO₃ was dissolved in 5 mL or less, and added to the aqueous solution. An off-white precipitate formed immediately, and the solution was cooled to room temperature before filtering. Ag[(C₄H₉)CB₁₁H₁₁] final yield of 960 mg, 79.7%. ¹H NMR (300 MHz, acetone-d₆, 25°C): δ = 2.83 – 0.45 (bm, 11H, B-H), 1.61 (d, 2H, ³J(*H,H*) = 2.0 Hz) 1.54

(m, 1H), 0.71 (d, 6H, $^3J(H,H) = 2.0$ Hz) ppm. $^{11}\text{B}[^1\text{H}]$ NMR (96 MHz, acetone- d_6 , 25°C): $\delta = -8.3, -9.7$ ppm. ^{11}B NMR (96 MHz, acetone- d_6 , 25°C): $\delta = -8.2$ ppm ($^1J(H,B) = 145.0$ Hz), -9.7 ppm ($^1J(H,B) = 128.6$ Hz).

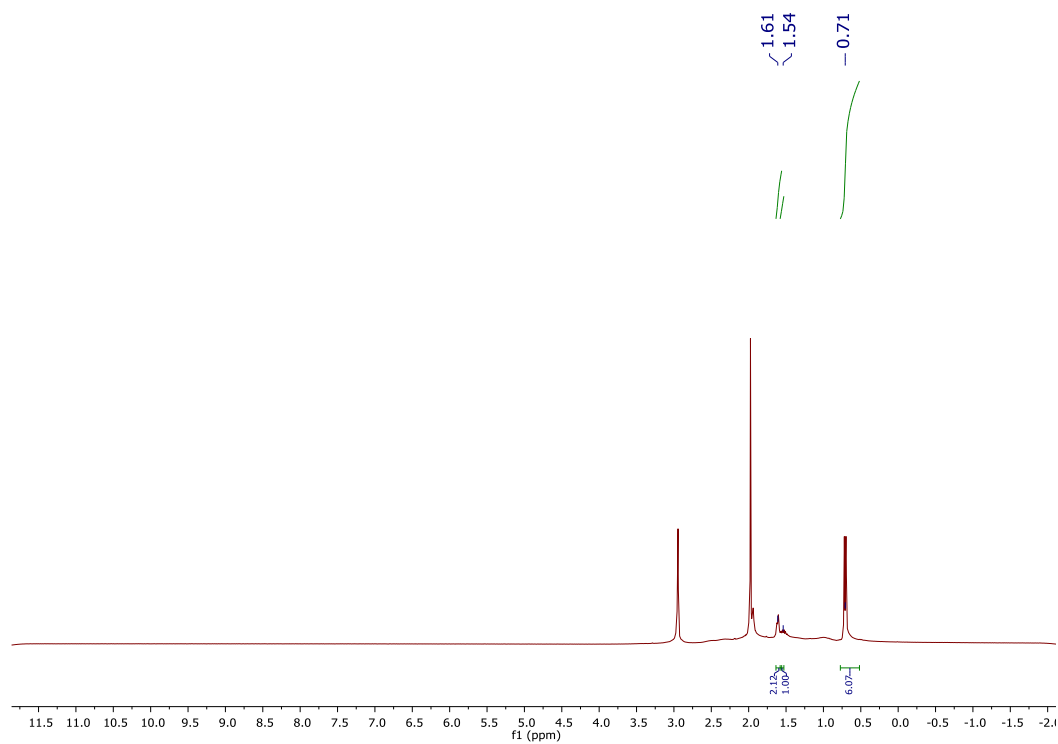


Figure S2.1A: ^1H -NMR spectrum of $\text{Ag}[(\text{C}_4\text{H}_9)\text{CB}_{11}\text{H}_{11}]$ in acetone- d_6 . Note: peak at 2.80 ppm is from H_2O .

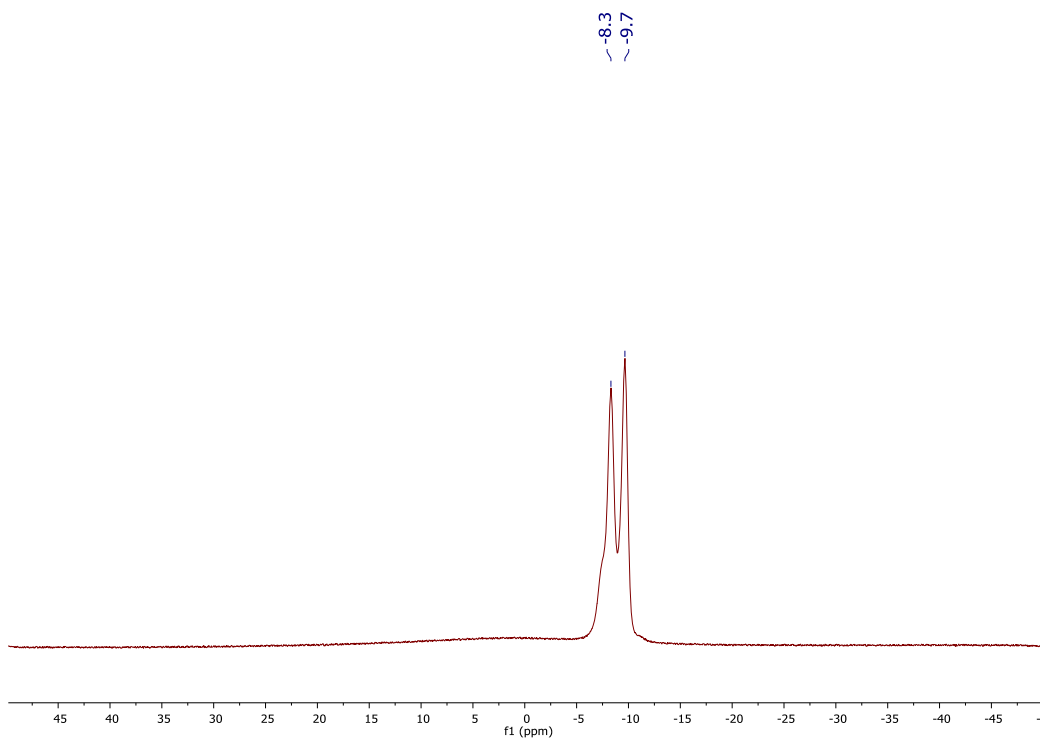


Figure S2.1B: $^{11}\text{B}\{^1\text{H}\}$ -NMR spectrum of $\text{Ag}[(\text{C}_4\text{H}_9)\text{CB}_{11}\text{H}_{11}]$ in acetone- d_6 .

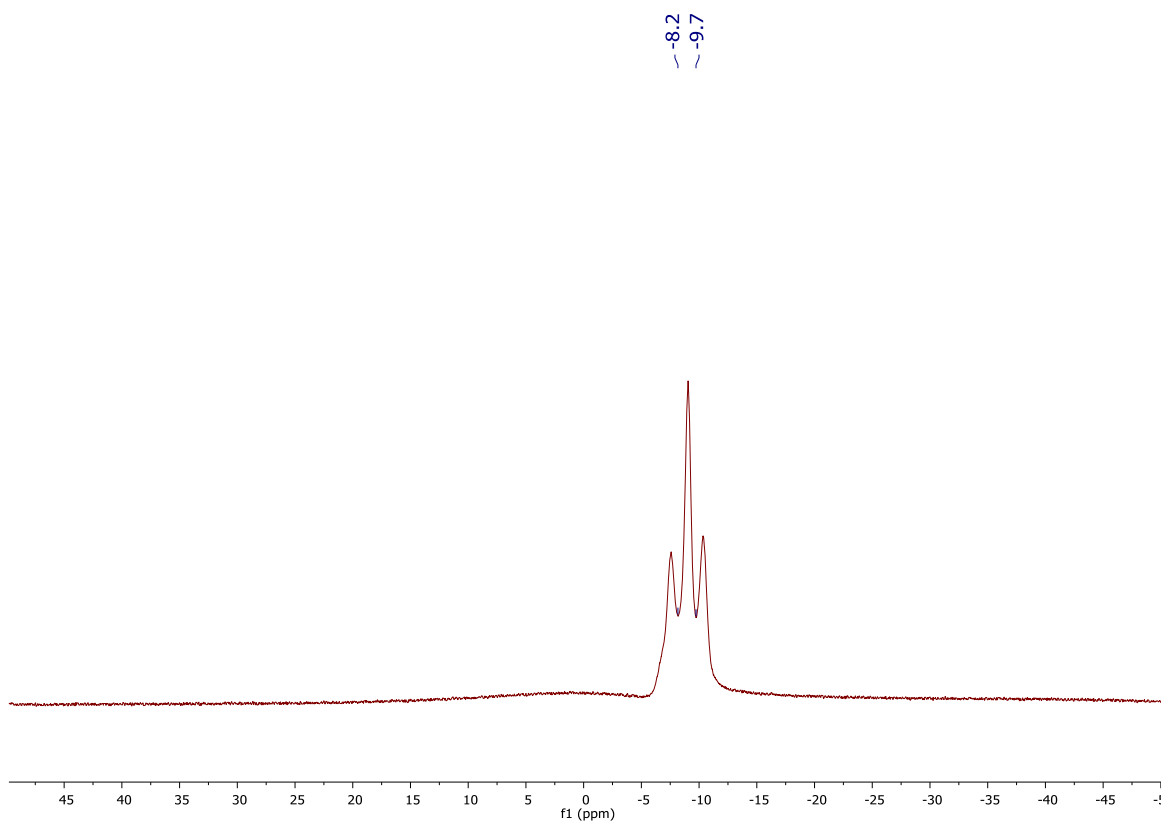


Figure S2.1C: ^{11}B -NMR spectrum of $\text{Ag}[(\text{C}_4\text{H}_9)\text{CB}_{11}\text{H}_{11}]$ in acetone- d_6 .

III. BCIL Formulation

BCILs were prepared as described in detail below. Generally, 1-butyl-3-methyl-imidazolium bromide ([BMIM]Br), silver monocarborane, and CuBr₂ were mixed in a 4 mL vial with gentle heating to ~50 °C to facilitate melting. Once the BCIL became homogeneous, atmospheric moisture was removed under vacuum with mild heating until the BCIL stopped outgassing. Note: extended exposure to atmospheric moisture leads to a teal colored BCIL, likely due to formation of copper aqua complexes. The original performance of the BCIL can be recovered by dehydrating the BCIL with mild heating under vacuum.

BCIL-1 / BCIL-1a: 63 mg (0.250 mmol) of Ag[HCB₁₁H₁₁] and 137 mg (0.625 mmol) of [BMIM]Br were mixed in a 4 mL vial with gentle heating to ~50 °C until the mixture became a clear, homogeneous liquid. The liquid was then heated under dynamic vacuum until the mixture began evolving moisture, this was continued until bubbling ceased.

BCIL-1b: 63 mg (0.250 mmol) of Ag[HCB₁₁H₁₁], 68 mg (0.312 mmol) of [BMIM]Br, and 54 mg (0.312 mmol) of [BMIM]Cl were mixed in a 4 mL vial with gentle heating to ~50 °C until the mixture became a clear, homogeneous liquid. The liquid was then heated under dynamic vacuum until the mixture began evolving moisture, this was continued until bubbling ceased.

BCIL-1c: 63 mg (0.250 mmol) of Ag[HCB₁₁H₁₁] and 108 mg (0.625 mmol) of [BMIM]Cl were mixed in a 4 mL vial with gentle heating to ~50 °C until the mixture became a clear, homogeneous liquid. The liquid was then heated under dynamic vacuum until the mixture began evolving moisture, this was continued until bubbling ceased.

BCIL-2: 63 mg (0.250 mmol) of Ag[HCB₁₁H₁₁], 137 mg (0.625 mmol) of [BMIM]Br, and 11 mg (0.05 mmol) CuBr₂ were mixed in a 4 mL vial with gentle heating to ~50 °C until the mixture

became a deep blue / purple liquid. The liquid was then heated under dynamic vacuum until the mixture began evolving moisture, this was continued until bubbling ceased.

BCIL-3: 77 mg (0.250 mmol) of Ag[s-butylCB₁₁H₁₁], 137 mg (0.625 mmol) of [BMIM]Br, and 11 mg (0.05 mmol) CuBr₂ were mixed in a 4 mL vial with gentle heating to ~50 °C until the mixture became a deep blue / purple liquid. The liquid was then heated under dynamic vacuum until the mixture began evolving moisture, this was continued until bubbling ceased.

IV. Normalization of CV Currents

All electrochemical current was normalized to the electrode area, 0.489 cm². The same working area was used for all studies.

V. Moisture Stability Studies

The assembled device was placed into an Associated Environmental Systems humidity chamber and set to 98% humidity at room temperature for 4 days. CVs (100 mV/s) exhibit equivalent currents and redox features even after 4 days of moisture exposure.

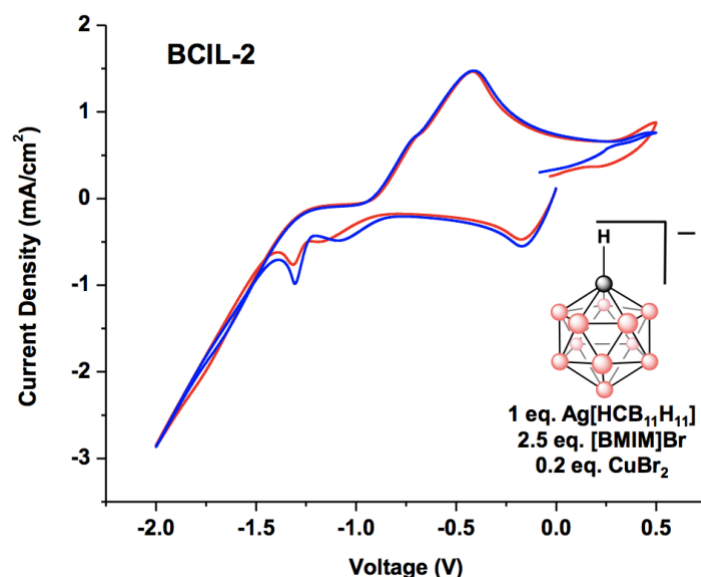


Figure S2.2: Cyclic voltammograms of BCIL-2 before placement into moisture chamber (blue) and after 4 days of exposure at 98% humidity (red).

VI. Electrochemical Current Reductions

BCIL-2 Current Loss

Gradual current decay was observed upon extended cycling (100 mV/s) of **BCIL-2**. After 100 cycles, current had dropped to zero. This decay in current is attributed to a loss of ion mobility caused by gradual crystallization.

ITO Degradation

A series of experiments on the reversible plating of Ag (100 mV/s) from **BCIL-3** were conducted on both FTO and ITO slides. Significant reduction in device current was seen for ITO sandwiched **BCIL-3** after only 100 cycles of current sweeping. Conversely, **BCIL-3** sandwiched between FTO substrates displayed current consistency up to 2,000 cycles. ITO degradation mechanism has been previously reported. Under the presence of an electric field, scratches at the ITO surface initiate degradation. Degradation is exacerbated by increased ITO surface area, the presence of external contaminants such as water and higher device operating temperatures. Measurement of resistivity increase across ITO surface has also been attributed to surface growths, leading to degradation. Such susceptibility to external factors presents manufacturing challenges if BCIL devices were to be implemented in spacecraft thermal control. FTO is a desirable alternative by introducing cycling stability without the need for strict monitoring of surface conditions.

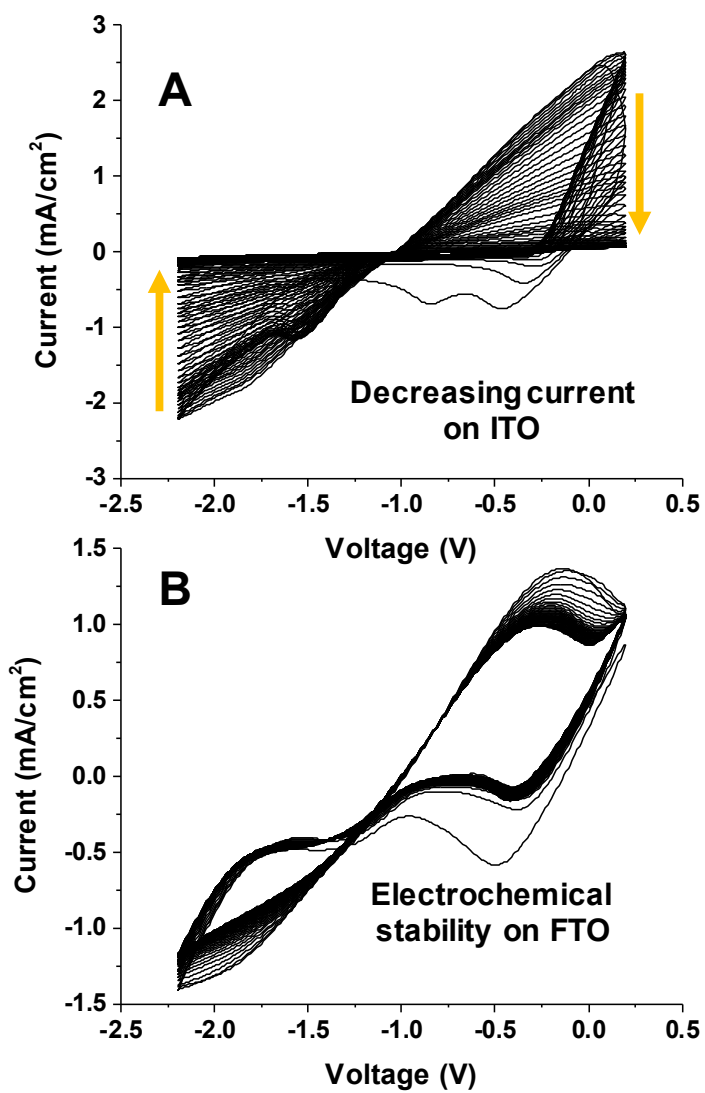


Figure S2.3 A: decreasing current of **BCIL-3** on ITO after 100 CV cycles, **B:** stable electrochemical performance of **BCIL-3** on FTO after 100 CV cycles. (100 mV/s scan rate)

Current Loss Upon Cooling to Room Temperature

As described in text, devices containing **BCIL-2** and **BCIL-3** were kept at room temperature overnight resulting in the decay of electrochemical features. To further display this “freeze-thaw” phenomenon a second figure detailing the before and after cooling state is attached herein.

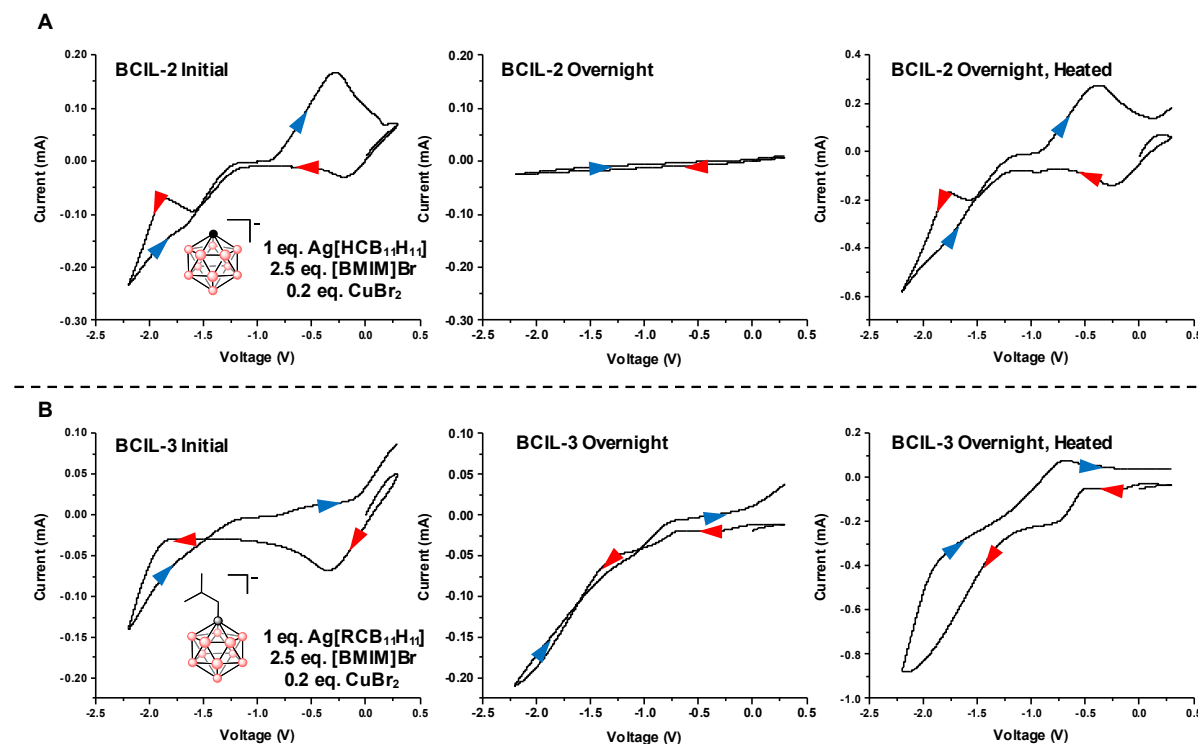


Figure S2.4 A: Two-electrode cyclic voltammograms of **BCIL-2** before and after equilibrating at ambient conditions overnight and after heating the equilibrated cell to 60 °C, top and bottom respectively. **B:** Two-electrode cyclic voltammograms of **BCIL-3** before and after equilibrating at ambient conditions overnight and after heating the equilibrated cell to 60 °C, top and bottom respectively.

VII. Variable IR Emission

Silver Modulates Emissivity

A heated glass slide, coated on one side with a 100 nm thick silver film displayed drastically different emissivity depending on which side is facing the detector. When the uncoated glass side is facing the camera, the glass slide appears “hot”, (Figure S5A). When the glass slide is flipped, the silver mirror is facing the detector and the substrate appears “cold”, (Figure S5B). This apparent difference in temperature is due to the different emissivity of the top surface. Glass appears “hot” because it is an IR absorber (IR absorber at $\lambda < 4 \mu\text{m}$), while silver films are IR reflective ($< 10\%$ IR absorption).⁴ Using this unique property, the thermal emissivity of a spacecraft could be controlled by deploying IR reflective surfaces (metallic films).

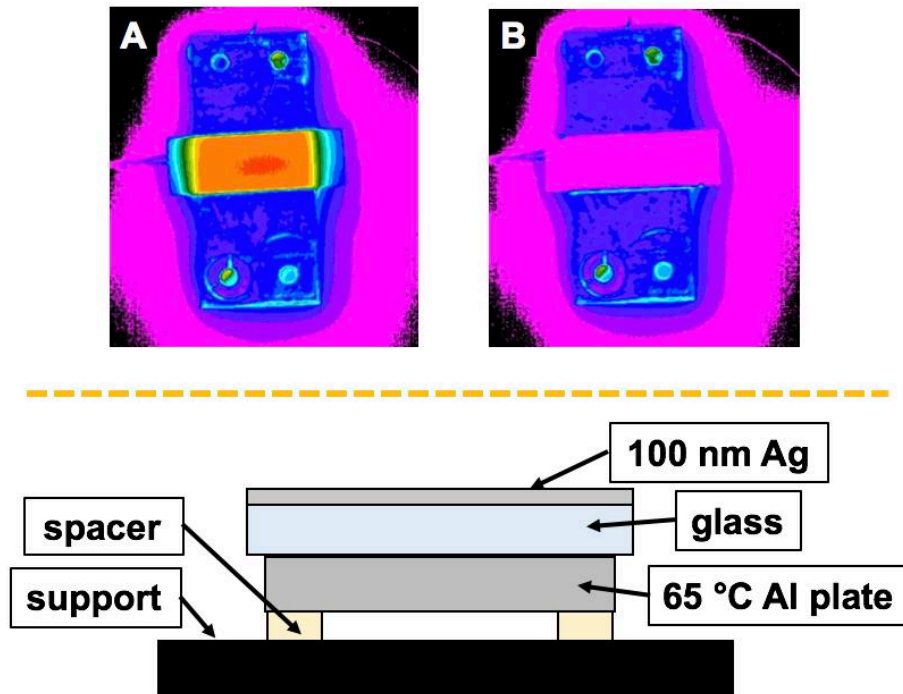


Figure S2.5 **A:** strong IR emission observed when the glass side is facing up, **B:** strong IR reflection when the 100 nm silver film is facing up. Bottom, cross-section schematic of substrate emissivity experiment.

ITO-Sapphire IR Absorption

Reported % change in transmittance value of 18% is believed to be largely affected by IR absorption of the sapphire substrate. Sapphire begins absorbing at $\sim 2500\text{ cm}^{-1}$ ($4\ \mu\text{m}$) and is not IR transparent beyond $\sim 1667\text{ cm}^{-1}$ ($6\ \mu\text{m}$), representing a majority of the IR range measured.⁵ The limit to IR transmittance can be seen by thermal imaging of an ITO-coated sapphire electrode and a sapphire window on a heated silver coated glass slide, (Figure. S6). Higher heat intensity is seen for the ITO coated sapphire window (green) than the uncoated sapphire window (blue). Importantly, the IR reflectivity of the silver surface is masked by the IR absorptive (emissive) sapphire and ITO-coated sapphire windows. Although we were unable to achieve large changes in IR transmission and reflectivity, these experiments support the feasibility of a BCIL variable emissivity device.

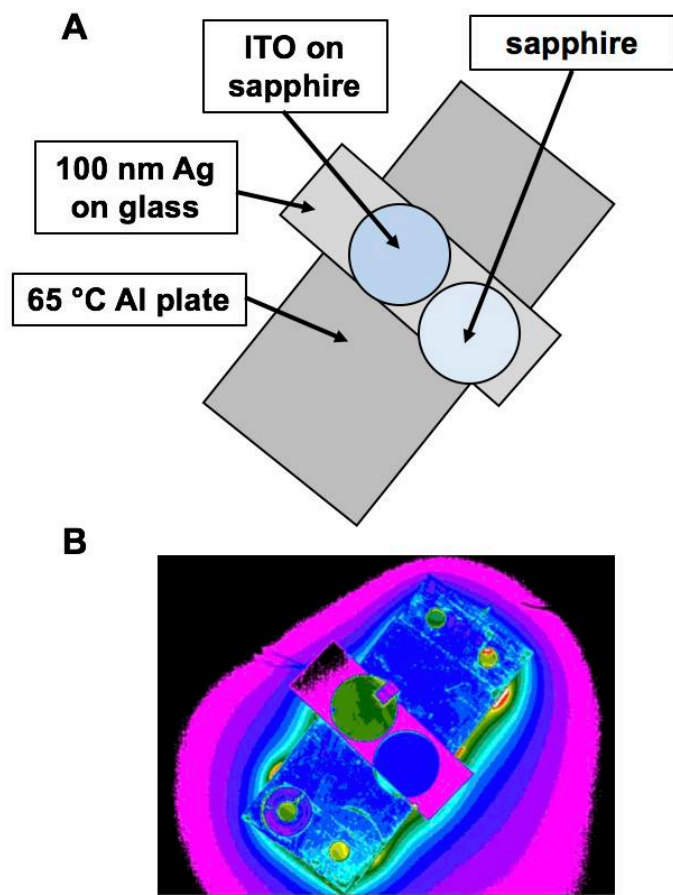


Figure S2.6 A: schematic of substrate emissivity experiment. **B:** near-IR thermal camera image of ITO coated and uncoated sapphire windows placed on an IR reflective (non-emissive) silver mirror on glass.

VIII. SEM Cross Section

In order to assess film thickness in the absence of acetonitrile washing, devices were disassembled and broken in half to image the cross section. An average film thickness of $(244 \pm 4) \mu\text{m}$ was determined. EDX measurements indicate excess carbon on towards the top of the film, likely residual ionic liquid. Silver is dispersed throughout, with pockets of higher concentration as consistent with a nucleation limited growth pattern.

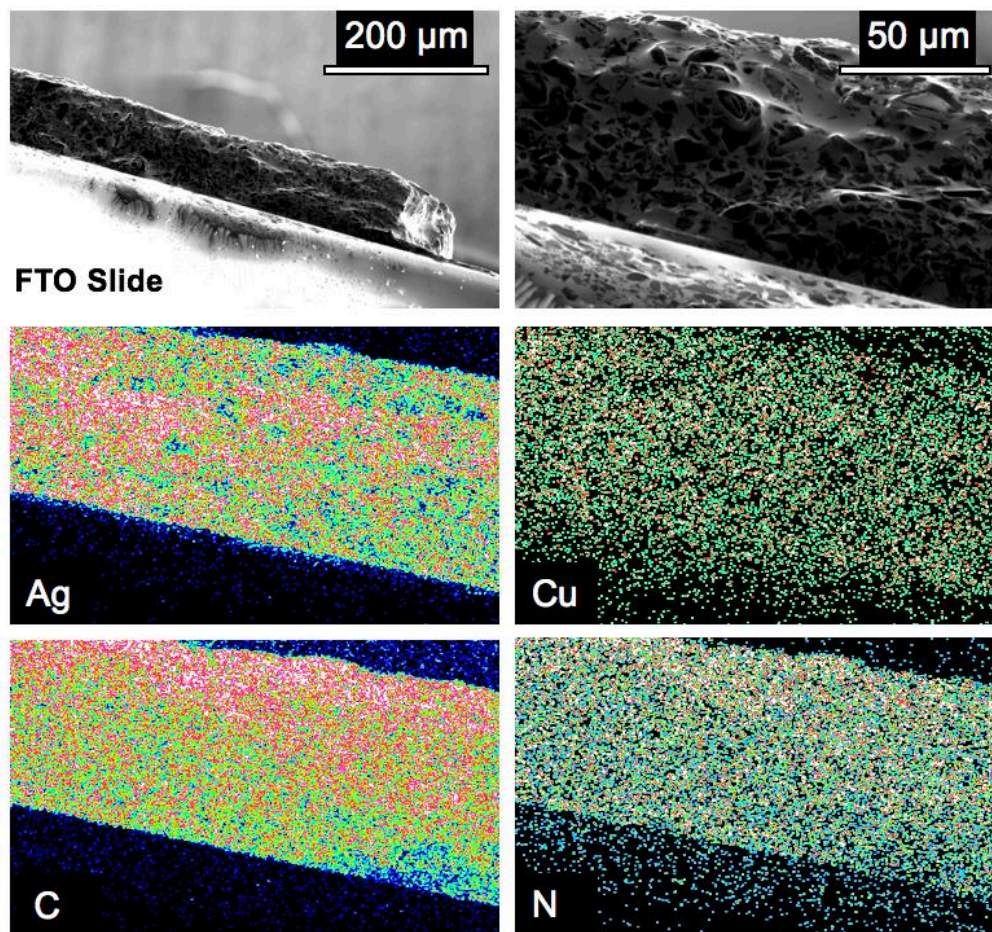


Figure S2.7: Cross-sectional scanning electron micrographs and EDX elemental mapping of **BCIL-3** working electrode after deposition of a silver film. Average film thickness was calculated to be $(244 \pm 4) \mu\text{m}$.

IX. SI References

1. Shelly, K.; Finster, D. C.; Lee, Y. J.; Scheidt, W. R.; Reed, C. A. (1985). η^1 -Benzene coordination: the synthesis and x-ray crystal structure of a novel silver salt of the weakly coordinating carborane anion $B_{11}CH_{12}^-$. *J. Am. Chem. Soc.* 1985, 107, 5955–5959.
2. Reed, C.A. H^+ , CH_3^+ , and R_3Si^+ Carborane Reagents: When Triflates Fail. *Acc. Chem. Res.* **2010**, 43, 121–128.
3. Jelinek, T.; Baldwin, P.; Scheidt, R.; Reed, C.A. New Weakly Coordinating Anions. 2. Derivatization of the Carborane Anion $CB_{11}H_{12}^-$. *Inorg. Chem.* **1993**, 32, 1982.
4. Clawson, J.F.; Tsuyuki, G.T.; Anderson, B.J.; Justus, C.G.; Batts, W.; Ferguson, D.; Gilmore, D.G. Spacecraft Thermal Environments. In *Spacecraft Thermal Control Handbook*; Ed.2; The Aerospace Press, 2002; vol. 1; 21-69.
5. Lowry, S. Analysis of Rubies and Sapphires by FT-IR Spectroscopy; *Thermo Fischer Scientific*; Madison, WI; Application Note 51124; 2008.

CHAPTER 3

Mixed Halogenation Strategy for Tuning Properties of a Dodecaborate Anion

Abstract

Considerable research effort has been devoted to developing weakly coordinating anions (WCAs) that can be produced on large scale, are soluble in a variety of solvents and exhibit both thermal and kinetic stability. Polyhedral boranes have emerged as a particularly attractive class of WCAs owing to the high degree of electron delocalization, exceptional stability profiles and low nucleophilicity associated with these species. Specifically, halogenated dodecaborates $[\text{B}_{12}\text{X}_{12}]^{2-}$ ($\text{X} = \text{Cl}, \text{Br}, \text{I}, \text{F}$) are polyhedral boranes that can be produced from facile and scalable syntheses; however, generally low solubility of these salts limits widespread utility. Herein we present a series of mixed halogenated $[\text{B}_{12}\text{X}_9(\text{OR})_3]^{2-}$ dodecaborates where $\text{X} = \text{Cl}, \text{Br}$ and $\text{R} = \text{H}, \text{CH}_3$. The present strategy allows for tuning of physical properties such as steric bulk, solubility and thermal stability of the anions. We demonstrate coordination to both tetrabutylammonium (TBA^+) and lithium (Li^+) cations. After, thermogravimetric analysis offers insights on the thermal stability of $[\text{B}_{12}\text{X}_9(\text{OR})_3]^{2-}$ anions. Finally, a preliminary assessment of solubility demonstrates enhanced solubility of $[\text{B}_{12}\text{X}_9(\text{OR})_3]^{2-}$ salts over perhalogenated analogues, providing future opportunities in applications such as Li conductivity, battery materials, ionic liquids and components for electrochemistry.

Introduction

WCAs are ubiquitous components in modern catalysis, electrochemistry, ionic liquids and battery materials.¹ While many WCAs (*i.e.* ClO_4^- , NO_3^- , BF_4^-) were once referred to as “non-coordinating” owing to their dissociation in aqueous solution,^{1c} this notion has largely been refuted as decades of spectroscopic and crystallographic characterization demonstrate the solvent dependency of anion coordination.^{1a,c} Generally, some non-nucleophilic anions with a large degree

of electron delocalization can be weakly coordinating.¹ However, kinetic and thermal stability are essential for practical application.¹ Anions such as BF_4^- and PF_6^- can undergo rapid fluoride abstraction in the presence of electrophiles, severely limiting their widespread usage.^{1c} BPh_4^- can be utilized to circumvent degradative fluoride abstraction but at the expense of oxidative stability.² Modification of the phenyl rings with electron withdrawing groups ($-\text{C}_6\text{F}_6$ or $-\text{C}_6\text{H}_3-3,5-(\text{CF}_3)_2$) increases the reduction potential of the $\text{B}(\text{Ar})_4^{0/1}$ redox couple, yielding commercially available perfluoroalkyl borates which are important precursors in homogeneous catalysis.¹ Replacement of the $-\text{C}_6\text{H}_3-3,5-(\text{CF}_3)_2$ withdrawing groups with $-\text{C}_6\text{H}_3-3,5-(n-\text{C}_6\text{F}_{13})$, $-\text{C}_6\text{H}_3-3,5-(n-\text{C}_4\text{F}_9)$, and $-\text{C}_6\text{H}_3-3,5-(2-\text{C}_3\text{F}_7)$ results in perfluoroalkyl borates which are more soluble in hydrocarbons while also reducing the coordinating effect of these anions.^{1b,c} Unfortunately, lengthy synthesis limits large scale distribution of these designer perfluoroalkyl borates¹, highlighting the challenges presented towards the generation of the “ideal” weakly coordinating anion. Recent toxicology data associated with biological persistence of perfluoroalkyl compounds also sheds additional doubts whether some of these anions could present long-term environmental and health concerns.^{3,4} Clearly, one must consider more than coordinating ability but also the solubility, synthetic accessibility, stability and environmental aspects associated with the anion.

The complexity of developing WCAs is further highlighted by the historical progression within the family of poly- or perfluorinated alkoxy- (OR^{F}) and aryloxymetallates (OAr^{F}). ($[\text{M}(\text{OR}^{\text{F}})_n]^-$ and $[\text{M}(\text{OAr}^{\text{F}})_n]^-$) salts can be generated from oxophilic, Lewis acidic metals such as B^{III} , Al^{III} , Nb^{V} , Ta^{V} , Y^{III} , and La^{III} to generate catalysts for polymerization.^{1,5} These metallates offer safer synthesis and larger scalability than related perfluoroalkyl borate, $[\text{B}(\text{C}_6\text{F}_5)_4]^-$, which can lead to explosive byproducts.¹ While various perfluoroaryloxymetallates have demonstrated efficient olefin polymerization, complexes such as $[\text{M}(\text{OC}_6\text{F}_5)_6]^-$ ($\text{M} = \text{Nb}$ or Ta) undergo

deleterious aryloxy abstraction in the presence of zirconocene catalysts.^{6,7} Additionally, the oxygen atom in many aryloxy moieties leads to enhanced anion coordination.¹ Poly- and perfluorinatedalkoxymetallates largely circumvent these coordination and stability issues through incorporation of sterically demanding moieties^{1,8} such as $-\text{OCH}(\text{CF}_3)_2$, $-\text{OCH}_3(\text{CF}_3)_2$ and $-\text{OC}(\text{CF}_3)_3$. Alkoxyaluminate $[\text{Al}\{\text{OC}(\text{CF}_3)_3\}_4]^-$ (Figure 3.1A) represents a particularly attractive complex owing to the scalable preparation, chemical stability, facile conversion to other synthetically useful precursors and low coordinative strength associated with this salt.^{1,5} For example, in contrast to many alkoxyaluminates, $[\text{Al}\{\text{OC}(\text{CF}_3)_3\}_4]^-$ is stable towards hydrolysis in nitric acid due to $-\text{CF}_3$ shielding of the oxygen atom.⁹ These examples demonstrate the capacity of halogenated, bulky ligands to provide a multifaced enhancement in the chemical properties and catalytic performance of WCAs. From this logic, a larger ligand should result in a more weakly coordinating anion, but what species are more encumbered than aryl or tertiary alkyl systems?

Early pioneers including Knoth¹⁰⁻¹¹, Reed¹²⁻¹³ and Štíbr¹⁴ answered this question through use of highly symmetrical, three-dimensional polyhedral monocarboranes, $[\text{HCB}_{11}\text{H}_{11}]^-$ and $[\text{HC}_9\text{H}_9]^-$. Monocarborane anions exhibit a large HOMO-LUMO gap with delocalized electron density

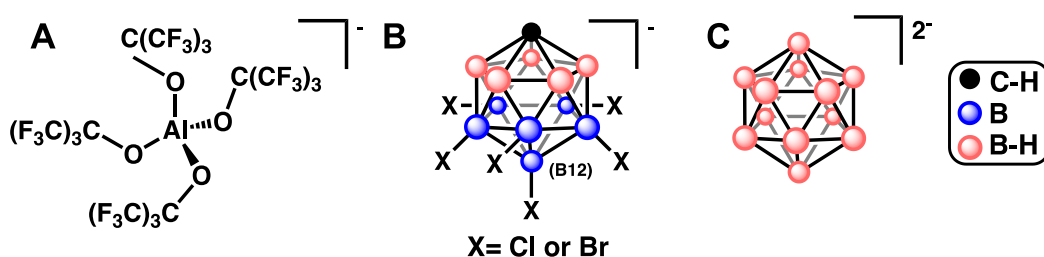


Figure 3.1: Structures of **A:** the perfluoroalkoxyaluminate anion $[\text{Al}\{\text{OC}(\text{CF}_3)_3\}_4]^-$ **B:** partially halogenated monocarborane anion $[\text{HCB}_{11}\text{H}_5\text{X}_6]^-$ and **C:** the dodecaborate anion $[\text{B}_{12}\text{H}_{12}]^{2-}$.

shared amongst σ bonds that contribute to the bonding of the boron cage.¹⁵ Owing to the strength of σ bonding, monocarboranes exhibit exceptional thermal and kinetic stability.¹⁵ After initial discovery by Knoth¹¹, Reed and coworkers coined monocarborane anion, $[\text{HCB}_{11}\text{H}_{11}]^-$, “the least coordinating anion” in a seminal report demonstrating the longest bonding distance to cation $\text{Fe}(\text{TPP})^+$ ever observed.¹⁶ Later, both Reed¹⁷ and Štíbr¹⁸ reported halogenated monocarboranes ($[\text{HCB}_{11}\text{H}_5\text{X}_6]^-$ where $\text{X} = \text{Cl}$ or Br) as the B-H bonds are amenable to electrophilic substitution—much like the C-H bonds of benzene. The boron (B12) directly opposite to carbon represents the most electrophilic site and can be substituted preferentially followed by the surrounding boron centers on the lower belt of the cluster, yielding one of the most chemically robust WCAs known (Figure 3.1B).¹ While many have demonstrated the capacity of monocarboranes to act as very WCAs in a variety of metal complexes, their widespread use is still limited by the lengthy and expensive synthetic processes involved in production of these molecules. Comparatively, synthesis of isostructural dodecaborane $[\text{B}_{12}\text{H}_{12}]^{2-}$ (Figure 3.1C) is facile and scalable.¹⁹ Initial preparation included reflux of 2-iodododecaborane with triethylamine in benzene to afford $[\text{C}_6\text{H}_{16}\text{N}^+]_2\text{B}_{12}\text{H}_{12}$.^{19a} A more convenient and widely utilized procedure was later reported by Hawthorne and coworkers who demonstrate the isolation of $\text{Na}_2\text{B}_{12}\text{H}_{12}$ from pyrolysis of NaB_3H_8 (Figure 3.2).^{19b} Initially, $[\text{B}_{12}\text{H}_{12}]^{2-}$ was dismissed as a WCA as it was believed the dianionic character of this cluster would lead to its metal coordination; however, early reports by Zakharova conclude that both unmodified and halogenated dodecaborate anions produce weakly coordinated complexes with Pd and Ni (*i.e.* $[\text{Ni}(\text{MeCN})_6][\text{B}_{12}\text{H}_{12}]$ and $[(\text{PPh}_3)_3\text{PdCl}]_2\text{B}_{12}\text{Cl}_{12}$)²⁰. Later, perfluorinated dodecaborate $[\text{B}_{12}\text{F}_{12}]^{2-}$ was found to stabilize $[\text{AlMe}_2]^{\delta+}$ and $[\text{SiR}_3]^{\delta+}$ further corroborating the capacity of $[\text{B}_{12}\text{X}_{12}]^{2-}$ anion platform to be weakly coordinating²¹.

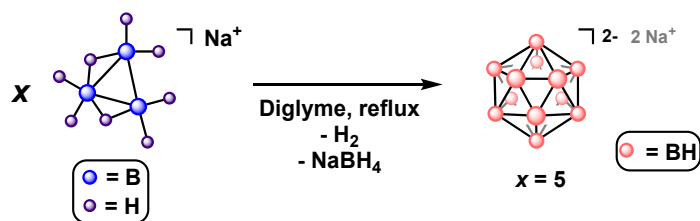


Figure 3.2: Schematic detailing the facile generation of $\text{Na}_2\text{B}_{12}\text{H}_{12}$ from the pyrolysis of NaB_3H_8 .^{19b}

While dodecaborate anions offer a promising platform for further development, Reed and coworkers²² have identified a significant limitation as “the generally lower solubilities of $[\text{B}_{12}\text{X}_{12}]^{2-}$ salts compared to those of $[\text{HCB}_{11}\text{H}_{11}]^-$.” Herein, we augment the scope of accessible dodecaborate-based WCAs through a mixed hydroxylation and halogenation strategy to generate $[\text{B}_{12}\text{X}_9(\text{OR})_3]^{2-}$ where $\text{X} = \text{Cl}, \text{Br}$ and $\text{R} = \text{H}, \text{CH}_3$. Through mixed halogenation we provide a platform for tuning the solubility of the resulting salts, circumventing this known limitation of dodecaborate anions. While incorporation of oxygen could enhance metal coordination, steric encumbering by B-X bonds may render the atom inaccessible to cations. Importantly, Alkoxylation offers further opportunities for steric blocking of hydroxyl oxygen while also allowing for enhanced modulation of stability and solubility. Coordination to both alkali metal lithium and organic cation tetrabutylammonium is demonstrated. We highlight the thermal stability profiles of the resulting salts and provide preliminary evidence of enhanced solubility of mixed halogenated clusters over the corresponding perhalogenated analogues. This library of anions expands the toolbox of accessible polyhedral borane WCAs with potential applications in lithium-ion conductivity, catalysis and ionic liquid components.

Results and Discussion

After initial discovery of $[\text{B}_{12}\text{X}_{12}]^{2-}$, a number of early pioneers explored various methods to modify $[\text{B}_{12}\text{H}_{12}]^{2-}$. Specifically, Muetterties reported the hydroxylation of $[\text{B}_{12}\text{H}_{12}]^{2-}$ by heating N-methyl-2-pyrrolidinone in nitric acid.²³ Subsequent treatment of the product with NaOH yielded $[\text{B}_{12}\text{H}_m(\text{OH})_n]^{2-}$ where $m=10-11$ and $n=1-2$. Decades later, a single-step hydroxylation in sulfuric acid was reported by Hawthorne and coworkers.²⁴ This high yielding and efficient method offered a higher degree of specificity in hydroxyl addition leading to the isolation of $[\text{B}_{12}\text{H}_m(\text{OH})_n]^{2-}$ clusters where $m=8-11$ and $n=1-4$. We utilized the preparation reported by Hawthorne with slight modification (49% sulfuric acid was increased to 53%) to generate $[\text{B}_{12}\text{H}_9(\text{OH})_3]^{2-}$ (Figure 3.3, See SI Section II). It should be noted that hydroxylation repeatedly led to ~5-10% $[\text{B}_{12}\text{H}_8(\text{OH})_4]^{2-}$ by-product. This compound could be removed through column chromatography; however, for ease of subsequent scale-up we chose to retain the slight $[\text{B}_{12}\text{H}_8(\text{OH})_4]^{2-}$ impurity in all subsequent reactions.

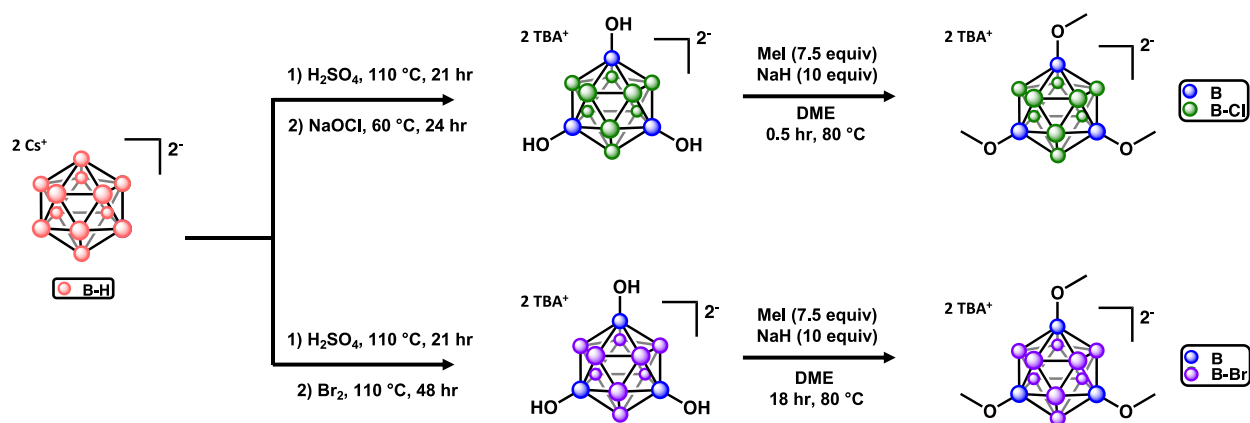


Figure 3.3: Schematic detailing the hydroxylation, halogenation and alkoxylation of $[\text{B}_{12}\text{X}_{12}]^{2-}$.

Following hydroxylation, $[\text{B}_{12}\text{H}_9(\text{OH})_3]^{2-}$ was subjected to either chlorination or bromination to yield $[\text{B}_{12}\text{Cl}_9(\text{OH})_3]^{2-}$ and $[\text{B}_{12}\text{Br}_9(\text{OH})_3]^{2-}$, respectively (Figure 3.2, See SI Section

II). Perchlorination of $[\text{B}_{12}\text{H}_{12}]^{2-}$ has been achieved through various preparations. First, Muetterties and coworkers heated $\text{Na}_2\text{B}_{12}\text{H}_{12}\cdot 2\text{H}_2\text{O}$ in a silver-lined pressure vessel containing chlorine gas for 2 hr under autogenous pressure.^{25a} Later, the method was improved by Uzun *et al.* who achieved perchlorination by bubbling chlorine gas into a solution of $\text{Na}_2\text{B}_{12}\text{H}_{12}$ for ~30 hr.^{25b} Finally, perhalogenation was achieved using thionyl chloride (SOCl_2) under refluxing in acetonitrile.²⁶ We envisioned an alternate approach utilizing sodium hypochlorite to generate Cl_2 *in situ* in order to circumvent the need for a chlorine tank or highly corrosive SOCl_2 , significantly enhancing the safety and scalability of the reaction. Sodium hypochlorite was previously utilized to chlorinate the B-H bonds within tertiary amine-boranes as outlined below²⁷:



Rate of chlorination increased with decreasing pH as formation of hypochlorous acid was determined to be the kinetically limiting step for monochlorination.²⁷ We applied a similar approach by treating $\text{Cs}_2\text{B}_{12}\text{H}_9(\text{OH})_3$ dissolved in sulfuric acid to dropwise addition of excess sodium hypochlorite (6%). Green gas (Cl_2) was observed upon addition of the sodium hypochlorite and the sealed vessel was allowed to stir at room temperature for two hours after which the temperature was increased to 60 °C. Following a 24 hr period, product was precipitated by addition of tetrabutylammonium bromide (TBA-Br), filtered and washed with water. Negative mode ESI(-) mass spectrometry of the isolated product was consistent with the formation of $[\text{B}_{12}\text{Cl}_9(\text{OH})_3]^{2-}$. Next, we analyzed the isolated product through ^{11}B NMR spectroscopic analysis. A singlet resonance was observed (-7.2 ppm) along with two overlapping resonances (-13.5 ppm and -15.2 ppm) with an integral ratio of 1 to 3 consistent with the expected splitting pattern for $[\text{B}_{12}\text{Cl}_9(\text{OH})_3]^{2-}$ (See SI Section I). After, the nature of the cation was probed through ^1H and ^{13}C

NMR spectroscopic analysis. A distinct singlet with an integration of 3 was observed in the ^1H NMR spectrum along with four multiplets in an integral ratio of 16:16:16:24, indicating the $[\text{B}_{12}\text{Cl}_9(\text{OH})_3]^{2-}$ anion had been isolated as a TBA salt. Four resonances in the ^{13}C NMR spectrum corresponding to the TBA cation lend additional support to the formation of $\text{TBA}_2\text{B}_{12}\text{Cl}_9(\text{OH})_3$ (see SI Section I). Finally, X-ray crystallography unequivocally confirmed the presence of $\text{TBA}_2\text{B}_{12}\text{Cl}_9(\text{OH})_3$ as well as the regioselectivity in hydroxyl placement which aligned well with previous hydroxylation reports.^{23,24} No evidence of cation coordination to the hydroxyl moiety is observed within the complex, suggesting the steric bulk of halogenation is sufficient to shield the oxygen atom from TBA^+ . Importantly, the reaction conditions could be applied to kilogram-scale chlorination at collaborator facilities, suggesting the facile and inexpensive preparation is amenable to industrially relevant quantities. Bromination of $[\text{B}_{12}\text{H}_9(\text{OH})_3]^{2-}$ was achieved using a reported method^{25a} with only slight modification (See SI Section I) and the $[\text{B}_{12}\text{Br}_9(\text{OH})_3]^{2-}$ anion was also isolated as a TBA salt in order to provide a more consistent analysis of anionic properties.

Next, we methylated both $\text{TBA}_2\text{B}_{12}\text{Cl}_9(\text{OH})_3$ and $\text{TBA}_2\text{B}_{12}\text{Br}_9(\text{OH})_3$ in order to enhance the steric hindrance of the $[\text{B}_{12}\text{X}_9(\text{OH})_3]^{2-}$ scaffold and offer new opportunities for tuning of physical properties. Taking inspiration from reports for the peralkoxylation²⁸ of $[\text{B}_{12}(\text{OH})_{12}]^{2-}$, we heated $\text{TBA}_2\text{B}_{12}\text{X}_9(\text{OH})_3$ to 80 °C in 1,2-dimethoxyethane (DME) with strong base, sodium hydride (NaH). After 5 min, the reaction vessel was charged with excess methyl iodide ($\text{CH}_3\text{-I}$) and allowed to react. Masses consistent with full methylation of $\text{TBA}_2\text{B}_{12}\text{Cl}_9(\text{OH})_3$ were observed by negative mode ESI(-) mass spectrometry within 30 min. In addition, a distinct singlet was observed at 3.5 ppm in the ^1H NMR spectrum along with four multiplets in an integral ratio of 9:16:16:16:24, further suggesting full methylation to $\text{TBA}_2\text{B}_{12}\text{Cl}_9(\text{OCH}_3)_3$ had occurred. Finally, five resonances were observed in the ^{13}C spectrum corresponding to four TBA cation resonances

and one resonance corresponding to the methoxy ^{13}C . Methylation of $\text{TBA}_2\text{B}_{12}\text{Br}_9(\text{OH})_3$ was more sluggish, requiring 18 hours to reach full conversion by negative mode ESI(-) mass spectrometry. The slower kinetics associated with methylation of $\text{TBA}_2\text{B}_{12}\text{Br}_9(\text{OH})_3$ are likely the result sterically encumbering B-Br pentagonal belt surrounding the hydroxyl groups, limiting access to the methylating reagent. In addition to mass spectrometry, ^1H NMR and ^{13}C NMR spectroscopy confirmed full conversion to $\text{TBA}_2\text{B}_{12}\text{Br}_9(\text{OCH}_3)_3$ (See SI Section II).

After generation of $\text{TBA}_2\text{B}_{12}\text{X}_9(\text{OR})_3$ ($\text{X} = \text{Br}, \text{Cl}$ and $\text{R} = \text{H}, \text{CH}_3$) salts, we utilized a resin-based cation exchange method to convert to the organic cation to lithium. Adapted from an elegant approach reported by Strauss and coworkers²¹, $\text{TBA}_2\text{B}_{12}\text{X}_9(\text{OR})_3$ was dissolved in various mixtures of acetone, acetonitrile and methanol depending on the solubility of the given salt and passed through a column packed with Amberlyst-15 proton resin exchange beads (See SI Section III). The eluted solvent was dried *in vacuo* until an oily residue remained. The residue was dissolved in water and the pH was brought up to 7 using LiOH. After drying *in vacuo*, white powders were isolated. Complete cation exchange was first indicated by the facile dissolution of the isolated powders in water as all $\text{TBA}_2\text{B}_{12}\text{X}_9(\text{OR})_3$ salts were completely insoluble in aqueous media. Secondly, a singlet resonance at ~ 0.0 ppm was observed by ^7Li NMR spectroscopy for all cation-exchanged salts further suggesting the organic cation had been removed. ^1H NMR and ^{13}C NMR spectroscopy provided additional evidence that lithium salts had been isolated. No resonances were observed in the ^1H NMR spectra for both $\text{Li}_2\text{B}_{12}\text{Cl}_9(\text{OH})_3$ and $\text{Li}_2\text{B}_{12}\text{Br}_9(\text{OH})_3$ providing indirect verification of TBA removal (See SI Section III). The ^1H NMR spectrum for $\text{Li}_2\text{B}_{12}\text{Cl}_9(\text{OCH}_3)_3$ contained only a singlet resonance at 3.7 ppm which can be ascribed to the methoxy ^1H nuclei. Similarly, a single resonance at 54.6 ppm was observed by ^{13}C NMR and corresponds to the methoxy ^{13}C nuclei. As with $\text{Li}_2\text{B}_{12}\text{Cl}_9(\text{OCH}_3)_3$, the ^1H NMR and ^{13}C NMR

spectra of $\text{Li}_2\text{B}_{12}\text{Br}_9(\text{OCH}_3)_3$ contained single resonances corresponding to methoxy at 3.7 ppm and 54.8 ppm, respectively (See SI Section III). These results highlight capacity ion exchange to dramatically alter the solubility properties of the anions and provides a useful path forward for many battery and Li-conductivity applications.

Next, we analyzed the thermal stability of the library of mixed halogenated dodecaborates as lithium salts using thermogravimetric analysis. In order to benchmark the stability, we prepared $\text{Li}_2\text{B}_{12}\text{Cl}_{12}$ and $\text{Li}_2\text{B}_{12}\text{Br}_{12}$ as control samples (See SI Section II). As seen in Figure 2.3A, the plot of weight (%) against temperature indicates that from 60 °C to 200 °C, 18% of the $\text{Li}_2\text{B}_{12}\text{Cl}_{12}$ sample weight is lost, suggesting three water molecules were coordinated to each lithium (See SI Section IV). As the temperature scans from 200 °C to 575 °C, no weight change is observed indicating $\text{Li}_2\text{B}_{12}\text{Cl}_{12}$ is thermally stable across this range. These results are in close agreement with the thermogravimetric analysis of $\text{Cs}_2\text{B}_{12}\text{Cl}_{12}$ where no mass changes were observed between

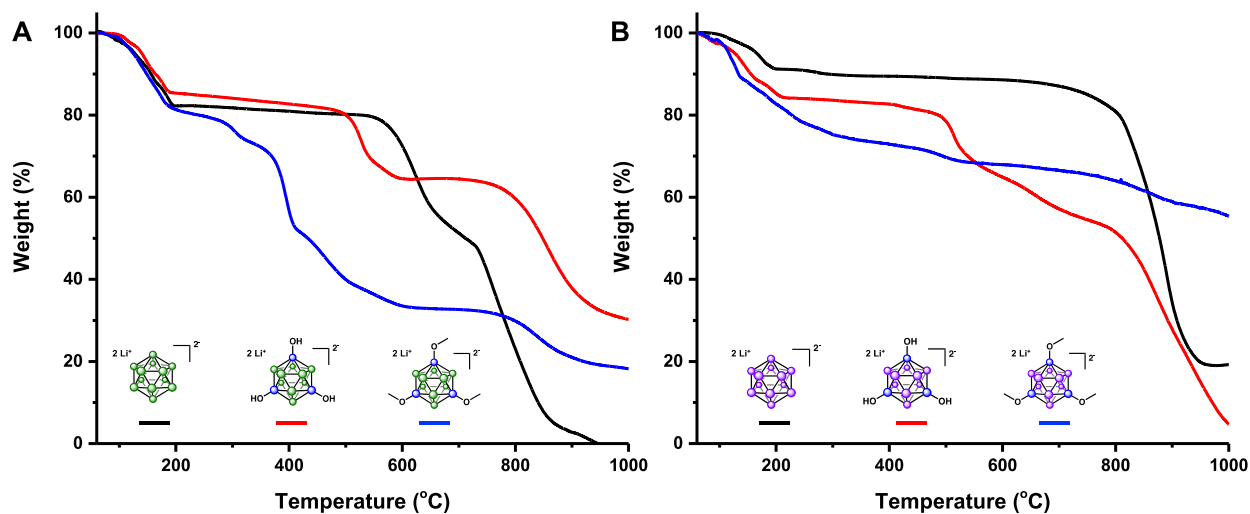


Figure 3.4 A: thermogravimetric analysis of $\text{Li}_2\text{B}_{12}\text{Cl}_{12}$, $\text{Li}_2\text{B}_{12}\text{Cl}_9(\text{OH})_3$ and $\text{Li}_2\text{B}_{12}\text{Cl}_9(\text{OCH}_3)_3$ and **B:** thermogravimetric analysis of $\text{Li}_2\text{B}_{12}\text{Br}_{12}$, $\text{Li}_2\text{B}_{12}\text{Br}_9(\text{OH})_3$ and $\text{Li}_2\text{B}_{12}\text{Br}_9(\text{OCH}_3)_3$. Samples were heated at a rate of 10 °C/min under a constant flow of argon (200 mL/min).

180 °C and 600 °C.²⁹ After 600 °C, decomposition of the sample and 85% mass loss was observed. Comparatively, a 14% dehydration was observed in the sample of $\text{Li}_2\text{B}_{12}\text{Cl}_9(\text{OH})_3$, corresponding to only two water molecules per lithium, possibly due to coordination of the anion hydroxy groups to the alkali metal (Figure 3.4A, See SI Section IV). Elevating the temperature from 200 °C to 500 °C results in negligible weight change; however, after 500 °C, a rapid loss in 20% of the sample weight is observed suggesting mixed halogenation lowers the thermal stability of the anion scaffold. After initial dehydration corresponding to the loss of three water molecules per lithium, heated sample of $\text{Li}_2\text{B}_{12}\text{Cl}_9(\text{OCH}_3)_3$ resulted in the most significant weight change profile as ~10% loss is observed at just 250 °C (Figure 3.4A, See SI Section IV). Continued mass loss is observed as heating extends to 1000 °C resulting in an overall 80% reduction in sample weight. The significant impact of methylation upon anion stability could be the result of thermally induced, lithium chloride-catalyzed demethylation which was previously observed in aryl methyl ether substrates by Bei and coworkers under microwave conditions.²⁹ We then treated the library of brominated lithium salts to thermogravimetric analysis. Samples of $\text{Li}_2\text{B}_{12}\text{Br}_{12}$, $\text{Li}_2\text{B}_{12}\text{Br}_9(\text{OH})_3$ and $\text{Li}_2\text{B}_{12}\text{Br}_9(\text{OCH}_3)_3$ dehydrated by 8%, 15% and 11%, corresponding to the coordination of three, four and three water molecules to lithium, respectively (Figure 3.4B, See SI Section IV). Heating $\text{Li}_2\text{B}_{12}\text{Br}_{12}$ beyond 200 °C resulted in no significant mass changes until 800 °C where 80% of the sample weight was lost. This remarkable stability is in close agreement with the thermogravimetric analysis of $\text{Cs}_2\text{B}_{12}\text{Br}_{12}$ where heating to 950 °C was required to induce decomposition.³⁰ Heating $\text{Li}_2\text{B}_{12}\text{Br}_9(\text{OH})_3$ beyond 200 °C resulted in little change in weight until 500 °C, after which continuous mass loss was observed indicating $\text{Li}_2\text{B}_{12}\text{X}_9(\text{OH})_3$ salts have similar thermal stability when X= Cl and X= Br. Finally, continuous weight loss is observed in the

thermogravimetric curve of $\text{Li}_2\text{B}_{12}\text{Br}_9(\text{OCH}_3)_3$ across the thermal scan from 60 °C to 1000 °C suggesting thermally induced reactivity is likely occurring in heated samples of both $\text{Li}_2\text{B}_{12}\text{Cl}_9(\text{OCH}_3)_3$ and $\text{Li}_2\text{B}_{12}\text{Br}_9(\text{OCH}_3)_3$ (Figure 3.4B, See SI Section IV). Overall, mixed halogenation lowers thermal stability when compared to perhalogenation; however, exceptional stability is still demonstrated, especially for $\text{Li}_2\text{B}_{12}\text{X}_9(\text{OH})_3$ salts which remain intact up to 500 °C. Importantly, halogen type (X= Cl or Br) did not substantially impact thermal stability and modulation of X could be used instead to modulate the steric and solubility properties of the resulting salt.

Finally, we completed a preliminary assessment of the solubility properties of anhydrous $\text{Li}_2\text{B}_{12}\text{Cl}_{12}$, $\text{Li}_2\text{B}_{12}\text{Cl}_9(\text{OH})_3$ and $\text{Li}_2\text{B}_{12}\text{Cl}_9(\text{OCH}_3)_3$ in acetonitrile, ethyl acetate, methanol, ethanol, isopropanol, and hexanes. $\text{Li}_2\text{B}_{12}\text{Cl}_{12}$ was insoluble in all solvents except ethyl acetate where partial solubility was observed (See Section VI). $\text{Li}_2\text{B}_{12}\text{Cl}_9(\text{OH})_3$ was insoluble in all solvents except ethyl acetate, ethanol and isopropanol where partial solubility was observed (See Section VI). The enhanced solubility could be a result of hydrogen bonding facilitated by hydroxylation of the cluster. In contrast to both $\text{Li}_2\text{B}_{12}\text{Cl}_{12}$ and $\text{Li}_2\text{B}_{12}\text{Cl}_9(\text{OH})_3$, $\text{Li}_2\text{B}_{12}\text{Cl}_9(\text{OCH}_3)_3$ was found to be insoluble only in hexanes (See Section VI). In all other solvents, partial or full solubility was observed indicating methylation affords significant enhancement to anion solubility which could be due to both enhanced intermolecular interactions (Van Der Waals and hydrogen bonding) as well as alterations to the polarity of the cluster. Computational modeling will be conducted in future studies in order to better understand the impact of mixed hydroxylation and halogenation upon solubility.

Conclusion and Outlook

In conclusion, we present a series of $[\text{B}_{12}\text{X}_9(\text{OR})_3]^{2-}$ ($\text{X} = \text{Br}, \text{Cl}$ and $\text{R} = \text{H}, \text{CH}_3$) WCAs from a mixed hydroxylation and halogenation strategy. We present a facile method for chlorination utilizing sodium hypochlorite which enhances the usability and safety of the reaction by eliminating the need for a chlorine gas tank or highly corrosive SOCl_2 .^{25,26} This developed procedure was amenable to both mixed halogenation as well as perhalogenation, suggesting a wide array of dodecaborate substrates could be modified. Importantly, kilogram-scale chlorination was demonstrated, suggesting these reaction conditions could be synthesized at industrially quantities. Coordination of all anions to both TBA^+ and Li^+ is demonstrated and thermogravimetric analysis of $\text{Li}_2\text{B}_{12}\text{X}_9(\text{OR})_3$ salts was conducted. A reduced thermal stability was observed for both $\text{Li}_2\text{B}_{12}\text{Cl}_9(\text{OH})_3$ and $\text{Li}_2\text{B}_{12}\text{Br}_9(\text{OH})_3$ when compared to the perhalogenated analogues; however, both salts were stable up to exceptionally high temperatures (~ 500 °C). Onset of decomposition within $\text{Li}_2\text{B}_{12}\text{Cl}_9(\text{OCH}_3)_3$ and $\text{Li}_2\text{B}_{12}\text{Br}_9(\text{OCH}_3)_3$ salts was observed at ~ 250 °C highlighting the impact enhanced organic character imparts upon anion stability. Finally, we conducted a preliminary assessment of the solubility of $\text{Li}_2\text{B}_{12}\text{Cl}_{12}$, $\text{Li}_2\text{B}_{12}\text{Cl}_9(\text{OH})_3$ and $\text{Li}_2\text{B}_{12}\text{Cl}_9(\text{OCH}_3)_3$ in selected solvents. The least soluble salt was $\text{Li}_2\text{B}_{12}\text{Cl}_{12}$ followed by $\text{Li}_2\text{B}_{12}\text{Cl}_9(\text{OH})_3$ and then $\text{Li}_2\text{B}_{12}\text{Cl}_9(\text{OCH}_3)_3$, suggesting the proposed strategy was effective at enhancing anion solubility. Computational modeling will be conducted to provide more insights into the nature of this enhancement and inform design of new salts. Overall, a promising platform for modification of the physical properties of halogenated dodecaborate anions is presented and could lead to interesting applications in battery materials, ionic liquids and catalysis.

References

1. (a) Krossing, I. & Raabe, I. Noncoordinating Anions- Fact or Fiction? A Survey of Likely Candidates. *Angew. Chem. Int. Ed.* **2004**, *43*, 2066-2090. (b) Riddlestone, I. M.; Kraft, A.; Schaefer, J.; Krossing, I. Taming the Cationic Beast: Novel Developments in the Synthesis and Application of Weakly Coordinating Anions. *Angew. Chem. Int. Ed.* **2018**, *57*, 13982-14024. (c) Strauss, S. H. The Search for Larger and More Weakly Coordinating Anions. *Chem. Rev.* **1993**, *93*, 927-942.
2. Williams, J. L. R.; Doty, J. C.; Grisdale, P. J.; Regan, T. H.; Borden, D. G. Boron Photochemistry: 1-Phenylcyclohexa-1,4-diene from Sodium Tetraphenylborate. *Chem. Commun.* **1967**, *3*, 109.
3. Post, G. B.; Gleason, J. A.; Cooper, K. R. Key scientific issues in developing drinking water guidelines for perfluoroalkyl acids: Contaminants of emerging concern. *PLOS Biology* **2017**, *15*, e2002855.
4. Lilienthal, H.; Dieter, H. H.; Hölzer, J.; Wilhelm, M. Recent experimental results of effects of perfluoroalkyl substances in laboratory animals – Relation to current regulations and guidance values. *Int. J. Hyg. Environ. Health* **2017**, *220*, 766–775.
5. Rupp, A. B. A. & Krossing, I. Ionic Liquids with Weakly Coordinating $[M^{III}(OR^F)_4]^-$ Anions. *Acc. Chem. Res.* **2015**, *48*, 2537-2546.
6. Metz, M. V.; Sun, Y.; Stern, C. L.; Marks, T. J. Weakly Coordinating Al-, Nb-, Ta-, Y-, and La-Based Perfluoroaryloxymetalate Anions as Cocatalyst Components for Single-Site Olefin Polymerization. *Organomet.* **2002**, *21*, 3691-3702.

7. Sun, Y.; Metz, M. V.; Stern, C. L.; Marks, T. J. Perfluoroaryloxy Anions as Cocatalysts for Metallocene-Mediated Ziegler–Natta Olefin Polymerization. *Organomet.* **2000**, *19*, 1625-1627.
8. Barbarich, T. J.; Handy, S. T.; Miller, S. M.; Anderson, O. P.; Grieco, P. A.; Strauss, S. H. $\text{LiAl}(\text{OC}(\text{Ph})(\text{CF}_3)_2)_4$: A Hydrocarbon-Soluble Catalyst for Carbon–Carbon Bond-Forming Reactions. *Organomet.* **1996**, *15*, 3776–3778.
9. Krossing, I. The facile Preparation of Weakly Coordinating Anions: Structure and Characterisation of Silverpolyfluoroalkoxyaluminates $\text{AgAl}(\text{OR}_F)_4$, Calculation of the Alkoxide Ion Affinity. *Chem.* **2001**, *7*, 490-502.
10. Knoth, W. H. Chemistry of Boranes. XXVI.¹ Inner Diazonium Salts $1,10\text{-B}_{10}\text{H}_8(\text{N}_2)_2^-$, $\text{B}_{10}\text{Cl}_8(\text{N}_2)_2^-$, and $\text{B}_{10}\text{I}_8(\text{N}_2)_2^-$. *J. Am. Chem. Soc.* **1966**, *88*, 935-939.
11. Knoth, W. H. $1\text{-B}_9\text{H}_9\text{CH}^-$ and $\text{B}_{11}\text{H}_{11}\text{CH}^-$. *J. Am. Chem. Soc.* **1967**, *89*, 1274-1275.
12. Shelly, K.; Finster, D. C.; Lee, Y. J.; Scheidt, W. R.; Reed, C. A. (1985). η^1 -Benzene coordination: the synthesis and x-ray crystal structure of a novel silver salt of the weakly coordinating carborane anion $\text{B}_{11}\text{CH}_{12}^-$. *J. Am. Chem. Soc.* **1985**, *107*, 5955–5959.
13. Liston, D. J.; Lee, Y. J.; Scheidt, W. R.; Reed, C. A. Observations on silver salt metathesis reactions with very weakly coordinating anions. *J. Am. Chem. Soc.* **1989**, *111*, 6643–6648.
14. Plešek, J.; Jelínek, T.; Drdáková, E.; Heřmánek, S.; Štíbr, B. A Convenient Preparation of $1\text{-CB}_{11}\text{H}_{12}^-$ and its C-amino Derivatives. *Collect. of Czech. Chem. Commun.* **1984**, *49*, 1559–1562.
15. Reed, C. A. Carboranes: A New Class of Weakly Coordinating Anions for Strong Electrophiles, Oxidants and Superacids. *Acc. Chem. Res.* **1998**, *31*, 133-139.

16. Shelly, K.; Lee, Y. J.; Scheidt, W. R.; Reed, C. A. The least coordinating anion. *J. Am. Chem. Soc.* **1986**, *108*, 3117–3118.
17. Xie, Z.; Manning, J.; Reed, R. W.; Mathur, R.; Boyd, P. D. W.; Benesi, A.; Reed, C. A. Approaching the Silylium (R_3Si^+) Ion: Trends with Hexahalo (Cl, Br, I) Carboranes as Counterions. *J. Am. Chem. Soc.* **1996**, *118*, 2922-2928.
18. Jelínek, T.; Plešek, J.; Heřmánek, S.; Štíbr, B. Chemistry of Compounds with the 1-Carba-closo-dodecaborane(12) Framework. *Collect. of Czech. Chem. Commun.* **1986**, *51*, 819-829.
19. (a) Pitochelli, A. R. & Hawthorne, M. F. The Isolation of the Icosahedral $B_{12}H_{12}^{-2}$ Ion. *J. Am. Chem. Soc.* **1960**, *82*, 3228-3229. (b) Miller, H. C.; Muetterties, E. L.; Boone, J. L.; Garrett, P.; Hawthorne, M. F. Borane Anions. In *Inorganic Syntheses*; McGraw-Hill, Inc., 1967; pp 81-91.
20. Zakharova, I. A. Closoborate Anions as a Means of Synthesizing New Coordination Compounds. *Coord. Chem. Rev.* **1982**, *43*, 313-324.
21. Ivanov, S. V.; Miller, S. M.; Anderson, O. P.; Solntsev, K.A; Strauss, S. H. Synthesis and Stability of Reactive Salts of Dodecafluoro-closo-dodecaborate(2-). *J. Am. Chem. Soc.* **2003**, *125*, 4694-4695.
22. Avelar, A.; Tham, F. S.; Reed, C. A. Superacidity of Boron Acids $H_2(B_{12}X_{12})$ (X= Cl, Br). *Angew. Chem. Int. Ed.* **2009**, *48*, 3491-3493.
23. Knoth, W. H.; Sauer, J. C.; England, D. C.; Hertler, W. R.; Muetterties, E. L. Chemistry of Boranes. XIX.¹ Derivative Chemistry of $B_{10}H_{10}^{-2}$ and $B_{12}H_{12}^{-2}$. *J. Am. Chem. Soc.* **1964**, *86*, 3973-3983.

24. Peymann, T.; Knobler, C. B.; Hawthorne, M. F. A Study of the Sequential Acid-Catalyzed Hydroxylation of Dodecahydro-*closo*-dodecaborate(2-). *Inorg. Chem.* **2000**, *39*, 1163-1170.
25. (a) Knoth, W. H.; Miller, H. C.; Sauer, J. C.; Balthis, J. H.; Chia, Y. T.; Muetterties, E. L. Chemistry of Boranes. IX.¹ Halogenation of B₁₀H₁₀⁻² and B₁₂H₁₂⁻². *Inorg. Chem.* **1964**, *3*, 159-167. (b) Geis, V.; Guttsche, K.; Knapp, C.; Scherer, H.; Uzun, R. Synthesis and Characterization of Synthetically Useful Salts of the Weakly-Coordinating Dianion [B₁₂Cl₁₂]²⁻. *Dalton Trans.* **2009**, *15*, 2649-2884.
26. Gu, W. & Ozerov, O. V. Exhaustive Chlorination of [B₁₂H₁₂]²⁻ without Chlorine Gas and the Use of [B₁₂Cl₁₂]²⁻ as a Supporting Anion in Catalytic Hydrodefluorination of Aliphatic C-F Bonds *Inorg. Chem.* **2011**, *50*, 2726-2728.
27. Kelly, H. C.; Yasui, S. C.; Twiss-Brooks, A. B. Hypochlorite Chlorination of Tertiary Amine-Boranes. *Inorg. Chem.* **1984**, *23*, 2220-2223.
28. Maderna, A.; Knobler, C. B.; Hawthorne, M. F. Twelfefold Functionalization of an Icosahedral Surface by Total Esterification of [B₁₂(OH)₁₂]²⁻: 12(12)-Closomers. *Angew. Chem. Int. Ed.* **2001**, *40*, 1661-1664.
29. Fang, Z.; Zhou, G.-C.; Zheng, S.-L.; He, G.-L.; Li, J.-L.; He, L.; Bei, D. Lithium chloride-catalyzed selective demethylation of aryl methyl ethers under microwave irradiation. *J. Mol. Catal. A Chem.* **2007**, *274*, 16.
30. Tiritiris, I., & Schleid, T. The crystal structures of the Dicaesium dodecahalogeno-*closo*-dodecaborates Cs₂[B₁₂X₁₂] (X = Cl, Br, I) and their hydrates. *Z. Anorg. Allg. Chem.* **2004**, *630*, 1555–1563.

Supporting Information

I. Materials and Methods

Materials:

All reagents were purchased from Sigma Aldrich, Strem Chemicals, ChemImpex, Oakwood Chemicals, TCI, Fisher Scientific, Carbosynth, Combi-Blocks, or Alfa Aesar, and used as received unless otherwise noted. Solvents (methanol (MeOH), acetone, acetonitrile (ACN), dichloromethane (DCM), dimethoxyethane (DME) and diethyl ether (Et₂O), were used as received without further purification unless otherwise specified. Milli-Q water was used for all experiments. Deuterated solvents (CDCl₃, and D₂O) were obtained from Cambridge Isotope Laboratories and used as received.

Methods:

NMR

All NMR spectra were obtained on a Bruker Avance 400 or a Bruker DRX 500 MHz broad band FT NMR spectrometer. ¹H NMR and ¹³C{¹H} NMR spectra were referenced to residual protio-solvent signals, and both ¹¹B and ¹¹B{¹H} chemical shifts were referenced to BF₃•Et₂O (15% in CDCl₃, δ 0.0 ppm).

TGA

Thermogravimetric analyses were performed on a PerkinElmer Pyris Diamond TG/DTA under a constant flow of Argon (200 mL/min). Samples were heated in ceramic trays (5 mm) from 60 °C to 1000 °C at 10 °C/min.

II. Synthesis

Synthesis of TBA₂B₁₂Cl₁₂:

Cs₂B₁₂H₁₂ (2.0 g, 5.0 mmol) and a dry stir bar were added to a clean, dry round bottom flask (250.0 mL). Under vigorous stirring, hydrochloric acid (3 M) was added dropwise using an addition funnel (60.0 mL). Excess sodium hypochlorite (40.0 mL, 6%) was slowly added to the round bottom via addition funnel (all joints were heavily greased and fitted with parafilm to trap any evolved gas) and the contents were stirred heavily. The sealed reaction was allowed to proceed at room temperature for 2 hrs. After, the round bottom was heated to 60 °C for 24 hrs. Unreacted chlorine was quenched with sodium sulfite until the reaction liquid was clear. Excess (2.2 equivalents per cluster) tetrabutylammonium bromide (TBA-Br) was dissolved in minimal water and added drop-wise to the reaction mixture. A white powder precipitated from solution and was collected via vacuum filtration. After 3 washes with water (10.0 mL), the product was collected and recrystallized from hot ethanol. **Note:** Conversion was monitored by ¹¹B NMR spectroscopy and ESI-MS(-).

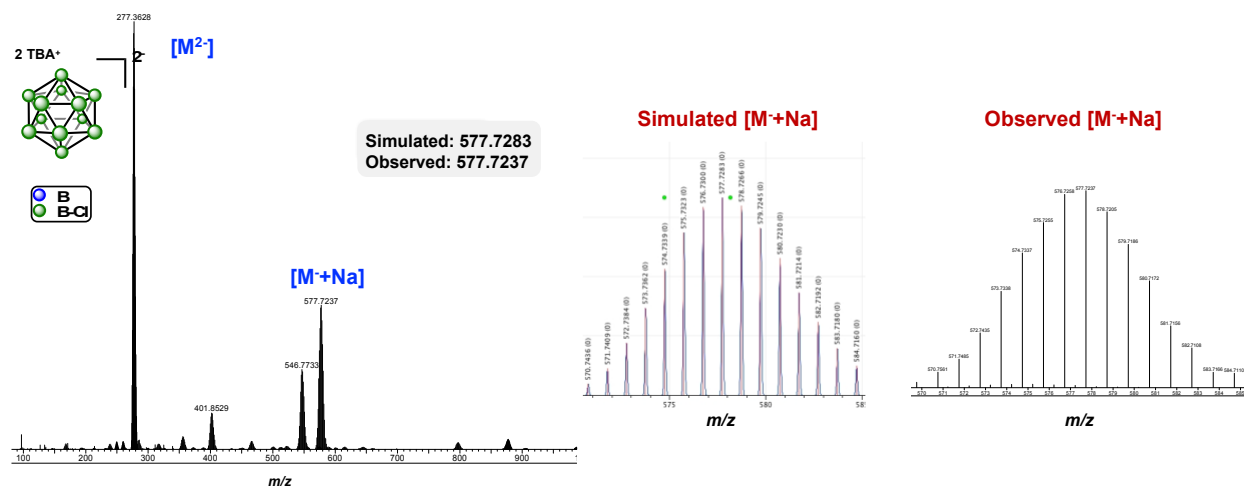


Figure S3.1: The negative mode ESI(-) mass profile of TBA₂B₁₂Cl₁₂.

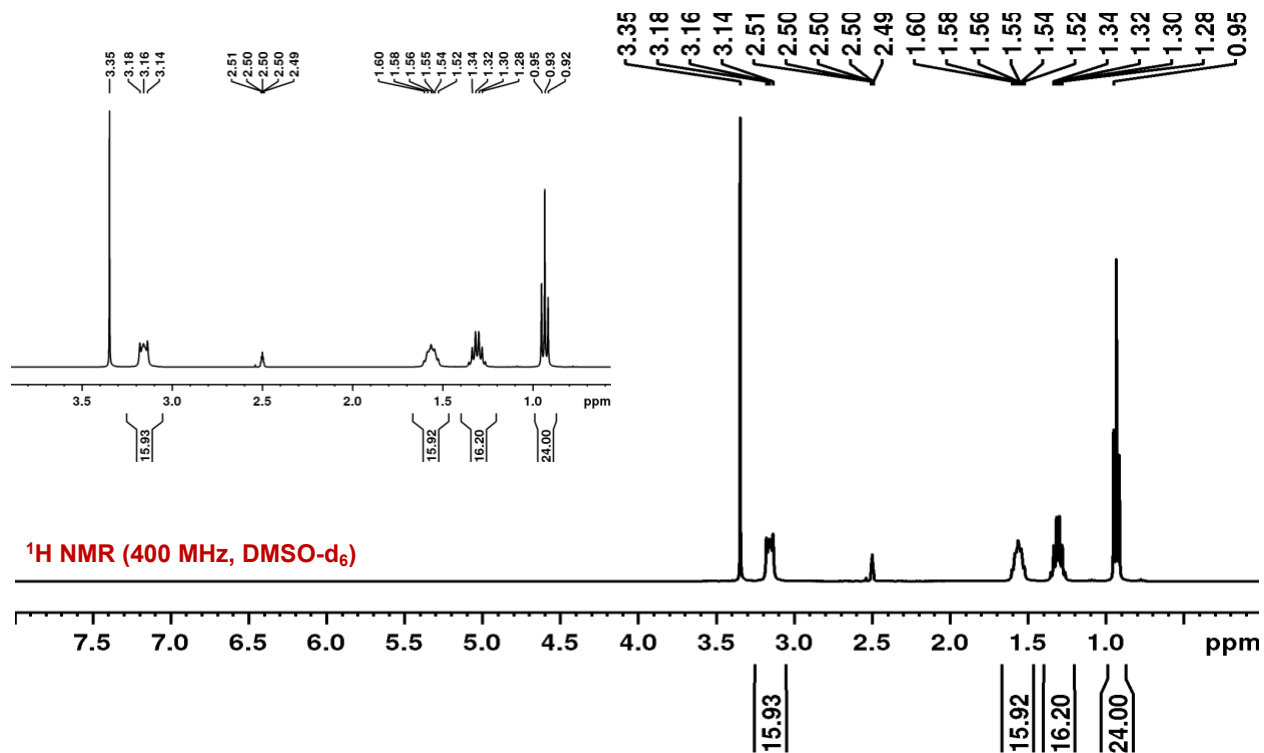


Figure S3.2: The ^1H NMR spectrum of $\text{TBA}_2\text{B}_{12}\text{Cl}_{12}$. Four multiplets are observed as consistent with the splitting pattern and integral ratio of the TBA cation.

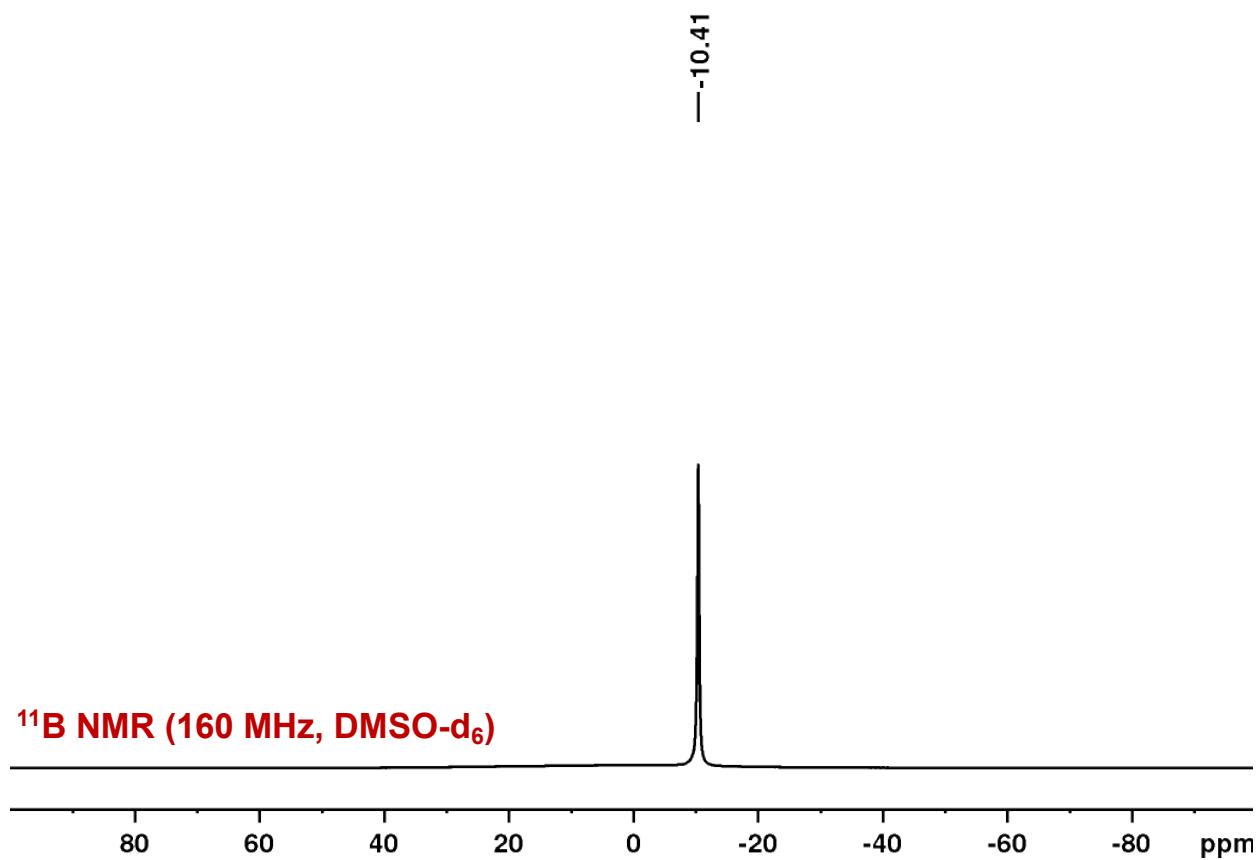


Figure S3.3: The ^{11}B NMR spectrum of $\text{TBA}_2\text{B}_{12}\text{Cl}_{12}$ with a singlet resonance consistent with perhalogenation of the cluster.

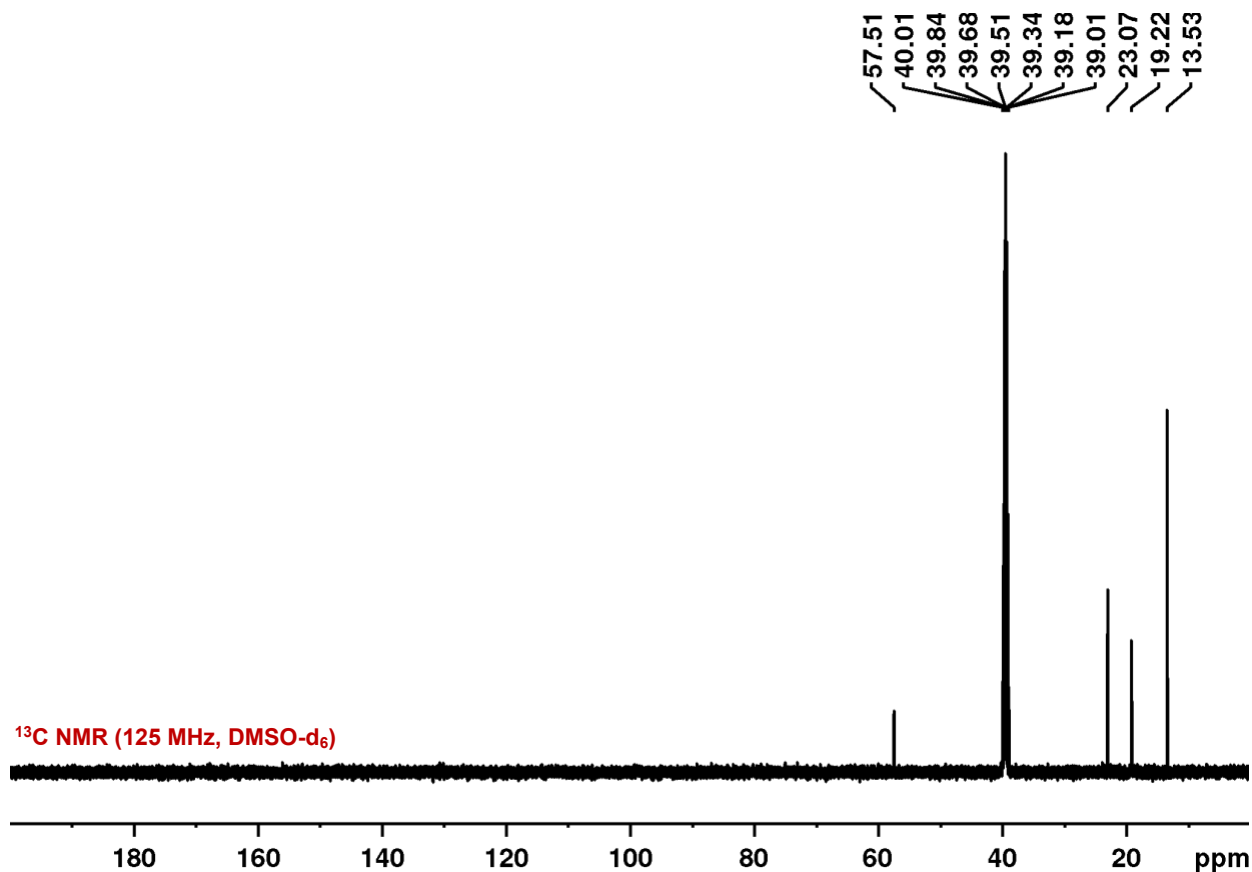


Figure S3.4: The ¹³C NMR spectrum of TBA₂B₁₂Cl₁₂ where all resonances are consistent with the splitting pattern and integral ratio of the TBA cation.

Synthesis of TBA₂B₁₂Cl₉(OH)₃:

Cs₂B₁₂H₁₂ (6.0 g, 15.0 mmol) and a dry stir bar were added to a clean, dry round bottom flask (300.0 mL) and the flask was placed into an ice bath. Under vigorous stirring, diluted sulfuric acid was added dropwise using an addition funnel (120.0 mL, 53% v/v). The round bottom flask was moved to an oil bath and fitted with a reflux condenser. The bath was heated to 110°C and the reaction was allowed to reflux for 20 hrs. After allowing the reaction to cool to room temperature after hydroxylation, the reflux condenser was removed and an addition funnel was fitted onto the round bottom flask. All joints were heavily greased and a stopper was placed on top of addition funnel to avoid any gas release. Additionally, parafilm was placed over all joints. Excess sodium

hypochlorite (120.0 mL, 6%) was slowly added to the round bottom via addition funnel while the contents were stirred heavily. The reaction was allowed to proceed at room temperature for 2 hrs. After, the round bottom was heated to 60 °C for 24 hrs. Unreacted chlorine was quenched with sodium sulfite until the reaction liquid was clear. Excess (2.2 equivalents per cluster) tetrabutylammonium bromide (TBA-Br) was dissolved in minimal water and added drop-wise to the reaction mixture. A white powder precipitated from solution and was collected via vacuum filtration. After 3 washes with water (10.0 mL), the product was collected and recrystallized from hot ethanol. **Note:** Conversion was monitored by ^{11}B NMR spectroscopy and ESI-MS(-).

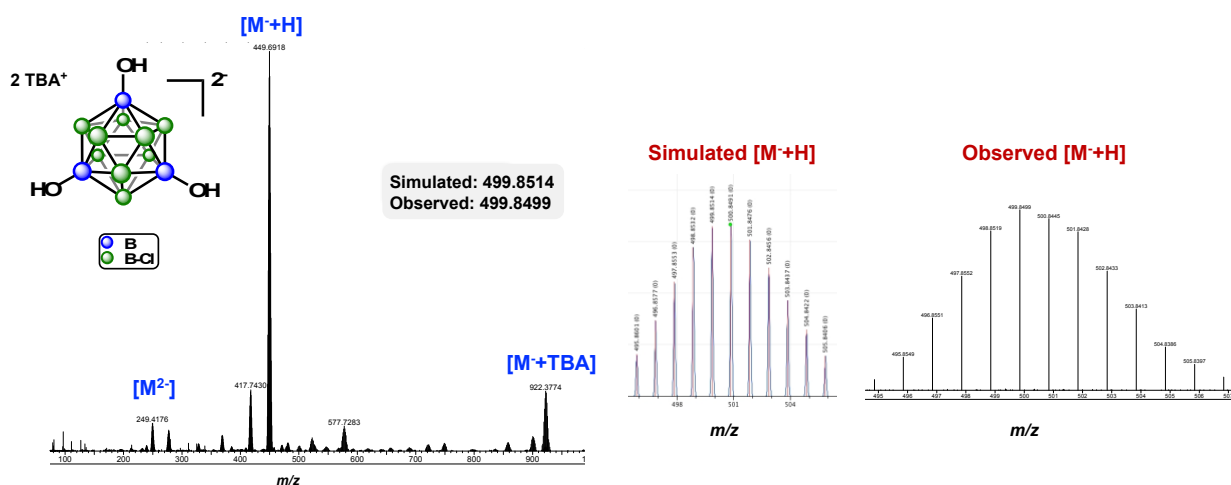


Figure S3.5: The negative mode ESI(-) mass profile of $\text{TBA}_2\text{B}_{12}\text{Cl}_9(\text{OH})_3$.

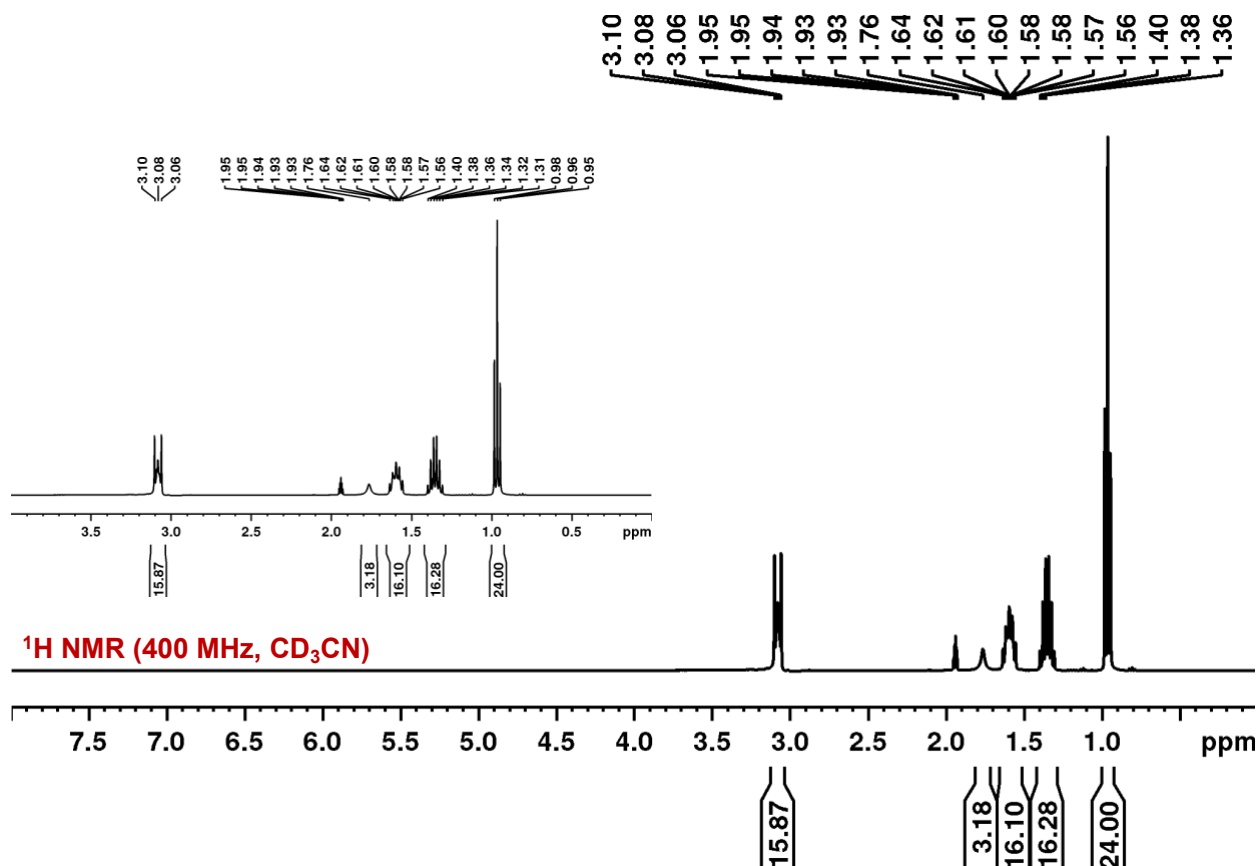


Figure S3.6: The ¹H NMR spectrum of TBA₂B₁₂Cl₉(OH)₃. Four multiplets are observed as consistent with the splitting pattern and integral ratio of the TBA cation. In addition, a singlet corresponding to the hydroxyl ¹H atoms is observed.

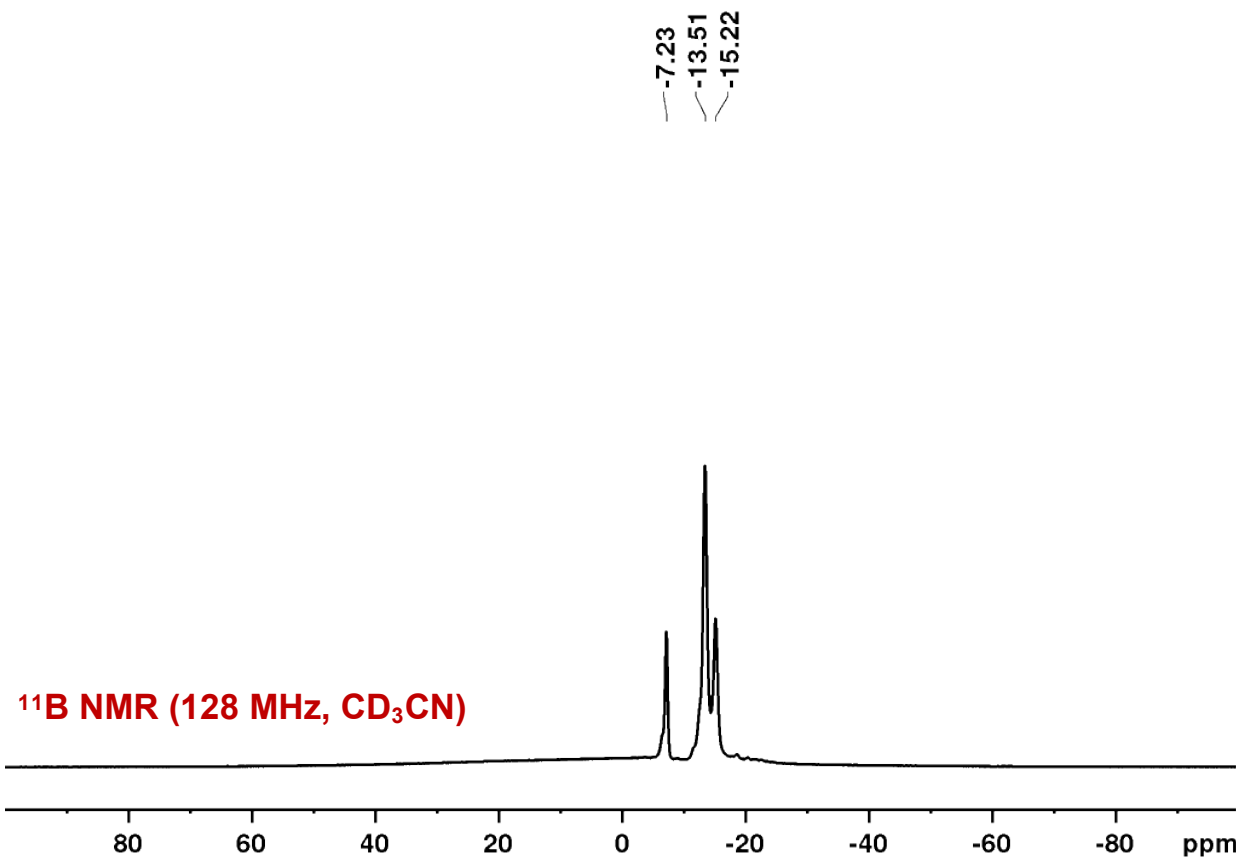


Figure S3.7: The ¹¹B NMR spectrum of TBA₂B₁₂Cl₉(OH)₃ with a resonance at -7.2 ppm ascribed to the B-O bonds and overlapping resonances at -13.5 ppm and -15.2 ppm corresponding to the B-Cl bonds.

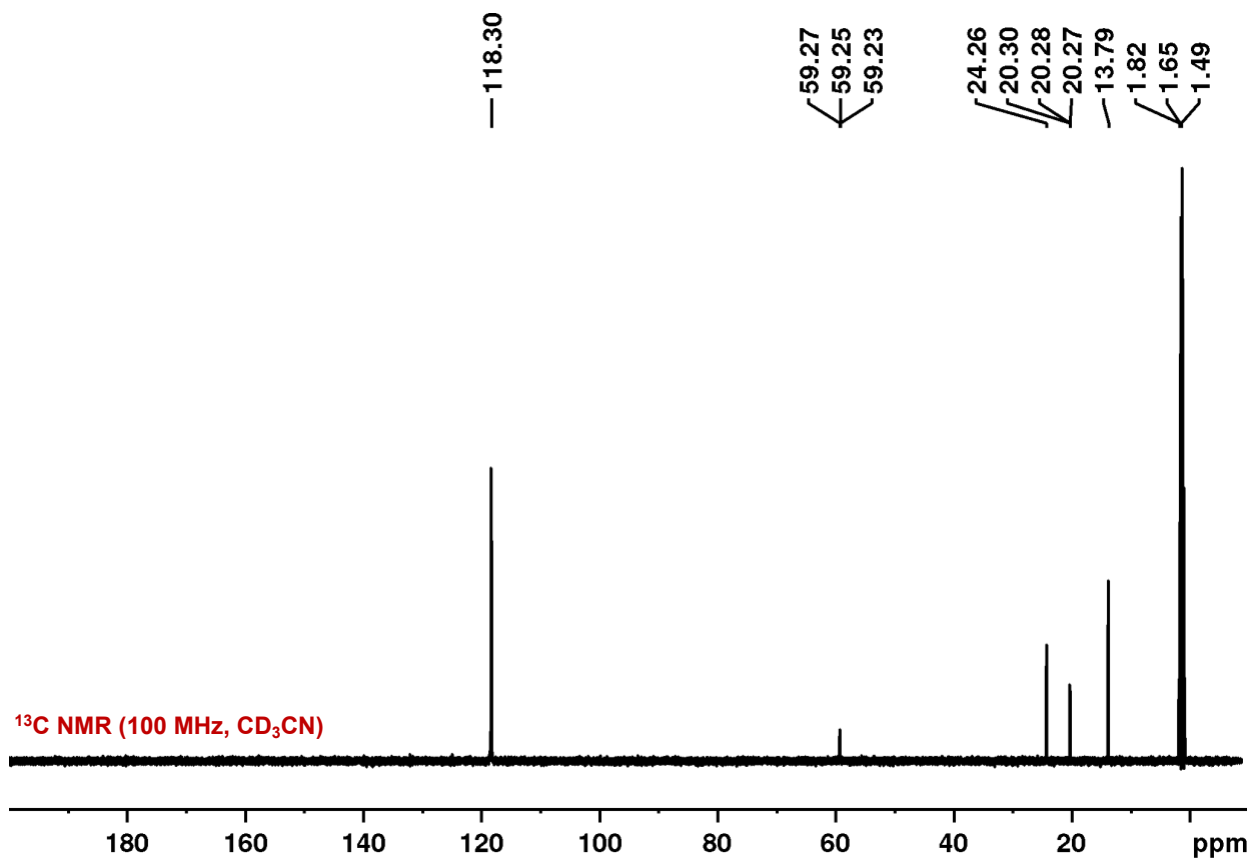


Figure S3.8: The ¹³C NMR spectrum of TBA₂B₁₂Cl₉(OH)₃ where all resonances are consistent with the splitting pattern and integral ratio of the TBA cation.

Synthesis of TBA₂B₁₂Cl₉(OCH₃)₃:

TBA₂B₁₂Cl₉(OH)₃ (2.0 g, 2.0 mmol) and a dry stir bar were placed into a dry Schlenk flask (50.0 mL) and transferred into a nitrogen filled glovebox. Sodium hydride (NaH, 0.5 g, 20.0 mmol) and DME (10.0 mL) were added to the flask and it was sealed and transferred out of the glovebox. The flask was then removed from the glovebox and transferred to an oil bath. The oil bath was heated to 80 °C and methyl iodide (0.9 mL, 15.0 mmol) was slowly injected into the sealed flask under a flow of nitrogen. The reaction was allowed to proceed for 0.5 hrs. After, the reaction mixture was quenched with MeOH so that all NaH had reacted. The DME and MeOH were removed under

vacuum and the product was dissolved in DCM (10.0-15.0 mL) and passed through a silica plug. The filtrate was collected and dried under vacuum.

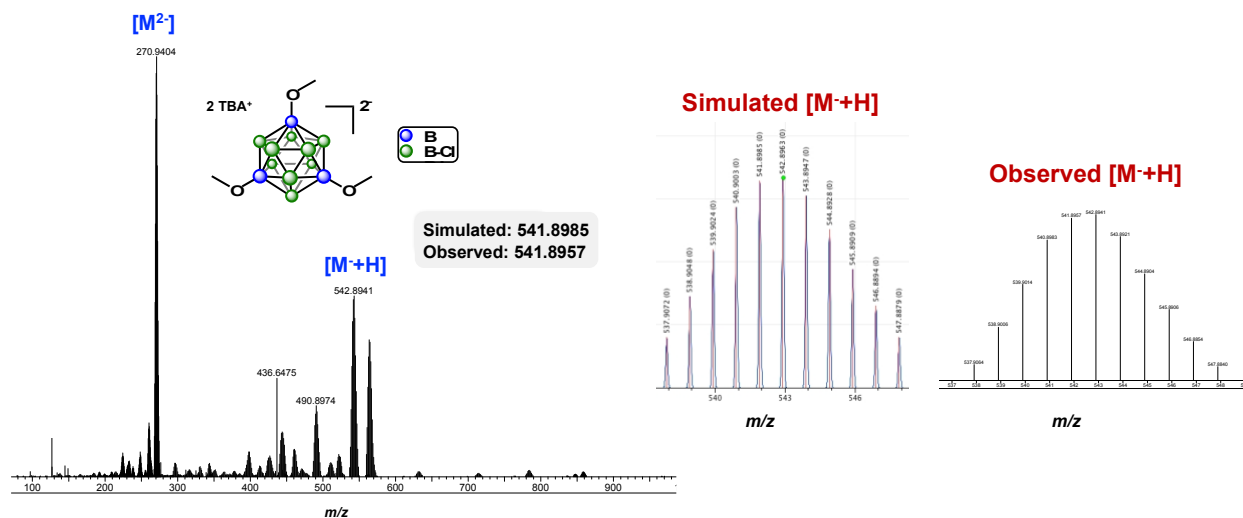


Figure S3.9: The negative mode ESI(-) mass profile of TBA₂B₁₂Cl₉(OCH₃)₃.

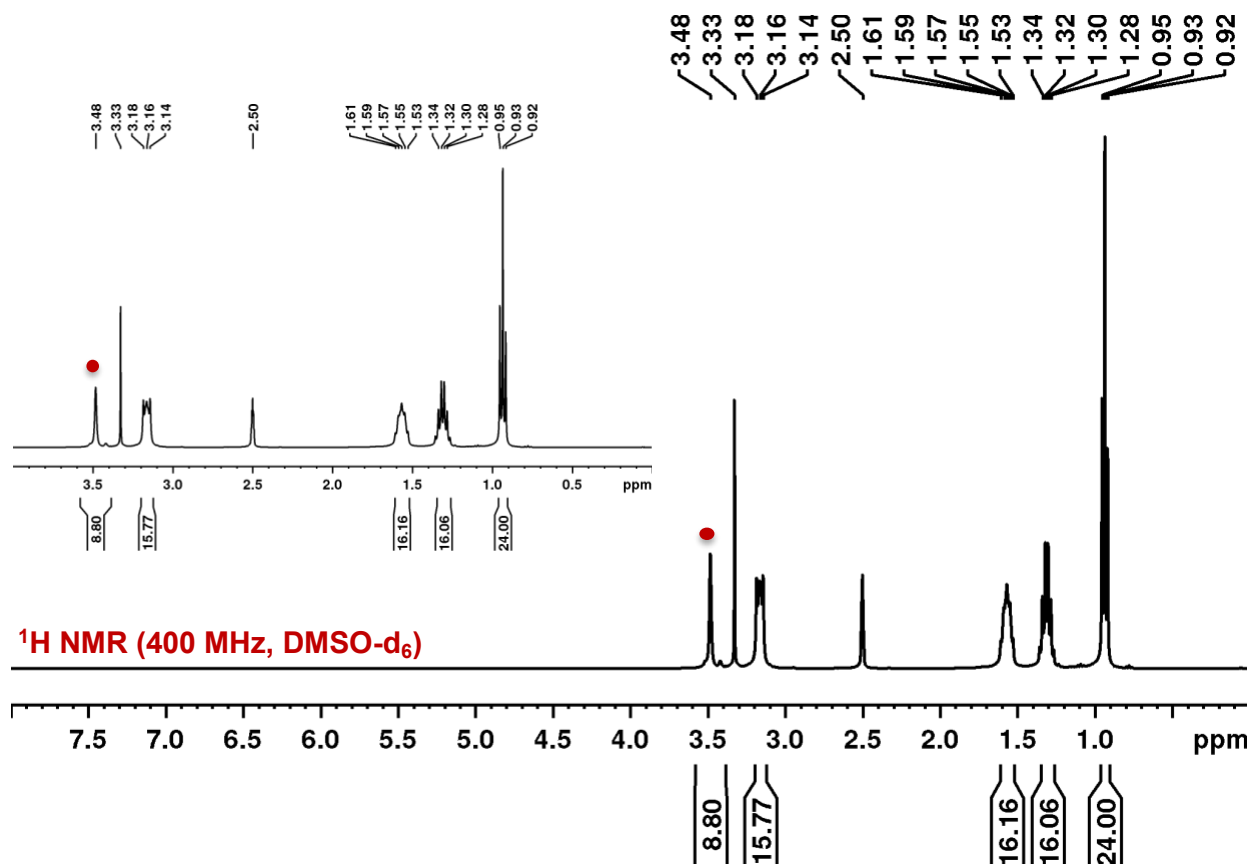


Figure S3.10: The ^1H NMR spectrum of $\text{TBA}_2\text{B}_{12}\text{Cl}_9(\text{OCH}_3)_3$. Four multiplets are observed as consistent with the splitting pattern and integral ratio of the TBA cation. In addition, a singlet denoted with a red dot is observed and corresponds to the methoxy ^1H .

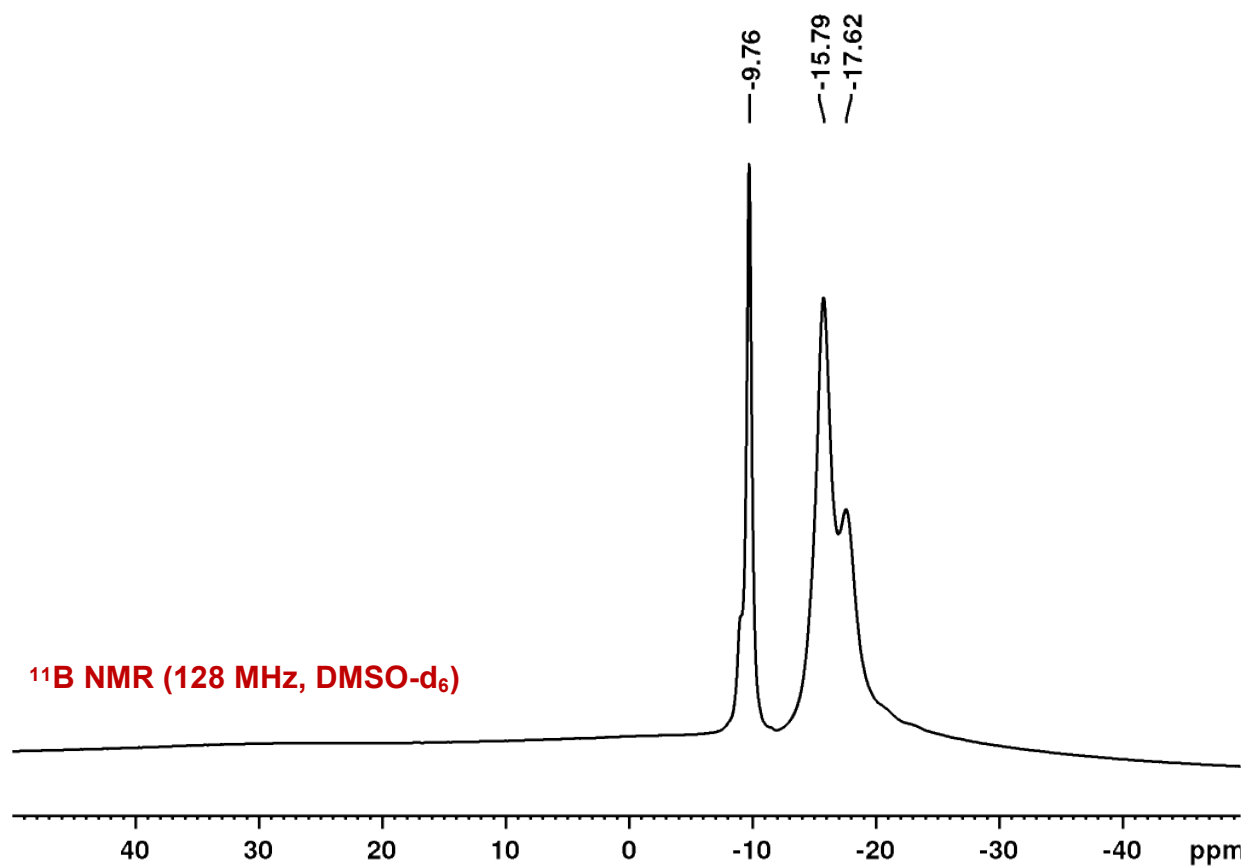


Figure S3.11: The ¹¹B NMR spectrum of TBA₂B₁₂Cl₉(OCH₃)₃ with a resonance at -9.8 ppm ascribed to the B-O bonds and overlapping resonances at -15.8 ppm and -17.6 ppm corresponding to the B-Cl bonds.

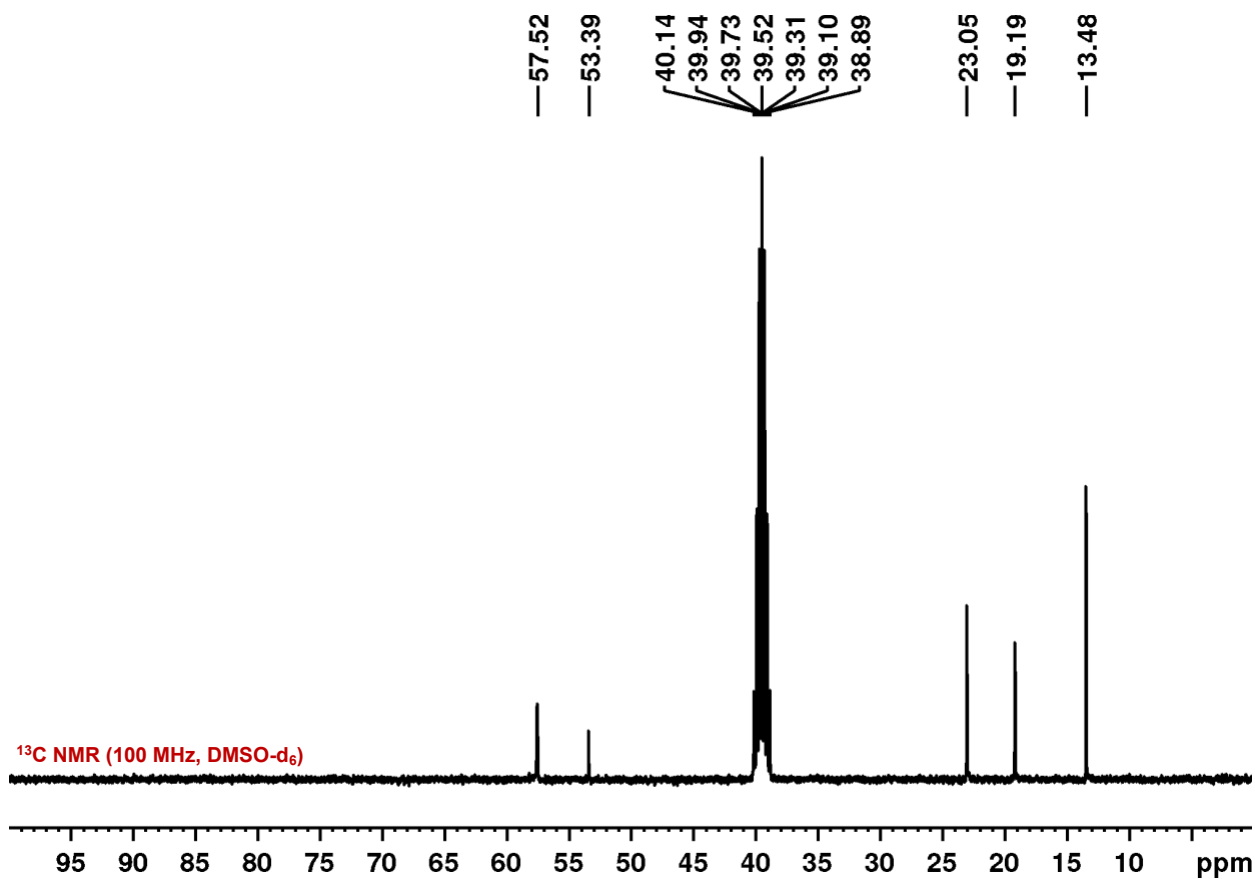


Figure S3.12: The ^{13}C NMR spectrum of $\text{TBA}_2\text{B}_{12}\text{Cl}_9(\text{OCH}_3)_3$ with four resonances that correspond to the TBA cation and a fifth resonance ascribed to the methoxy ^{13}C .

Synthesis of $\text{Cs}_2\text{B}_{12}\text{Br}_{12}$:

The procedure was adapted from Muetterties.²⁵ A solution of $\text{Cs}_2\text{B}_{12}\text{H}_{12}$ (2.0 g, 5.0 mmol) in 50 mL of aqueous methanol (50% v/v) was cooled to 5 °C. Under vigorous stirring 5.0 mL (187.5 mmol) of Br_2 were added dropwise. Once at room temperature the reaction was moved to an oil bath and fitted with a reflux condenser. An additional 5.0 mL of Br_2 were added and the reaction was allowed to reflux (90 °C) for 48 hrs. The solvent and unreacted Br_2 were removed in vacuo. The white powder was recrystallized from water overnight. The recrystallized product was then introduced to 50 mL of aqueous methanol (50% v/v) in a clean round bottom flask (250.0 mL). 5.0 mL of Br_2 were then added dropwise. The reaction was left under reflux (90 °C) for 24 hrs.

The solvent and excess Br₂ were removed in vacuo. The resulting white powder was recrystallized from water until full conversion was observed. Note: Conversion was monitored by ¹¹B NMR spectroscopy and ESI-MS(-). ¹H NMR and ¹³C NMR are omitted as no resonances were anticipated for this sample.

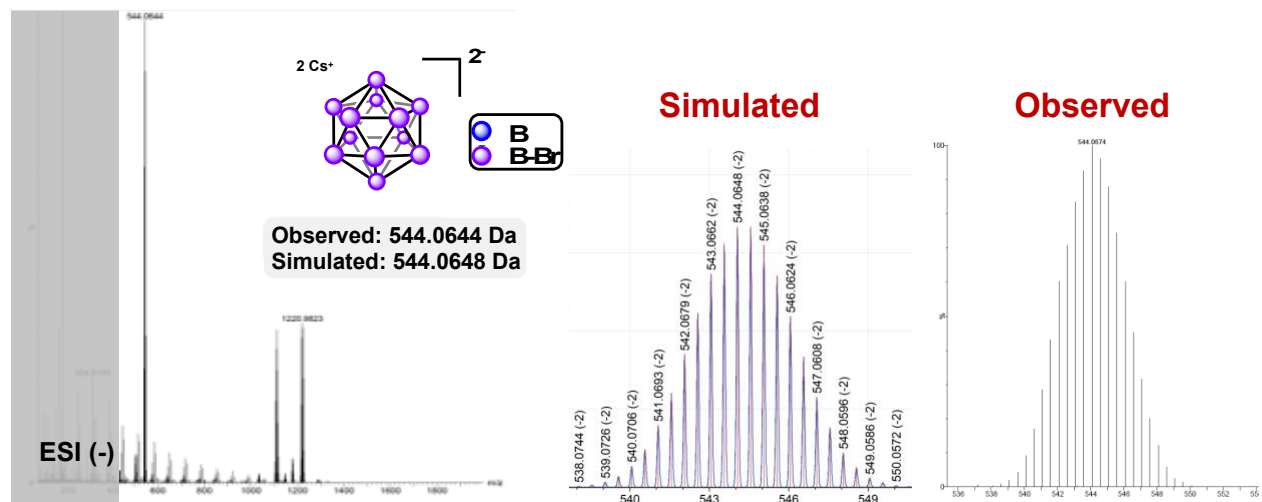


Figure S3.13: The negative mode ESI(-) mass profile of Cs₂B₁₂Br₁₂.

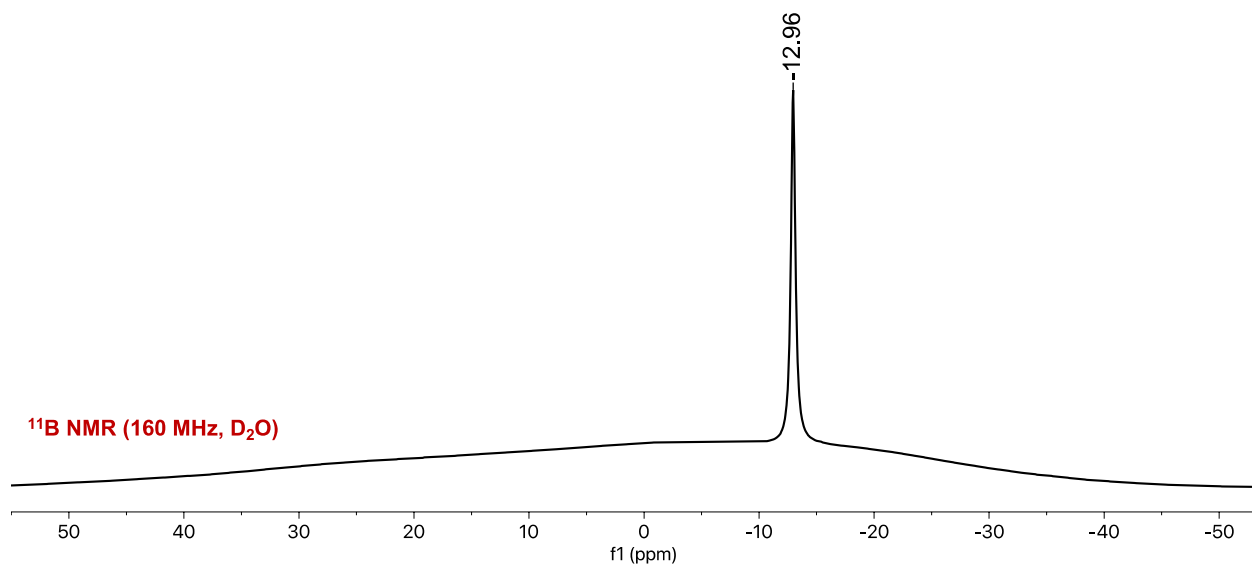


Figure S3.14: The negative mode ESI(-) mass profile of Cs₂B₁₂Br₁₂.

Synthesis of $\text{TBA}_2\text{B}_{12}\text{Br}_9(\text{OH})_3$:

$\text{Cs}_2\text{B}_{12}\text{H}_{12}$ (2.0 g, 5.0 mmol) and a dry stir bar were added to a clean, dry round bottom flask (250.0 mL) and the flask was placed into an ice bath. Under vigorous stirring, diluted sulfuric acid was added dropwise using an addition funnel (120 mL, 53% v/v). The round bottom flask was moved to an oil bath and fitted with a reflux condenser. The bath was heated to 110°C and the reaction was allowed to reflux for 20 hrs. After allowing the reaction to cool, the reaction was diluted with MeOH (120.0 mL) and the vessel was charged with bromine (5.0 mL). The reaction was again fitted with a reflux condenser and heated to 80°C for 48 hrs. Excess (2.2 equivalents per cluster) tetrabutylammonium bromide (TBA-Br) was dissolved in minimal water and added drop-wise to the reaction mixture. The precipitate was isolated by vacuum filtration and washed with water (10.0 mL x 3). After, the product was dried *in vacuo*.

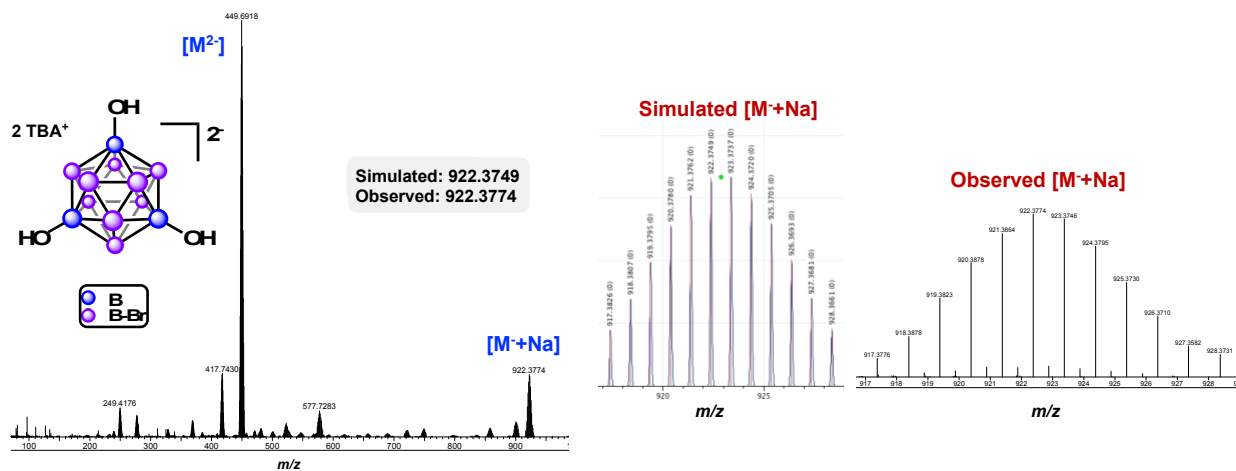


Figure S3.15: The negative mode ESI(-) mass profile of $\text{TBA}_2\text{B}_{12}\text{Br}_9(\text{OH})_3$.

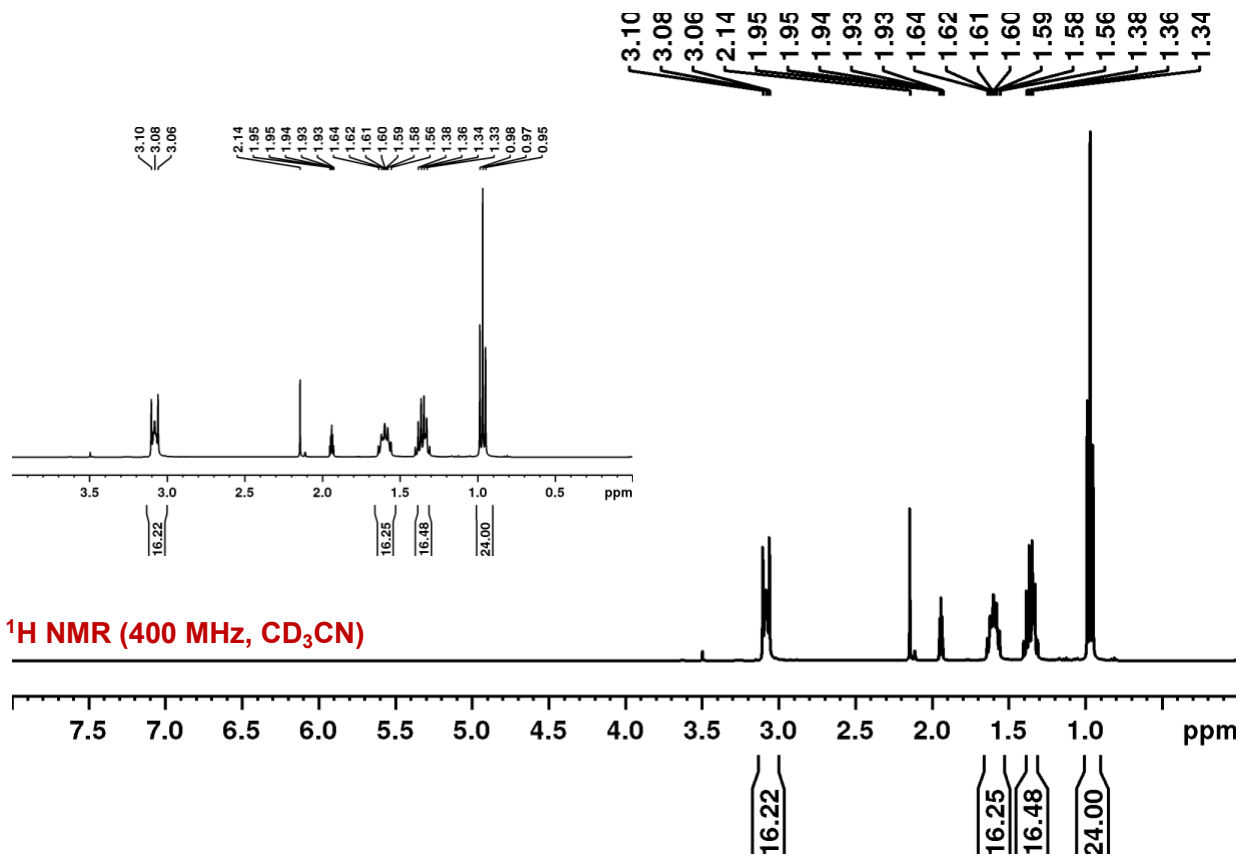


Figure S3.16: The ^1H NMR spectrum of $\text{TBA}_2\text{B}_{12}\text{Br}_9(\text{OH})_3$. Four multiplets are observed as consistent with the splitting pattern and integral ratio of the TBA cation.

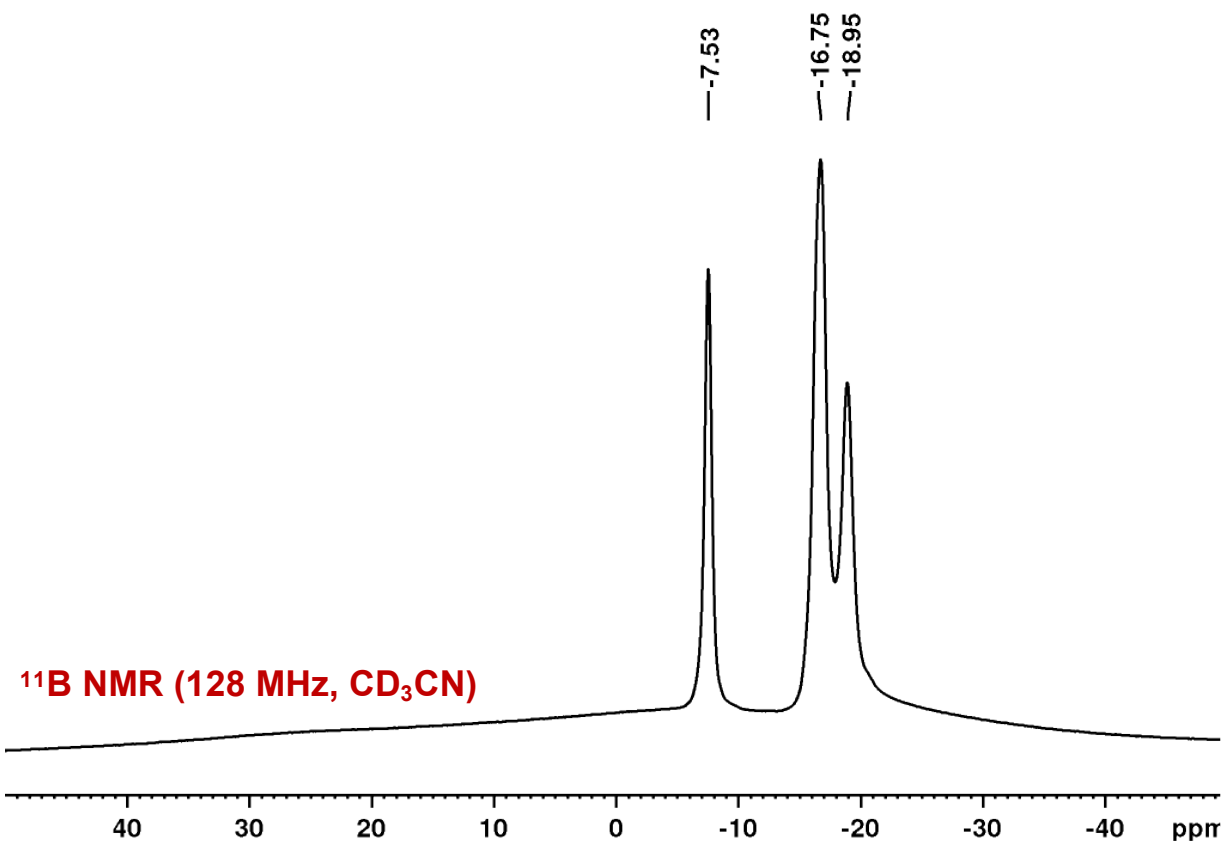


Figure S3.17: The ^{11}B NMR spectrum of $\text{TBA}_2\text{B}_{12}\text{Br}_9(\text{OH})_3$ with a resonance at -7.5 ppm ascribed to the B-O bonds and overlapping resonances at -16.8 ppm and -19.0 ppm corresponding to the B-Cl bonds.

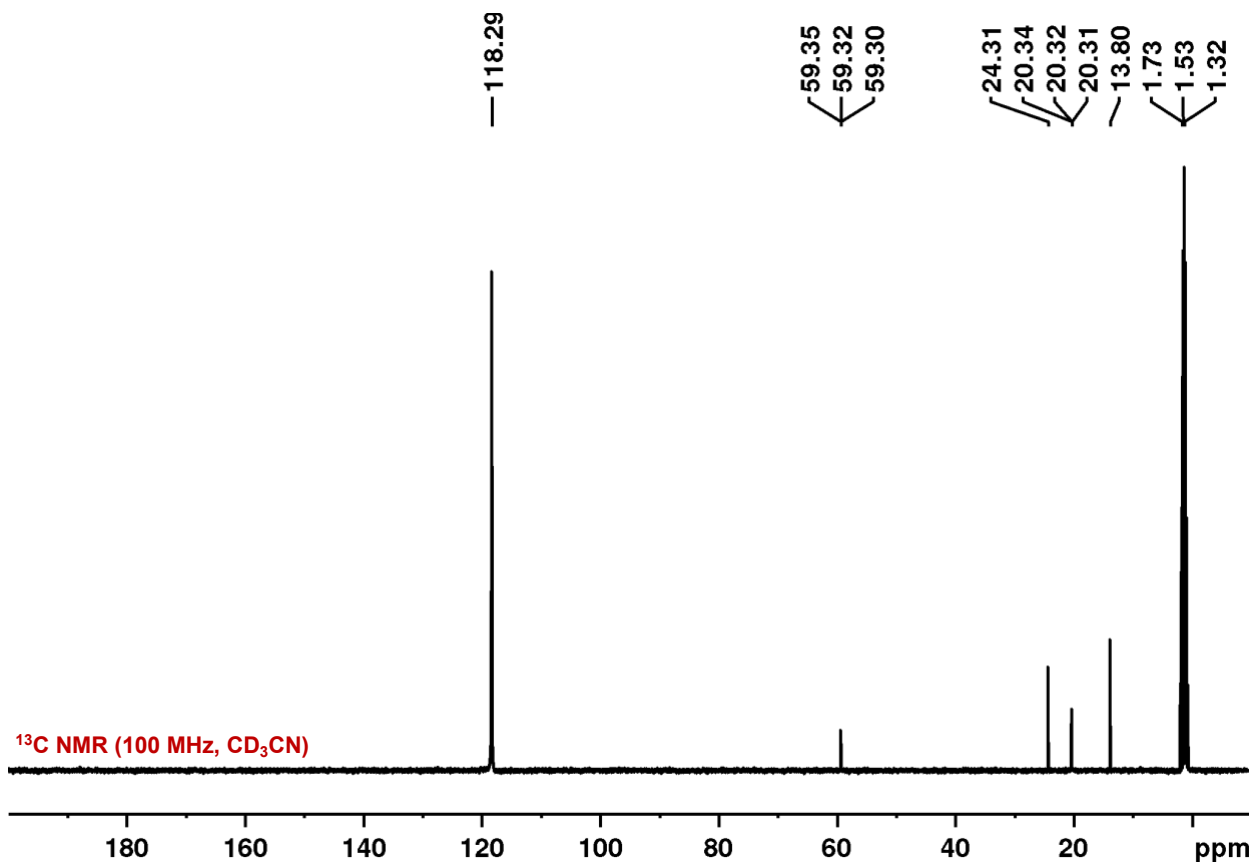


Figure S3.18: The ¹³C NMR spectrum of TBA₂B₁₂Br₉(OH)₃ where all resonances are consistent with the splitting pattern and integral ratio of the TBA cation.

Synthesis of TBA₂B₁₂Br₉(OCH₃)₃:

TBA₂B₁₂Br₉(OH)₃ (0.5 g, 0.35 mmol) and a dry stir bar were placed into a dry Schlenk flask (50.0 mL) and transferred into a nitrogen filled glovebox. Sodium hydride (NaH, 0.9 g, 3.5 mmol) and DME (10.0 mL) were added to the flask and it was sealed and transferred out of the glovebox. The flask was then removed from the glovebox and transferred to an oil bath. The oil bath was heated to 80 °C and methyl iodide (0.16 mL, 2.6 mmol) was slowly injected into the sealed flask under a flow of nitrogen. The reaction was allowed to proceed for 18 hrs. After, the reaction mixture was quenched with MeOH so that all NaH had reacted. The DME and MeOH were removed under

vacuum and the product was dissolved in DCM (10.0-15.0 mL) and passed through a silica plug. The filtrate was collected and dried under vacuum.

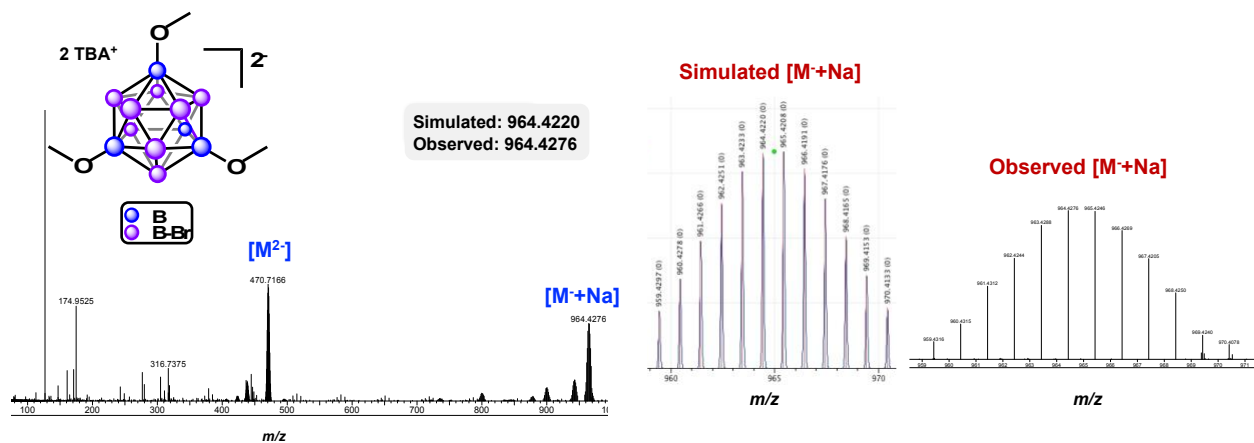


Figure S3.19: The negative mode ESI(-) mass profile of $\text{TBA}_2\text{B}_{12}\text{Br}_9(\text{OCH}_3)_3$.

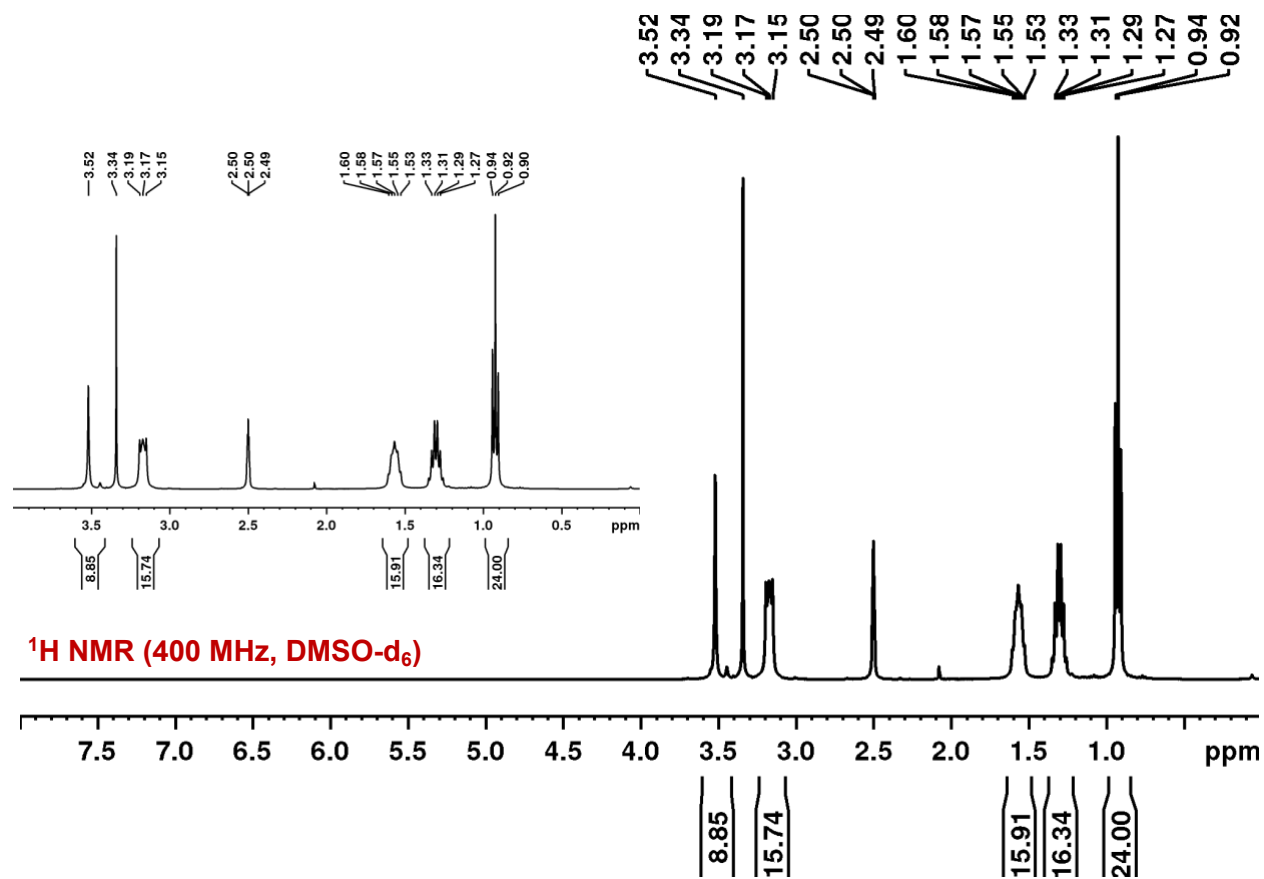


Figure S3.20: The ^1H NMR spectrum of $\text{TBA}_2\text{B}_{12}\text{Cl}_9(\text{OCH}_3)_3$. Four multiplets are observed as consistent with the splitting pattern and integral ratio of the TBA cation. In addition, a singlet at 3.5 ppm is observed and corresponds to the methoxy ^1H .

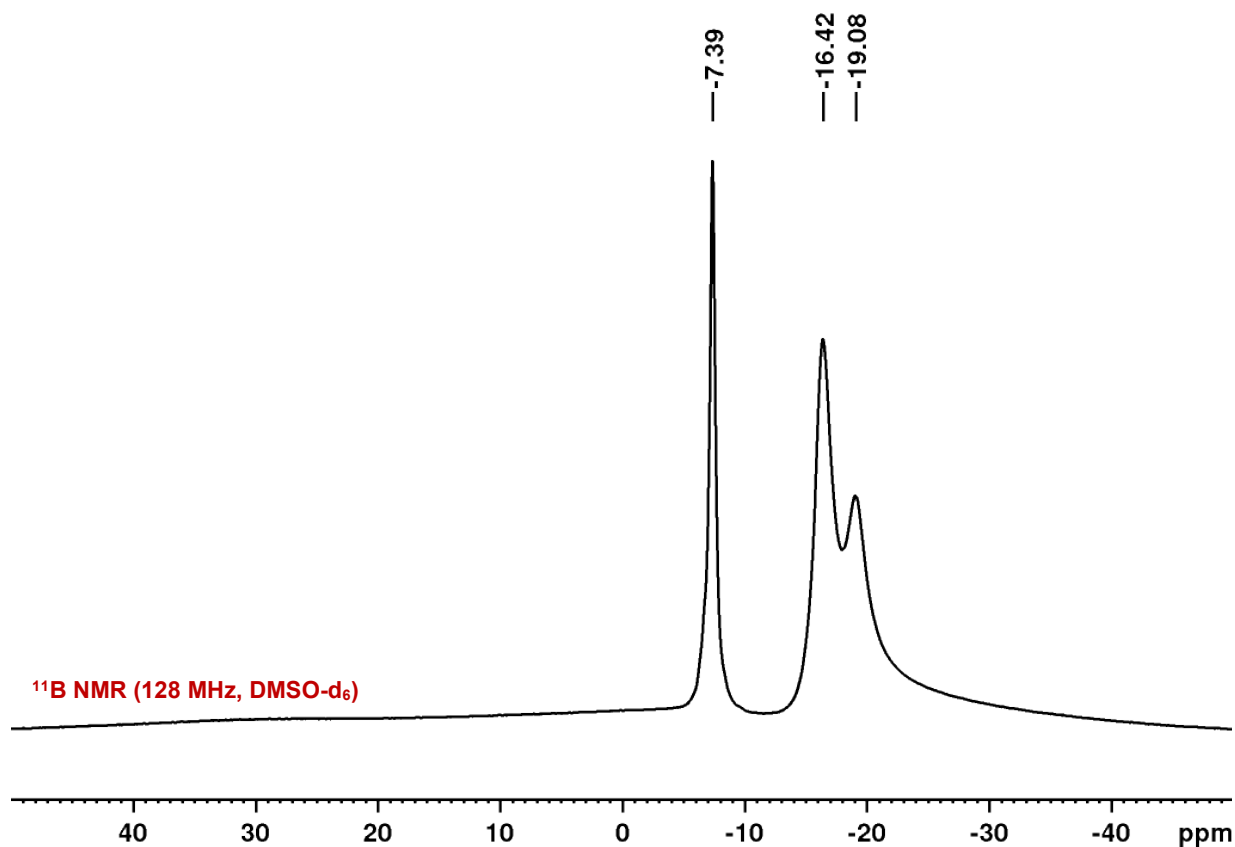


Figure S3.21: The ^{11}B NMR spectrum of $\text{TBA}_2\text{B}_{12}\text{Br}_9(\text{OCH}_3)_3$ with a resonance at -7.4 ppm ascribed to the B-O bonds and overlapping resonances at -16.4 ppm and -19.0 ppm corresponding to the B-Cl bonds.

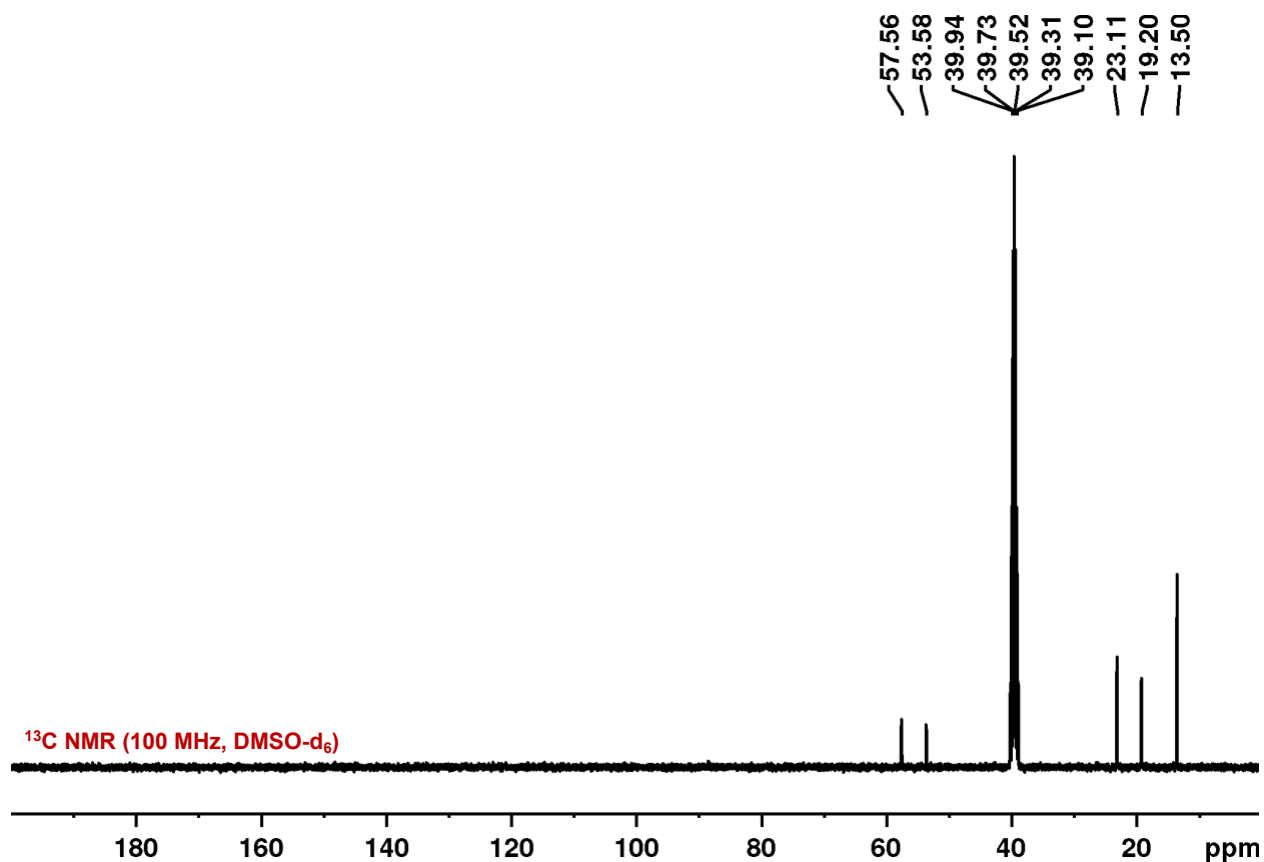


Figure S3.22: The ^{13}C NMR spectrum of $\text{TBA}_2\text{B}_{12}\text{Br}_9(\text{OCH}_3)_3$ with four resonances that correspond to the TBA cation and a fifth resonance ascribed to the methoxy ^{13}C .

III. Cation Exchange Procedures

Cation exchange was achieved by adapting the procedure of Strauss and coworkers.²¹ Salts were dissolved in the following solvents and volumes:

Compound	Acetonitrile (mL)	Methanol (mL)	Acetone (mL)
$\text{TBA}_2\text{B}_{12}\text{Cl}_{12}$	5	5	
$\text{TBA}_2\text{B}_{12}\text{Cl}_9(\text{OH})_3$	10	10	20
$\text{TBA}_2\text{B}_{12}\text{Cl}_9(\text{OCH}_3)_3$	5	15	15
$\text{Cs}_2\text{B}_{12}\text{Br}_{12}$	10	15	
$\text{TBA}_2\text{B}_{12}\text{Br}_9(\text{OH})_3$	5	5	
$\text{TBA}_2\text{B}_{12}\text{Br}_9(\text{OCH}_3)_3$	5	10	5

Figure S3.23: Solvent mixtures utilized to solubilize all compounds for cation exchange.

After dissolution, the Amberlyst-15 column (15 in) was prepared by passing 3 column volumes of the solvent mixture used to dissolve the given compound through the resin. After, the dissolved compound was loaded to the top of the column and allowed to elute (~1-2 drops/sec). The solvent was collected and dried *in vacuo*. An oily residue was collected, and deionized water (10 mL) was added. After, the pH was brought up to 7 using LiOH•H₂O (200 mg/mL). Activated charcoal (1 g) was charged into the vessel and allowed to stir for 3-4 hrs. After, the activated charcoal was removed under vacuum filtration, washed with water (20 mL x 3) and the filtrate was collected. The filtrate was dried under vacuum and stored at 10 °C. ¹¹B NMR confirmed the presence of intact cluster, ⁷Li NMR confirmed the presence of the alkali cation and ¹H NMR indicates loss TBA. All samples were prepared in D₂O.

$\text{Li}_2\text{B}_{12}\text{Cl}_{12}$

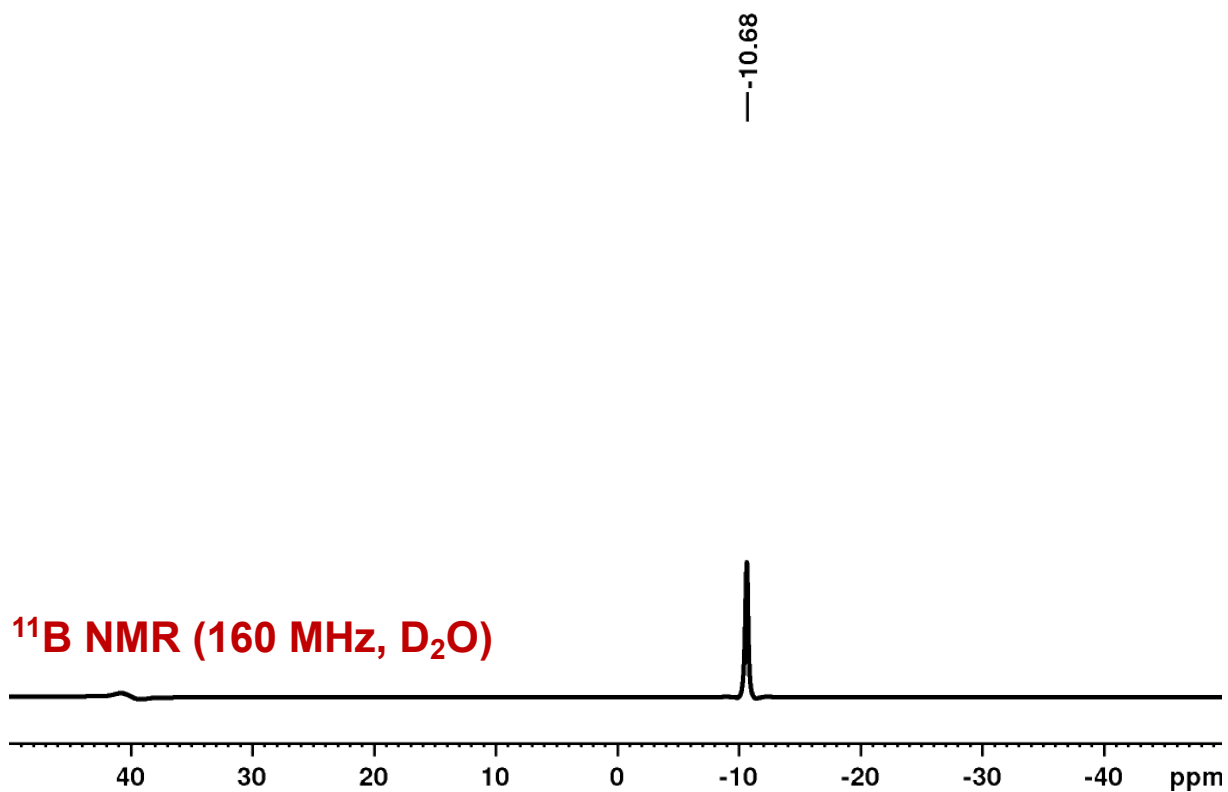


Figure S3.24: ^{11}B NMR spectrum of $\text{Li}_2\text{B}_{12}\text{Cl}_{12}$ confirming no changes to the cluster occurred during cation exchange.

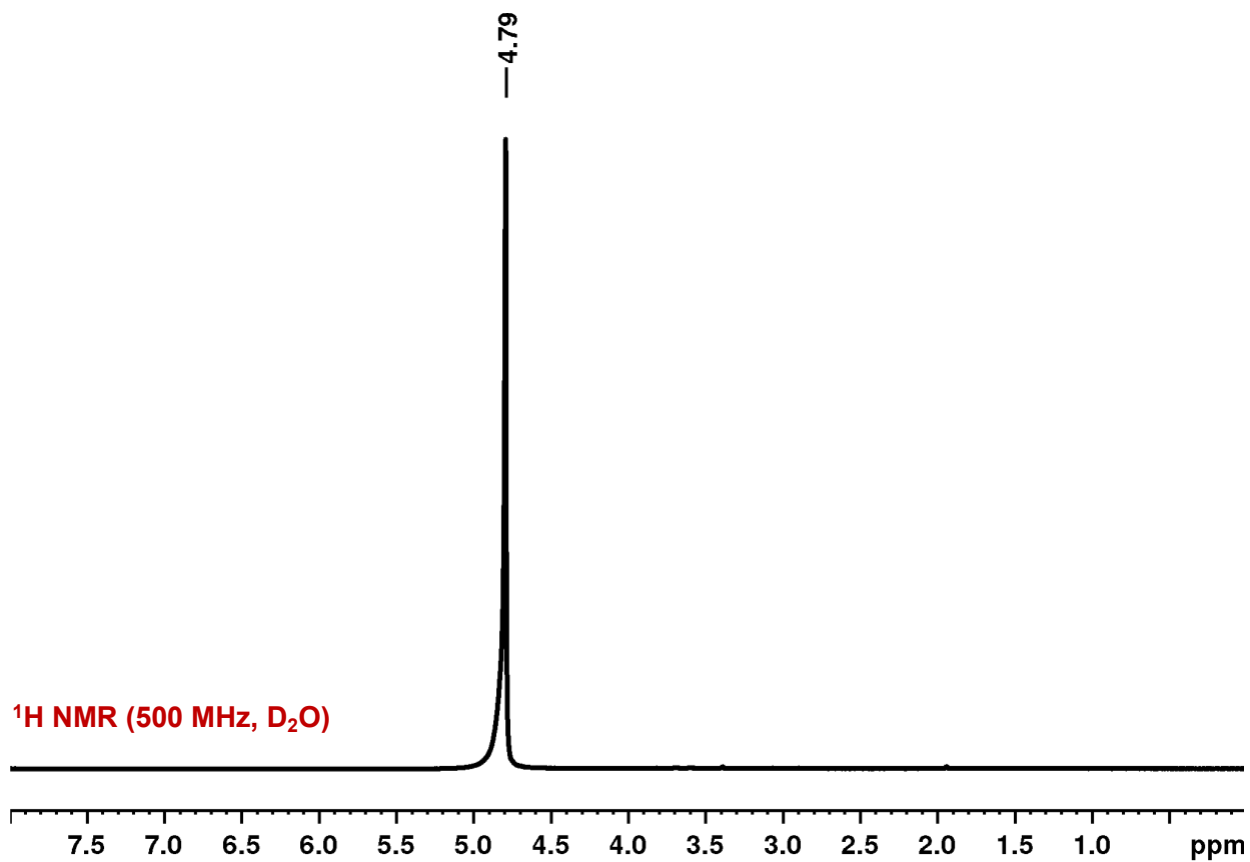


Figure S3.25: ^1H NMR spectrum of $\text{Li}_2\text{B}_{12}\text{Cl}_{12}$. The only resonance observed can be attributed to residual water in D_2O , suggesting all TBA cation had been exchanged.

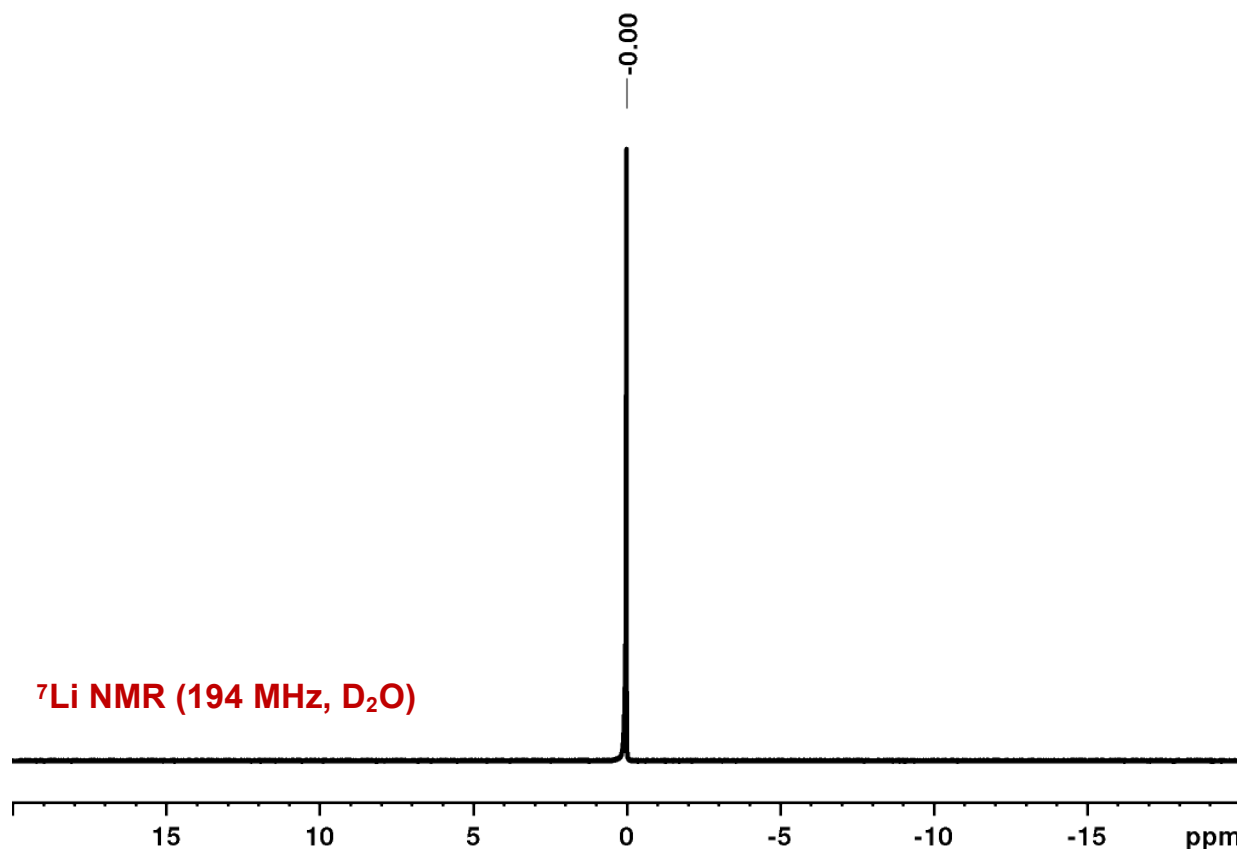


Figure S3.26: ${}^7\text{Li}$ NMR spectrum of $\text{Li}_2\text{B}_{12}\text{Cl}_{12}$. The observed singlet confirms the presence of ${}^7\text{Li}$ in the sample.

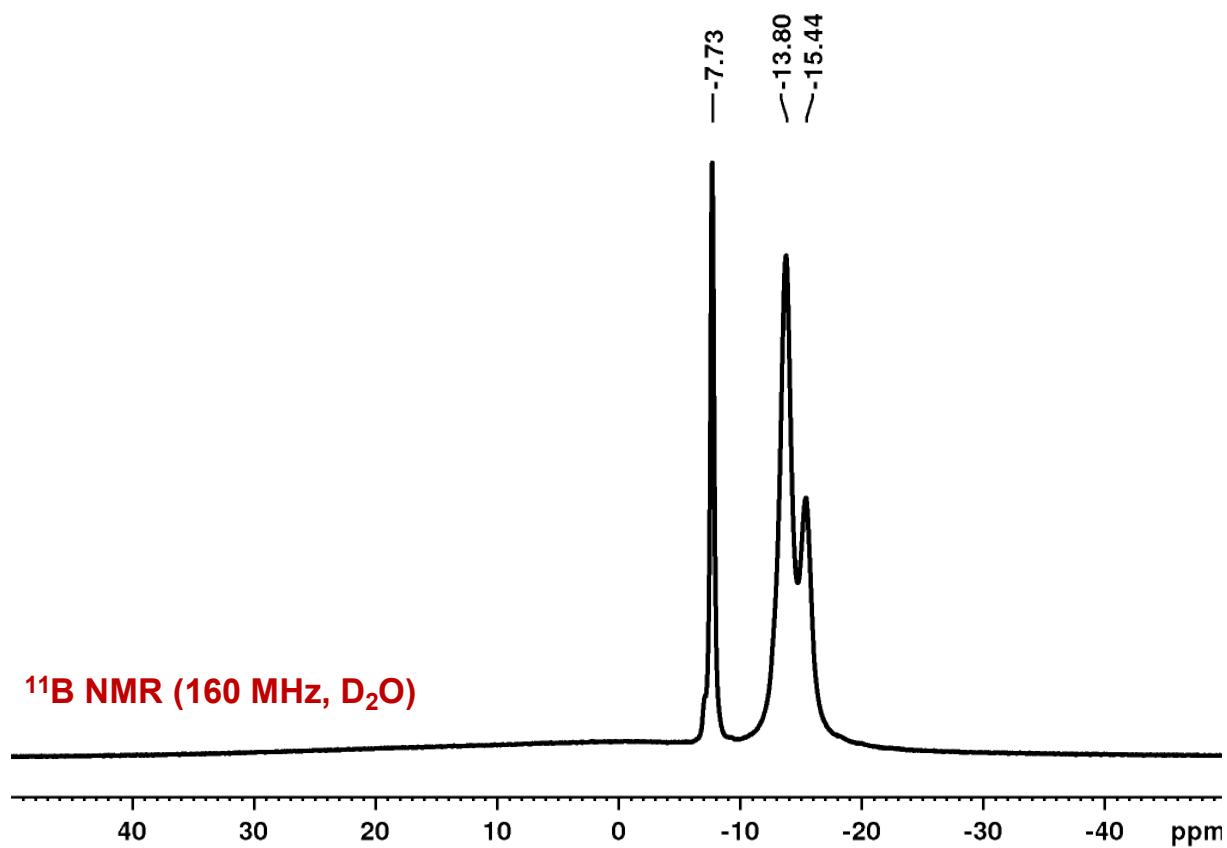


Figure S3.27: ^{11}B NMR spectrum of $\text{Li}_2\text{B}_{12}\text{Cl}_9(\text{OH})_3$ confirming no changes to the cluster occurred during cation exchange.

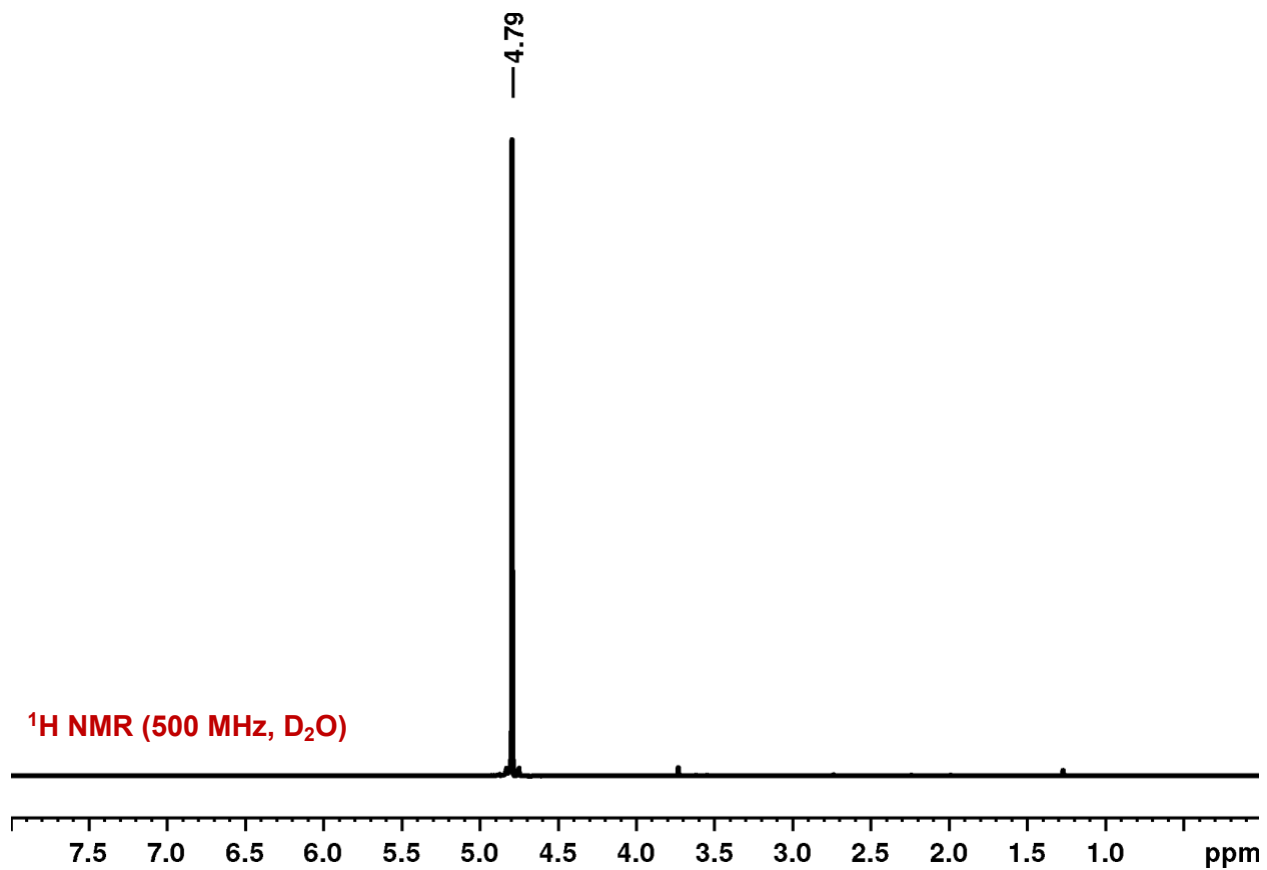


Figure S3.28: ¹H NMR spectrum of Li₂B₁₂Cl₉(OH)₃. The only resonance observed can be attributed to residual water in D₂O, suggesting all TBA cation had been exchanged.

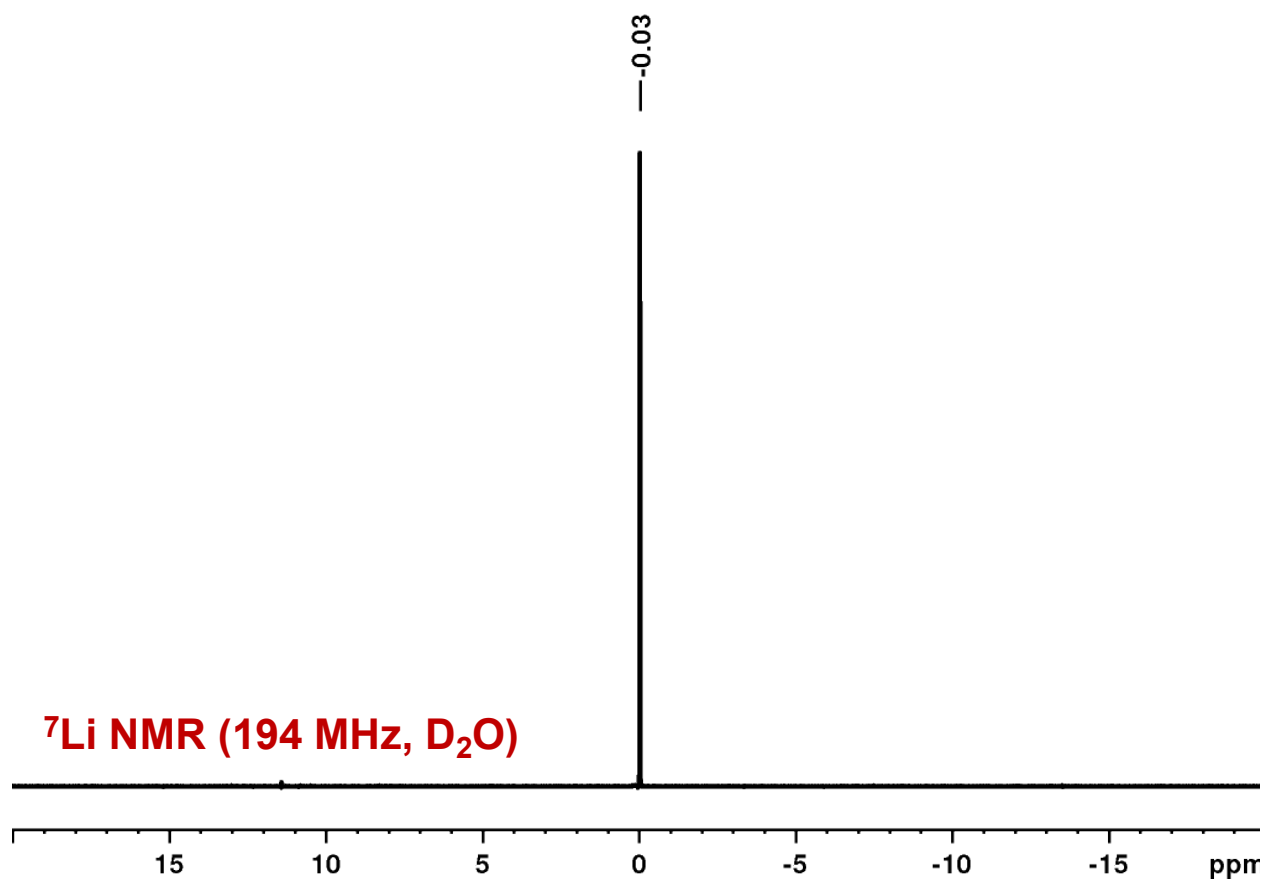


Figure S3.29: ⁷Li NMR spectrum of Li₂B₁₂Cl₉(OH)₃. The observed singlet confirms the presence of ⁷Li in the sample.

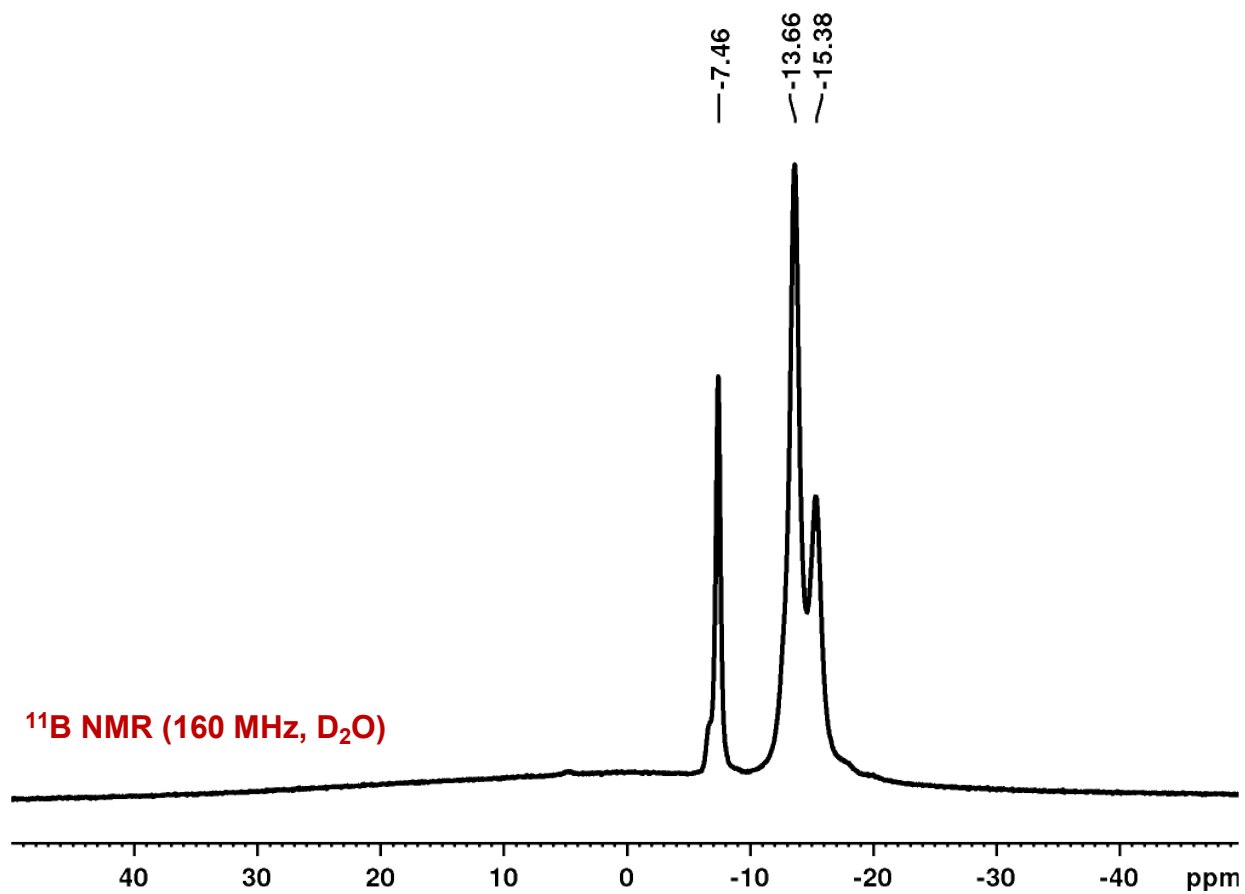
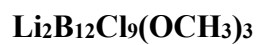


Figure S3.30: ^{11}B NMR spectrum of $\text{Li}_2\text{B}_{12}\text{Cl}_9(\text{OCH}_3)_3$ confirming no changes to the cluster occurred during cation exchange.

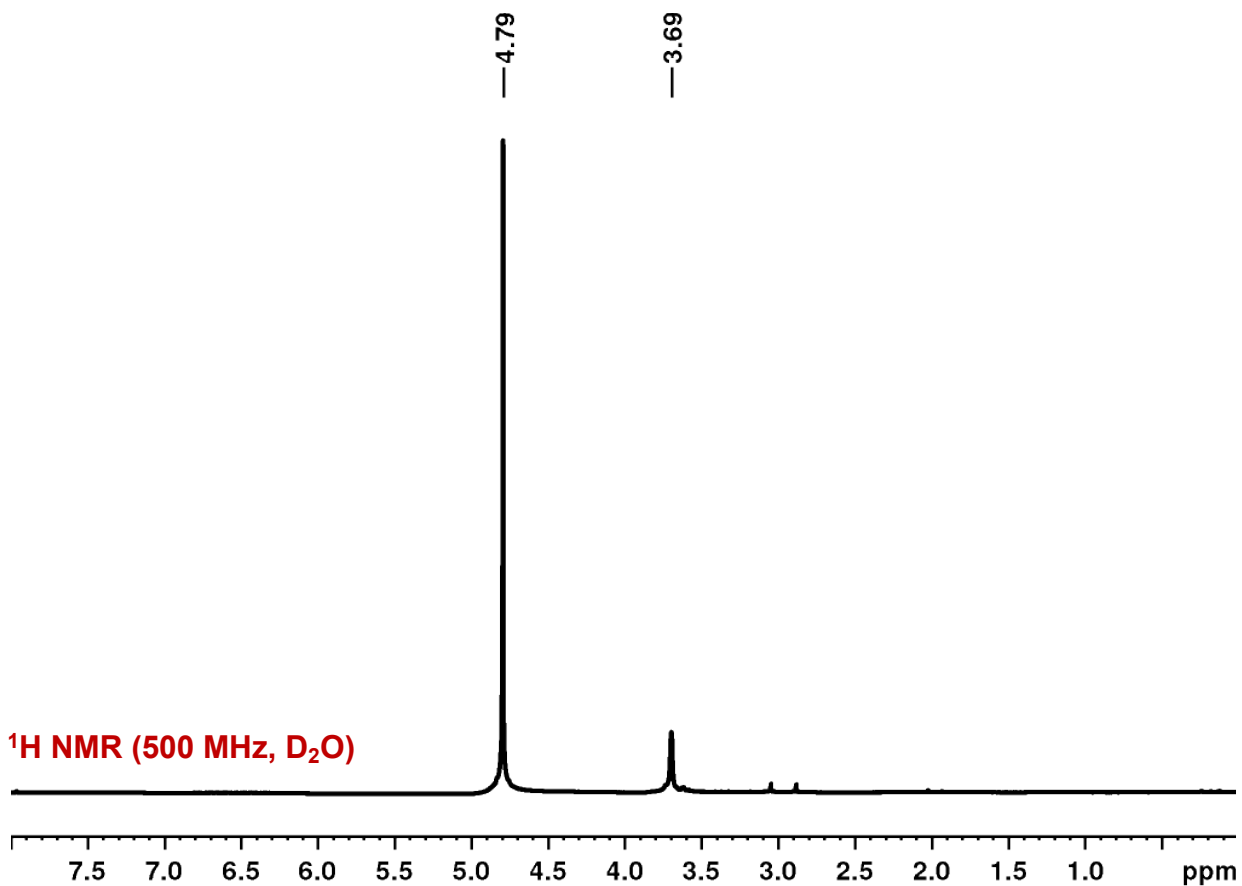


Figure S3.31: ¹H NMR spectrum of Li₂B₁₂Cl₉(OCH₃)₃. Two resonances are observed and are attributed to residual water in D₂O and methoxy ¹H indicating all TBA cation had been exchanged.

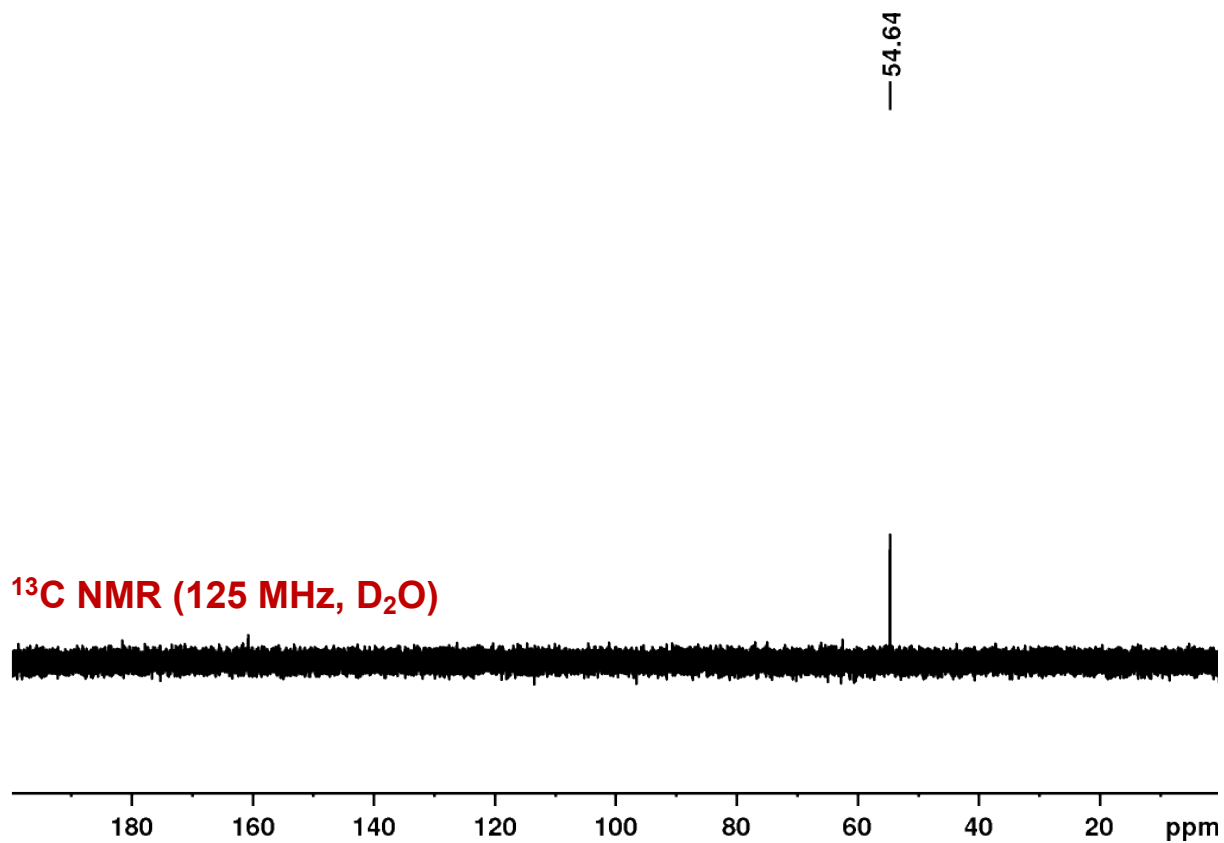


Figure S3.32: ¹³C NMR spectrum of Li₂B₁₂Cl₉(OCH₃)₃. A singlet resonance is observed and is attributed to methoxy ¹³C indicating all TBA cation had been exchanged. The ¹³C NMR was referenced externally to 10% ethylbenzene in CDCl₃.

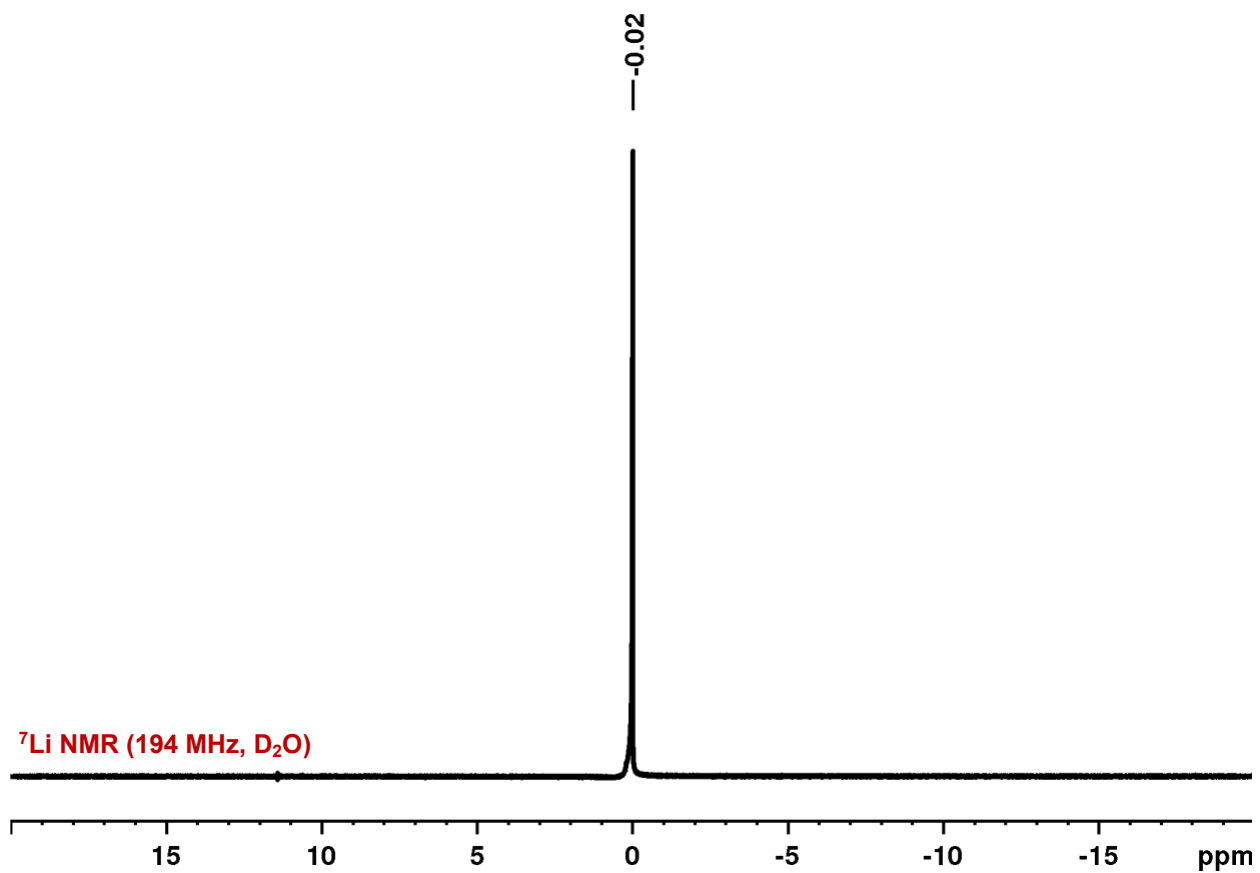


Figure S3.33: ${}^7\text{Li}$ NMR spectrum of $\text{Li}_2\text{B}_{12}\text{Cl}_9(\text{OCH}_3)_3$. The observed singlet confirms the presence of ${}^7\text{Li}$ in the sample.

$\text{Li}_2\text{B}_{12}\text{Br}_{12}$

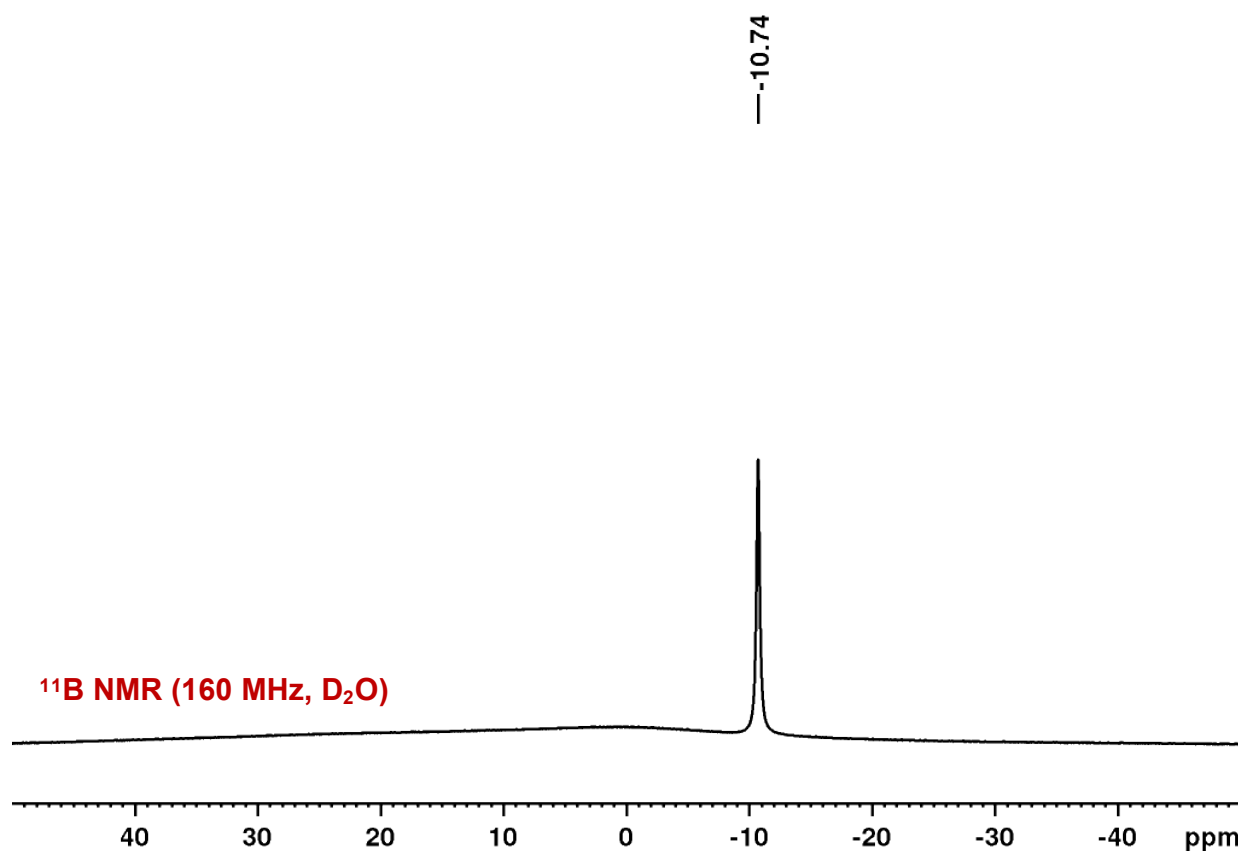


Figure S3.34: ^{11}B NMR spectrum of $\text{Li}_2\text{B}_{12}\text{Br}_{12}$ confirming no changes to the cluster occurred during cation exchange.

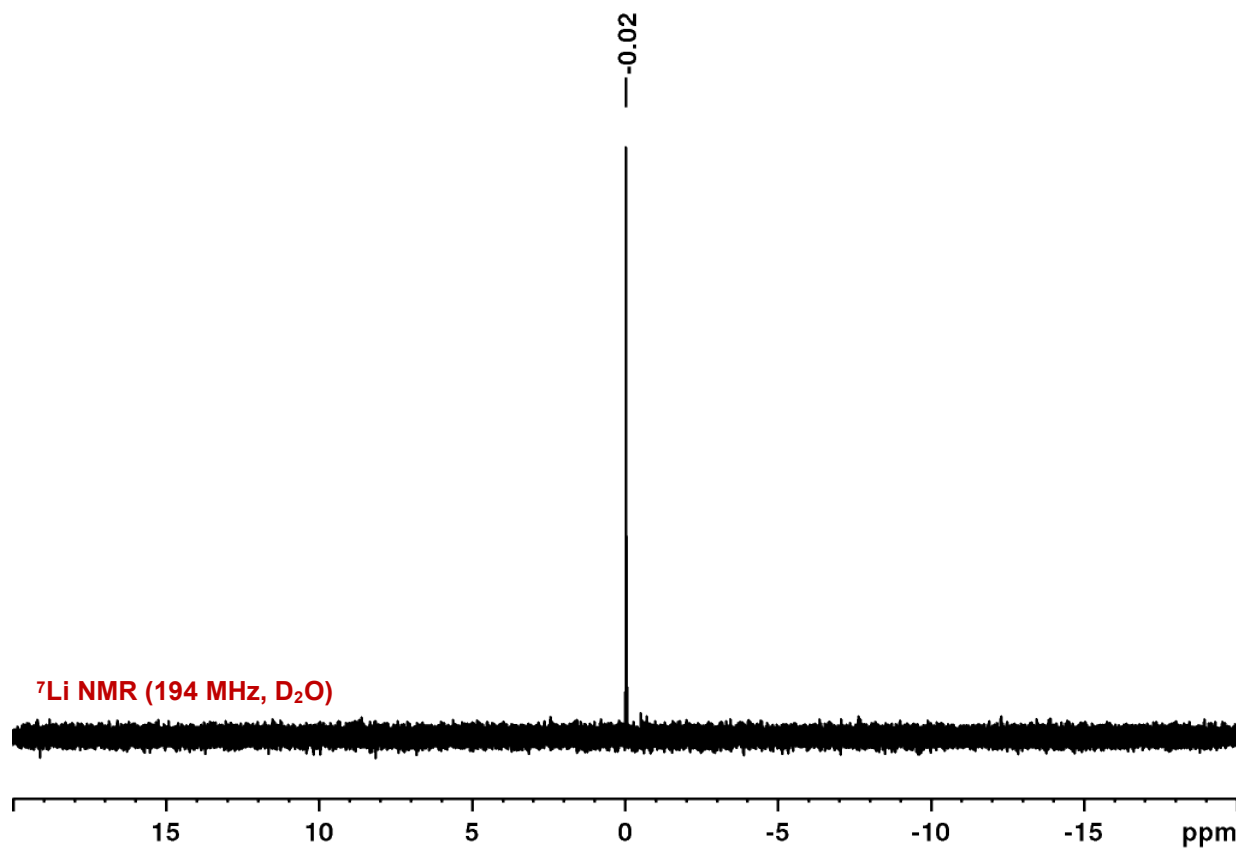


Figure S3.35: ⁷Li NMR spectrum of Li₂B₁₂Br₁₂. The observed singlet confirms the presence of ⁷Li in the sample.

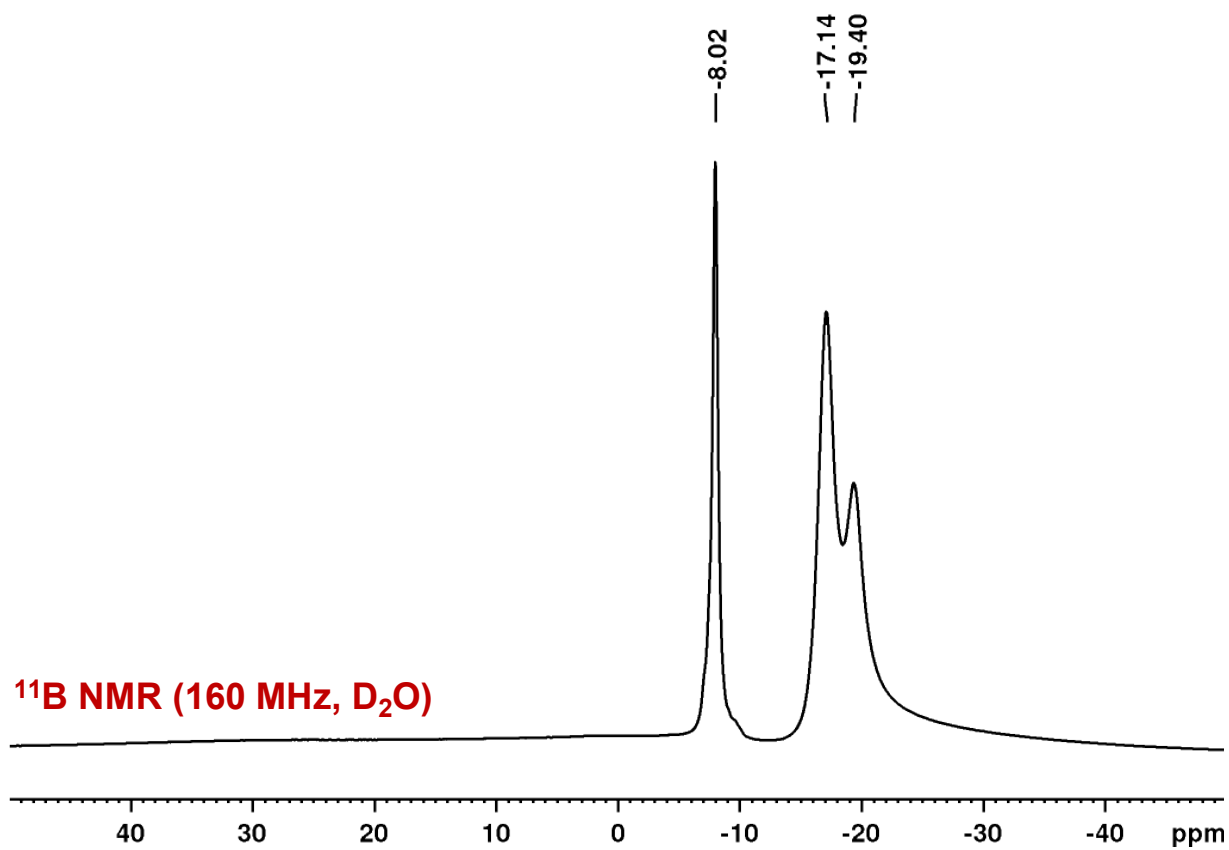


Figure S3.36: ^{11}B NMR spectrum of $\text{Li}_2\text{B}_{12}\text{Br}_9(\text{OH})_3$ confirming no changes to the cluster occurred during cation exchange.

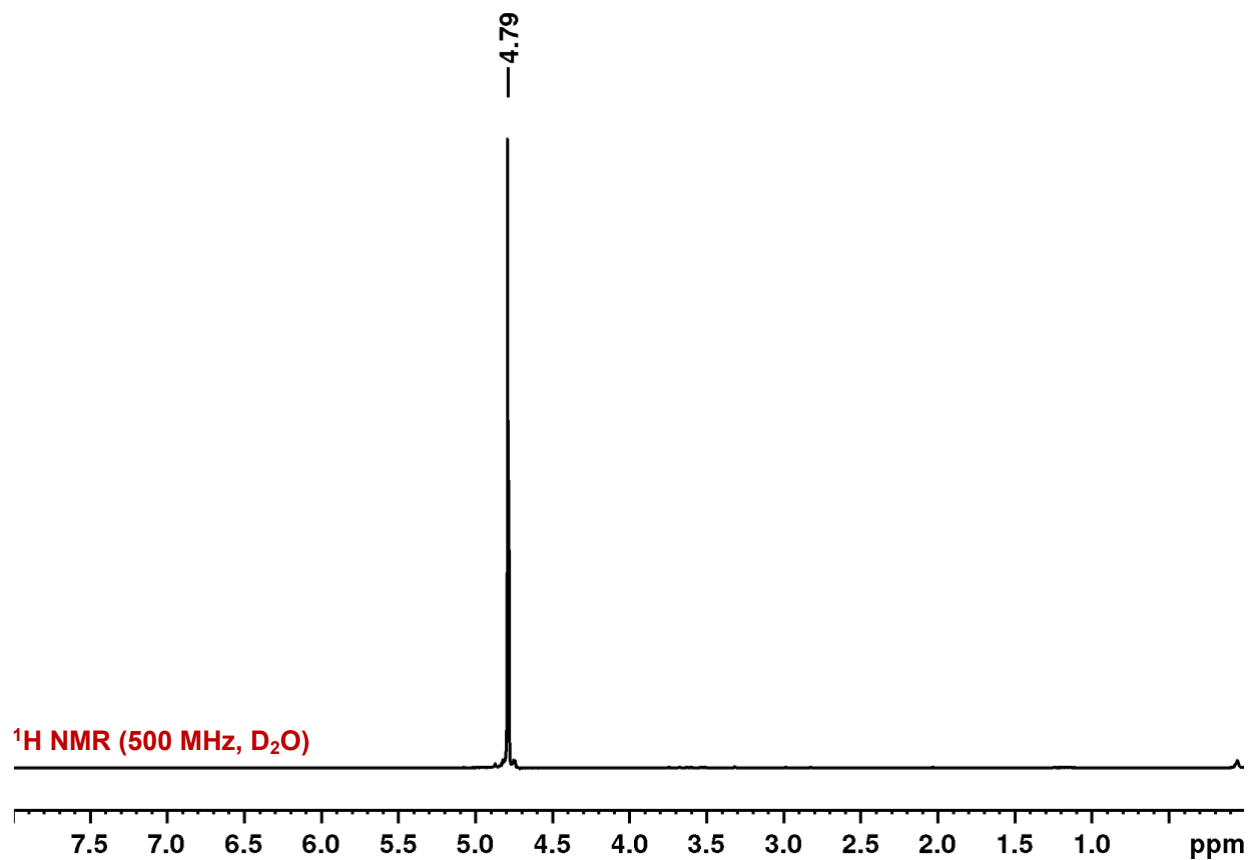


Figure S3.37: ^1H NMR spectrum of $\text{Li}_2\text{B}_{12}\text{Br}_9(\text{OH})_3$. The only resonance observed can be attributed to residual water in D_2O , suggesting all TBA cation had been exchanged.

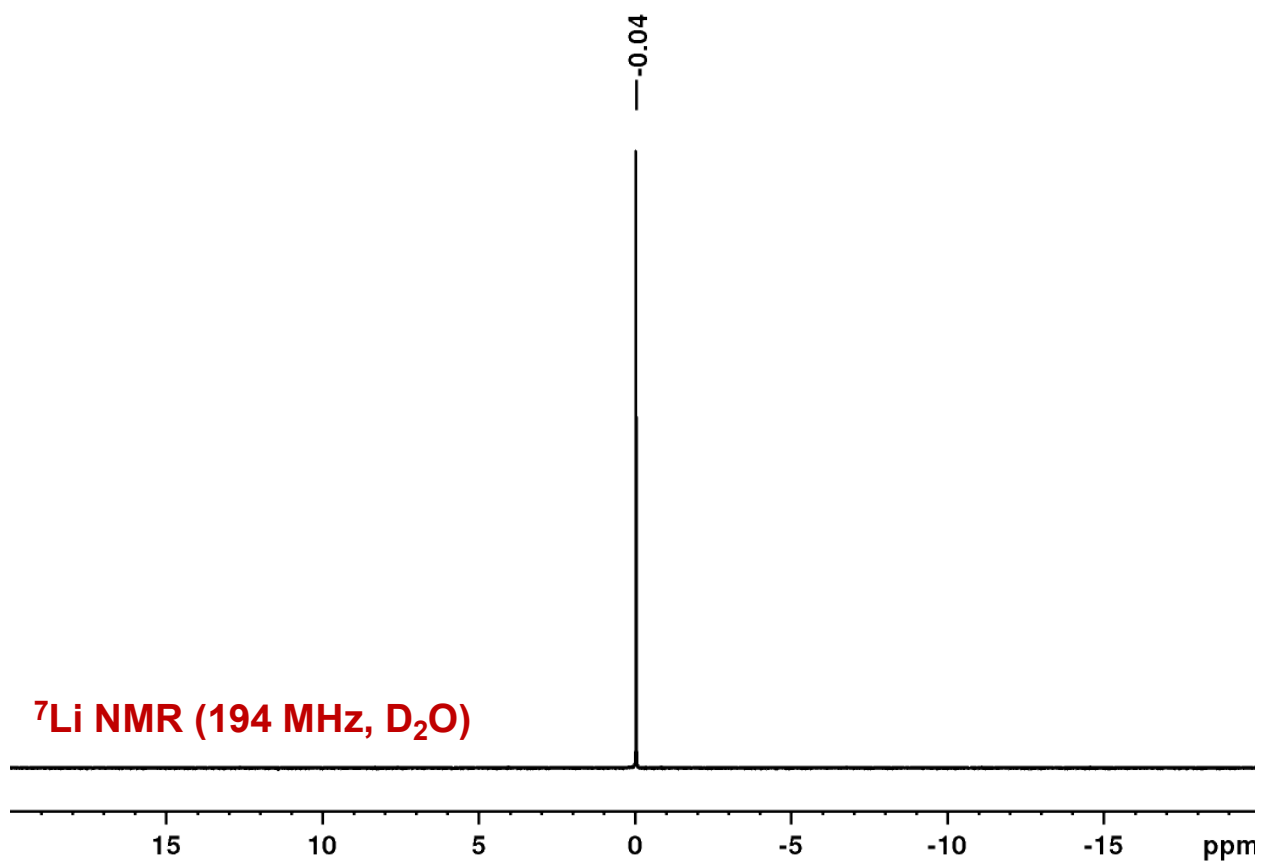


Figure S3.38: ${}^7\text{Li}$ NMR spectrum of $\text{Li}_2\text{B}_{12}\text{Br}_9(\text{OH})_3$. The observed singlet confirms the presence of ${}^7\text{Li}$ in the sample.

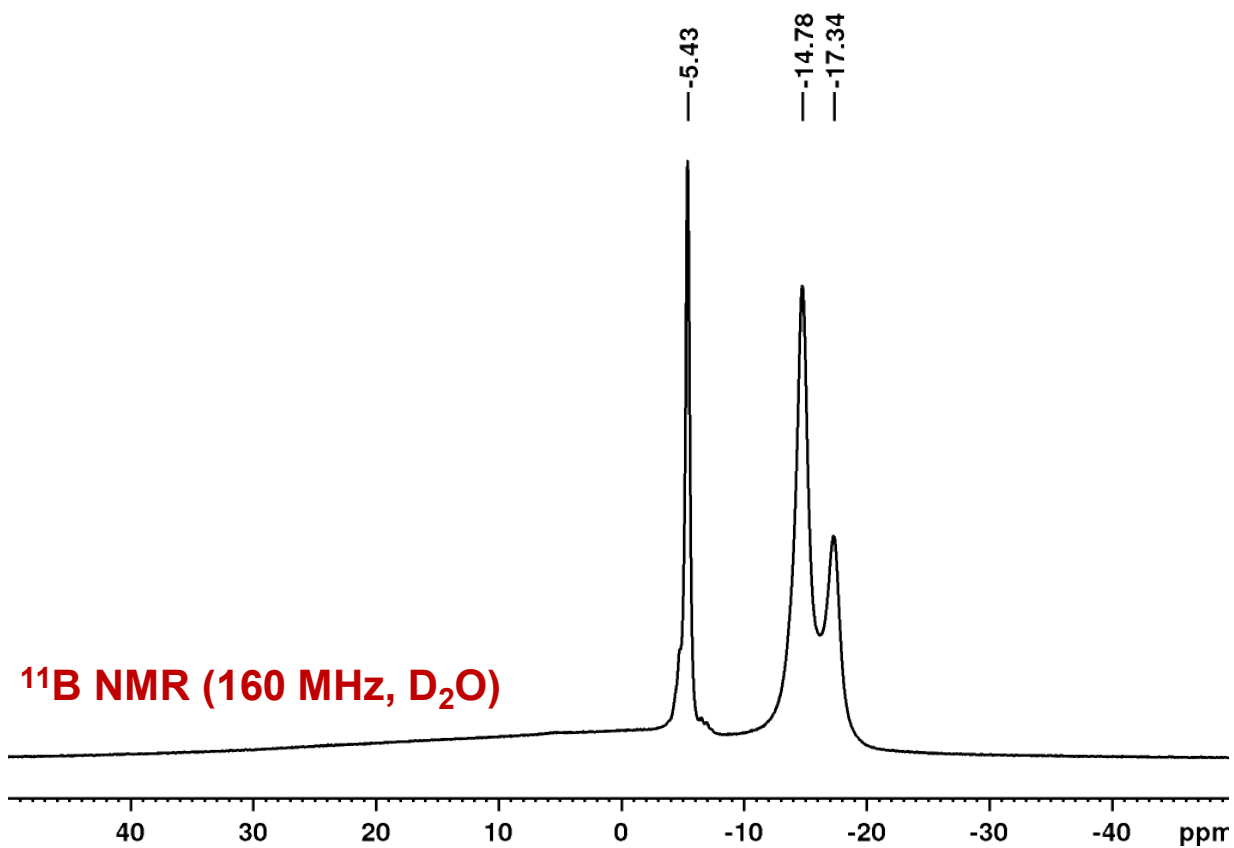


Figure S3.39: ^{11}B NMR spectrum of $\text{Li}_2\text{B}_{12}\text{Br}_9(\text{OCH}_3)_3$ confirming no changes to the cluster occurred during cation exchange.

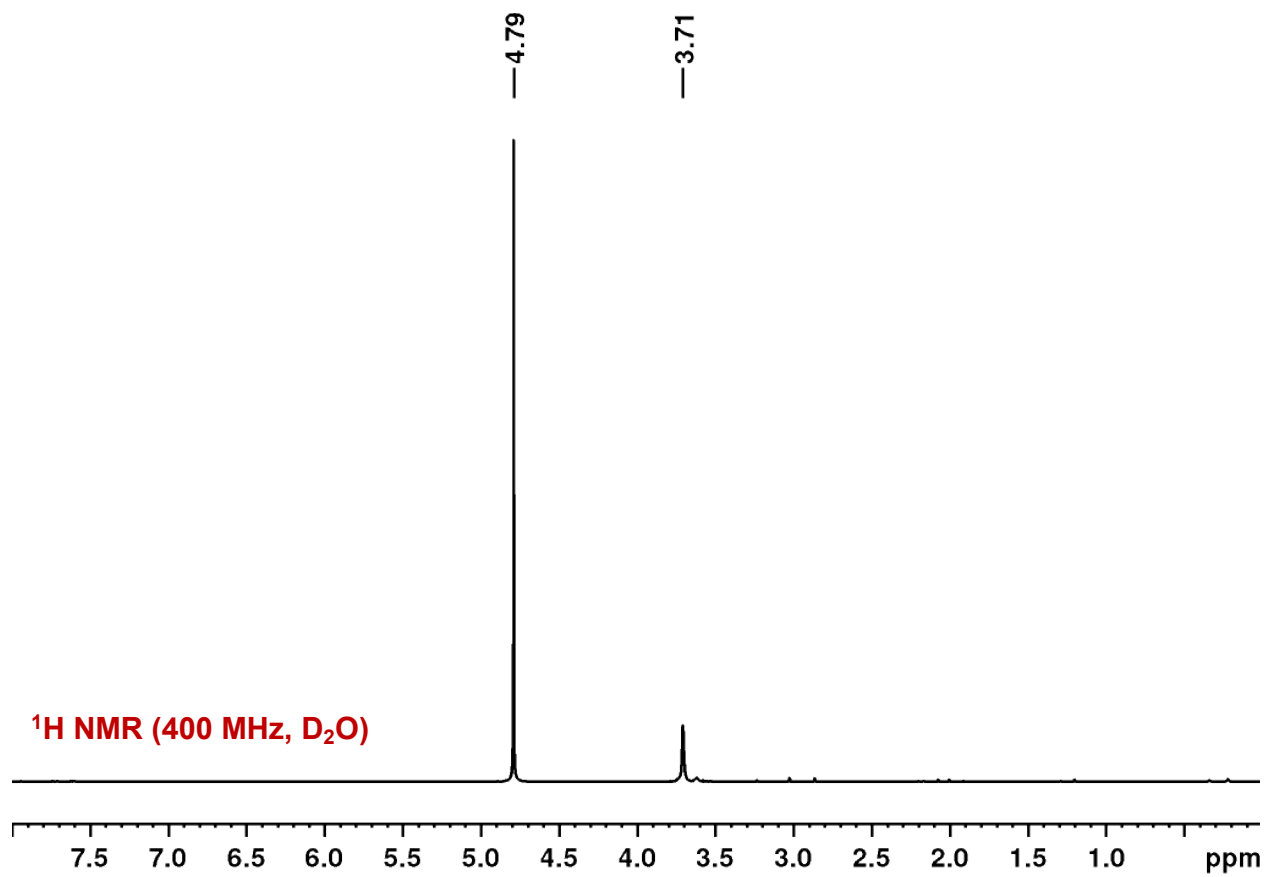


Figure S3.40: ¹H NMR spectrum of Li₂B₁₂Br₉(OCH₃)₃. Two resonances are observed and are attributed to residual water in D₂O and methoxy ¹H indicating all TBA cation had been exchanged.

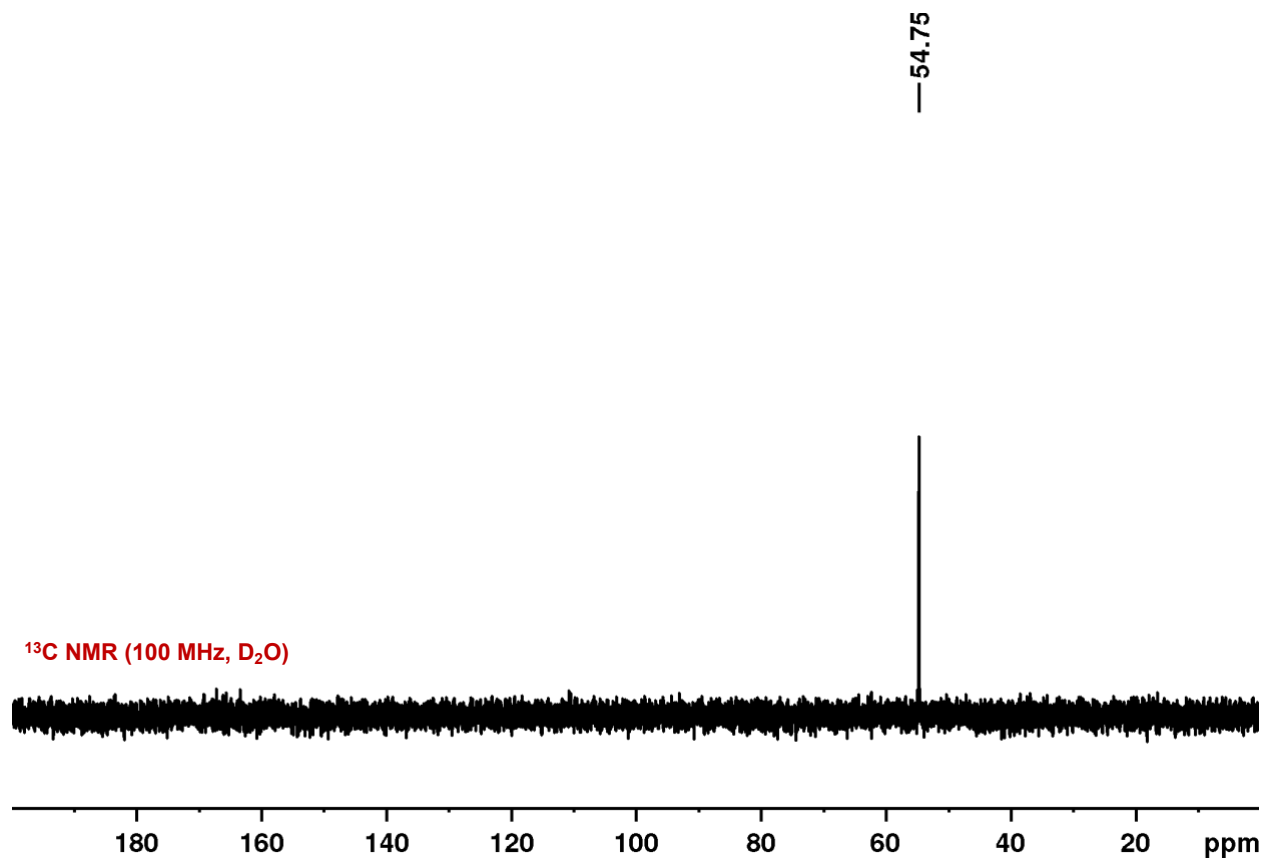


Figure S3.41: ¹³C NMR spectrum of Li₂B₁₂Br₉(OCH₃)₃. A singlet resonance is observed and is attributed to methoxy ¹³C indicating all TBA cation had been exchanged. The ¹³C NMR was referenced externally to 10% ethylbenzene in CDCl₃.

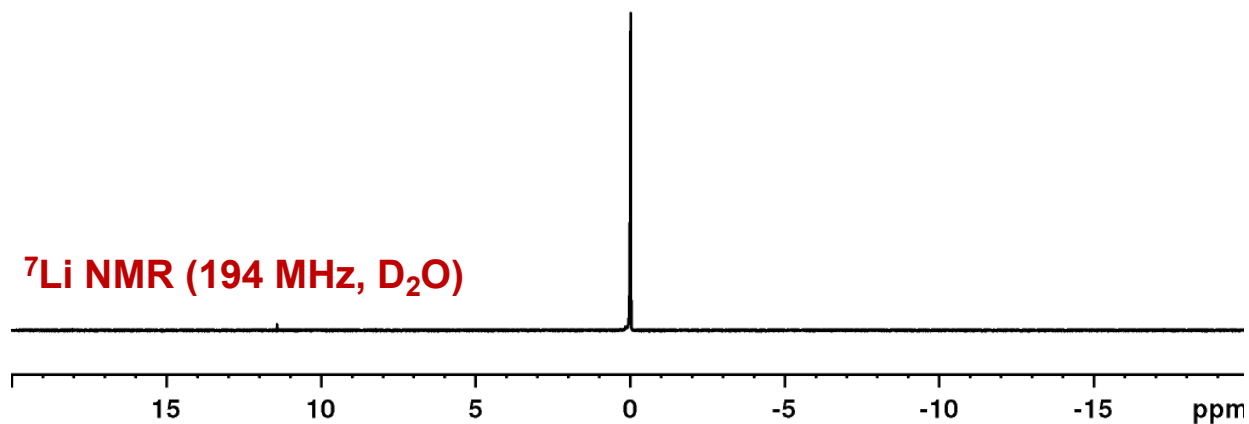


Figure S3.42: ⁷Li NMR spectrum of Li₂B₁₂Br₉(OH)₃. The observed singlet confirms the presence of ⁷Li in the sample.

IV. Thermogravimetric Analysis

Thermogravimetric analyses were performed on a PerkinElmer Pyris Diamond TG/DTA under a constant flow of Argon (200 mL/min). Samples were heated in ceramic trays (5 mm) from 60 °C to 1000 °C at 10 °C/min. The following equation was used to assess the number of water molecules lost per lithium per sample:

$$\frac{X(H_2O)}{Li} = \frac{X(18.02\frac{g}{mol})}{Li} \times 2Li = X(36.04\frac{g}{mol}) \quad (1)$$

$$\frac{X(36.04\frac{g}{mol})}{Molecular\ Weight} = \% \text{ Water Loss} \quad (2)$$

V. Crystal Structures

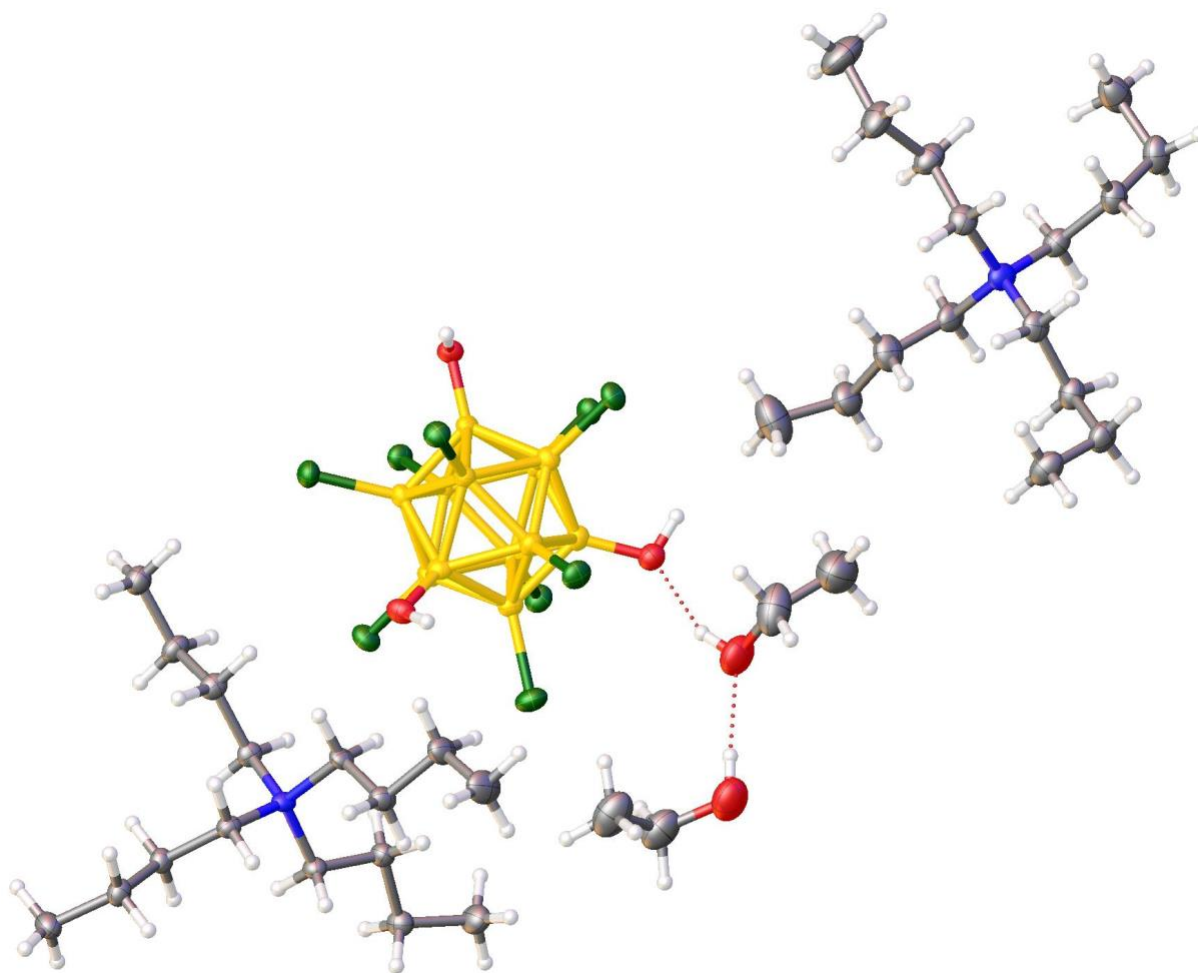


Figure S3.43: Crystal structure of $\text{TBA}_2\text{B}_{12}\text{Cl}_9(\text{OH})_3$ crystallized from hot ethanol.

Empirical formula	$C_{36}H_{87}B_{12}Cl_9N_2O_5$	
Formula weight	1076.84	
Temperature	100.0 K	
Wavelength	1.54178 Å	
Crystal system	Monoclinic	
Space group	P 21/c	
Unit cell dimensions	a = 11.2017(10) Å	∠ = 90°.
	b = 12.5612(14) Å	∠ = 95.402(5)°.
	c = 40.716(3) Å	∠ = 90°.
Volume	5703.6(9) Å ³	
Z	4	
Density (calculated)	1.254 Mg/m ³	
Absorption coefficient	4.335 mm ⁻¹	
F(000)	2280	
Crystal size	0.31 x 0.29 x 0.07 mm ³	
Theta range for data collection	2.180 to 68.394°.	
Index ranges	-12 ≤ h ≤ 13, -15 ≤ k ≤ 15, -49 ≤ l ≤ 48	
Reflections collected	111639	
Independent reflections	10434 [R(int) = 0.0960]	
Completeness to theta = 67.679°	99.8 %	
Absorption correction	None	
Max. and min. transmission	0.7531 and 0.4757	
Refinement method	Full-matrix least-squares on F ²	
Data / restraints / parameters	10434 / 2 / 598	
Goodness-of-fit on F ²	1.097	
Final R indices [I > 2σ(I)]	R1 = 0.0610, wR2 = 0.1488	
R indices (all data)	R1 = 0.0704, wR2 = 0.1565	
Extinction coefficient	n/a	
Largest diff. peak and hole	0.488 and -0.468 e.Å ⁻³	

Figure S3.44: Crystal data and structure refinement parameters for TBA₂B₁₂Cl₉(OH)₃.

VI. Assessment of Solubility

$\text{Li}_2\text{B}_{12}\text{Cl}_{12}$, $\text{Li}_2\text{B}_{12}\text{Cl}_9(\text{OH})_3$ and $\text{Li}_2\text{B}_{12}\text{Cl}_9(\text{OCH}_3)_3$ were added to a 96-well plate with enough compound to cover the bottom of the well. The following solvents were added: (A) acetonitrile, (B) ethyl acetate, (C) methanol, (D) ethanol, (E) isopropanol and (F) hexanes.

Compound	A	B	D	E	F	G
$\text{Li}_2\text{B}_{12}\text{Cl}_{12}$	I	P	I	I	I	I
$\text{Li}_2\text{B}_{12}\text{Cl}_9(\text{OH})_3$	I	P	I	P	P	I
$\text{Li}_2\text{B}_{12}\text{Cl}_9(\text{OCH}_3)_3$	P	S	P	S	S	I

Figure S3.45: Preliminary assessment of solubility for $\text{Li}_2\text{B}_{12}\text{Cl}_{12}$, $\text{Li}_2\text{B}_{12}\text{Cl}_9(\text{OH})_3$ and $\text{Li}_2\text{B}_{12}\text{Cl}_9(\text{OCH}_3)_3$. P indicates partially soluble, S indicates soluble and I indicates insoluble

CHAPTER 4

An Organometallic Strategy for Cysteine Borylation

This chapter is a version of Waddington, M. A.; Zheng, X.; Stauber, J. M.; Hakin Mouilly, E.; Montgomery, H. R.; Saleh, L. M. A.; Král, P.; Spokoyny, A. “An Organometallic Strategy for Cysteine Borylation.” *J. Am. Chem. Soc.* **2021**, *in press*.

Abstract

Synthetic bioconjugation at cysteine (Cys) residues in peptides and proteins has emerged as a powerful tool in chemistry. Soft nucleophilicity of the sulfur in Cys renders an exquisite chemoselectivity with which various functional groups can be placed onto this residue under benign conditions. While a variety of reactions have been successful at producing Cys-based bioconjugates, the majority of these feature sulfur-carbon bonds. We report Cys-borylation, wherein a benchtop stable Pt(II)-based organometallic reagent can be used to transfer a boron-rich cluster onto a sulfur moiety in unprotected peptides forging a boron-sulfur bond. Cys-borylation proceeds at room temperature and tolerates a variety of functional groups present in complex polypeptides. Further, the bioconjugation strategy can be applied to a model protein modification of Cys-containing DARPin (designed ankyrin repeat protein). The resultant bioconjugates show no additional toxicity compared to their Cys alkyl-based congeners. Finally, we demonstrate how the developed Cys-borylation can enhance the proteolytic stability of the resultant peptide bioconjugates while maintaining the binding affinity to a protein target.

Introduction

Synthetic bioconjugation has emerged as a powerful tool towards understanding and altering biomolecular interactions. Mimicking the post-translational modifications ubiquitous to natural biological systems, a variety of C-S, C-O, C-N and C-C bond forming reactions have been

previously reported.^{1,2} These synthetic tools have been used to install handles on biomolecules for applications ranging from imaging^{3,4} to enhancement of therapeutic efficacy.^{5,6}

Cysteine (Cys) residues in proteins and peptides represent a historically attractive site for synthetic bioconjugation development owing to its soft nucleophilicity and low natural abundance which contributes to its capacity to undergo site-directed mutagenesis and subsequent selective modification.⁷ These chemoselective Cys conjugations can be achieved through both metal-free and recently developed metal-mediated routes (Figure 4.1A). Conjugate addition to Michael acceptors (e. g., maleimides and vinyl sulfones^{1,2}) as well as S_N2 reactions with alkyl electrophilic centers^{1,2} represent the most common metal-free transformations; however, a number of noteworthy other alkylation and arylation strategies have been reported.^{1,7, 10-16} Recently, transition metal-mediated C-S bond forming reactions have attracted considerable attention due to the rapid kinetics, mild reaction conditions and high functional group tolerance often associated with these metal-based transformations (Figure 4.1A).^{1,17} For example, Buchwald, Pentelute and co-workers demonstrated a unique approach towards chemoselective Cys modification via arylation using well-defined and benchtop-stable Pd-based organometallic reagents.¹⁷ The reaction conditions were amenable to covalent linkage of fluorescent and affinity tags, drug molecules and handles for further conjugation. This concept was also demonstrated using a stoichiometric Au(I/III) platform^{18,19} as well as several notable catalytic strategies.^{15,24}

While a large breadth of chemoselective C-S bond forming bioconjugations have been reported, analogous transformations resulting in the formation of boron-sulfur bonds (B-S) are conspicuously absent. While substrates containing free thiols have been borylated through metal-mediated and metal-free routes (Figure 4.1B), these methods generally lack selectivity for thiols over other competing nucleophilic centers which is a key prerequisite for successful

boranes represent a promising platform to probe this hypothesis given their three-dimensional delocalized aromaticity²⁷⁻³³ analogous to the carbon-based aromatic molecules previously employed for bioconjugation. Here, we show that a Pt(II) complex³⁴ supported by a boron-bound carboranyl cluster (**1**) is capable of chemoselective Cys borylation across multiple unprotected peptide substrates to generate the first B-S bond linkages post-synthetically, which was a previously inaccessible modality in bioconjugation. Importantly, the borylated peptides were stable towards excess base, acid and external thiol and did not display any appreciable toxicity up to 50 μ M in cell culture. In addition to providing a new chemical connectivity, the developed Cys borylation offers new opportunities in areas of multivalent binding and tuning of ligand-receptor interactions in biomolecular targeting.

Results and Discussion

To test whether one can use boron-cluster supported organometallic reagents for successful Cys borylation, we subjected model peptide H₂N-VKALGVCG-CONH₂ (**2a**) with **1** under various conditions. Nearly quantitative conversion to a peptide containing a mass consistent with a Cys-borylated peptide was observed within 1.5 h when **2a** (5 mM) was treated with 1.2 equivalents of **1** at 25 °C in the presence of Tris•HCl buffer (30 mM) in dimethylformamide (DMF) as assessed by LC-MS analysis of the crude reaction mixture (Figure 4.2A). In order to verify that the reaction conditions were selective for Cys over other nucleophiles within the model peptide substrate, tandem MS/MS of Cys-borylated peptide **2b** was conducted. Fragmentation patterns support exclusive Cys borylation (Figure S4.20). Analogous to arylation bioconjugation involving Pd-based reagents¹⁷, we propose this chemoselectivity arises from the transmetallation of the soft nucleophilic Cys sulfur residue that has a high propensity towards binding a Pt(II) metal center (Figure 4.2B).^{35,36} A subsequent reductive elimination process affords Cys-borylated

peptide and Pt-based byproducts (Figure 4.1B). Importantly, this process proceeds efficiently despite the carboranyl group being significantly more sterically encumbering than the previously demonstrated aryl-based species²⁷ ultimately highlighting the advantages of the organometallic approach used.

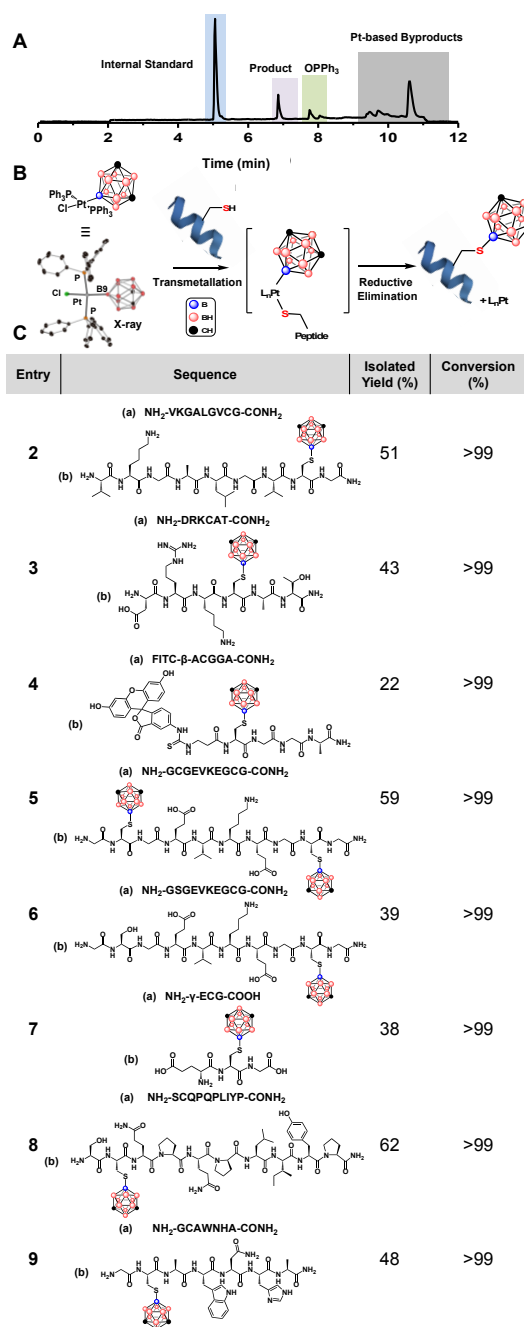


Figure 4.2A: Representative LC trace collected after **1** (1.2 equiv) and $\text{H}_2\text{N-VKGALGVCG-CONH}_2$ (5 mM) were allowed to react for 1.5 h at 25 °C in the presence of Tris•HCl buffer (30 mM) in dimethylformamide (DMF). Internal standard was produced through alkylation of $\text{H}_2\text{N-VKGALGVCG-CONH}_2$ (see SI section I). **B:** Proposed reaction scheme between **1** and cysteine-containing peptide **C:** Peptide substrate scope with isolated yields (%) and conversion (%).

To ensure generality of this method, we then applied the reaction conditions used to generate **2b** towards other peptide sequences (Figure 4.2C). Across all peptide substrates tested (entries **2-9**), we observed nearly quantitative conversion towards the corresponding borylated product with isolated yields ranging from 22-59% after HPLC purification (Figure 4.2C). Furthermore, the borylation reaction conditions were tolerant to the common labeling dye, fluorescein isothiocyanate (FITC) attached to the N-terminus of the peptide chain despite the presence of a thiourea linkage which could also serve as a chelating ligand towards the metal center (entry **4**). Even though carboranyl ligands are sterically bulky, diborylation of a peptide containing two Cys residues is possible; nearly quantitative conversion of **5a** to **5b** was observed under the optimized reaction conditions (entry **5**). Importantly, only monoborylation was observed when **6a**, which contains identical residues as **5a** except one Cys is mutated to a serine residue, was subjected to identical treatment (Figures S4.12 and S4.13). Overall, the borylation selectivity towards Cys thiols in unprotected peptides using **1** as a transfer reagent mirrors the selectivity of both Pd(II) and Au(III) organometallic Cys arylation reagents.^{17,19}

After assuring Cys-borylation was successful across multiple thiol containing peptides, we decided to perform an additional robustness screen for additional reagents that are often used in bioconjugation reactions on peptides. Diluting the DMF reaction mixture with water did not diminish conversion up to 25% water when model peptide H₂N-VKGALGVCG-CONH₂ (**2a**) was treated with **1**. Reaction mixtures exceeding 25% water resulted in a significant reduction in conversion, likely due to the poor solubility of **1** in water (Figure S4.17). Further, the bioconjugation was compatible with a common denaturing agent guanidine•HCl (3 M, Figure S4.18A), suggesting the organometallic complex **1** is stable under highly ionic conditions on the timescale of the reaction. Further, addition of Tris(2-carboxyethyl)phosphine hydrochloride

(TCEP HCl), a common reducing agent for disulfide moieties in biomolecules, does not significantly alter the conversion efficiency of the reaction (Figure S4.18B) indicating excess phosphine does not shut down the reactivity of **1** on the timescale of the reaction.

In order to probe the local environment of the carboranyl cluster on the purified Cys-borylated peptides using ^{11}B NMR spectroscopy, we decided to apply the borylation reaction to a peptide substrate with a low molecular weight to increase the signal to noise outcome of this experiment. Commercially available L-glutathione (**7a**) was thus chosen for these studies. Successfully Cys-borylated glutathione (**7b**) was subjected to a routine HPLC purification followed by ^{11}B NMR spectroscopic analysis. A distinct singlet resonance was observed at 2 ppm along with multiple broad doublets in an integral ratio of 1:9 consistent with the splitting pattern of a B(9)-substituted, intact *m*-carboranyl cluster (Figure S4.21A). Importantly, the $^{11}\text{B}\{^1\text{H}\}$ NMR spectrum of the same sample indicates that the doublets observed stem from the ^{11}B - ^1H coupling and the resonance at 2 ppm is consistent with a ^{11}B atom that is not bound to a ^1H nucleus (Figure S4.21B). Based on these observations and previously reported NMR spectroscopy data collected on *B*₉ substituted carborane thiols and thioether species³⁴, the resonance at 2 ppm was assigned to the $^{11}\text{B}(9)\text{-S}$ nucleus on the intact *m*-carborane cluster attached to the peptide. Finally, IR spectroscopy was used to further corroborate structural elements of **7b**. A diagnostic stretching band ascribed to the B-H bond vibrations on the cluster (2532-2681 cm^{-1}) was observed in samples of **7b** and was absent in **7a** when both samples were analyzed as powders by ATR IR spectroscopy (Figure S4.22). Additional evidence that Cys thiol conjugation had proceeded is provided by the disappearance of a free S-H stretch (2454-2545 cm^{-1}) in the spectrum of **7b** compared to the spectrum of **7a** (Figure S4.22). The spectroscopic techniques outlined above unequivocally confirm successful B-S bond formation using **1** and unprotected peptides containing Cys residues.

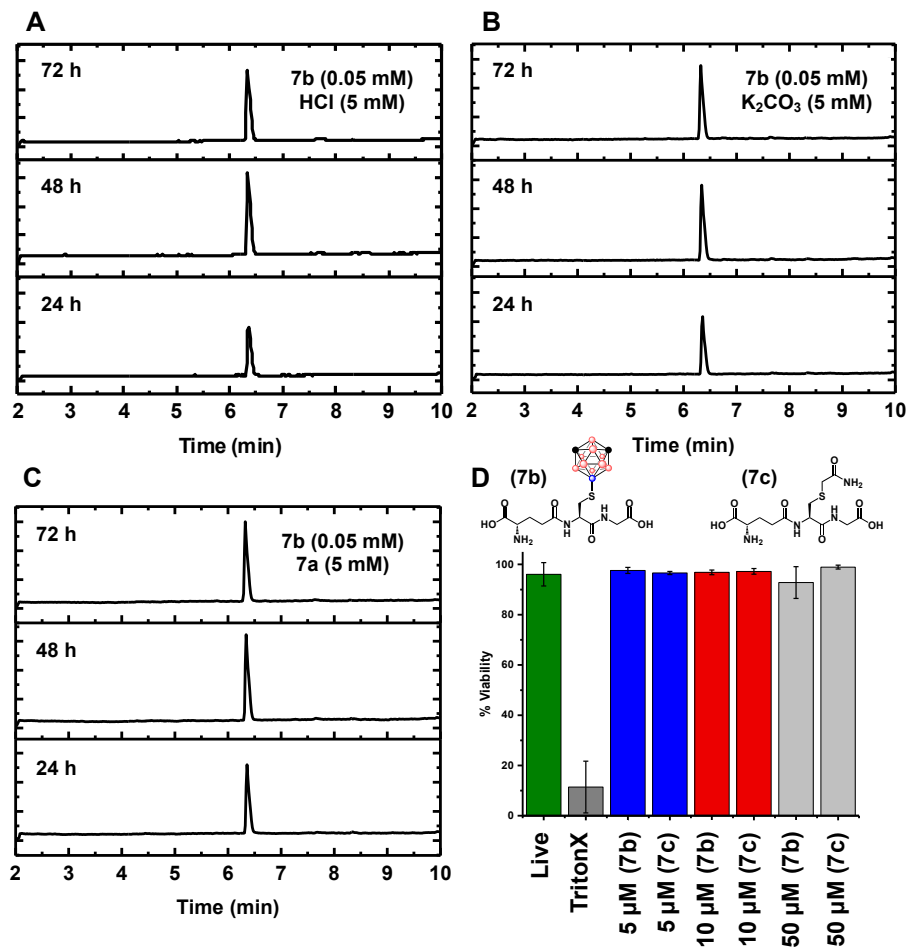


Figure 4.3: LC-MS traces of **7b** incubated with 100 excess **A**: hydrochloric acid **B**: potassium carbonate and **C**: **7a** after 24 hrs at r.t. followed by 48 and 72 hrs at 37 °C (See SI Section VII for full details). **D**: The % cell viability assessed after four-hour incubation of **7b** and **7c** with Chinese Hamster Ovarian (CHO) cells at 5 μM, 10 μM and 50 μM concentration of analyte (See SI Section IX for full details).

We then extended the bioconjugation to a more complex substrate, DARPin (designed ankyrin repeat protein), which has been previously shown to successfully undergo Cys arylation with various organometallic reagents.^{17,19} After treatment of DARPin with excess **1** for 6.5 hr, a deconvoluted mass consistent with complete DARPin borylation was observed by LCMS (Figure S4.23). The capacity to fully conjugate a protein target further highlights the potential of this Pt-

mediated route to transfer carboranyl clusters directly to large biomacromolecules at micromolar concentrations.

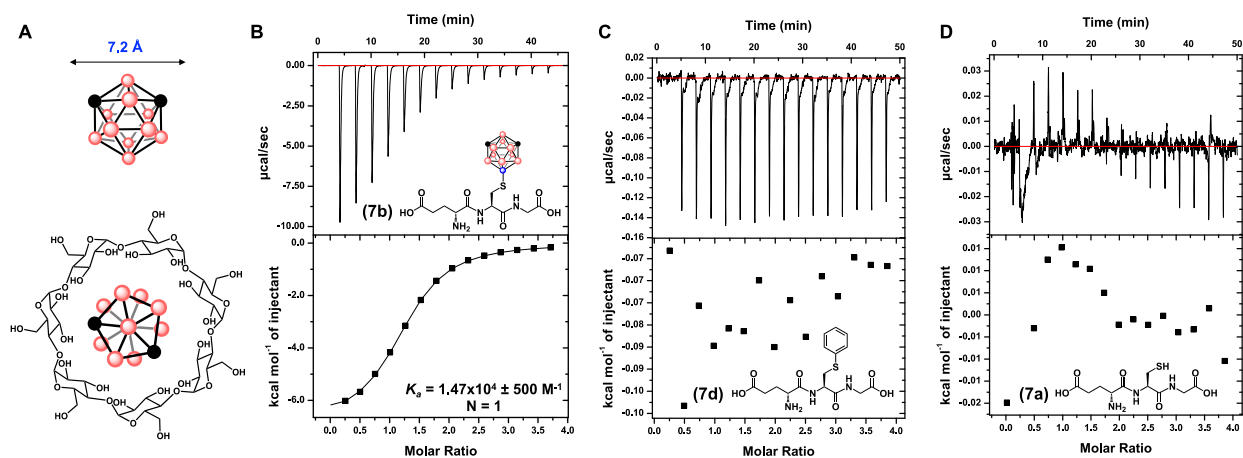


Figure 4.4 A: Representation of the inclusion complex formed between *m*-carborane and β-cyclodextrin.^{53,54} **B:** ITC binding plot for carboranylated glutathione and β-cyclodextrin to yield an association constant ($K_a = 1.47 \times 10^4 \pm 500 \text{ M}^{-1}$) and binding stoichiometry ($N = 1$). **C:** ITC binding plot for phenyl-glutathione and β-cyclodextrin. **D:** ITC binding plot for unmodified glutathione and β-cyclodextrin.

Next, we evaluated the stability of the B-S bond using **7b** as a model Cys-borylated peptide. Specifically, we assessed the fidelity of **7b** towards an acidic environment with a pH of 2.3 as this value falls within the normal pH range for stomach acid (pH= 1-3).³⁷ Sample of **7b** (0.05 mM) was incubated in the presence of hydrochloric acid (5 mM) at 25 °C and 37 °C for 72 hours (Figure 4.3A). No fragmentation was observed by LC-MS analysis of the mixture, indicating the S-B bond within **7b** stays intact at pH 2.3 under the timeframe of the experiment. Further, stability towards highly acidic environments suggests Cys-boryl conjugates could be compatible with harsh reagents used normally to cleave synthesized peptides from solid supports.²ⁱ To probe this hypothesis, we

treated a model peptide bound to Rink amide resin with excess **1** under buffered conditions for 1.5 hr (SI Figure S4.24). Resin was then isolated and peptide was globally cleaved using a standard solution of trifluoroacetic acid, water and triisopropyl silane (90%, 5%, 5% v/v) (SI Section VIII). Full conversion of Cys-borylated peptide was observed by LC-MS (SI Figure S4.24) indicating the bioconjugation could be also successfully applied to peptides appended to the solid supports. After assessment of stability towards acid, we probed the resistance of **7b** towards basic conditions. While intracellular pH remains close to neutral, published reports suggest alkaline microenvironments could be important in cellular signaling.³⁸ To rigorously determine the tolerance of Cys-borylated peptides towards base, we incubated **7b** at pH 11, a significantly more alkaline environment than would be anticipated for human cells. Sample of **7b** (0.05 mM) was incubated in the presence of potassium carbonate (5 mM) at 25 °C and 37 °C for 72 hours. No fragmentation was observed by LC-MS analysis of the mixture, indicating the stability of the S-B bond within **7b** (Figure 4.3B). Finally, we evaluated the stability of **7b** towards external thiol source. Glutathione (**7a**) was selected as it represents the most abundant non-protein source of thiol in eukaryotic cells with intracellular concentrations ranging from 1-10 mM.³⁹ Sample of **7b** (0.05 mM) was incubated in the presence of **7a** (5 mM) at 25 °C and 37 °C for 72 hours. No fragmentation was observed by LC-MS analysis of the mixture, indicating the S-B bond within **7b** does not undergo thiol exchange chemistry in the presence of large excess of external thiol (Figure 4.3C). Importantly, this stability towards external thiol is in contrast to classical Cys-based bioconjugation tools that employ Michael acceptors which often undergo retro-Michael addition when subjected to the presence of other thiol substrates.¹ Altogether, the stability of **7b** demonstrated herein suggests the S-B bond within Cys-borylated peptides can be bioorthogonal towards harsh biological milieu.

After confirming the stability of these constructs, we decided to evaluate the toxicity of Cys-borylated peptides towards Chinese Hamster Ovarian (CHO) cells using **7b** as a model peptide. As Pt(II) complexes have well described toxicity⁴⁰, we first assessed the efficiency of the purification method towards removing all metal-based byproducts. ICP-AES analysis of **7b** purified by reversed-phase HPLC indicated >99.9% platinum content had been removed (See SI Section II, Figure S4.1). Four-hour incubation of pure, isolated **7b** with CHO cells resulted in no appreciable toxicity up to 50 μM (Figure 4.3D). As a control sample, acetamide-glutathione (**7c**) was also incubated under the same conditions and exhibited no appreciable toxicity up to 50 μM (Figure 4.3D). The similar cell viability profiles for Cys-boryl glutathione and Cys-acetamide glutathione suggest no inherent cytotoxicity is added through forging a B-S bond by appending a boron cluster to unprotected peptides.

Few post translational modifications are competent towards the chemoselective transfer of bulky substrates containing large cone angles directly at amino acid sites. A rare example was demonstrated independently by both Park⁴¹ and Davis⁴² who prepared *tert*-Leu residues via dehydroalanine; however, the bioconjugates formed are racemates. The present strategy offers the first organometallic-based route towards unprotected peptide modification with a highly bulky moiety that does not alter the local stereochemistry, affording unique opportunities to assess the role steric encumbering at amino acid sites has upon downstream peptidic properties. Specifically, we probed the capacity of Cys-boryl peptides to participate in receptor binding by titrating **7b** as a model peptide to β -cyclodextrin, a sugar macrocycle which is widely used in catalysis, analytical separation and solubilization.⁴³ Isothermal titration calorimetry (ITC) experiment was carried out where peptide **7b** (10 mM) was titrated to β -cyclodextrin (0.25 mM) in an aqueous buffered solution at pH 3.4 revealing a binding stoichiometry ($N = 1$) and an association constant ($K_a = 1.47$

$\times 10^4 \pm 500 \text{ M}^{-1}$) (Figure 4.4A and 4.4B). The approximated binding stoichiometry of $N=1$ is consistent with a 1:1 **7b**– β -cyclodextrin inclusion complex promoted by the chaotropic properties of the cluster cage inserting into the macrocycle cavity.^{44,45} The observed K_d is an order of magnitude higher than was observed between unmodified *m*-carborane and β -cyclodextrin when measured by a displacement binding technique⁴⁶, which could be attributed to the enhanced solubility of **7b** over unmodified *m*-carborane in aqueous media. Cys-modified S-phenyl glutathione (**7d**, Figure 4.4C) and **7a** (Figure 4.4D) were used as controls and did not exhibit any appreciable binding affinity to β -cyclodextrin by ITC under the same measurement conditions. These controls highlight the receptor specificity and the capacity of borylation to engender a unique binding profile between **7b** and a macrocyclic sugar.

Finally, we evaluated the stability of Cys-boryl peptides towards a broadly acting serine protease, Proteinase K. Specifically, Cys-boryl peptide **2b** was chosen as a model substrate owing to the many aliphatic amino acid residues in the sequence which are cleavable by Proteinase K.⁴⁶ We envisaged **2b** might resist the activity of Proteinase K to a higher degree than **2a** owing to the steric hindrance of the carboranyl group positioned proximally to the peptide backbone thereby blocking access to cleavable residues. To test this hypothesis, **2b** was incubated with Proteinase K for 5 min at 60 °C in the presence of Tris•HCl buffer (50 mM, pH=8.2) and CaCl₂ (5 mM). After treatment, $45 \pm 1\%$ **2b** remained intact as assessed by integration of the peak compared to integration of the internal standard (Table 4.1, Entry G). In contrast, no intact peptide remained when **2a** was subjected to the same reaction conditions (Table 4.1, Entry A), indicating Cys-borylation is competent towards inhibiting the action of Proteinase K within this timeframe. We then subjected Cys-aryl peptide **2c** to Proteinase K treatment for 5 min at 60 °C in the presence of buffer (50 mM) and CaCl₂ (5 mM) (Table 4.1, Entry D). No intact peptide was observed under

these conditions, suggesting inhibition of proteolytic degradation is unique to Cys-boryl conjugates compared to aryl-based congeners.

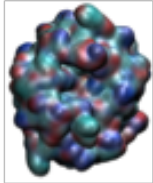
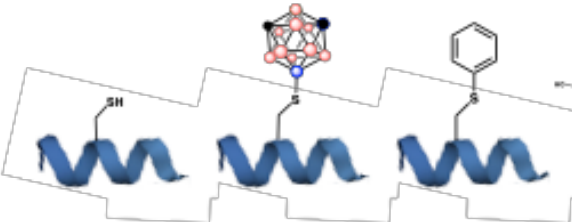
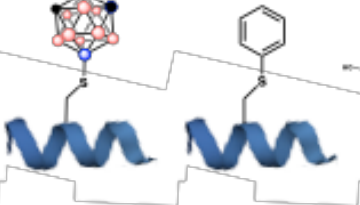
Entry	Proteinase K	Unmodified Peptide (2a)	Borylated Peptide (2b)	Arylated Peptide (2c)	β -cyclodextrin	% Peptide Intact*
						
A	+	+	-	-	-	0
B	+	+	-	-	+	0
C	-	-	-	+	-	100
D	+	-	-	+	-	0
E	+	-	-	+	+	0
F	-	-	+	-	-	100
G	+	-	+	-	-	45 ± 1
H	+	-	+	-	+	70 ± 10

Table 4.1: The reaction schemes and the observed corresponding degradation of **2a**, **2b** and **2c** with Proteinase K under various conditions.

To extend the steric hindrance surrounding the Cys moiety, we next subjected the **2b**- β -cyclodextrin inclusion complex to Proteinase K treatment (see SI for further details on the characterization of **2b**- β -cyclodextrin). The complex **2b**- β -cyclodextrin was heated for 5 min at 60 °C in the presence of buffered Proteinase K (Tris•HCl, 50 mM, pH=8.2) and CaCl₂ (5 mM). After this treatment, 70 ± 10% intact **2b** remained (Table 4.1, Entry H). Importantly, incubation of **2a** and **2c** with β -cyclodextrin prior to treatment with the same Proteinase K reaction conditions resulted in full degradation (Table 4.1, Entries B and E), indicating the presence of β -cyclodextrin

alone is insufficient towards inhibiting degradation. Overall, these experiments suggest that Cys-borylation can render peptides more proteolytically stable.

Molecular dynamics (MD) simulations were used to elucidate possible nature of the stability enhancement towards proteolysis. MD simulations of **2a**, **2b** and **2c** with Proteinase K demonstrated stable binding of all peptides to the reported substrate recognition site⁴⁷ by two segments, Gly100 to Tyr104 and Ser132 to Gly136. A second binding pocket (Figure 4.5A) formed by Gly134-Gly135-Gly-136 and Gly160-Asn161-Asn162 was identified for the unique capacity to bind the carborane of **2b** as a result of B-H···H-N dihydrogen⁴⁸ and C-H···O or C-H···N hydrogen bonding interactions²⁷ (Figure 4.5B). This binding might prevent the peptide from approaching the Asp39-His69-Ser224 catalytic triad, since **2b** was on average 2.12 Å further away from the catalytic triad than **2a** over the entire simulation timeframe (Figure 4.5C). Importantly, **2c** did not exhibit stable binding to the pocket formed by Gly134-Gly135-Gly-136 and Gly160-Asn161-Asn162 (Figure 4.5D) indicating the proteolytic protection is unique to Cys-borylation and is likely a result of placing a sterically encumbering functional group like carborane in close proximity to the polypeptide chain.

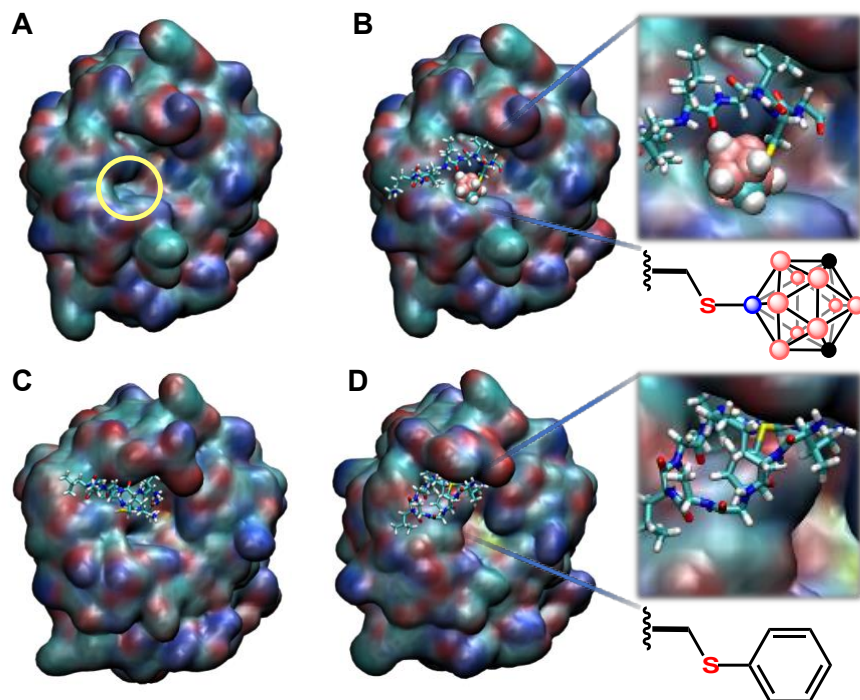


Figure 4.5: Molecular dynamics simulations of **A:** the secondary binding pocket identified as an important docking site **B:** **2b** binding with Proteinase K, **C:** **2a** binding with Proteinase K and **D:** **2c** binding with Proteinase K at 120 ns of equilibration. Proteinase K is represented using QuickSurf representation in VMD.

While Cys-borylation can render peptides more resistant towards proteolytic degradation, we wondered whether one can design hybrid agents with preserved binding capabilities to the protein target. To probe protein binding, we designed a model peptide (**8a**) containing a Ile-Tyr-Pro sequence which was previously identified as active towards inhibiting the activity of angiotensin-converting enzyme (ACE)⁴⁹, an important protein class implicated in the regulation of blood pressure and, recently, SARS-CoV-2 infection.⁵⁰ Specifically, at 5 μM unmodified **8a** and Cys-borylated **8b** were found to inhibit the activity of ACE by $24 \pm 5\%$ and $17 \pm 4\%$, respectively (See SI Section XII). Increasing the concentration of **8a** and **8b** to 50 μM enhanced the inhibition

of ACE activity by $54 \pm 7\%$ and $52 \pm 1\%$, respectively (See SI Section XII). The observed similarity in rates of inhibition between **8a** and **8b** suggests that Cys-borylation could maintain binding efficacy of the therapeutically relevant peptides while at the same time enhancing their proteolytic stability.

Conclusion and Outlook

In conclusion, an organometallic strategy for borylating Cys residues within unprotected peptide sequences and a model protein has been demonstrated. This work significantly expands our fundamental ability to construct new bioconjugates via a Cys residue by introducing a new room-temperature boron-sulfur forming pathway in unprotected peptides. Importantly, Cys-borylation can engender stable hybrid peptides featuring unique recognition and binding properties towards a macrocyclic sugar as well as render the resulting peptides more proteolytically stable while maintaining their binding affinity towards a protein target. This work further demonstrates the growing importance of organometallic chemistry in the field of bioconjugation,⁵¹⁻⁶⁰ where a designer post-translational synthetic modification can forge a chemoselective delivery of a sterically encumbering, abiotic functional group (e.g., carborane) directly to a native amino acid residue in a complex biomolecule.

References

1. Hermanson, G. T. *Bioconjugate Techniques*, 3rd ed.; Academic Press: San Diego, CA, 2013.
2. Recent representative reviews on general methods: (a) Stephanopoulos, N. & Francis, M. B. Choosing an Effective Protein Bioconjugation Strategy. *Nature Chem. Bio.* **2011**, *7*, 876-884. (b) McKay, C. S. & Finn, M. G. Click Chemistry in Complex Mixtures: Biorthogonal Bioconjugation. *Chem. Biol.* **2014**, *21*, 1075-1101. (c) Boutureira, O. & Bernardes, G. J. L. Advances in Chemical Protein Modification. *Chem. Rev.* **2015**, *115*, 2174-2195. (d)

- Albaba, B. & Metzler-Nolte, N. Organometallic-Peptide Bioconjugates: Synthetic Strategies and Medicinal Applications. *Chem. Rev.* **2016**, *116*, 11797-11839. (e) Hu, Q.-Y.; Berti, F.; Adamo, R. Towards the Next Generation of Biomedicines by Site-Selective Conjugation. *Chem. Soc. Rev.* **2016**, *45*, 1691-1719. (f) Vinogradova, E. V. Organometallic Chemical Biology: An Organometallic Approach to Bioconjugation. *Pure & Appl. Chem.* **2017**, *89*, 1619-1640. (g) Jbara, M.; Maity, S. K.; Brik, A. Palladium in the Chemical Synthesis and Modification of Proteins. *Angew. Chem., Int. Ed.* **2017**, *56*, 10644-10655. (h) Ohata, J.; Martin, S. C.; Ball, Z. T. Metal-Mediated Functionalization of Natural Peptides and Proteins: Panning for Bioconjugation Gold. *Angew. Chem., Int. Ed.* **2019**, *58*, 6176-6199. (i) Conibear, A. C.; Watson, E. E.; Payne, R. J.; Becker, C. F. W. Native Chemical Ligation in Protein Synthesis and Semi-Synthesis. *Chem. Soc. Rev.* **2019**, *47*, 9046-9068. (j) Isenegger, P. G. & Davis, B. G. Concepts of catalysis in site-selective protein modifications. *J. Am. Chem. Soc.* **2020**, *141*, 8005-8013. (k) Latocheski, E.; Dal Forno, G. M.; Ferreira, T. M.; Oliveira, B. L.; Bernardes, G. J. L.; Domingos, J. B. Mechanistic insights into transition metal-mediated bioorthogonal uncaging reactions *Chem. Soc. Rev.* **2020**, *49*, 7710-7729. (l) Szijj, P. A.; Kostadinova, K. A.; Spears, R. J.; Chudasama, V. Tyrosine Bioconjugation - An Emergent Alternative. *Org. Biomol. Chem.* **2020**, *18*, 9018-9028. (m) Patra, M. & Gasser, G. Organometallic Compounds: An Opportunity for Chemical Biology? *ChemBioChem* **2021**, *13*, 1232-1252.
3. Lavis, L. D. Teaching Old Dyes New Tricks: Biological Probes Built from Fluoresceins and Rhodamines. *Annu. Rev. Biochem.* **2017**, *86*, 825-43.
 4. Li, Y. Commonly Used Tag Combinations for Tandem Affinity Purification. *Biotechnol. Appl. Biochem.* **2010**, *55*, 73-83.

5. Liu, H.; Bolleddula, J.; Nichols, A.; Tang, L.; Zhao, Z.; Prakash, C. Metabolism of Bioconjugate Therapeutics: Why, When and How? *Drug Metab. Rev.* **2020**, *52*, 66-124.
6. Acar, H.; Ting, J. M.; Srivastava, S.; LaBelle, J. L.; Tirrell, M. V. Molecular Engineering Solutions for Therapeutic Peptide Delivery. *Chem. Soc. Rev.* **2017**, *46*, 6553-6569.
7. Chalker, J. M.; Bernardes, G. J. L.; Lin, Y. A.; Davis, B. G. Chemical Modification of Proteins at Cysteine: Opportunities in Chemistry and Biology. *Chem. Asian J.* **2009**, *4*, 630-640.
8. Masri, M. S. & Friedman, M. Protein Reactions with Methyl and Ethyl Vinyl Sulfones. *J. Protein Chem.* **1988**, *7*, 49-54.
9. Morales-Sanfrutos, J.; Lopez-Jaramillo, J.; Ortega-Muñoz, M.; Megia-Fernandez, A.; Perez-Balderas, F.; Hernandez-Mateo, F.; Santoyo-Gonzales, F. Vinyl Sulfone: a Versatile Function for Simple Bioconjugation and Immobilization. *Org. Biomol. Chem.* **2010**, *8*, 667-675.
10. Spokoyny, A. M.; Zou, Y.; Ling, J. J.; Yu, H.; Lin, Y.-S.; Pentelute, B. L. A Perfluoroaryl-Cysteine S_NAr Chemistry Approach to Unprotected Peptide Stapling. *J. Am. Chem. Soc.* **2013**, *135*, 5946-5949.
11. Kalhor-Monfared, S.; Jafari, M. R.; Patterson, J. T.; Kitov, P. I.; Dwyer, J. J.; Nuss, J. M.; Derda, R. Rapid Biocompatible Macrocyclization of Peptides with Decafluorodiphenylsulfone. *Chem. Sci.* **2016**, *7*, 3785-3790.
12. Valkevich, E. M.; Guenette, R. G.; Sanchez, N. A.; Chen, Y.-C.; Ge, Y.; Strieter, E. R. Forging Isopeptide Bonds Using Thiol-Ene Chemistry: Site-Specific Coupling of Ubiquitin Molecules for Studying the Activity of Isopeptidases. *J. Am. Chem. Soc.* **2012**, *134*, 6916-6919.

13. Conte, M. L.; Staderini, S.; Marra, A.; Sanchez-Navarro, M.; Davis, B. G.; Dondoni, A. Multi-molecule Reaction of Serum Albumin Can Occur Through Thiol-yne Coupling. *Chem. Commun.* **2011**, *47*, 11086-11088.
14. Bottechia, C.; Rubens, M.; Gunnoo, S. B.; Hessel, V.; Madder, A.; Noël, T. Visible-Light-Mediated Selective Arylation of Cysteine in Batch and Flow. *Angew. Chem., Int. Ed.* **2017**, *56*, 12702-12707.
15. Vara, B. A.; Li, X.; Berritt, S.; Walters, C. R.; Petersson, E. J.; Molander, G. A. Scalable Thioarylation of Unprotected Peptides and Biomolecules Under Ni/Photoredox Catalysis. *Chem. Sci.* **2018**, *9*, 336-344.
16. Chan, A. O.-Y.; Tsai, J. L.-L.; Lo, V. K.-Y.; Li, L.-G.; Wong, M.-K.; Che, C.-M. Gold-mediated Selective Cysteine Modification of Peptides Using Allenes. *Chem. Commun.* **2013**, *49*, 1428-1430.
17. Vinogradova, E. V.; Zhang, C.; Spokoyny, A. M.; Pentelute, B. L.; Buchwald, S. L. Organometallic Palladium Reagents for Cysteine Bioconjugation. *Nature* **2015**, *526*, 687-691.
18. Kung, K. K.-Y.; Ko, H.-M.; Cui, J.-F.; Chong, H.-C.; Leung, Y.-C.; Wong, M.-K. Cyclometalated Gold(III) Complexes for Chemoselective Cysteine Modification via Ligand Controlled C-S Bond-forming Reductive Elimination. *Chem. Commun.* **2014**, *50*, 11899-11902.
19. Messina, M. S.; Stauber, J. M.; Waddington, M. A.; Rheingold, A. L.; Maynard, H. D.; Spokoyny, A. M. Organometallic Gold(III) Reagents for Cysteine Arylation. *J. Am. Chem. Soc.* **2018**, *140*, 7065-7069.

20. Yang, Z.; Zhong, M.; Ma, X.; Nijesh, K.; De, S.; Parameswaran, P.; Roesky, H. W. An Aluminum Dihydride Working as a Catalyst in Hydroboration and Dehydrocoupling. *J. Am. Chem. Soc.* **2016**, *138*, 2548-2551.
21. Fernández-Salas, J. A.; Manzini, S.; Nolan, S. P. Efficient Ruthenium-Catalysed S-S, S-Si and S-B Bond Forming Reactions. *Chem. Commun.* **2013**, *49*, 5829-5831.
22. Romero, E. A.; Peltier, J. L.; Jazzar, R.; Bertrand, G. Catalyst-free Dehydrocoupling of Amines, Alcohols, and Thiols with Pinacol Borane and 9-Borabicyclononane (9-BBN). *Chem. Commun.* **2016**, *52*, 10563-10565.
23. Rochette, É.; Boutin, H.; Fontaine, F.-G. Frustrated Lewis Pair Catalyzed S-H Bond Borylation. *Organometallics* **2017**, *36*, 2870-2876.
24. Al-Shuaeeb, R. A. A.; Kolodych, S.; Koniev, O.; Delacroix, S.; Erb, S.; Nicoläy, S.; Cintrat, J.-C.; Brion, J.; Cianféroni, S.; Alami, M.; Wagner, A.; Messaoudi, S. Palladium-Catalyzed Chemoselective and Biocompatible Functionalization of Cysteine-Containing Molecules at Room Temperature. *Chem. Eur. J.* **2016**, *22*, 11365-11370.
25. Willwacher, J.; Raj, R.; Mohammed, S.; Davis, B. G. Selective Metal-Site-Guided Arylation of Proteins. *J. Am. Chem. Soc.* **2016**, *138*, 8678-8681.
26. Hanaya, K.; Ohata, J.; Miller, M. K.; Mangubat-Medina, A. E.; Swierczynski, M. J.; Yang, D. C.; Rosenthal, R. M.; Popp, B. V.; Ball, Z. T. Rapid Nickel(II)-Promoted Cysteine S-Arylation with Arylboronic Acids. *Chem. Commun.* **2019**, *55*, 2841-2844.
27. Scholz, M. & Hey-Hawkins, E. Carbaboranes as Pharmacophores: Properties, Synthesis, and Application Strategies. *Chem. Rev.* **2011**, *111*, 7035-7062.
28. Leitao, E. M.; Jurca, T.; Manners, I. Catalysis in Service of Main Group Chemistry Offers a Versatile Approach to *p*-Block Molecules and Materials. *Nature Chem.* **2013**, *5*, 817-829.

29. Keener, M.; Hunt, C.; Carroll, T. G.; Kampel, V.; Dobrovetsky, R.; Hayton, T. W.; Ménard, G. Redox-Switchable Carboranes for Uranium Capture and Release. *Nature* **2020**, *577*, 652-655.
30. Fisher, S. P.; Tomich, A. W.; Lovera, S. O.; Kleinsasser, J. F.; Guo, J.; Asay, M. J.; Nelson, H. M.; Lavallo, V. Nonclassical Applications of *closo*-Carborane Anions: From Main Group Chemistry and Catalysis to Energy Storage. *Chem. Rev.* **2019**, *119*, 8262-8290.
31. Quan, Y. & Xie, Z. Controlled Functionalization of *o*-Carborane via Transition Metal Catalyzed B-H Activation. *Chem. Rev.* **2019**, *48*, 3660-3673.
32. Lin, F.; Yu, J.-L.; Shen, Y.; Zhang, S.-Q.; Spingler, B.; Liu, J.; Hong, X.; Duttwyler, S. Palladium-Catalyzed Selective Five-Fold Cascade Arylation of the 12-Vertex Monocarborane Anion by B-H Activation. *J. Am. Chem. Soc.* **2018**, *140*, 13798-13807.
33. Yin, Y.; Ochi, N.; Craven, T. W.; Baker, D.; Takigawa, N.; Suga, H. De Novo Carborane-Containing Macrocyclic Peptides Targeting Human Epidermal Growth Factor Receptor. *J. Am. Chem. Soc.* **2019**, *141*, 19193-19197.
34. Saleh, L. M. A.; Dziejczak, R. M.; Khan, S. I.; Spokoyny, A. M. Forging Unsupported Metal-Boryl Bonds with Icosahedral Carboranes. *Chem. Eur. J.* **2016**, *22*, 8466-8470.
35. Pearson, R. G. The Principle of Maximum Hardness. *Acc. Chem. Res.* **1993**, *26*, 250-255.
36. Dedon, P. C. & Borch, R. F. Characterization of the Reactions of Platinum Antitumor Agents with Biologic and Nonbiologic Sulfur-Containing Nucleophiles. *Biochem. Pharmacol.* **1987**, *36*, 1955-1964.
37. Machen, T. E. & Paradiso, A. M. Regulation of Intracellular pH in the Stomach. *Ann. Rev. Physiol.* **1987**, *49*, 19-33.

38. Ro, H.-A. & Carson, J. H. pH Microdomains in Oligodendrocytes. *J. Biol. Chem.* **2004**, *279*, 37115-37123.
39. Forman, H. J.; Zhang, H.; Rinna, A. Glutathione: Overview of its Protective Roles, Measurement, and Biosynthesis. *Mol. Aspects Med.* **2009**, *30*, 1-12.
40. Hartmann, J. T. & Lipp, H. Toxicity of Platinum Compounds. *Expert Opin. Pharmacol.* **2003**, *6*, 889-901.
41. Yang, A.; Ha, S.; Ahn, J.; Kim, R.; Kim, S.; Lee, Y.; Kim, J.; Söll, D.; Lee, H.-Y.; Park, H.-S. A Chemical Biology Route to Site-Specific Authentic Protein Modifications. *Science* **2016**, *354*, 623-626.
42. Wright, T. H.; Bower, B. J.; Chalker, J. M.; Bernardes, G. J. L.; Wiewiora, R.; Ng, W.-L.; Raj, R.; Faulkner, S.; Vallée, M. R. J.; Phantumrithiwath, A.; Coleman, O. D.; Thézénas, M.-L.; Khan, M.; Galan, S. R. G.; Lercher, L.; Schombs, M. W.; Gerstberger, S.; Palm-Espling, M. E.; Baldwin, A. J.; Kessler, B. M.; Claridge, T. D. W.; Mohammed, S.; Davis, B. G. Posttranslational Mutagenesis: A Chemical Strategy for Exploring Protein Side-Chain Diversity. *Science* **2016**, *354*, aag1465-1 – aag1465-11.
43. Singh, M.; Sharma, R.; Banerjess, U. C. Biotechnological Applications of Cyclodextrins. *Biotechnol. Adv.* **2002**, *20*, 341-359.
44. Assaf, K. I. & Nau, W. M. The Chaotropic Effect as an Assembly Motif in Chemistry. *Angew. Chem., Int. Ed.* **2018**, *57*, 13968-13981.
45. Sadrerafi, K.; Moore, E. E.; Lee, M. W. Association Constant of β -cyclodextrin with Carboranes, Adamantane, and Their Derivatives Using Displacement Binding Technique. *J. Incl. Phenom. Macrocycl. Chem.* **2015**, *83*, 159-166.

46. Ebeling, W.; Hennrich, N.; Klockow, M.; Metz, H.; Orth, H. D.; Lang, H. Proteinase K From *Tritirachium Album* Limber. *Eur. J. Biochem.* **1974**, *47*, 91-97.
47. Wolfs, W. M.; Bajorath, J.; Muller, A.; Raghunathan, S.; Singh, T. P.; Hinrichs, W.; Saenger, W. Inhibition of Proteinase K by Methoxysuccinyl-Ala-Ala-Pro-Ala-Chloromethyl Ketone. *J. Biol. Chem.* **1991**, *266*, 17695-17699.
48. Fanfrlík, J.; Lepšík, M.; Horinek, D.; Havlas, Z.; Hobza, P. Interaction of Carboranes with Biomolecules: Formation of Dihydrogen Bonds. *ChemPhysChem* **2006**, *7*, 1100-1105.
49. Kohmura, M.; Nio, N.; Kubo, K.; Minoshima, Y.; Munekata, E.; Ariyoshi, Y. Inhibition of Angiotensin-Converting Enzyme by Synthetic Peptides of Human β -Casein. *Agric. Biol. Chem.* **1989**, *53*, 2107-2114.
50. Ghafouri-Farda, S.; Noroozib, R.; Omrania, M. D.; Branickib, W.; Pośpiechb, E.; Sayada, A.; Pyrcb, K.; Łabajb, P. P.; Vafaec, R.; Taherid, M.; Sanak, M. Angiotensin Converting Enzyme: A review on Expression Profile and its Association with Human Disorders with Special Focus on SARS-CoV-2 Infection. *Vascul. Pharmacol.* **2020**, *130*, 106680.
51. Antos, J. M.; McFarland, J. M.; Iavarone, A. T.; Francis, M. B. Chemoselective Tryptophan Labeling with Rhodium Carbenoids at Mild pH. *J. Am. Chem. Soc.* **2009**, *131*, 6301-6308.
52. Schischko, A.; Ren, H.; Kaplaneris, N.; Ackermann, L. Bioorthogonal Diversification of Peptides through Selective Ruthenium(II) Catalyed C-H Activation. *Angew. Chem., Int. Ed.* **2017**, *129*, 1598-1602.
53. Bauer, M.; Wang, W.; Lorion, M. M.; Dong, C.; Ackermann, L. Internal Peptide Late-Stage Diversification: Peptide-Isosteric Triazoles for Primary and Secondary C(sp³)-H Activation. *Angew. Chem., Int. Ed.* **2018**, *57*, 203-207.

54. Lee, H. G.; Lautrette, G.; Pentelute, B. L.; Buchwald, S. L. Palladium-Mediated Arylation of Lysine in Unprotected Peptides. *Angew. Chem., Int. Ed.* **2017**, *56*, 3177-3181.
55. Kubota, K.; Dai, P.; Pentelute, B. L.; Buchwald, S. L. Palladium Oxidative Addition Complexes for Peptide and Protein Cross-Linking. *J. Am. Chem. Soc.* **2018**, *140*, 3128-3133.
56. Stenton, B. J.; Oliveira, B. L.; Matos, M. J.; Sinatra, L.; Bernardes, G. J. L. A Thioether-Directed Palladium-Cleavable Linker for Targeted Biorthogonal Drug Decaging. *Chem. Sci.* **2018**, *9*, 4184-4189.
57. Zhao, W.; Lee, H. G.; Buchwald, S. L.; Hooker, J. M. Direct ¹¹CN-Labeling of Unprotected Peptides via Palladium-Mediated Sequential Cross-Coupling Reactions. *J. Am. Chem. Soc.* **2017**, *139*, 7152-7155.
58. Schlatzer, T.; Kriegesmann, J.; Schroder, H.; Trobe, M.; Lembacher-Fadum, C.; Santner, S.; Kravchuk, A. V.; Becker, C. F. W.; Breinbauer, R. Labeling and Natural Post-Translational Modification of Peptides and Proteins via Chemoselective Pd-Catalyzed Prenylation of Cysteine. *J. Am. Chem. Soc.* **2019**, *141*, 14931-14937.
59. Stauber, J. M.; Qian, E. A.; Han, Y.; Rheingold, A. L.; Kral, P.; Fujita, D.; Spokoyny, A. M. An Organometallic Strategy for Assembling Atomically Precise Hybrid Nanomaterials. *J. Am. Chem. Soc.* **2020**, *142*, 327-334.
60. Dhanjee, H. H.; Saebi, A.; Buslov, I.; Loftis, A. R.; Buchwald, S. L.; Pentelute, B. L. Protein-Protein Cross-Coupling via Palladium-Protein Oxidative Addition from Cysteine Residues. *J. Am. Chem. Soc.* **2020**, *142*, 9124-9129.

Supporting Information

I. Materials and Methods

Materials:

All reagents were purchased from Sigma Aldrich, Strem Chemicals, ChemImpex, Oakwood Chemicals, TCI, Fisher Scientific, Carbosynth, Combi-Blocks, or Alfa Aesar, and used as received unless otherwise noted. Solvents (acetone, acetonitrile (MeCN), diethyl ether (Et₂O), N,N-dimethylformamide (DMF)) were used as received without further purification unless otherwise specified. Milli-Q water was used for all experiments. Fisher Water Optima™ LC-MS Grade and Fisher Acetonitrile Optima™ LC-MS Grade were used exclusively for LC-MS mobile phase solvents. MilliQ water and Fisher Acetonitrile, gradient grade, ≥99.9% were used as mobile phases for HPLC. Deuterated solvents (CDCl₃, and D₂O) were obtained from Cambridge Isotope Laboratories and used as received. Trifluoroacetic acid (TFA, 99%) was purchased from EMD Millipore Corporation. Angiotensin converting enzyme derived from rabbit lung (0.25 units/mL) and N-[3-(2-Furyl)acryloyl]-L-phenylalanyl-glycyl-glycine (FA-PGG) were purchased from Sigma Aldrich.

Methods:

Peptide Synthesis:

Peptide synthesis vessels (CG-1860) containing a coarse porosity fritted glass resin support and polytetrafluoroethylene (PTFE) cap were purchased from Chemglass. All peptide vessel shaking (to ensure mixing during solid phase peptide synthesis) was performed using a Burrell Wrist Action Shaker (Model 75). Specific synthetic details are summarized in Section II. All peptides were stored at -20 °C prior to use.

Peptide Purification and Characterization:

All peptide purification was carried out on an Agilent Technologies 1260 Infinity II HPLC system equipped with an Agilent ZORBAX 300SB-C18 column (5 μ m, 9.4 \times 250 mm) using 0.1% TFA in water and 0.1% TFA in acetonitrile as the eluent. Specific methods are described in Section III. Samples were prepared by dissolution of 20-25 mg crude peptide in water (1 mL spiked with 0.1% TFA). The borylated peptide was separated from reaction byproducts by dissolution of the crude product (0.5-5 mg) in water (1 mL spiked with 0.1% TFA), filtered using a 0.2 μ m PTFE Pall syringe filter followed by purification by HPLC as described in Section III.

LC-MS analysis was utilized to assess efficiency of all bioconjugation reactions using an Agilent 6530 ESI-Q-TOF with an Agilent ZORBAX 300SB C18 column (5 μ m, 2.1 \times 150 mm) heated to 40 $^{\circ}$ C and an injection volume of 0.3 μ L. All mobile phase solvents were acidified with formic acid (0.1%).

LC-MS Method for Analysis of Peptide-Containing Samples:

Time (min)	Water %	Acetonitrile %	Flow (mL/min)	Max. Pressure (bar)
0.00	99.0	1.0	0.800	300.0
2.00	99.0	1.0	0.800	300.0
11.00	9.0	91.0	0.800	300.0
12.00	5.0	95.0	0.800	300.0

Table S4.1: LC-MS method used to characterize all peptides and products.

For all peptide-containing samples, the detector was switched on at 2 min, with the exception of **7a/7b**, **3a/3b** and **2b** when used in Proteinase K experiments (see Section IX). For these samples, the detector was switched on immediately when the run started. All samples were prepared by dissolution of the sample (0.1 mg/mL) in either water or acetonitrile spiked with 0.1% TFA. All

data were analyzed using the program mMass version 5.4.1.0. Masses were collected in positive mode and are reported as protonated species. All LC traces are plotted time against the total ion count (TIC); however, the y-axis is omitted for simplicity.

Protein Purification and Characterization

Protein was purified using Pall™ microsep advance centrifugal devices with omega membrane 3K. The sample was dissolved in water (5 mL) and centrifuged at 18,000 x g for 1 hr. After, the volume beneath the membrane was discarded and the reservoir above the membrane was refilled with a second aliquot of water (5 mL) for 1 hr. The process was repeated a third time until purified protein was isolated.

LC-MS analysis was utilized to assess efficiency of all bioconjugation reactions using an Agilent 6530 ESI-Q-TOF with an Agilent ZORBAX 300SB C3 column (3.5 μm, 3 × 150 mm) heated to 40 °C and an injection volume of 0.3 μL. All mobile phase solvents were acidified with formic acid (0.1%). All samples were prepared in water spiked with 0.1% TFA. Masses were collected in positive mode and deconvolution was conducted using Agilent Mass Hunter Qualitative Analysis software.

LC-MS Method for Analysis of Protein-Containing Samples:

Time (min)	Water %	Acetonitrile %	Flow (mL/min)	Max. Pressure (bar)
0.00	90.0	10.0	0.500	300.0
2.00	90.0	10.0	0.500	300.0
11.00	9.0	91.0	0.500	300.0
12.00	5.0	95.0	0.500	300.0

Table S2: LC-MS method used to characterize all peptides and products.

Tandem MS/MS

MS/MS was performed on purified peptide samples, both before and after borylation. Fragments before and after borylation were compared. MS/MS analysis was performed using a 30 eV collision energy and the method and fragment analysis were carried out using ProSight Lite software.

Infrared Radiation (IR)

All IR spectra were collected on a PerkinElmer UATR Two FT-IR spectrometer. PerkinElmer Spectrum Software version 10.4.4 was used to process all data. All spectra were collected on solid powders with background subtraction between samples.

NMR

All NMR spectra were obtained on a Bruker Avance 400 or a Bruker DRX 500 MHz broad band FT NMR spectrometer. ^1H and $^{13}\text{C}\{^1\text{H}\}$ NMR spectra were referenced to residual protio-solvent signals, and both ^{11}B and $^{11}\text{B}\{^1\text{H}\}$ NMR chemical shifts were referenced to $\text{BF}_3\cdot\text{Et}_2\text{O}$ (15% in CDCl_3 , δ 0.0 ppm).

Isothermal Titration Calorimetry

All titrations were performed on a GE MicroCal iTC 200 and analyzed on MicroCal Data Analysis software.

Internal Standard

For all reactions, the internal standard was prepared by alkylation of $\text{H}_2\text{N-VKGALGVCG-CONH}_2$ using iodoacetamide as described by Pentelute and Buchwald *et al.*¹ Internal standard ($\text{H}_2\text{N-VKGALGV}(\text{H}_2\text{NCOCH}_2\text{-})\text{CG-CONH}_2$) was added to the indicated reactions (See Section III and IV) after quenching.

Inductively Coupled Plasma Atomic Emission (ICP-AE)

ICP-AES data were obtained using a Shimadzu ICPE-9000 spectrometer. Prior to measurements, samples were diluted in 4% nitric acid (Trace Metal Grade, Fisher) and a calibration curve was obtained using a platinum standard solution (1 mg/mL, Sigma-Aldrich), and diluted to 50, 75, 100, and 200 ppb Pt with 4% nitric acid.

Organometallic Reagent Synthesis

$[(\text{Me-DalPhos})\text{AuCl}]_2\text{C}_6\text{H}_4[\text{SbF}_6]_2$ was prepared following a previously reported procedure.² $[\text{PtCl}(\text{PPh}_3)_2(9\text{-B-}m\text{-C}_2\text{B}_{10}\text{H}_{11})]$ was prepared according to procedures outlined by Spokoyny *et al.*³

Fluorescein Isothiocyanate (FITC) Labeling of Peptides

Peptide $\text{H}_2\text{N-FITC-}\beta\text{-ACGGA-CONH}_2$ was labeled with FITC following a procedure previously described.⁴

Buffers

Buffer for proteinase K experiments (Section IX) were adjusted with hydrochloric acid (50 mM) or sodium hydroxide (50 mM). All other aqueous buffers were adjusted with either potassium acetate (50 mM) or glacial acetic acid (50 mM) in MilliQ water.

Note on Calculation of Peptide Molecular Weight

For all peptides synthesized by solid phase synthesis, additional mass (114.02 g/mol) was added for each basic residue side chain as trifluoroacetate counterion balances the protonated basic residue.

Centrifugation

A Thermo (Sorvall) LEGEND RT+ centrifuge was utilized for all protein centrifugations. A Fisher Scientific accuSpin Micro 17 centrifuge was utilized for all peptide and CHO cell centrifugations.

Molecular Dynamics Simulations

Molecular dynamics (MD) simulations of **2a**, **2b** and **2c** solvated in 5 mM CaCl₂ aqueous solution was performed using NAMD⁵ where a TIP3P model⁶ was used to describe water and the CHARMM force field^{7,8} was used to parameterize the nonapeptide and the proteinase K (PDB ID: 3PRK⁹). Ab initio calculations were done with *Gaussian09*¹⁰ to determine unknown parameters for the carborane cluster. The carborane was optimized at the MP2/6-31g(d) level of theory, with partial charges derived with a CHELPG algorithm¹¹. Bonds, angles, and dihedrals force constants containing boron atoms were determined at the MP2/6-31g(d)//HF/6-31g level of theory with the VMD Force Field Toolkit plugin^{12,13}. The alpha-carbons of residues that are 10 residues away from the substrate recognition site, which constitutes of two segments, Gly100-Tyr104 and Ser132-Gly136, in proteinase K was constrained in a harmonic potential with force constant 0.8 kcal mol⁻¹ Å⁻². Nonbonded van der Waals interactions were modeled using Lennard-Jones potentials and electrostatic interactions were described by a Coulombic coupling, where the cutoff distance was 10 Å in both interactions. The Particle Mesh Ewald algorithm¹⁴ with a grid spacing of 1 Å was used to describe long-range electrostatic interactions. A Langevin dynamics with a damping coefficient of 0.1 ps⁻¹ was applied in the simulations, where the time step was 1 fs in all simulations. Each system is first minimized for 50,000 steps. Afterwards, it is heated to 300 K, with 1 K increments per 5 steps until the system reaches a temperature of 300 K. A canonical ensemble with a constant temperature and pressure (NPT, P = 1 bar, T = 300 K) was used with periodic boundary conditions applied in all directions.

II. Peptide Synthesis and Purification

The following general protocol was followed for all solid-phase peptide syntheses.

Preparation of Resin:

Rink amide resin (1.0 g, 0.44 mmol/g) was added to a 250 mL peptide synthesis vessel fitted with a coarse-porosity fritted glass resin support. Dimethylformamide (10 mL) was added to the vessel, and the mixture was shaken for a minimum of 1 h to allow the resin to swell. The resin was subsequently washed with DMF (5×10 mL).

First Deprotection:

A 20% solution of 4-methylpiperidine in DMF (10-15 mL/g of resin) was added to the vessel, and the mixture was shaken for 20 min. After shaking, the 4-methylpiperidine solution was removed and the resin was washed with DMF (1 x 10 mL). A fresh solution of 4-methylpiperidine in DMF (10-15 mL/g of resin) was added to the vessel, and the and the vessel was shaken for an additional 5 min. The resin was then washed with DMF (5×10 mL) to ensure complete removal of 4-methylpiperidine.

Amino Acid Coupling Conditions:

Amino acid (3 equiv to resin) and hexafluorophosphate benzotriazole tetramethyl uronium (HBTU, 2.9 equiv to resin) were dissolved in DMF (10 mL). N,N-Diisopropylethylamine (DIPEA, 6 equiv to resin) was then added to the mixture, and the solution was stirred for 1 min. This mixture was then added to the peptide synthesis vessel containing the resin, and the vessel was shaken for 45 min. After shaking, the solution was removed, and the resin was washed with DMF (5×10 mL) to ensure complete removal of excess amino acid, HBTU, and DIPEA.

Cysteine Coupling Conditions:

Cysteine coupling was performed following a procedure previously reported.¹⁵

Fmoc-Cys(Trt)-OH (3 equiv to resin), hexafluorophosphate azabenzotriazole tetramethyl uronium (HATU, 4 equiv to resin), and 1-hydroxy-7-azabenzotriazole (HOAt, 0.6 M in DMF, 4 equiv to resin) were combined in DMF (6 mL) and CH₂Cl₂ (6 mL). Once dissolved, 2,4,6-trimethylpyridine (4 equiv to resin) was added and the mixture stirred quickly (1-2 sec) and added to the resin. The mixture was shaken for 1 h. After shaking, the resin was washed with DMF (5 × 10 mL) to ensure the removal of excess Fmoc-Cys(Trt)-OH, HATU, and HOAt. After cysteine coupling, the normal protocol was followed.

Amino Acid Deprotection Conditions:

A 20% solution of 4-methylpiperidine in DMF (10-15 mL/g of resin) was added to the vessel and the mixture was shaken for 15 min. After shaking, the 4-methylpiperidine solution was removed and the resin was washed once with DMF (10 mL). A fresh solution of 4-methylpiperidine in DMF (10-15 mL/g of resin) was added to the vessel, and the mixture was shaken for an additional 5 min. The solution was removed, and the resin was washed with DMF (5 x 10 mL) to ensure the complete removal of 4-methylpiperidine.

Cleavage from Resin:

After the final deprotection, the resin was washed with EtOH (2 x 10 mL), followed by DCM (3 × 10 mL). The washed resin was transferred to a 50 mL round bottom flask equipped and a magnetic stir bar was added. Nitrogen gas was flowed over the open vessel for 5 min. A cleavage cocktail (20 mL) consisting of a 95:2.5:2.5 mixture of TFA:H₂O:TIPS (TIPS = triisopropylsilane) was added to the resin. The slurry was stirred for 3-4 hours under an atmosphere of nitrogen. Cleavage time was dependent on the amino acid composition of the peptide. Aliquots of the slurry were analyzed *via* LC-MS after filtration through a small pipette filter and dilution with water to

determine full removal of peptide protecting groups. After 3-4 h, the cleavage cocktail was filtered and the filtrate was concentrated under a stream of nitrogen until 1 mL remained. To this solution was added cold (-20 °C) diethyl ether, resulting in the precipitation of the crude peptide. The supernatant was removed and the crude peptide was collected and then dried under reduced pressure.

*It is important to use fresh TIPS. TIPS stored longer than two months is less effective.

All crude peptides were purified by reversed-phase HPLC (see HPLC methods). The pure fractions were combined and lyophilized. All crude and purified peptides were stored in sealed containers at -20 °C.

Cleavage from Resin for Peptide Containing Tryptophan (9a):

After the final deprotection, the resin was washed with EtOH (2 x 10 mL), followed by DCM (3 x 10 mL). The washed resin was transferred to a 25 mL round bottom flask equipped and a magnetic stir bar was added. Nitrogen gas was flowed over the open vessel for 5 min. A cleavage cocktail (20 mL) consisting of a 95:2.5:2.5 mixture of TFA:H₂O:EDT (EDT = 1,2-ethanedithiol) was added to the resin. The slurry was stirred for 3 hours under an atmosphere of nitrogen. Aliquots of the slurry were analyzed *via* LC-MS after filtration through a small pipette filter and dilution with water to determine full removal of peptide protecting groups. After 3 h, the cleavage cocktail was filtered and the filtrate was concentrated under a stream of nitrogen until 1 mL remained. To this solution was added cold (-20 °C) diethyl ether, resulting in the precipitation of the crude peptide. The supernatant was removed and the crude peptide was collected and then dried under reduced pressure.

HPLC Methods:

For instrumentation information see Section I. The following methods were used to purify both the unmodified and borylated peptides:

- A. Isocratic flush water (99%), acetonitrile (1%) for 5 min. Gradient from water (99%), acetonitrile (1%) to water (60%), acetonitrile (40%) from 5 to 45 min. Flush with 100% acetonitrile from min 45 to 48.
- B. Isocratic flush water (100%) for 5 min Gradient from water (100%), acetonitrile (0%) to water (90%), acetonitrile (10%) over 85 min. Flush with 100% acetonitrile from min 85 to 88.
- C. Isocratic flush water (99%), acetonitrile (1%) for 5 min. Gradient from water (99%), acetonitrile (1%) to water (40%), acetonitrile (60%) from 5 min to 80 min. Flush with 100% acetonitrile from min 80 to 83.
- D. Gradient from water (99%), acetonitrile (1%) to water (65%), acetonitrile (35%) over 5 min followed by gradient from water (65%), acetonitrile (35%) to water (40%), acetonitrile (60%) from 5 min to 85 min. Flush with 100% acetonitrile from min 85 to 91 min.
- E. Isocratic flush water (99%), acetonitrile (1%) for 5 min. Gradient from water (99%), acetonitrile (1%) to water (80%), acetonitrile (20%) from 5 to 85 min. Flush with 100% acetonitrile from min 85 to 88.

Sequence	Purification Method (unmodified)	Purification Method (borylated)
H ₂ N-g-ECG-CONH ₂	-	A
H ₂ N-DRKCAT-CONH ₂	A	A
H ₂ N-FITC-β-ACGGA-CONH ₂	C	C
H ₂ N-VKGALGVCG-CONH ₂	A	A
H ₂ N-GCGEVKEGCG-CONH ₂	B	A
H ₂ N-GSGEVKEGCG-CONH ₂	B	A
H ₂ N-SCQPQLIYP-CONH ₂	D	D
H ₂ N-GCAWNHA-CONH ₂	E	C

Table S4.3: Summary of purified peptides and HPLC purification methods.

Inductively Coupled Plasma Atomic Emission Spectroscopy (ICP-AES)

In order to assess the removal of Pt-based byproducts, ICP-AES of HPLC-purified peptide (**7b**) was conducted (see section IV for borylation of glutathione). All standards and samples were measured with a 30 sec exposure time and conducted in triplicate. An R^2 value of 1.000 was obtained and less than 50 ppb Pt was detected representing >99.9% removal of Pt by HPLC purification.

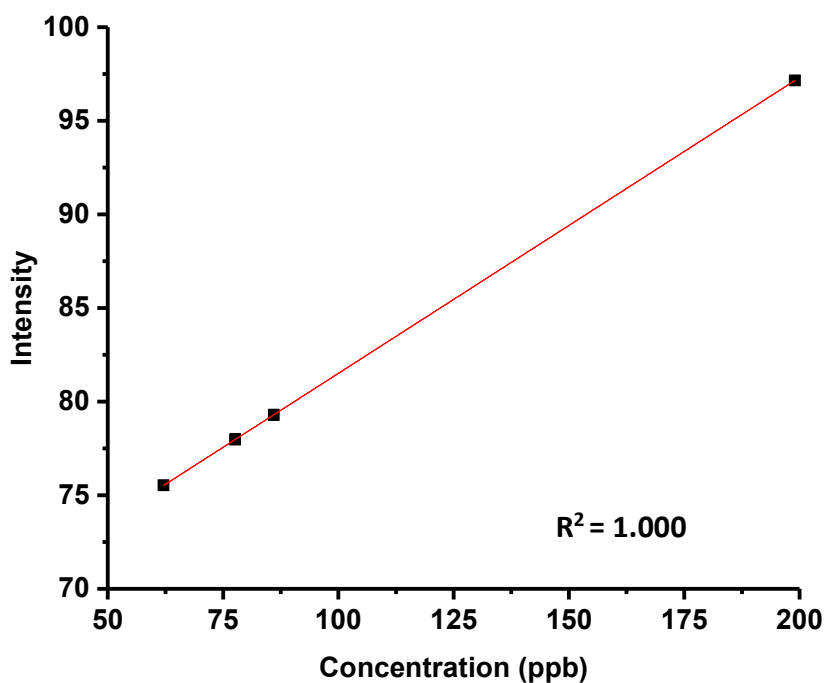


Figure S4.1: ICP-AES calibration curve used to measure Pt content remaining after HPLC purification of borylated peptide products.

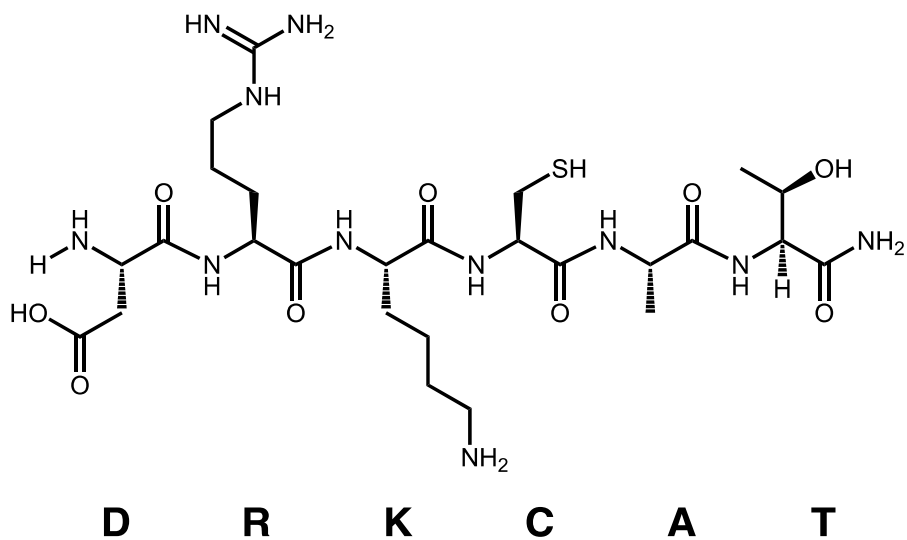
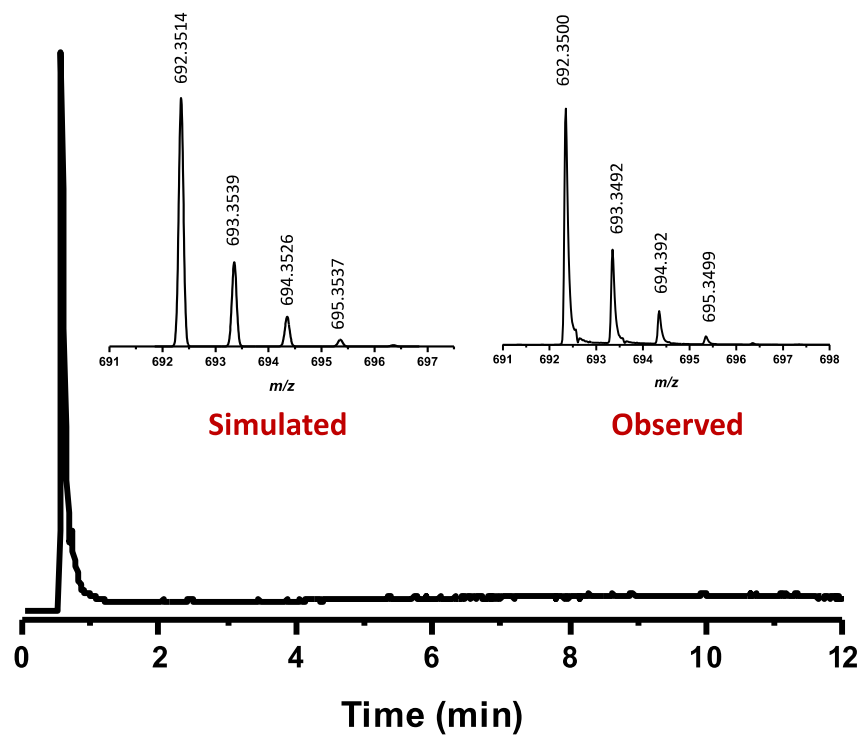


Figure S4.2: LC-MS data of purified peptide, $\text{H}_2\text{N-DRKCAT-CONH}_2$, **3a**, with simulated and observed masses.

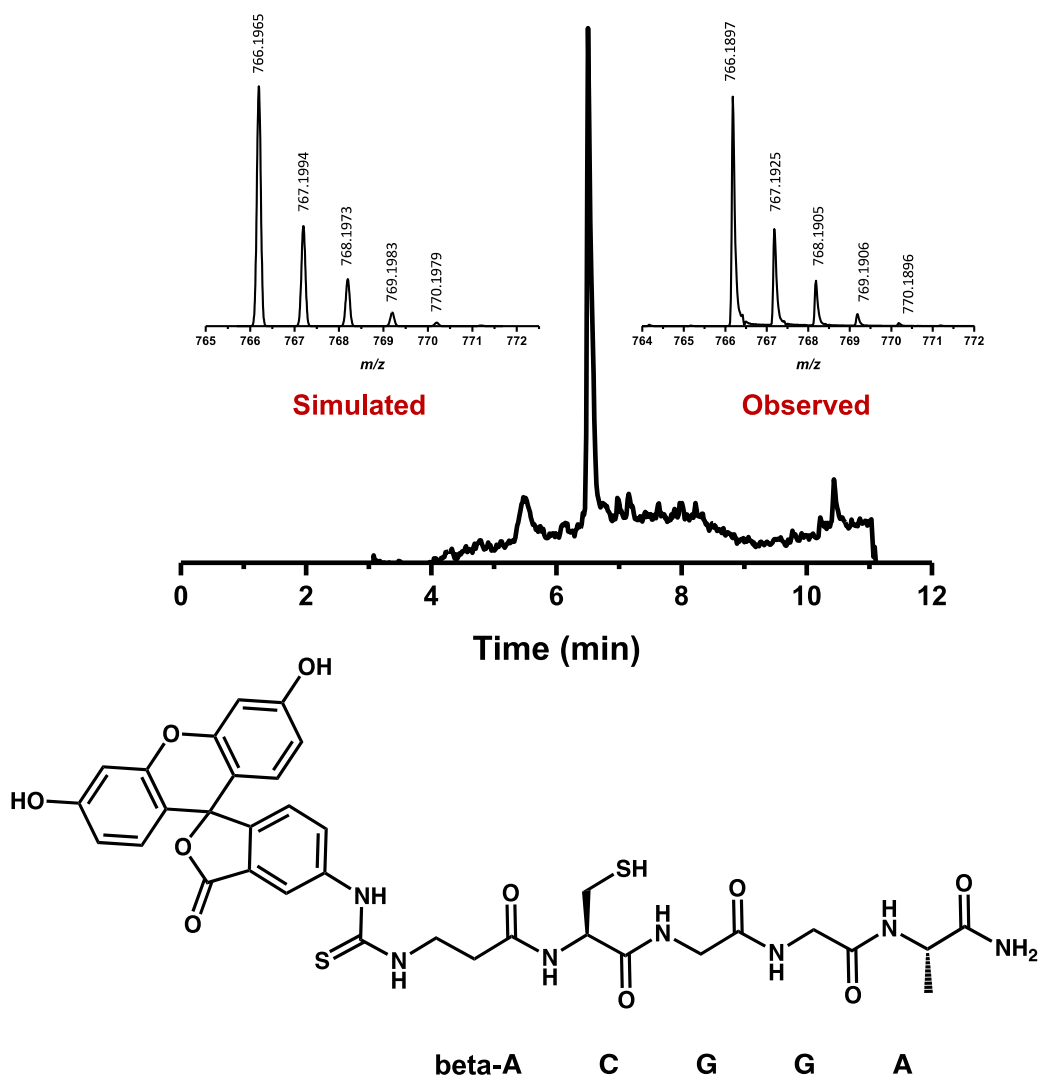


Figure S4.3: LC-MS data of purified peptide, FITC- β -ACGGA-CONH₂, **4a**, with simulated and observed masses.

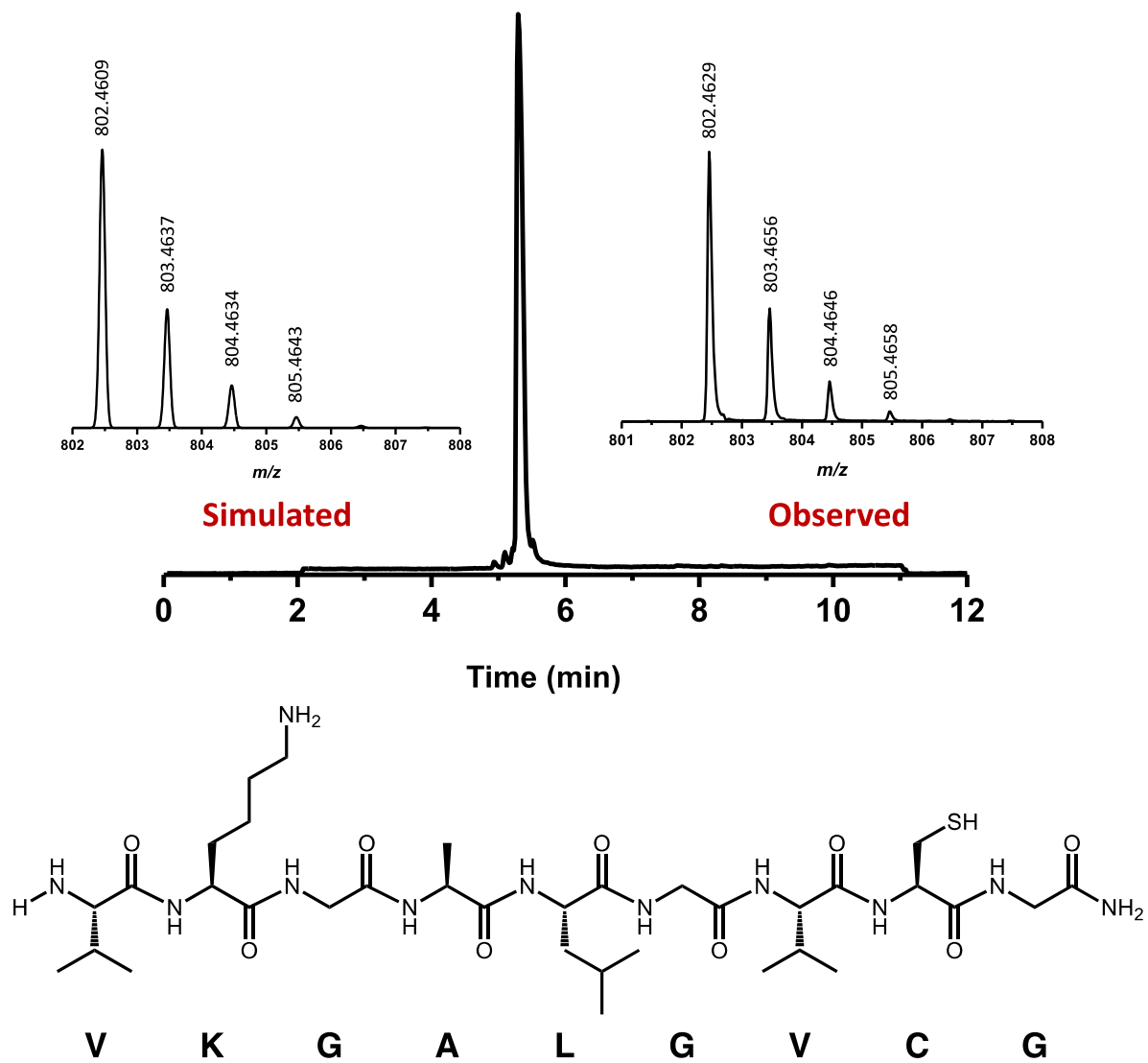


Figure S4.4: LC-MS data of purified peptide, H₂N-VK GALGVCG-CONH₂, **2a**, with simulated and observed masses.

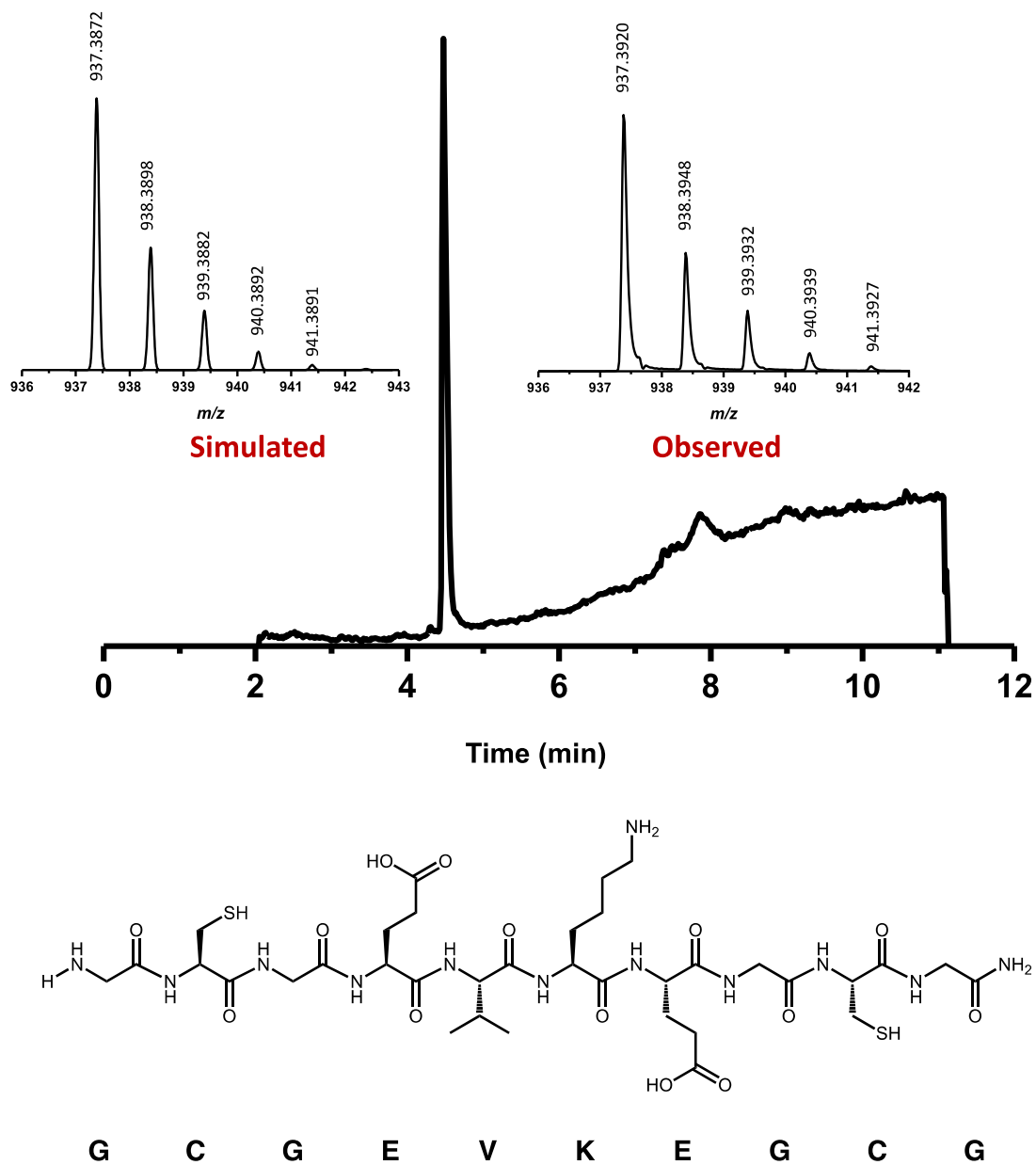


Figure S4.5: LC-MS data of purified peptide, H₂N-GCGEVKEGCG-CONH₂, **5a**, with simulated and observed masses.

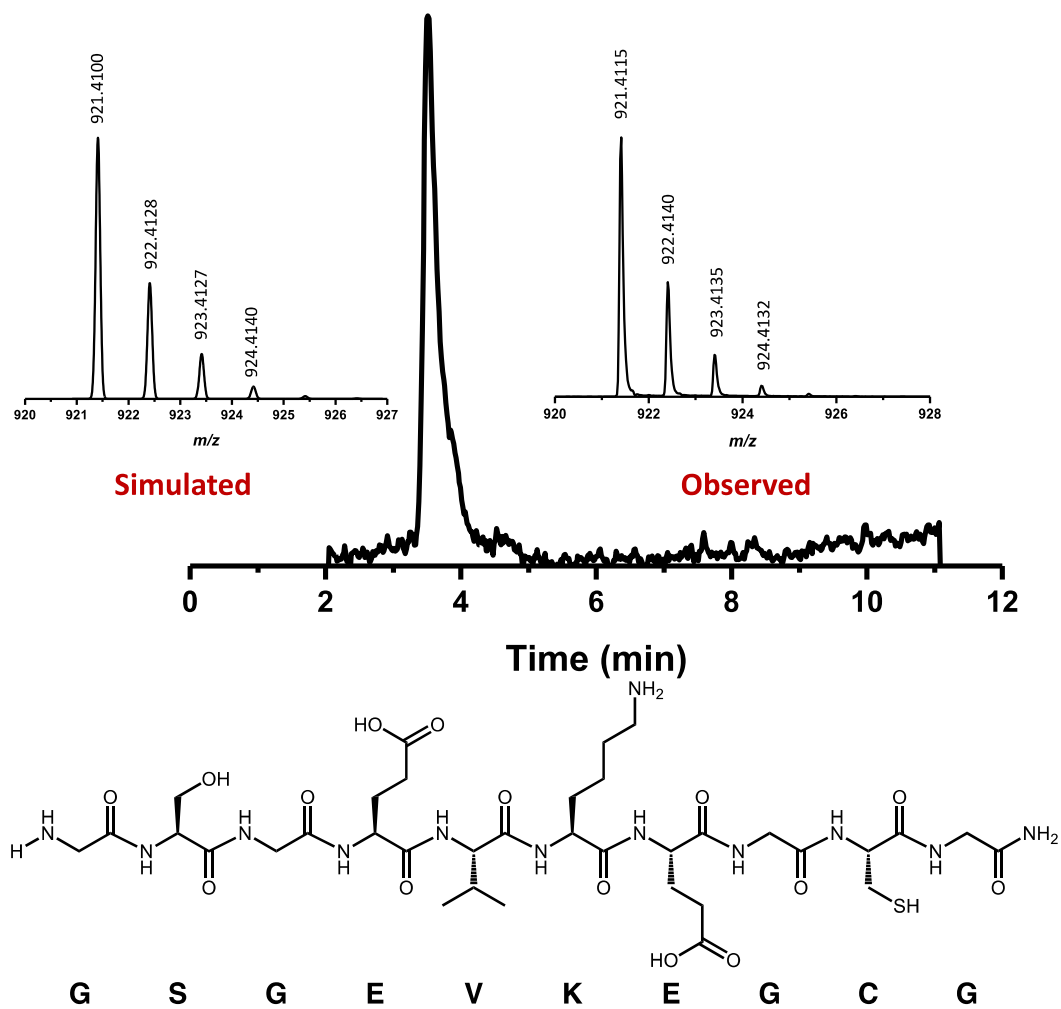


Figure S4.6: LC-MS data of purified peptide, H₂N-GSGEVKEGCG-CONH₂, **6a**, with simulated and observed masses.

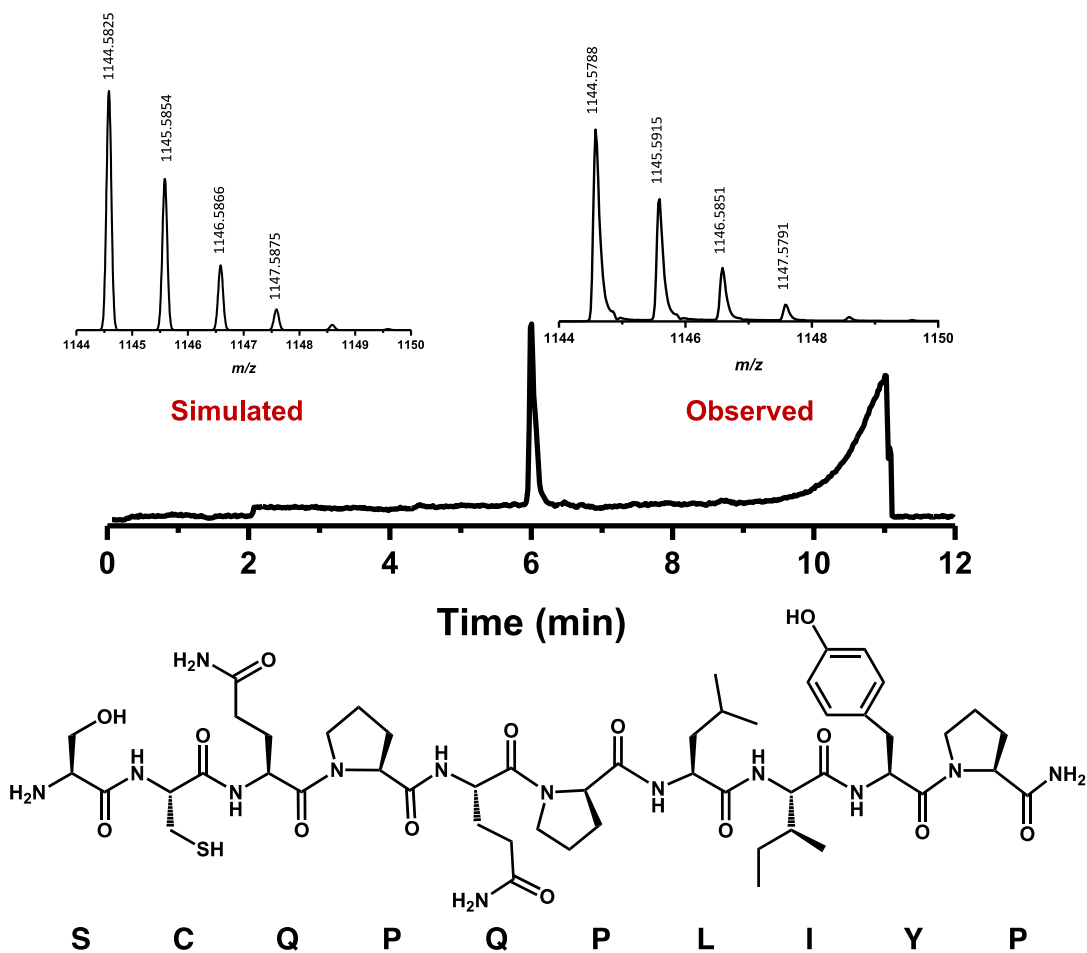


Figure S4.7: LC-MS data of purified peptide, H₂N-SCQPQPLIYP-CONH₂, **8a**, with simulated and observed masses.

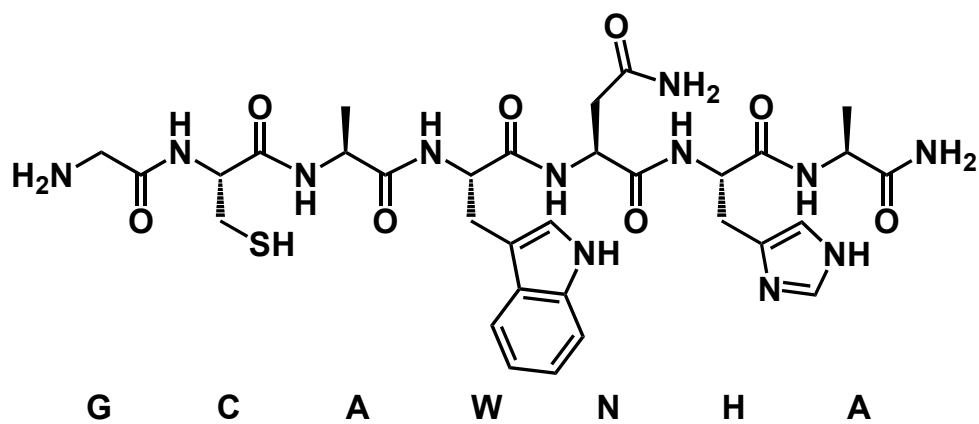
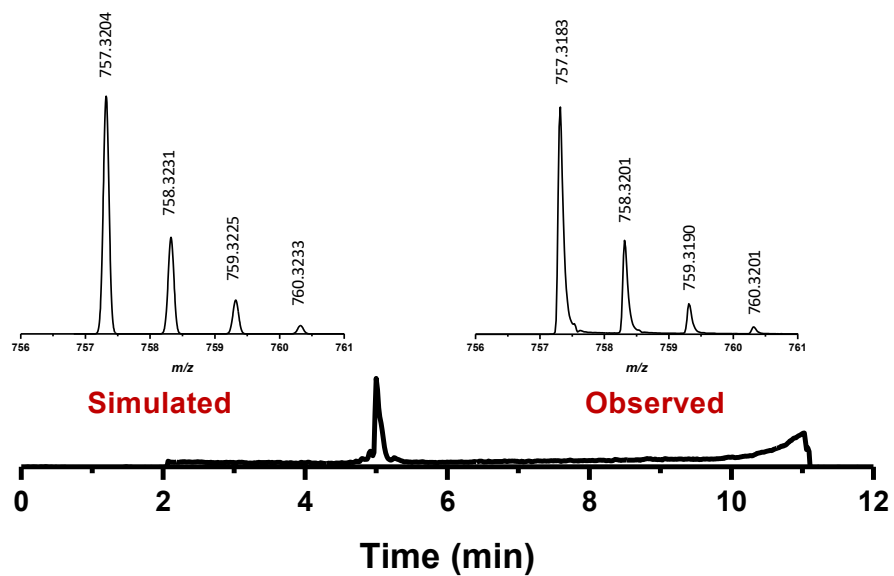


Figure S4.8: LC-MS data of purified peptide, H₂N-GCAWNHA-CONH₂, **9a**, with simulated and observed masses.

III. Peptide Borylation Reactions

General Borylation Procedure:

Each peptide (5 mM) was dissolved in Tris•HCl DMF buffer (30 mM). To this solution was added a dry stir bar and PtCl(PPh₃)₂-(9-B-*m*-C₂B₁₀H₁₁) (1.2 equiv per cysteine). The reaction was sonicated for 5 min to ensure complete solubilization of reagents, and was then allowed to stir for 1.5 h. An aliquot of the reaction mixture was removed (5 μL) and quenched with a 2:1 water:acetonitrile (v/v, spiked with 0.1% TFA) solution (175 μL). Finally, internal standard (20 μL, 1.25 mM, see Section I) was added to yield a final volume sample of 200 μL. This sample was then subjected to LCMS analysis. After ensuring conversion, the remainder of the reaction mixture was quenched through addition of a 2:1 water:acetonitrile (spiked with 0.1% TFA) mixture equaling 5 x the total reaction volume. Solvent was removed *in vacuo*, and the crude product was suspended in water (1 mL). The suspension was sonicated and then filtered with a Pall syringe filter (0.2 μm, PTFE). The filtrate was dried under reduced pressure, and purification of borylated peptides away from Pt-based byproducts was performed through reversed phase HPLC (Section II).

Depending on quantities, stock solutions of peptide (10-50 mM) and PtCl(PPh₃)₂-(9-B-*m*-C₂B₁₀H₁₁) (10-100 mM), were prepared, although storage (>24 h) of peptides in solution often resulted in disulfide bond formation between cysteine residues. Disulfide bond formation was also observed when peptide stock solutions were prepared in buffered solution and stored for >0.5 hr so concentrated stock solutions were always prepared in DMF and used immediately. Fresh PtCl(PPh₃)₂-(9-B-*m*-C₂B₁₀H₁₁) solutions were always prepared prior to use.

Borylation of Glutathione:

Glutathione (1.5 mg, 0.005 mmol, 1 equiv) was dissolved in a Tris • HCl DMF buffer (20 mL, 30 mM). To this mixture, a dry stir bar and PtCl(PPh₃)₂-(9-B-*m*-C₂B₁₀H₁₁) (5.0 mg, 0.006 mmol, 1.2 equiv) were added. The reaction was sonicated for 5 minutes to ensure solubilization and allowed to proceed for 1.5 h under constant stirring. To terminate the reaction, 5 x the reaction volume of 2:1 water:acetonitrile (0.1% TFA) was added. Quenched reactions were then sonicated for an additional 5 minutes before verifying borylation by LC-MS. After removing solvent *in vacuo*, borylated peptides were suspended in water under sonication and solutions were filtered through a Pall syringe filter (0.2 μm, polytetrafluoroethylene). Purification away from Pt byproducts was performed through reversed phase HPLC (Method A, Section III) to afford the product (0.5 mg, 30% yield).

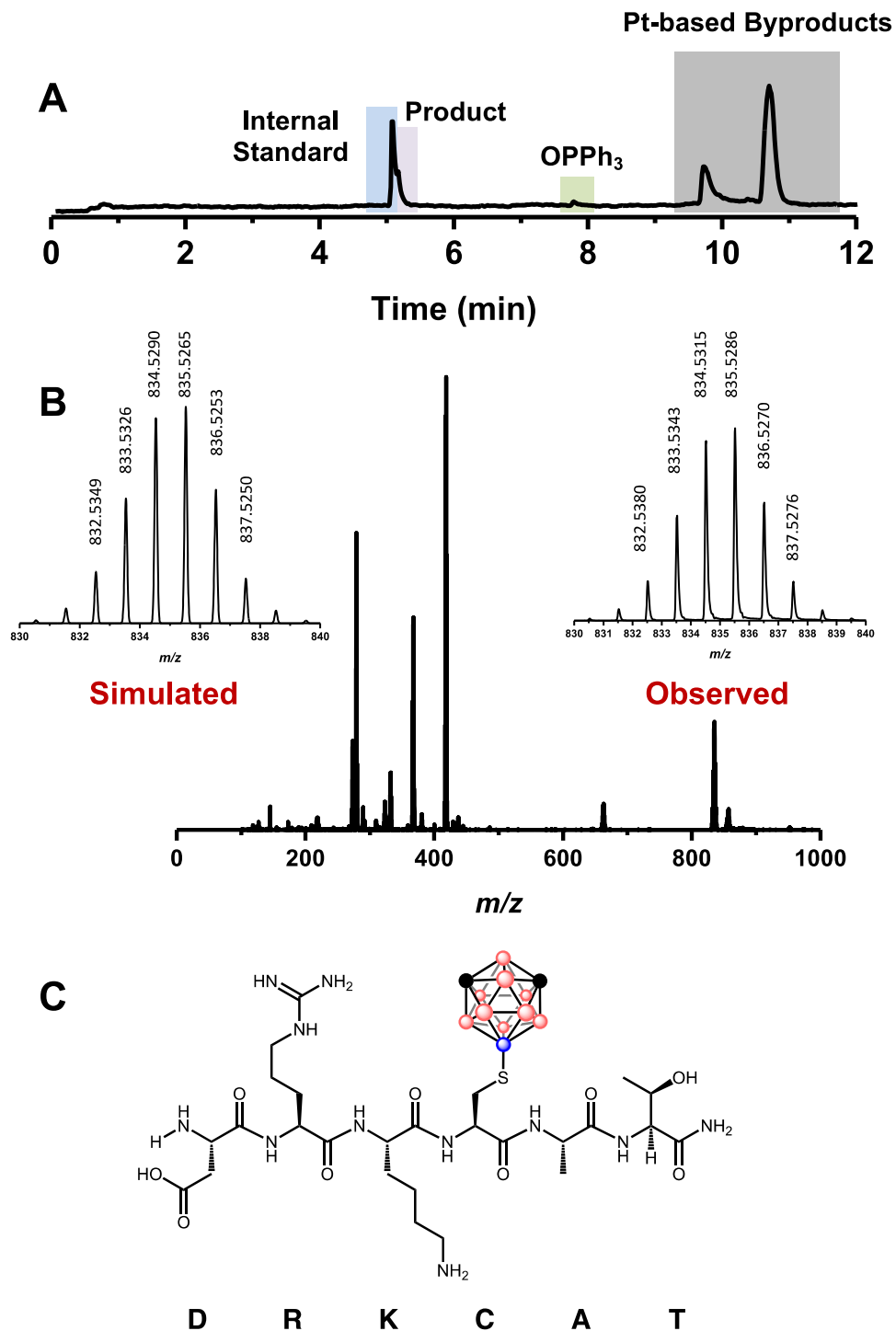


Figure S4.9 **A:** LC trace of the crude H₂N-DRKCAT-CONH₂ borylation reaction mixture. **B:** Simulated and observed masses for the borylated product **C:** Line drawing of the borylated product, **3b**.

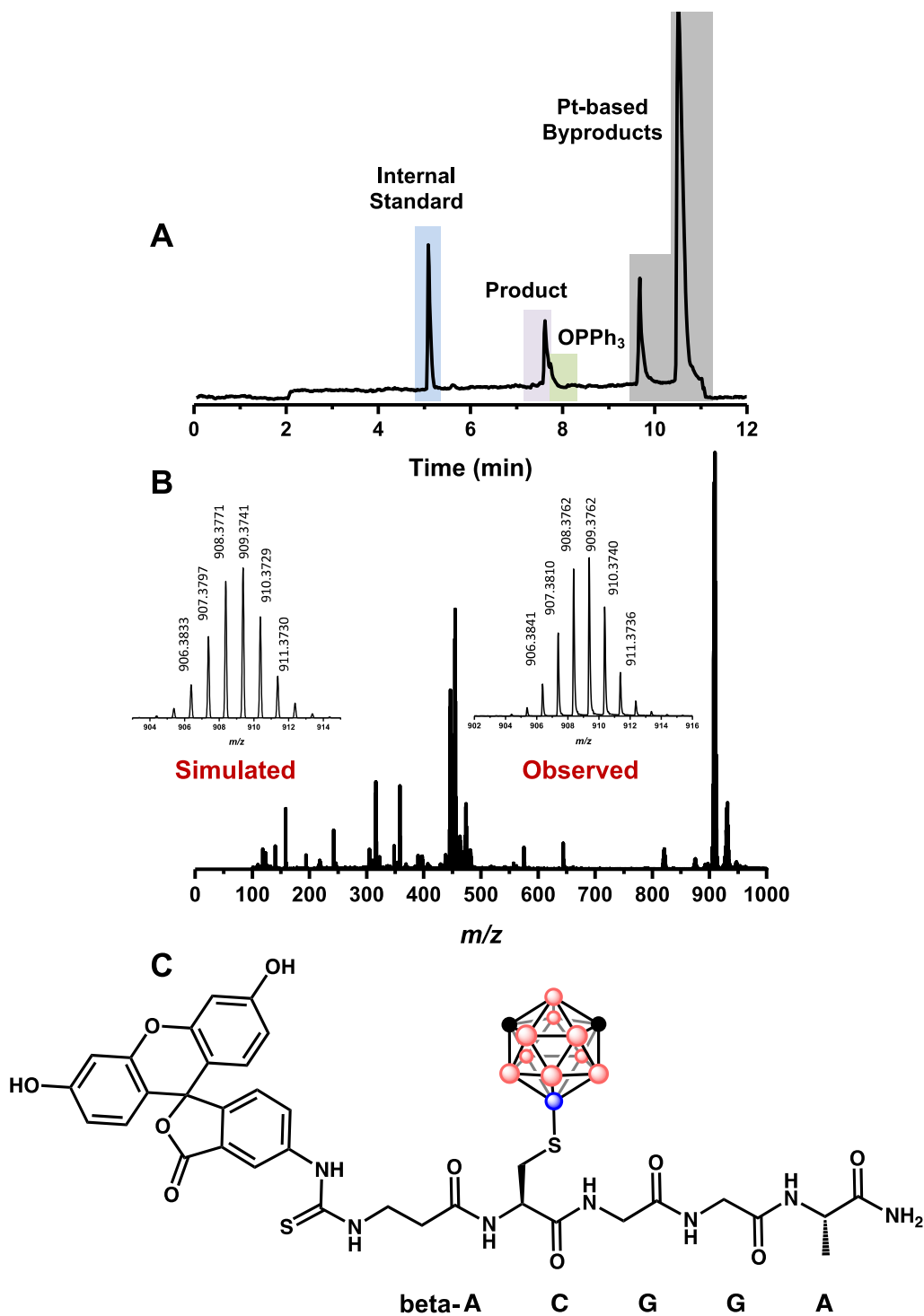


Figure S4.10 **A:** LC trace of the crude FITC-ACGGA-CONH₂ borylation reaction mixture. **B:** Simulated and observed masses for the borylated product **C:** Line drawing of the borylated product, **4b**.

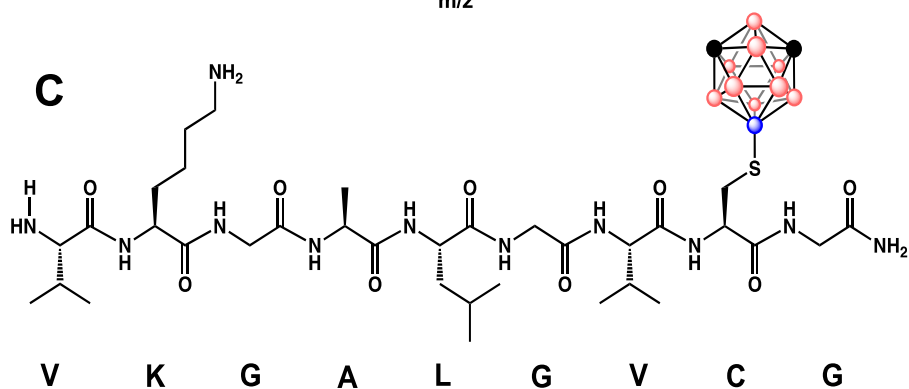
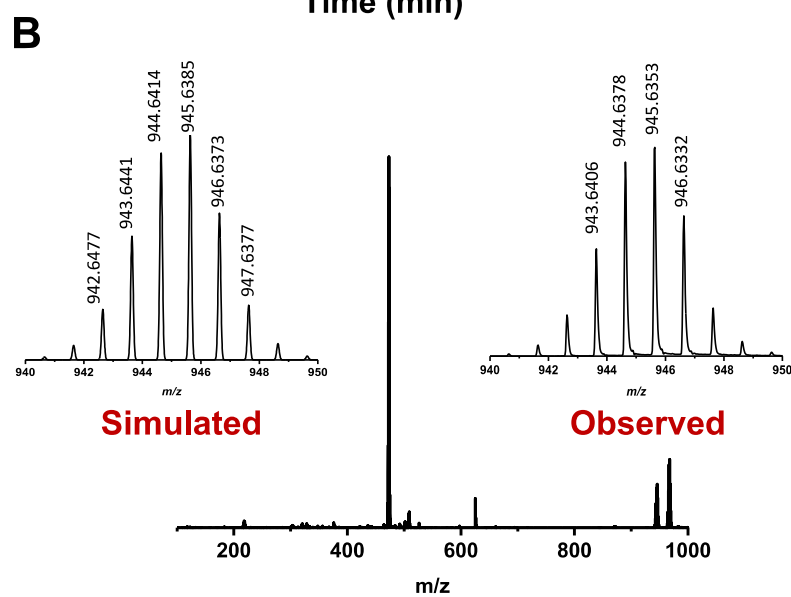
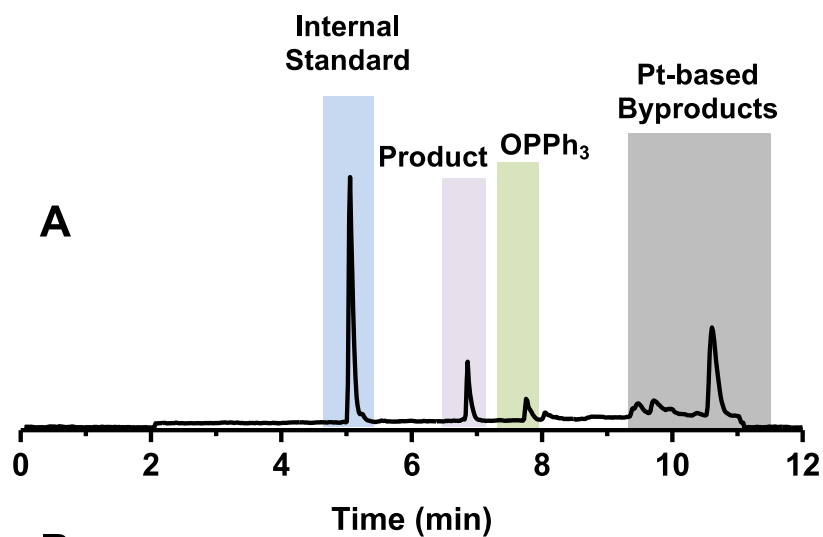


Figure S4.11 A: LC trace of the crude H₂N-VK GALGVCG-CONH₂ borylation reaction mixture.

B: Simulated and observed masses for the borylated product

C: Line drawing of the borylated product, **2b**.

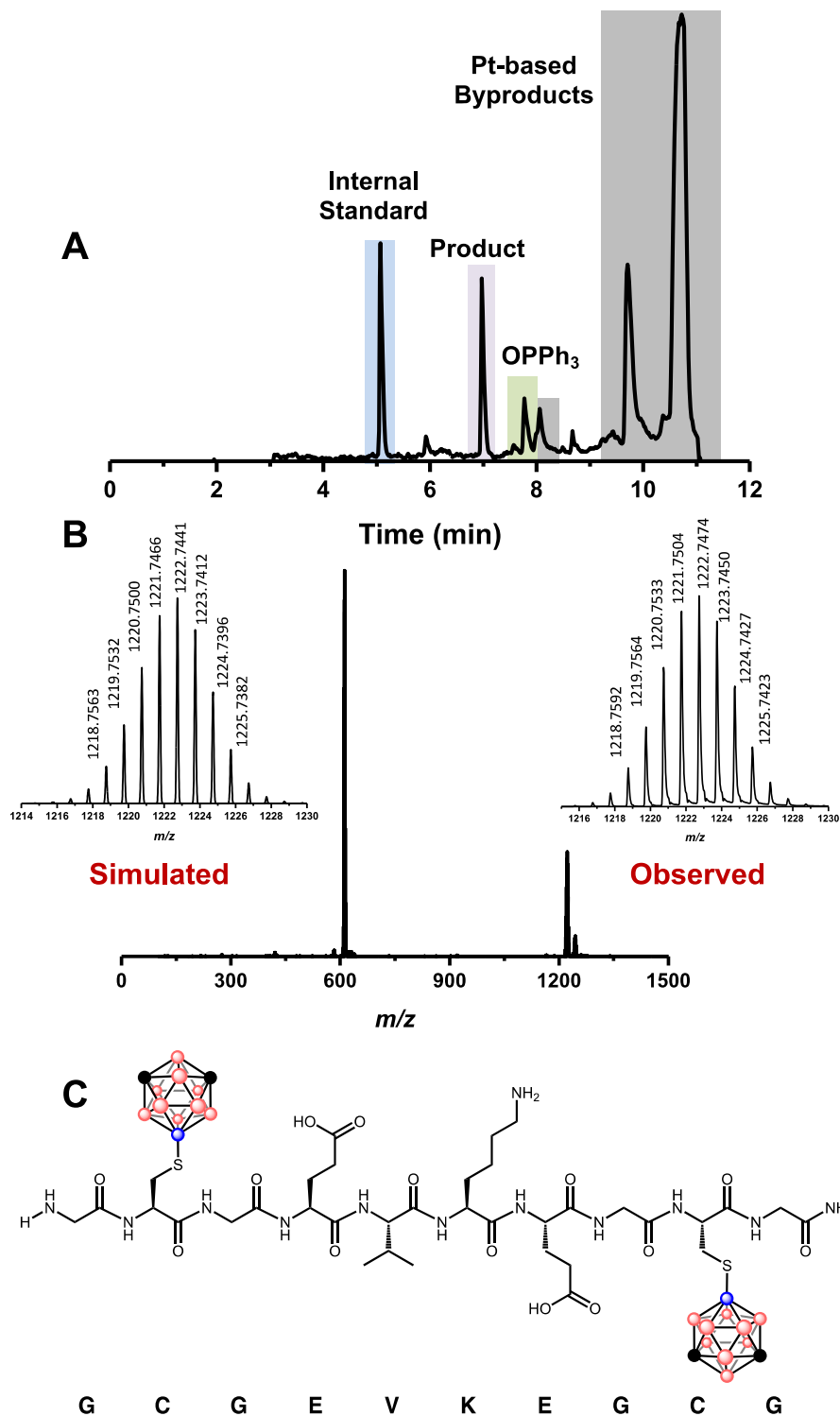


Figure S4.12 A: LC trace of the crude $\text{H}_2\text{N-GCGEVKEGCG-CONH}_2$ borylation reaction mixture.

B: Simulated and observed masses for the borylated product **C:** Line drawing of the borylated product, **5b**.

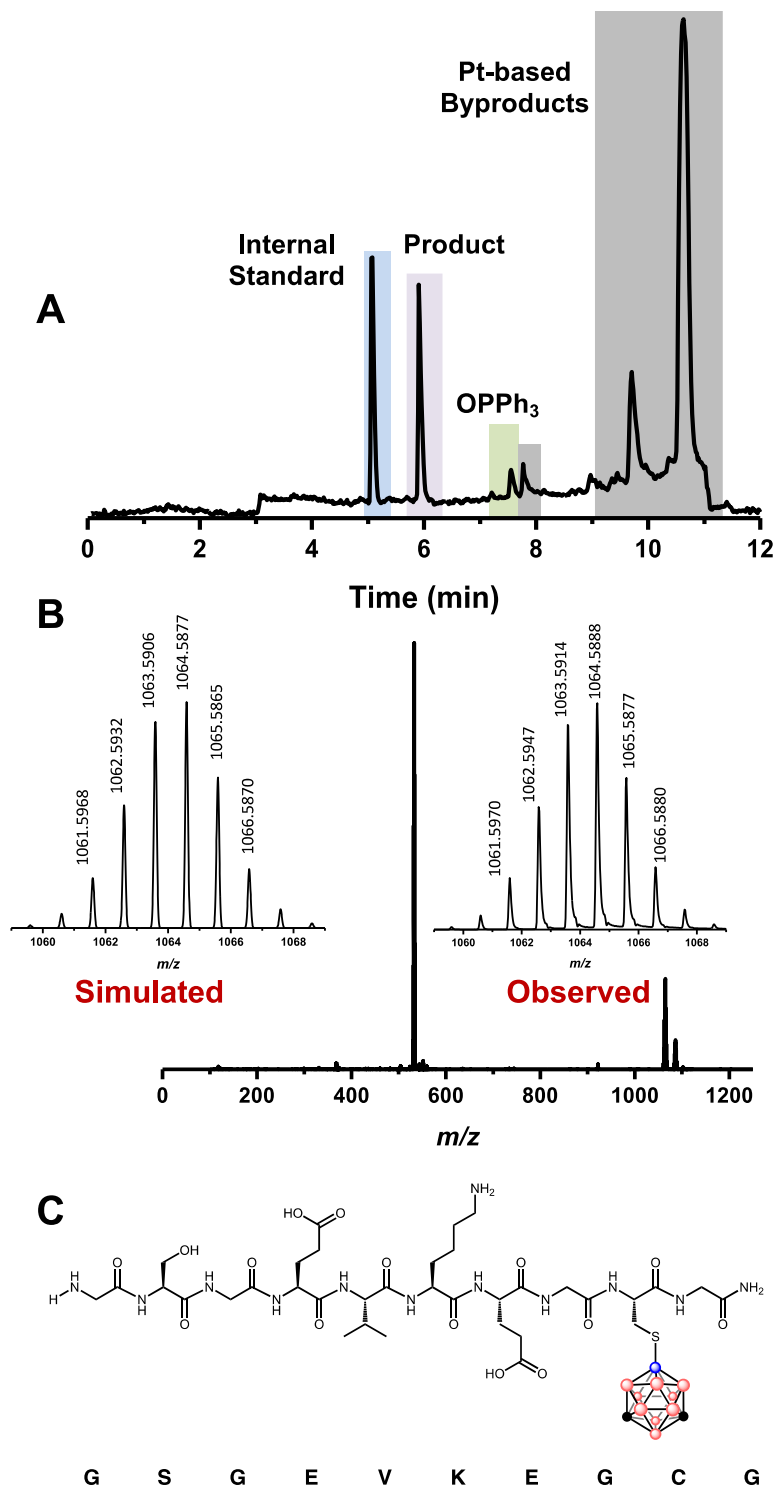


Figure S4.13 A: LC trace of the crude $\text{H}_2\text{N-GSGEVKEGCG-CONH}_2$ borylation reaction mixture. **B:** Simulated and observed masses for the borylated product **C:** Line drawing of the borylated product, **6b**.

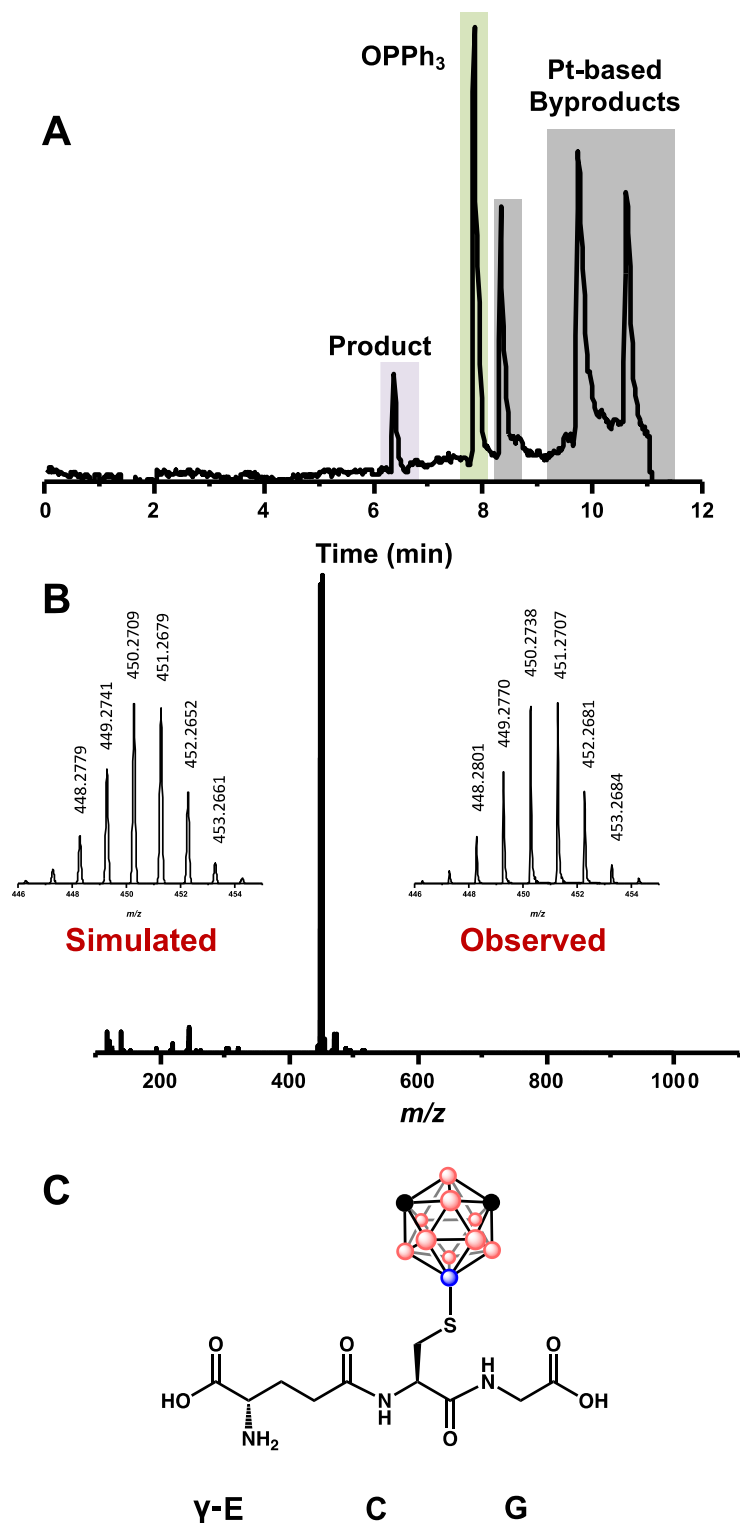


Figure S4.14 A: LC trace of the crude glutathione borylation reaction mixture. **B:** Simulated and observed masses for the borylated product **C:** Line drawing of the borylated product, **7b**.

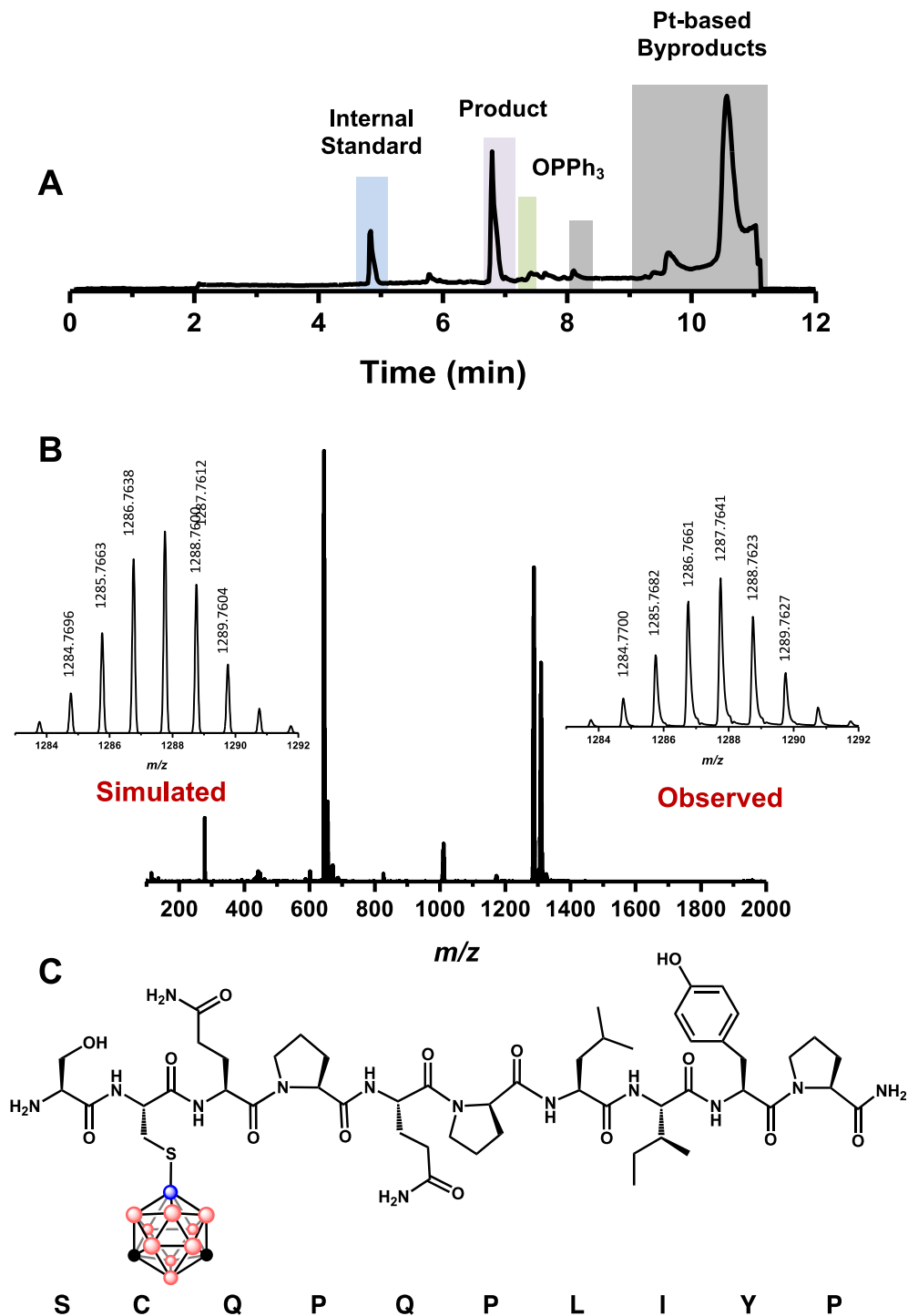


Figure S4.15 A: LC trace of the crude H₂N-SCQPQPLIYP-CONH₂ borylation reaction mixture.

B: Simulated and observed masses for the borylated product

C: Line drawing of the borylated product, **8b**.

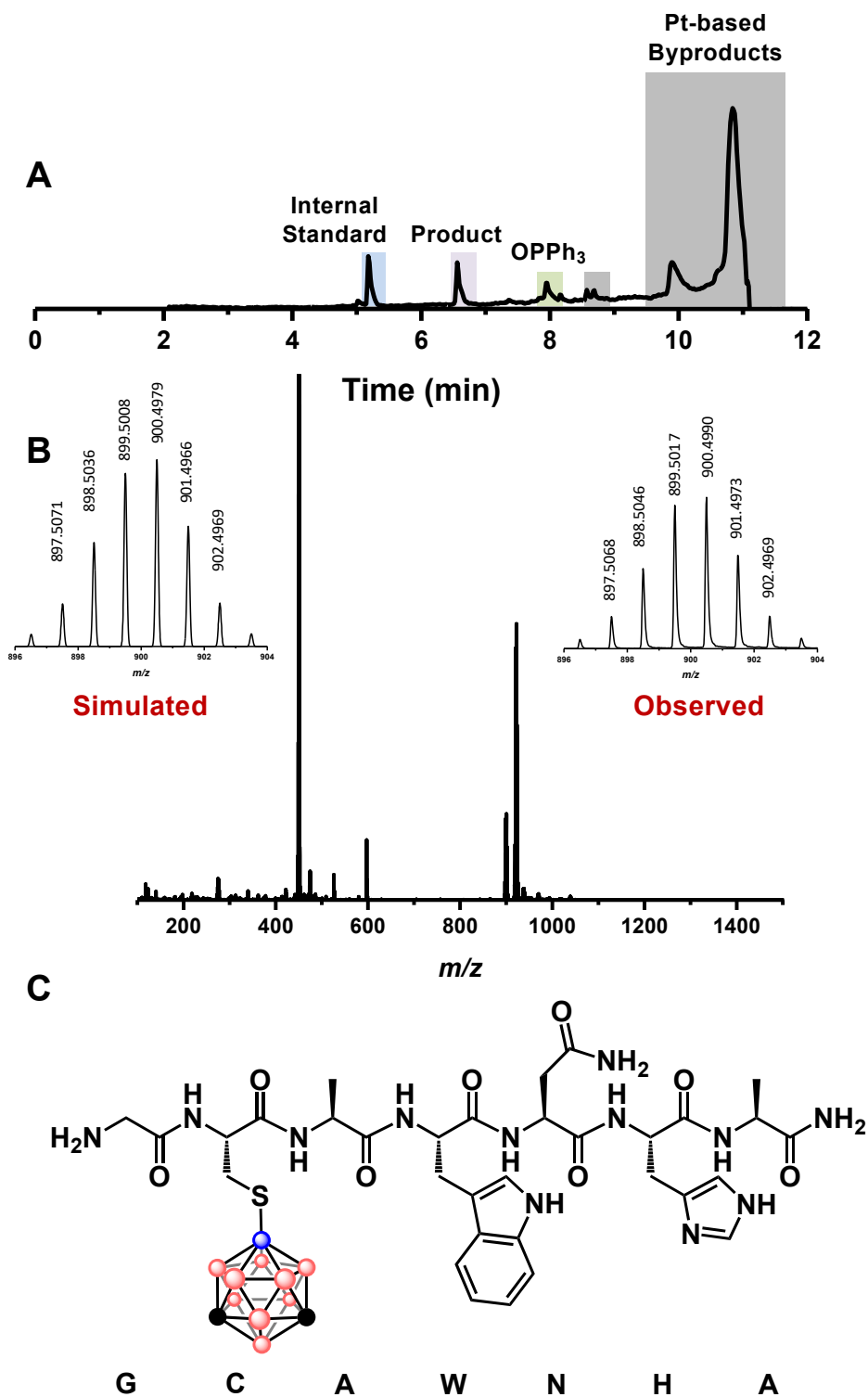


Figure S4.16 **A:** LC trace of the crude H₂N-GCAWNHA-CONH₂ borylation reaction mixture. **B:** Simulated and observed masses for the borylated product **C:** Line drawing of the borylated product, **9b**.

IV. Reagent Robustness Assessment

Reaction Tolerance to Water

In order to assess the borylation reaction tolerance to water, the following stock solutions were prepared in DMF: peptide (**2a**, 20 mM), Tris•HCl (200 mM) and PtCl(PPh₃)₂-(9-B-*m*-C₂B₁₀H₁₁) (50 mM). Two reaction mixtures were prepared in 1.5 mL Eppendorf tubes by the addition of dry stir bars and stock solutions and solvents as outlined in Table S4.4. An aliquot of the reaction mixture was removed (5 μL) and quenched with a 2:1 water:acetonitrile (v/v, spiked with 0.1% TFA) solution (175 μL). Finally, internal standard (20 μL, 1.25 mM, see Section I) was added to yield a final volume sample of 200 μL. This sample was then subjected to LCMS analysis as described in the General Borylation Procedure (Section III).

Total Volume (μL)	Water (μL)	DMF (μL)	Tris•HCl Buffer (μL)	Pt Stock (μL)	Peptide Stock (μL)
200	10	86	30	24	50
200	50	26	30	24	50

Table S4.4: Components of reaction mixtures used to assess the tolerance of peptide borylation to both 5% and 25% water.

To assess the reaction tolerance to the presence of 50% and 75% v/v water, the contents of Table S4.5 were mixed, sonicated (5 min) and allowed to react for 90 min. Again, an aliquot of the reaction mixture was removed (5 μL) and quenched with a 2:1 water:acetonitrile (v/v, spiked with 0.1% TFA) solution (175 μL). Finally, internal standard (20 μL, 1.25 mM, see Section I) was added to yield a final volume sample of 200 μL. This sample was then subjected to LCMS analysis.

Total Volume (μL)	Water (μL)	DMF (μL)	Tris-HCl Buffer (μL)	Pt Stock (μL)	Peptide (mg)
194	100	40	30	24	1
233	150	33	30	24	1

Table S4.5: Reaction mixtures to assess the tolerance of the reaction to both 50% and 75% water.

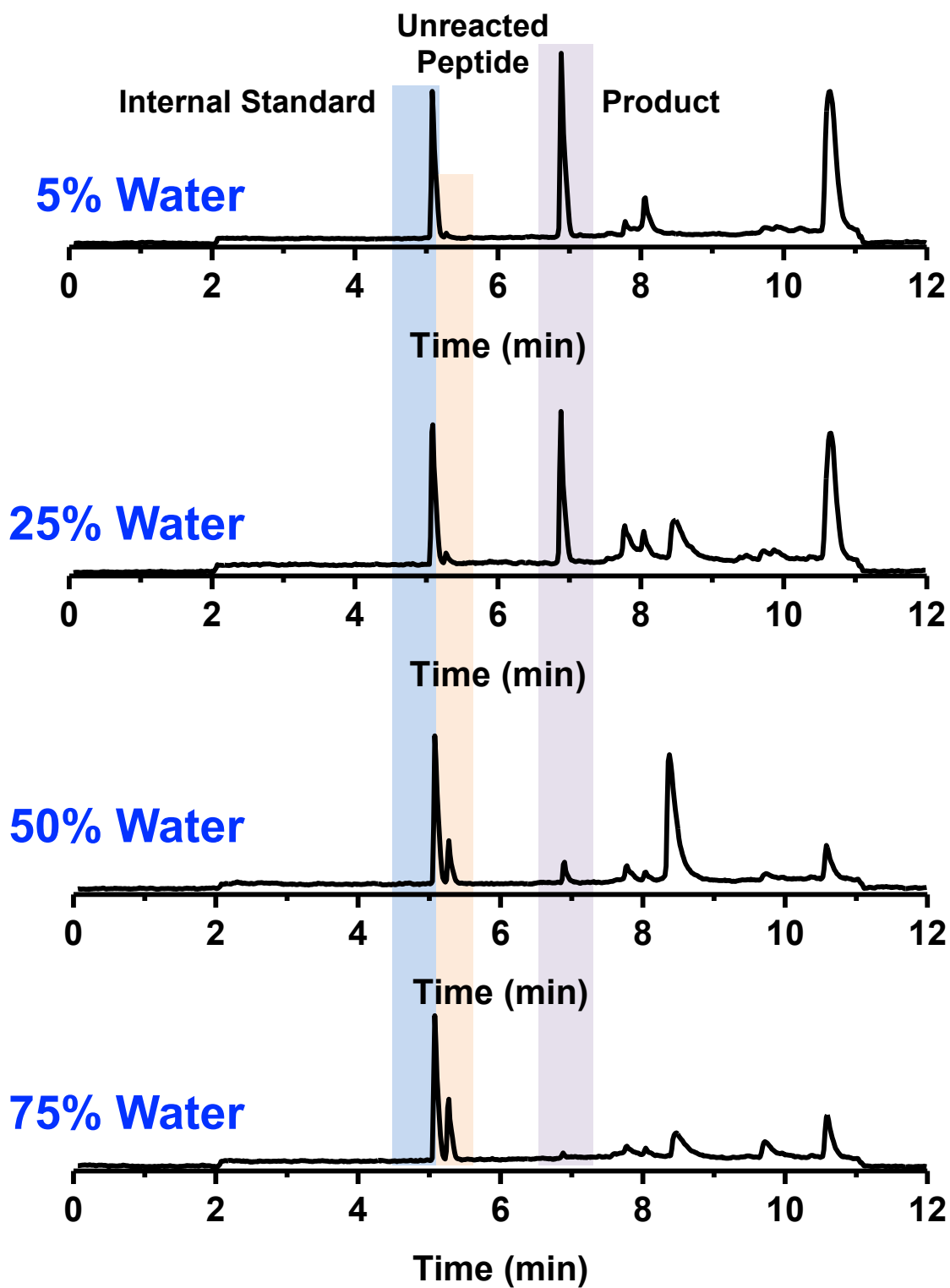


Figure S4.17: LC traces displaying the reaction tolerance to 5%, 25%, 50%, and 75% water.

Reaction Tolerance to Guanidine Hydrochloride (GuHCl) and Tris(2-carboxyethyl)phosphine Hydrochloride (TCEP HCl)

GuHCl:

In order to assess the reaction tolerance to GuHCl, the following stock solutions were prepared in DMF: peptide (**2a**, 20 mM), Tris•HCl (200 mM) and PtCl(PPh₃)₂-(9-B-*m*-C₂B₁₀H₁₁) (50 mM). To a 1.5 mL volume Eppendorf tube, Tris•HCl buffer (30 μL), PtCl(PPh₃)₂-(9-B-*m*-C₂B₁₀H₁₁) (24 μL), and peptide (50 μL) solutions were added. GuHCl (57 mg, 3M) and DMF (96 μL) were also added to yield a total reaction volume of 200 μL. A dry stir bar was added to the Eppendorf tube and the reaction mixture was sonicated to ensure dissolution of all reagents. The reaction was then allowed to stir for 90 min at room temperature. An aliquot of the reaction mixture was removed (5 μL) and quenched with a 2:1 water:acetonitrile (v/v, spiked with 0.1% TFA) solution (175 μL). Finally, internal standard (20 μL, 1.25 mM, see Section I) was added to yield a final volume sample of 200 μL. This sample was then subjected to LCMS analysis.

TCEP:

In order to assess the reaction tolerance to TCEP HCl, peptide **2a** (1.5 mg) was dissolved in Tris•HCl buffer (291 μL, 30 mM) to produce a 5 mM solution of **2a**. A molar excess of TCEP HCl (4.2 mg, 10 x) was added to this mixture and sonicated for 5 min. After sonication, PtCl(PPh₃)₂-(9-B-*m*-C₂B₁₀H₁₁) (1.3 mg) and a dry stir bar were added and the mixture was sonicated again for 30 sec. The reaction was then allowed to stir for 90 min at room temperature. An aliquot of the reaction mixture was removed (5 μL) and quenched with a 2:1 water:acetonitrile (v/v, spiked with 0.1% TFA) solution (175 μL). Finally, internal standard (20 μL, 1.25 mM, see Section I) was added to yield a final volume sample of 200 μL. This sample was then subjected to LCMS analysis.

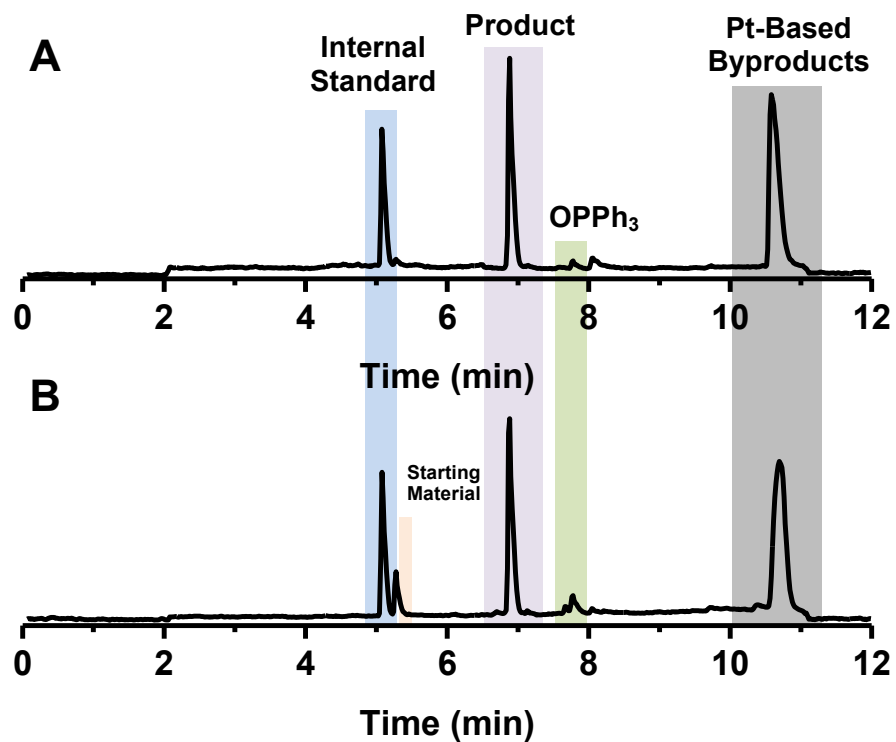


Figure S4.18: LC traces displaying the reaction tolerance between 1 and 2a to **A:** 3 M guanidine HCl and **B:** TCEP HCl.

V. Data Supporting S-B Bond Formation

Tandem MS/MS

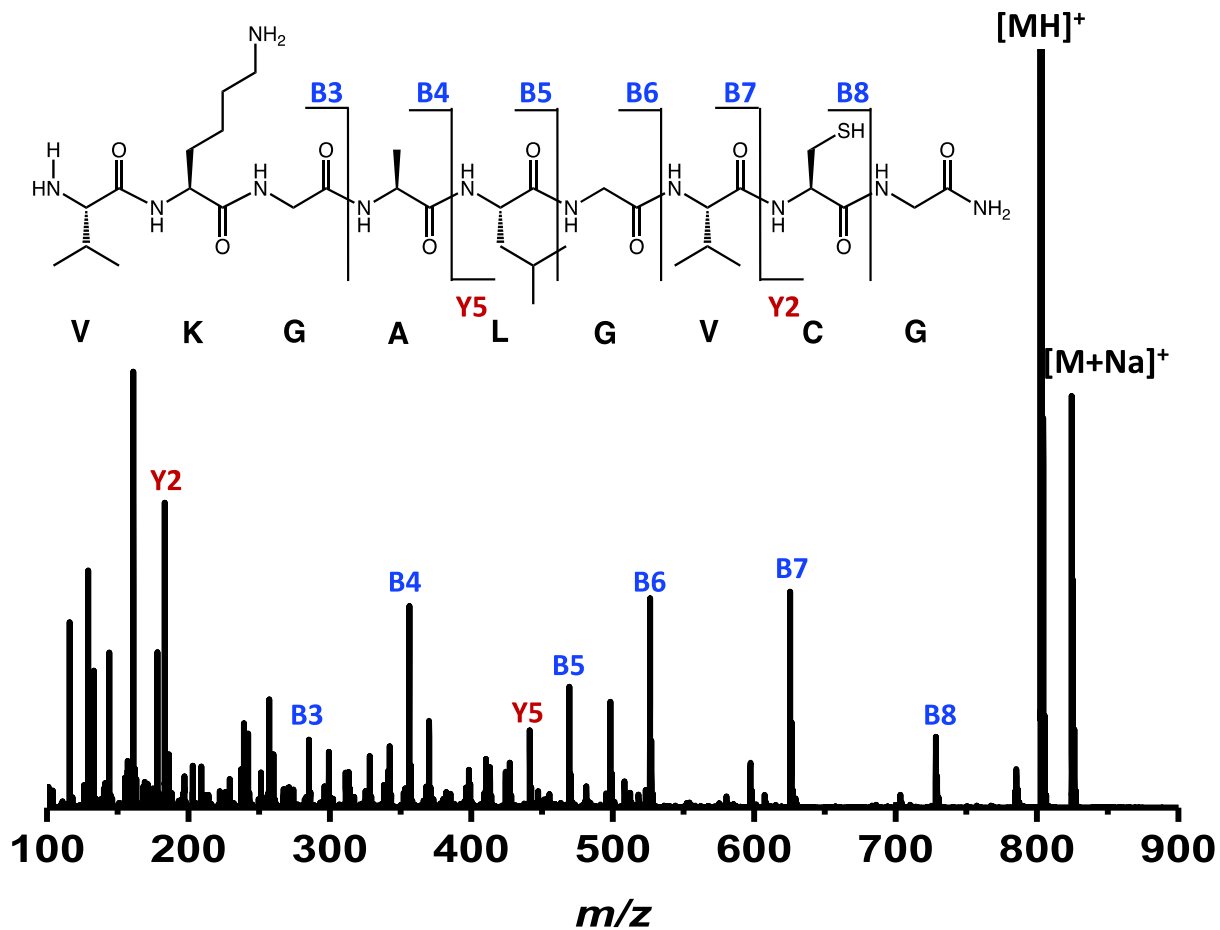


Figure S4.19: Mass spectrum of 2a when 30 eV collision energy was applied.

Fragment	Type	Calculated Mass	Observed Mass
B3	B	285.193	285.191
B4	B	356.230	356.233
B5	B	469.314	469.314
B6	B	526.335	526.339
B7	B	625.404	625.408
B8	B	728.413	728.417
Y2	Y	178.065	178.067
Y5	Y	447.240	447.243

Table S4.6: Summary of the calculated and observed masses when **2a** was fragmented under 30 eV collision energy. These data correspond to the spectrum in Figure S4.17.

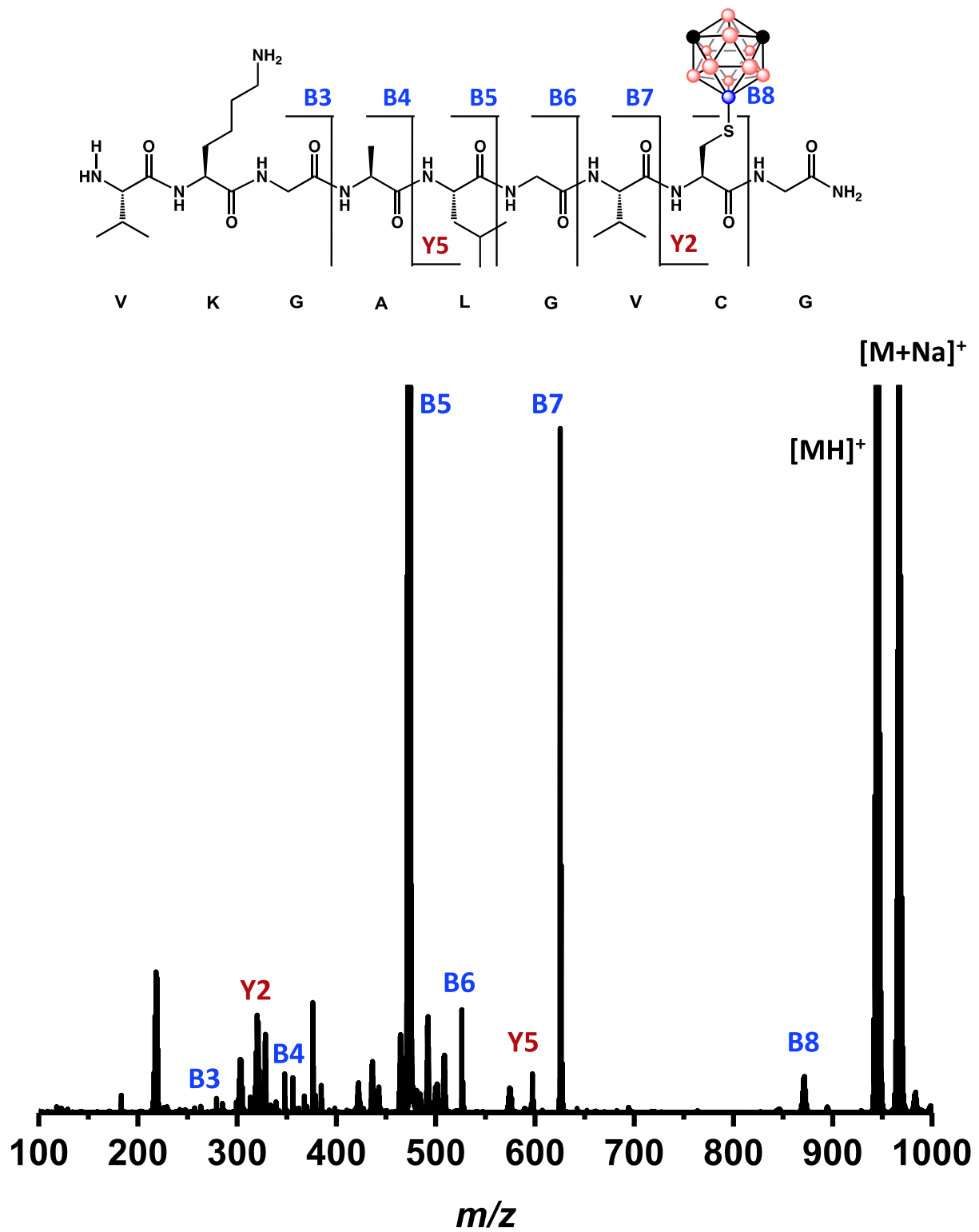


Figure S4.20: Mass spectrum of borylated peptide **2b** when 30 eV collision energy was applied.

Name	Type	Calculated Mass	Observed Mass
B3	B	285.193	285.191
B4	B	356.230	356.233
B5	B	469.314	469.314
B6	B	526.335	526.339
B7	B	625.404	625.408
B8	B	728.413	728.417
Y2	Y	178.065	178.067
Y5	Y	447.240	447.243

Table S4.7: Summary of the calculated and observed masses when **2b** was fragmented under 30 eV collision energy. These data correspond to the spectrum in Figure S4.18.

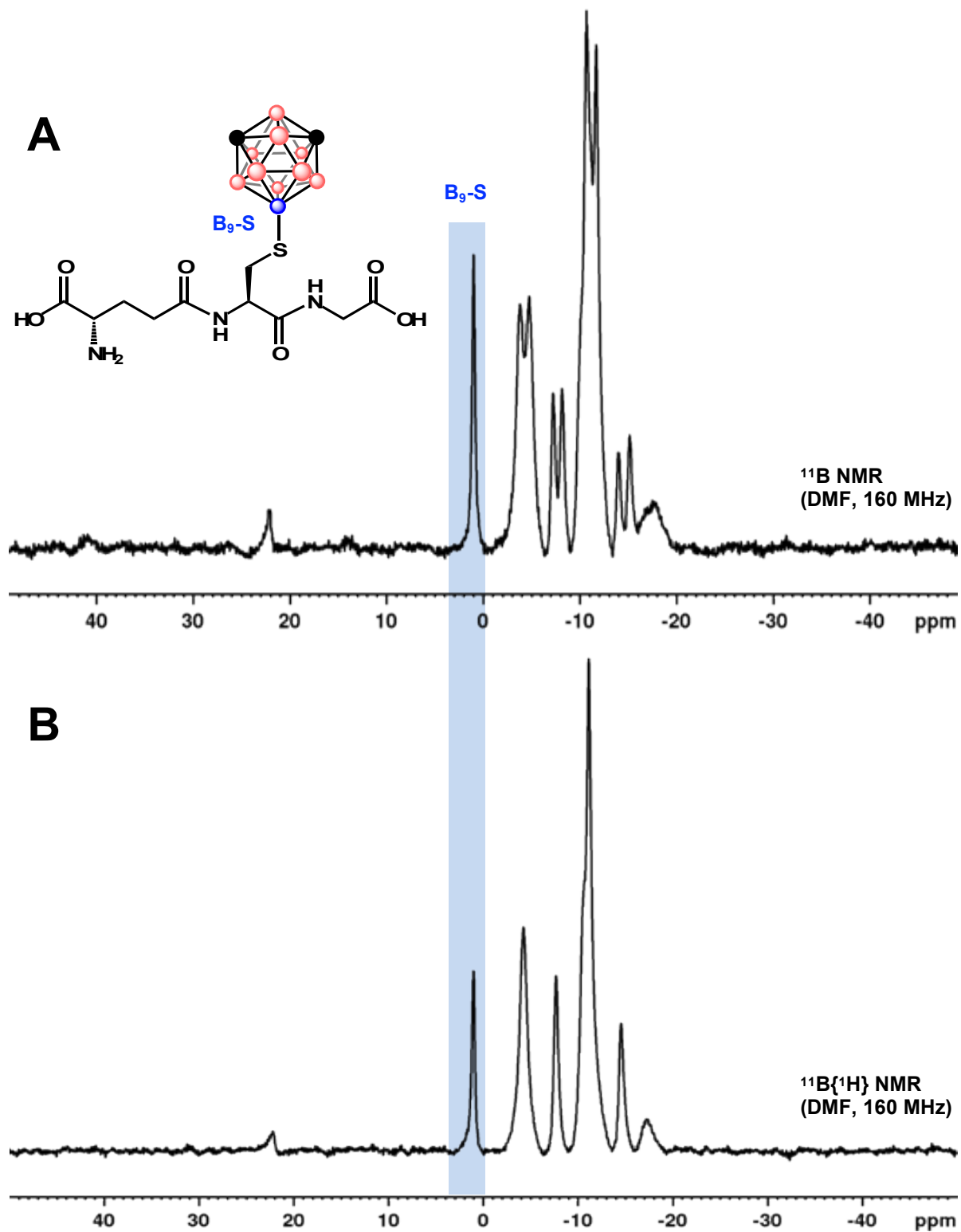


Figure S4.21 A: ^{11}B NMR spectrum of **7b** (DMF, 160 MHz). **B:** $^{11}\text{B}\{^1\text{H}\}$ NMR spectrum of **7b** (DMF, 160 MHz).

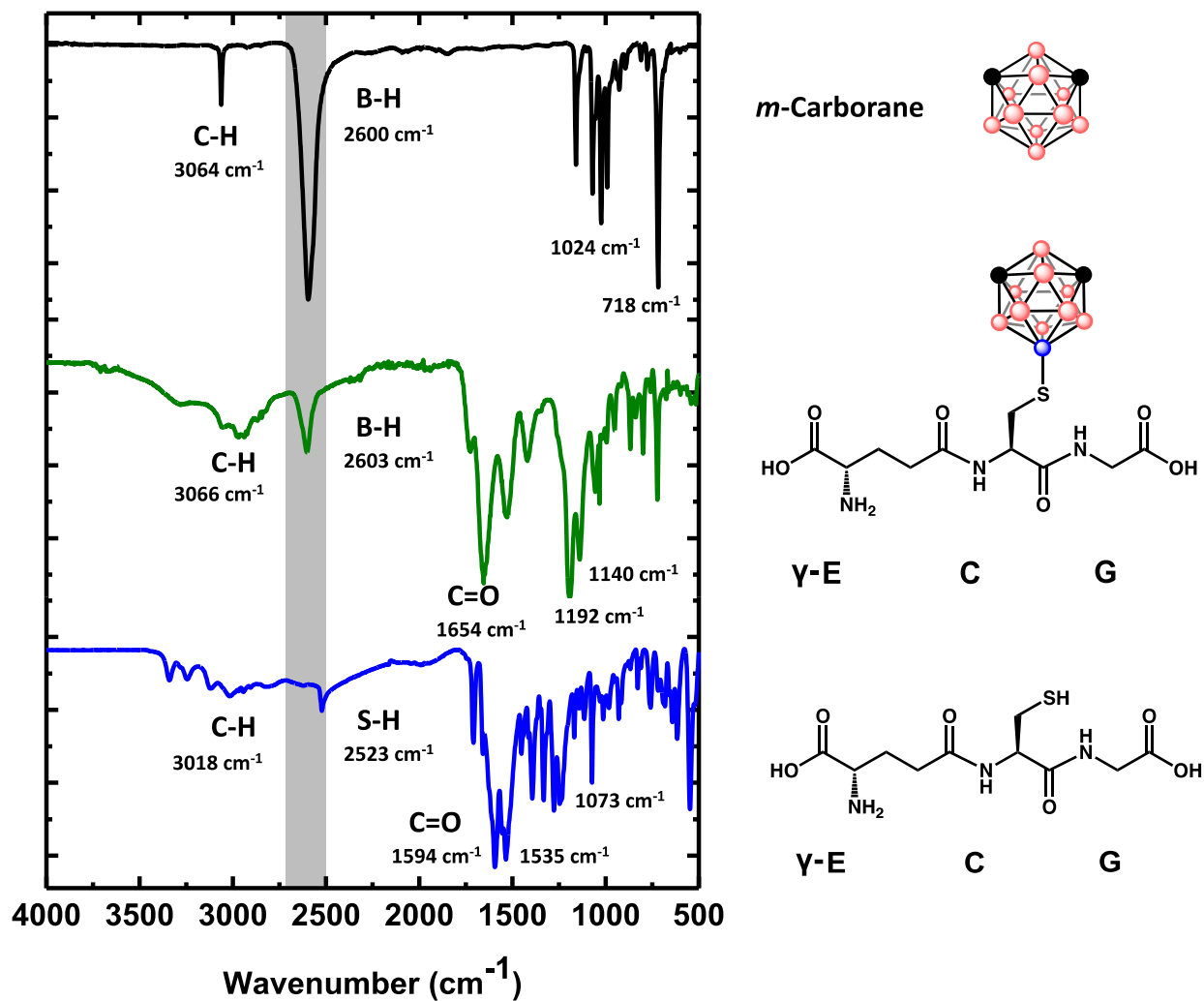


Figure S4.22: A comparison of the infrared spectra of peptide 7a (blue), peptide 7b (green) and *m*-carborane (black). The S-H stretch observed in unmodified glutathione at 2523 cm^{-1} is absent in the spectrum for borylated glutathione.

I. DARPin Expression, Purification and Borylation

DARPin Expression and Purification

DARPin-Cys protein expression and purification was adapted from literature procedures.¹

DARPin-Cys Sequence (Calculated Mass: 15996.84 Da):

MGSDKIHSHHHHENLYFQGGCGGSDLGKKLLEAARAGQDDEVRILMANGADVNAVYD
DNGVTPLHLAAFLGHLEIVEVLLKYGADVNAADSWGTTPLHLAATWGHLEIVEVLLKH
GADVNAQDKFGKTAFDISIDNGNEDLAEILQKLN

The plasmid was designed to have an N-terminal His₆ tag followed by a TEV protease which was left on for our purposes (model bioconjugation protein). The plasmid purchased from Twist Bioscience is a pET29b(+) vector with kanamycin resistance and the DARPin-Cys gene was cloned in via NdeI and XhoI restriction sites.

Prior to expression, the plasmid was transformed into BL21-Gold cells (Agilent) using the standard manufacturer's procedure. Overnight cultures were grown and from these, two glycerol stocks were made and stored in the -80°C freezer. To two flasks (2 L) containing 750 ml of previously autoclaved LB Broth (Miller) with kanamycin (50 ug/ml), a saturated overnight culture inoculated (5 mL) was added from one of the aforementioned glycerol stocks. The culture was grown at 37°C with 250 rpm shaking for about 4 hours before the OD₆₀₀ reached ~0.4 and the culture was induced with 1 mM IPTG. The temperature was lowered and the culture was continued to shake at 30°C and 250 rpm for approximately 17 hours overnight. The final OD₆₀₀ was observed to be 1.39. Uninduced and induced cell pellets from ~3 ml of culture each were normalized to 1 OD₆₀₀ unit/ml and analyzed by SDS-PAGE and Coomassie Blue staining. The cultures were harvested by centrifugation at 6000 rpm for 30 min to yield a cell pellet.

The pellet was resuspended in lysis buffer containing Tris•HCl (20 mM), NaCl (150 mM), lysozyme (15 mg) and of protease inhibitor cocktail (0.5 tablet) at pH 7.5. The resulting suspension was homogenized (Avestin Emulsiflex C-3) and centrifuged at 17,000 rpm for 30 min to remove cell debris. The supernatant was loaded onto a 5 mL gravity Ni-NTA column (Qiagen) and washed with the following solutions which were prepared in buffer (Tris•HCl (20 mM) and NaCl (150 mM)): 30ml (10ml X 3) imidazole (5mM) followed by 20ml (10ml X 2) imidazole (20mM). Protein was eluted with 25ml (5ml x 5) imidazole (200mM). SDS-PAGE was run on all fractions and under reducing conditions and stained with Coomassie Blue. Pure fractions were combined and solvent exchanged into storage buffer (20mM Tris, 150mM NaCl, pH 7.5) and concentrated to ~15 ml using a using Amicon 3K Ultra-15 Centrifugal Filter (Millipore).

The purified protein was analyzed by LC-MS* and SDS-PAGE confirming sample purity and molecular weight. Concentration was determined by A280 (extinction coefficient = $15470 \text{ M}^{-1} \text{ cm}^{-1}$) and confirmed by Ellman's (5,5'-Dithio-bis-(2-nitrobenzoic acid) Assay after treatment with and subsequent removal of (Amicon 3K Ultra-0.5 mL Centrifugal Filters) two equivalents TCEP HCl (Tris (2-carboxyethyl) phosphine hydrochloride). The protein sample was diluted with storage buffer to 300 μM and aliquots were flash frozen and stored in $-80 \text{ }^\circ\text{C}$ freezer.

* The observed mass by LC-MS of purified protein is 15,866 Da corresponding to the calculated mass of the sequence without the initial methionine which was likely cleaved during expression.²⁵

DARPin Borylation

A sample of DARPin (50 μL , 300 μM) prepared in Tris•HCl (20 mM) and NaCl (150 mM) at pH 7.5 was treated with TCEP HCl (5 μL , 17 mM) for 30 minutes. After, an aliquot of this sample (30 μL) was added to an Eppendorf tube (1 mL) containing a dry stir bar. Compound **1** dissolved in DMF (56 equiv, 100 μL , 5 mM) was added. Additionally, Tris•HCl buffer in DMF was added to

bring the final reaction conditions to 15% water v/v, 85% DMF v/v under buffered conditions of Tris•HCl (33 mM) and NaCl (23 mM). The Eppendorf tube for vortexed for 5 min and the reaction was allowed to proceed for 6.5 hours. The progress of the reaction was monitored by LCMS as described in Section I.

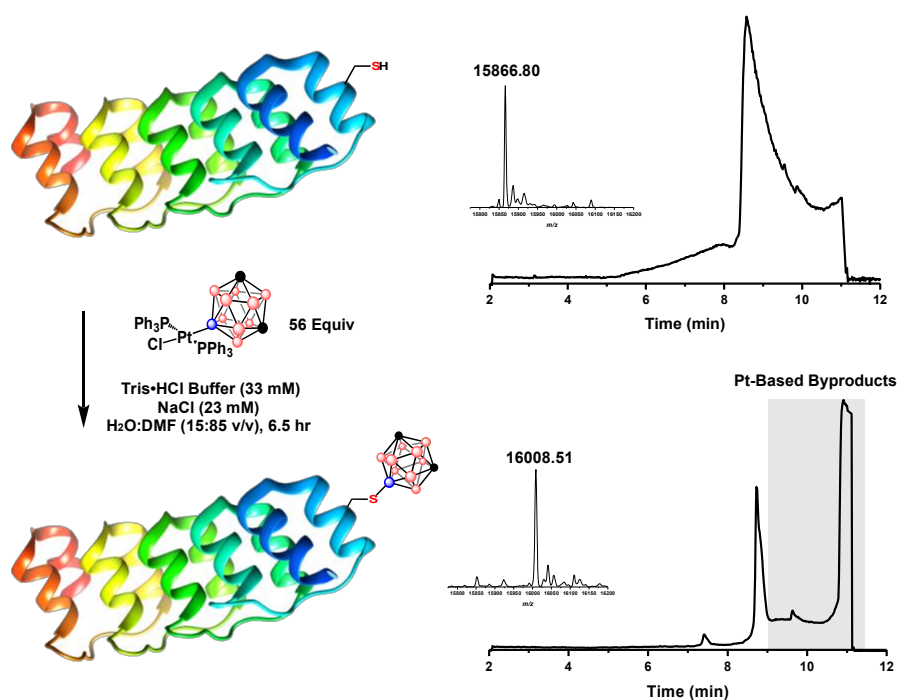


Figure S4.23: Borylation of DARPin with the corresponding LC traces and deconvoluted masses.

II. Peptide Stability Assessment

Aqueous solutions of **7b** (5 mM), potassium carbonate (50 mM), hydrochloric acid (50 mM) and **7a** (50 mM) were prepared. To three 1.5 mL volume Eppendorf tubes, 20 μ L of the **7b** solution was added followed by addition of the potassium carbonate solution (21 μ L) to one of the three Eppendorf tubes. To the second and third tubes, the hydrochloric acid (21 μ L) and **7a** (21 μ L) solutions were added, respectively. All three mixtures were vortexed and allowed to sit for 24 h at r.t., after which 20 μ L aliquots were removed from each tube and subjected to LC-MS analysis (see Section I). Each Eppendorf tube was then submerged in a sand bath at 37 °C for an additional 48 h. After each 24 h time period, a 20 μ L aliquot was removed from each sample and subjected to LC-MS analysis.

III. Borylation of Peptide on Solid-Phase Resin

Peptide H₂N-QNACG-CONH₂ was synthesized as described in Section II. However, prior to cleavage from the resin, beads (50 mg) were removed and subjected to TIPS (1 mL), Hydroxybenzotriazole (1 mL, 0.5 M in DMF) and 2,2,2-trifluoroethanol (3 mL) to remove trityl protecting groups. After reaction for 30 minutes, the beads were isolated by vacuum filtration and washed with DMF (5 mL, 3x). A sample of beads (3 mg) were added to an Eppendorf tube (1 mL) and subjected to excess **1** (3.5 mM) in DMF Tris•HCl buffer (30 mM). After 1.5 hr, the beads were subjected to centrifugation at 18,000 x g for 3 min and the supernatant was removed. To the Eppendorf, trifluoroacetic acid (200 µL), TIPS (10 µL) and water (10 µL) were added. After 30 min, an aliquot (20 µL) was removed and diluted with 180 µL of a 2:1 water:acetonitrile mixture (spiked with 0.1% TFA). The sample was then analyzed by LCMS using the peptide characterization method described in Section I.

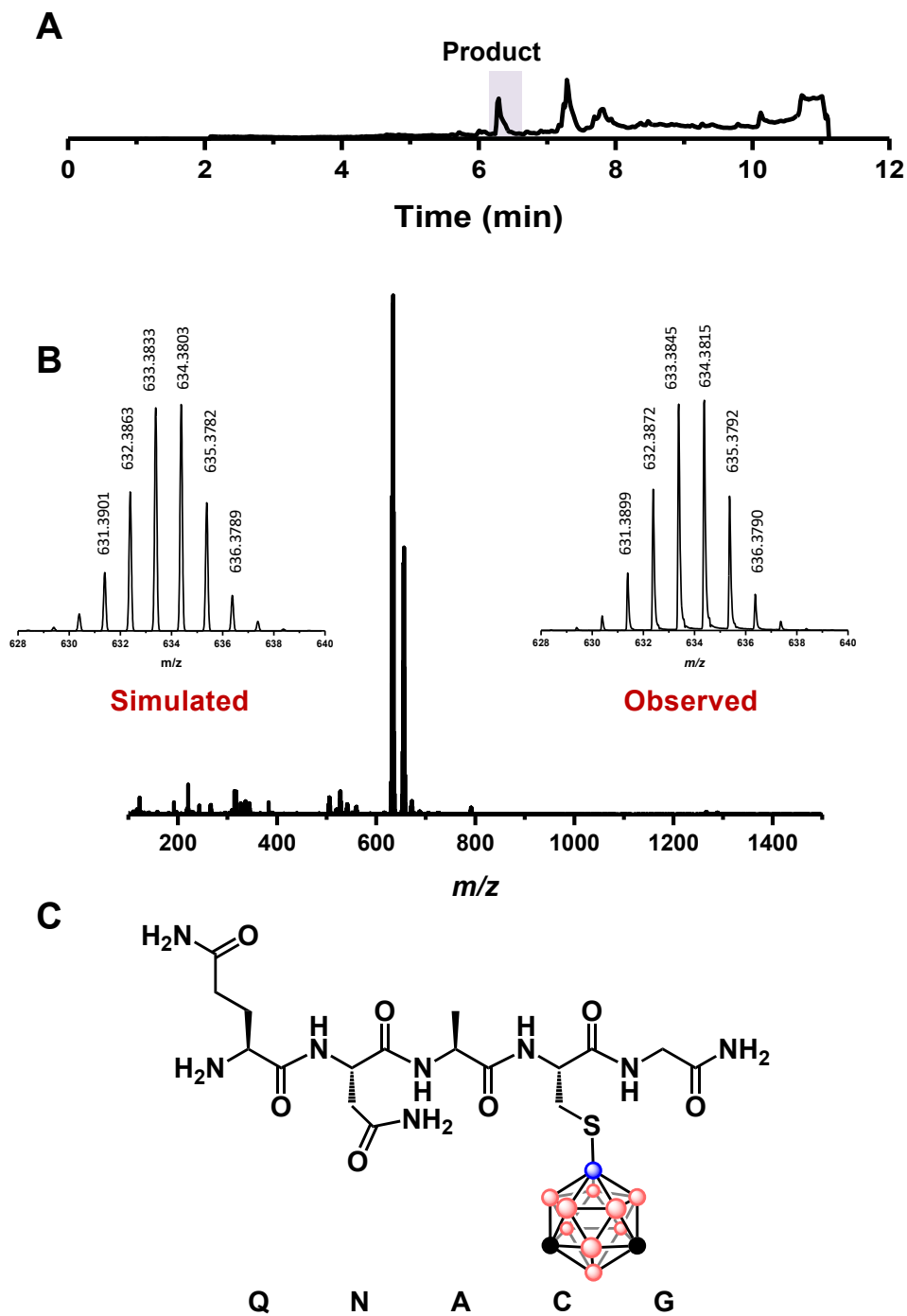


Figure S4.24 A: LC trace corresponding to peptide $\text{H}_2\text{N-QNAC(boryl)G-CONH}_2$. Masses corresponding to Trt-H, $\text{H}_2\text{N-QNAC(Trt)G-CONH}_2$ and $\text{H}_2\text{N-NAC(Trt)G-CONH}_2$ were observed at ~ 7.3 and 7.8 min. **B:** Simulated and observed masses for the borylated product **C:** Line drawing of the resulting borylated peptide.

IV. Cellular Toxicity Studies

Two stock solutions were prepared in phosphate buffered saline (1x concentration): borylated glutathione, **7b**, (1.0 mg, 356 μ M) and acetamide glutathione, **7c**, (0.5 mg, 549 μ M). **7c** was prepared using a previously reported procedure (see Internal Standard Procedure Section I)¹. Both stock solutions were then filtered into autoclaved Eppendorf tubes (1.5 mL) using a 0.2 μ m PTFE Pall syringe filter. To an unopened, sterile 96-well plate, Chinese hamster ovarian cells were plated to a density of 60k per well. Wells A1-C1 were allotted for the live control, A2-C2 the dead control, A3-C3 for 5 μ M **7b**, D3-F3 for 5 μ M **7c**, A4-C4 for 15 μ M **7b**, D4-F4 for 15 μ M **7c**, A5-C5 for 50 μ M **7b** and D5-F5 for 50 μ M **7c**. To each well, the stock solution to generate the indicated concentrations was added and the final volume was brought to 200 μ L using cell media. The well plate was then incubated at 37 °C under a 5% CO₂ atmosphere for 4 h. The well plate was then removed and ~150 μ L of the contents in each well was removed. Trypsin (100 μ L) was added to each well and the solutions were allowed to incubate at 37 °C under a 5% CO₂ atmosphere for 5 min. After incubation, cell media (100 μ L) was added to each well and the entire contents of each well was removed and transferred to 1.5 mL volume Eppendorf tubes, and centrifuged at 17,000 x g for 2 min at 4 °C. The supernatant was discarded, and the cell pellet was resuspended in phosphate buffered saline (1x concentration, 200 μ L). After a second centrifugation at 17,000 x g for 2 min, the supernatant was again removed and phosphate buffered saline (1x concentration, 100 μ L) and trypan blue (0.4%, 100 μ L) were added to each Eppendorf tube except the tubes from cells A2-C2. To these tubes, Triton X (45%, 40 μ L) was added followed by phosphate buffered saline (1x concentration, 60 μ L) and trypan blue (0.4%, 100 μ L). After, 10 μ L of each solution was pipetted onto two sides of a hemocytometer. The number of live and dead cells between both

the top and bottom sides of the hemocytometer were recorded. The average measurement between triplicate solutions (e.g.: A1-C1) was then used to calculate cell viability.

Calculation of % Viability

		1		2		3		4		5	
		L	D	L	D	L	D	L	D	L	D
A	T	241	8	0	4	147	3	116	2	99	2
	B	276	1	0	2	109	1	103	0	86	4
B	T	324	5	1	2	108	4	90	3	58	9
	B	226	10	0	4	98	4	82	3	48	9
C	T	316	2	2	3	138	4	115	1	81	3
	B	192	2	0	5	130	1	115	4	65	3
D	T					117	3	56	1	96	0
	B					103	6	50	1	80	1
E	T					72	2	101	2	75	1
	B					88	4	90	6	84	0
F	T					125	3	123	3	91	0
	B					93	3	76	2	57	3

Table S4.8: Live (L) and dead (D) cell counts observed on hemocytometer where T is the top plate of the hemocytometer and B is the bottom plate of the hemocytometer.

	A1	B1	C1	A2	B2	C2	A3	B3	C3	D3	E3	F3
Sum T	249	277	318	4	3	5	150	112	142	120	74	128
Sum B	277	329	194	2	4	5	110	102	131	109	92	96
Avg Total	263	303	256	3	3.5	5	130	107	136.5	114.5	83	112
Avg Live	258.5	275	254	0	0.5	1	128	103	134	110	80	109
% Viability	98.3	90.8	99.2	0	14.3	20	98.5	96.3	98.2	96.1	96.4	97.3
Average	96			10			98			96.6		
STDEV	5			10			1			0.7		

Table S4.9: The % viability calculated for columns 1-3 with the average and standard deviation reported.

	A4	B4	C4	D4	E4	F4	A5	B5	C5	D5	E5	F5
Sum T	118	93	116	57	103	126	101	67	84	96	76	91
Sum B	110	85	119	51	96	78	90	57	68	81	84	60
Avg Total	114	89	117.5	54	99.5	102	95.5	62	76	88.5	80	75.5
Avg Live	109.5	86	115	53	95.5	99.5	92.5	53	73	88	79.5	74
% Viability	96.0	96.6	97.9	98.1	95.98	97.5	96.9	85.5	96.1	99.4	99.4	98.0
Average	96.8			97			93			98.9		
STDEV	0.9			1			6			0.8		

Table S4.10: The % viability calculated for columns 4-5 with the average and standard deviation reported.

V. ITC and $^{11}\text{B}\{^1\text{H}\}$ NMR Binding Studies

ITC Binding of **7a**, **7b** and **7c** to β -Cyclodextrin

The following solutions were prepared in acetic acid (10 mM, pH = 3.4): **7a** (1.0 mg, 10 mM), **7b** (1.8 mg, 10 mM) and **7c** (2.0, 10 mM). A solution of β -cyclodextrin (2.8 mg, 0.5 mM) was also prepared in acetic acid (10 mM, pH = 3.4). This pH represents the isoelectric point of glutathione. All solutions were sonicated (5 min) and vortexed to ensure complete solubilization. The following parameters were set for the titration of all peptide solutions into β -cyclodextrin solutions: 16 total injections at 25 °C with a reference power set to 10 $\mu\text{cal}/\text{sec}$ at a stirring rate of 750 rpm. After an initial delay of 120 sec, 0.2 μL of peptide solution was injected into the cell for a duration of 0.4 sec (with a filter period of 5 sec). After this first injection, 180 sec were allowed to pass before an additional 2.4 μL was injected for 4.8 sec (with a filter period of 5 sec). This process was repeated 14 times to reach saturation. The enthalpic output (kcal mol^{-1} of injectant) of unmodified peptide was subtracted from the borylated peptide titration enthalpic output to ensure all observed binding events were due to the boryl fragment rather than side chains. The subtracted data (Figures 4.4B and 4.4C) are plotted alongside the data of the unmodified peptide control (Figure 4.4D).

Binding of **2a** and **2b** to β -Cyclodextrin

Binding of **2b** towards β -cyclodextrin was verified through ITC to yield a binding constant, $K_a = 1.1 \times 10^3 \pm 700 \text{ M}^{-1}$ (SI Figure S4.25). After, inclusion was also probed through $^{11}\text{B}\{^1\text{H}\}$ NMR spectroscopy by titration of a solution containing β -cyclodextrin to a solution containing **2b**. The singlet assigned to the $^{11}\text{B}(9)\text{-S}$ nucleus on the intact *m*-carborane cluster attached to the peptide was shifted downfield as β -cyclodextrin was titrated to the solution. Scatchard treatment¹⁶ of the data resulted in a binding constant, $K_a = 1.49 \times 10^3 \text{ M}^{-1}$ (SI Figure S4.27).

ITC Parameters

Solutions of **2b** (0.5 mg, 5 mM) and **2a** (0.3 mg, 5 mM) were prepared in Tris•HCl/Trizma buffer (10 mM, pH = 8.2) containing guanidine hydrochloride (3M). A solution of β -cyclodextrin (7.1 mg, 0.25 mM) was also prepared in Tris•HCl/Trizma buffer (10 mM, pH = 8.2) containing guanidine hydrochloride (3M). This pH represents the isoelectric point of **2a**. All solutions were subjected to sonication (5 min) and mixing under vortex to ensure solubility. Guanidine hydrochloride was incorporated as a denaturing agent. The following parameters were set for the titration of all peptide solutions into β -cyclodextrin solutions: 16 total injections at 25 °C with a reference power set to 10 μ cal/sec at a stirring rate of 750 rpm. After an initial delay of 120 sec, 0.2 μ L of peptide solution was injected into the cell for a duration of 0.4 sec (with a filter period of 5 sec). After this first injection, 180 sec were allowed to pass before an additional 2.4 μ L was injected for 4.8 sec (with a filter period of 5 sec). This process was repeated 14 times to reach saturation. The enthalpic output (kcal mol^{-1} of injectant) of unmodified peptide was subtracted from the borylated peptide titration enthalpic output to ensure all observed binding events were due to the boryl fragment rather than side chains.

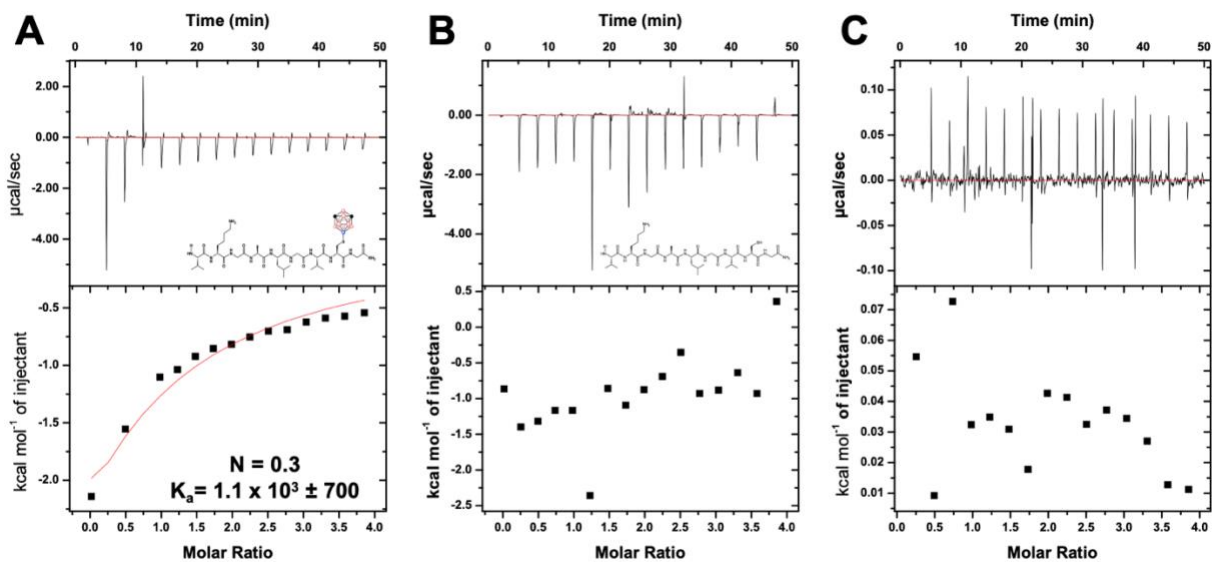


Figure S4.25 **A:** ITC plot of the titration of **2b** to β -cyclodextrin **B:** ITC plot of the titration of **2a** to β -cyclodextrin **C:** ITC plot of the titration of buffer to β -cyclodextrin.

$^{11}\text{B}\{^1\text{H}\}$ NMR Binding Studies

Solutions of peptide **2b** (0.5 mg, 1.6 mM) and β -cyclodextrin (5.7 mg, 5.0 mM) were prepared in D_2O . The solution containing peptide **2b** was added to an NMR tube and a $^{11}\text{B}\{^1\text{H}\}$ NMR spectrum was collected as summarized by Entry A of Table S4.11. After, an aliquot of β -cyclodextrin solution (25 μL) was added to the NMR tube and mixed by tilting the NMR up and down 5 times to yield Entry B. After, a $^{11}\text{B}\{^1\text{H}\}$ NMR spectrum was collected. This process was repeated 5 times as described by Entries C-G of Table S4.11. Downfield shift in the singlet ascribed to the $^{11}\text{B}(9)$ nucleus was used to assess the **2b** $\subset\beta$ -cyclodextrin inclusion complex as described by Figure S4.26. Scatchard treatment¹⁶ of the data yielded an association constant $K_a = 1.49 \times 10^3 \text{ M}^{-1}$ with an $R^2 = 0.862$ as summarized by Figure S4.27.

Entry	Chemical Shift (δ) Ascribed to $^{11}\text{B}(9)$ Nucleus	Δ Chemical Shift (δ)	Concentration 2b (M)	Concentration β -Cyclodextrin (M)
A	-0.70	-	0.0016	-
B	-0.48	0.94	0.0015	0.00037
C	-0.30	0.158	0.0014	0.00069
D	-0.11	0.2	0.0013	0.00096
E	-0.02	0.104	0.0012	0.0012
F	0.1	0.102	0.0011	0.0014
G	0.15	0.014	0.0011	0.0016

Table S4.11: The reaction mixtures and corresponding chemical shifts associated with the titration of β -cyclodextrin to **2b**.

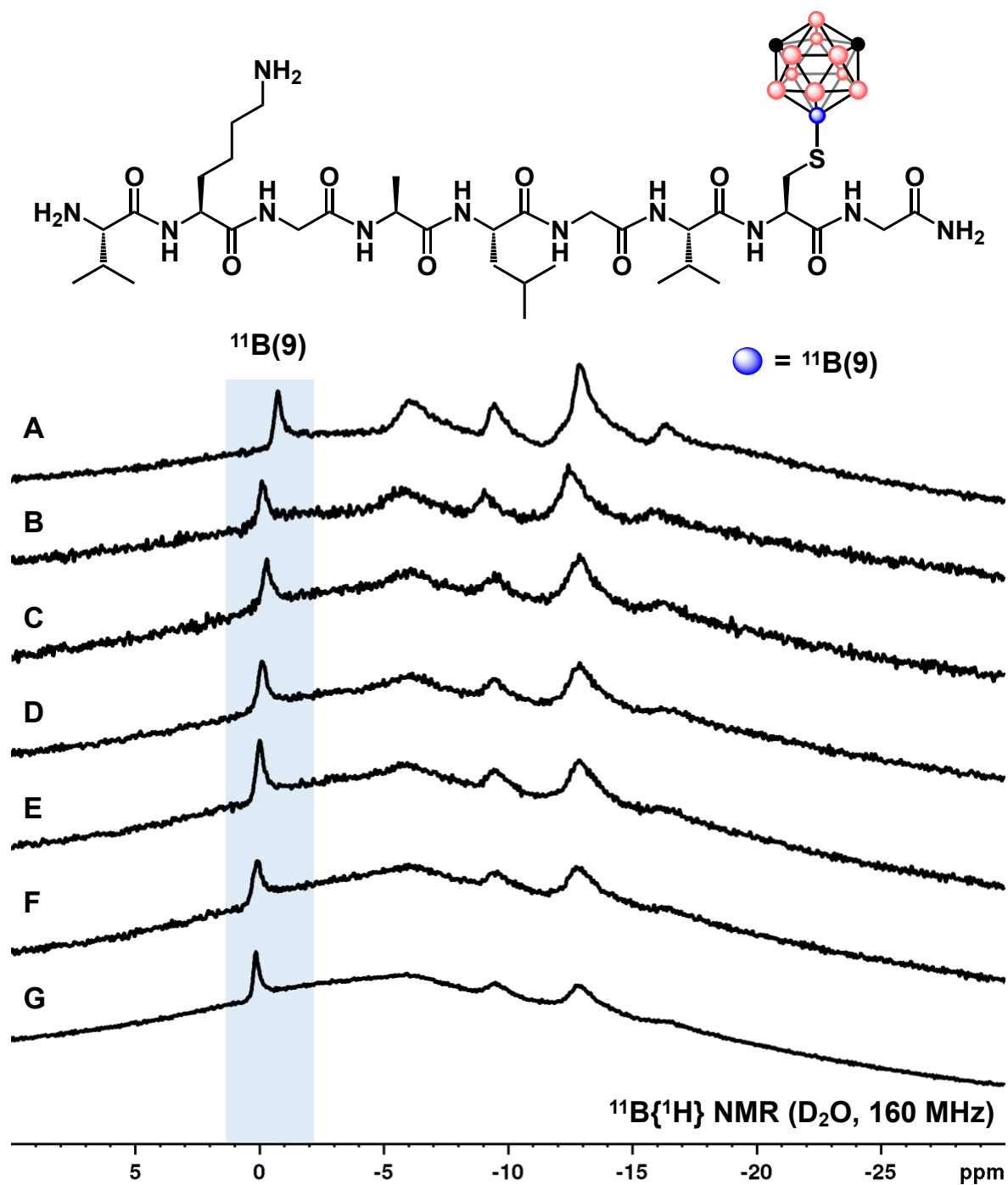


Figure S4.26: $^{11}\text{B}\{^1\text{H}\}$ NMR (D_2O , 160 MHz) spectra of the titration of β -cyclodextrin to **2b** as described by Entries A-G in Table S4.7.

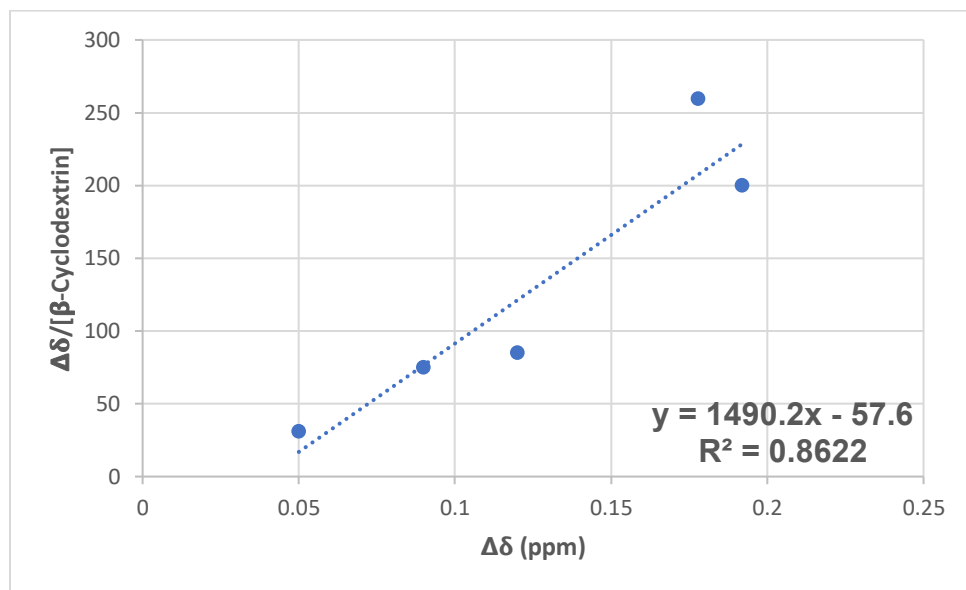


Figure S4.27: Scatchard plot of the titration of β -cyclodextrin to **2b** as described by Entries A-G in Table S4.11 to yield an association constant $K_a = 1.49 \times 10^3 \text{ M}^{-1}$ with an $R^2 = 0.862$.

VI. Proteinase K Degradation Studies

Stock solutions (10 $\mu\text{g}/\mu\text{L}$) of peptides **2a**, **2b** and **2c** were prepared in water. Additionally, Proteinase K (0.8 mg) was dissolved in 1.0 mL deionized water to produce a 0.8 $\mu\text{g}/\mu\text{L}$ solution in an Eppendorf tube (1.5 mL). After, the following stock solutions were prepared in Falcon tubes (10.0 mL): calcium chloride dihydrate (37.0 mg) in 5.0 mL deionized water to produce a 50 mM solution and β -cyclodextrin (57.0 mg) in 10.0 mL deionized water to produce a 5 mM solution. Finally, a Tris•HCl/Trizma buffered solution (50.0 mL, 100 mM) was prepared at pH 8.0. Aliquots of these stock solutions were added to an Eppendorf tube (1.5 mL) in volumes described by Table X. All entry components except Proteinase K were combined and vortexed for \sim 30 sec prior to the addition of Proteinase K. Finally, the Proteinase K was added and the Eppendorf tube was vortexed for \sim 10 sec and placed into a sand bath at 55 $^{\circ}\text{C}$ for 5 min. After 5 min, an aliquot of each reaction mixture (50 μL) was removed and placed into an Eppendorf containing protease inhibitor phenylmethyl sulfonyl fluoride (1.0 mM, 100 μL), water acidified with 0.1% TFA (25 μL) and 3-bromomethyl pyridine HBr (23.7 mM, 25 μL) as an internal standard. This entire process was repeated a second time with fresh stock solutions for error analysis. The reaction mixtures were then analyzed by LCMS (Figure S4.24) as described in Section I except the injection volume was increased from 0.3 μL to 5 μL .

Entry	Water (αL)	Buffer (αL)	Peptide 2a (αL)	Peptide 2b (αL)	Peptide 2c (αL)	CaCl ₂ (αL)	b-Cyclodextrin (αL)	Proteinase K (αL)
A	65.0	100.0	10.0	-	-	20.0	-	5.0
B	45.0	100.0	10.0	-	-	20.0	20.0	5.0
C	70.0	100.0	-	-	10.0	10.0	-	-
D	45.0	100.0	-	-	10.0	20.0	-	5.0
E	65.0	100.0	-	-	10.0	20.0	20.0	5.0
F	70.0	100.0	-	10.0	-	20.0	-	-
G	45.0	100.0	-	10.0	-	20.0	-	5.0
H	65.0	100.0	-	10.0	-	20.0	20.0	5.0

Table S4.12: The reaction mixtures corresponding to entries A-H.

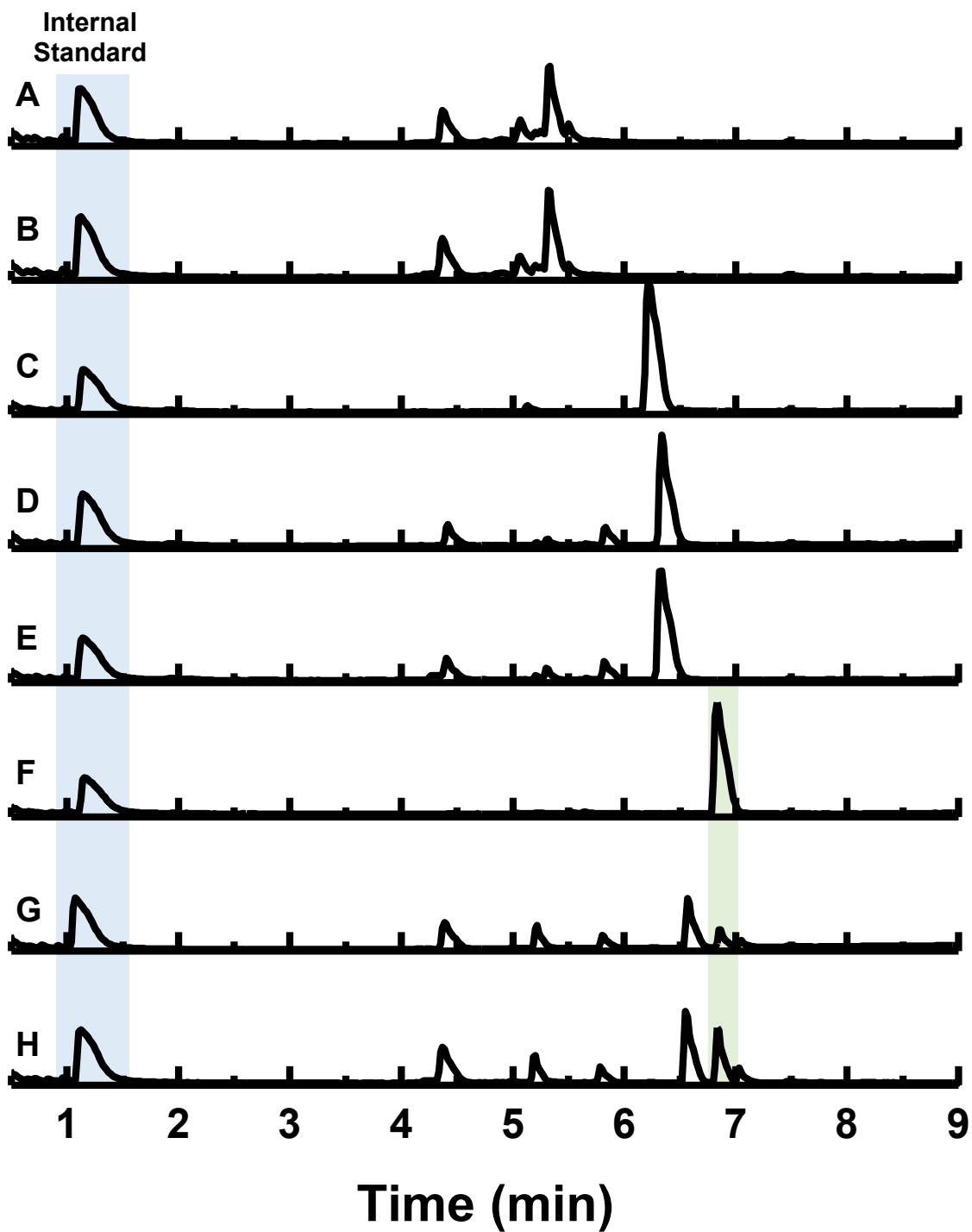


Figure S4.28: Representative LC traces corresponding to entries A-H described in **Table S8**. The retention time of intact **2c** is highlighted in red while intact **2b** is highlighted in green.

Calculation of % Degraded

All data are reported as an average of two trials as described by Table S4.13. As no peptide remained intact for entries A-E, a percentage of peptide remaining could not be calculated. A corrective response factor, F , was calculated using equation (1):

$$(1) F = \frac{\text{Area}_{\text{Intact Peptide in Entry F}} / \text{Concentration}_{\text{Intact Peptide in Entry F}}}{\text{Area}_{\text{Internal Standard in Entry F}} / \text{Concentration}_{\text{Internal Standard in Entry F}}}$$

The concentration of peptide in each entry was then calculated using this corrective factor as described by equation (2):

$$\text{Peptide Remaining} = \frac{F \times \text{Concentration}_{\text{Internal Standard}} \times \text{Area}_{\text{peptide}}}{\text{Area}_{\text{Internal Standard}}}$$

The percentage of peptide remaining represents the ratio of the concentration of peptide calculated to the concentration of peptide theoretically in solution given the reactants described by Table S4.13. All data were normalized to control sample Entry F where no Proteinase K was incorporated and no degradation was observed.

Entry	Trial	Internal Standard Integration by LCMS	Intact Peptide Integration by LCMS	Response Factor, F	Concentration of Peptide in Trace (M)	Peptide Remaining (%)	Normalization	Average	Standard Deviation
F	-	1802918467	3170687750		1.83007E-05	87.98118269	100.000003	-	-
G	1	2088289113	237290391		1.18244E-06	32.11028636	44.1291064	45	1
H	2	3983531140	483082504	2.70560	1.26195E-06	51.62640758	63.6452276		
G	1	1962549068	414868096		2.19978E-06	63.54564758	75.5644676	70	10
H	2	3689486520	1462184537		4.12408E-06	65.21454314	77.2333631		

Table S4.13: Calculation of peptide remaining across multiple trials of entries G and H.

VII. Angiotensin-Converting Enzyme (ACE) Studies

ACE inhibition studies were derived from Otte, J. *et al.*¹⁷ ACE from rabbit lung was prepared as a 0.25 unit/mL solution. Stock solutions of peptide **8a** (0.5 mg, 100 μ M) and peptide **8b** (0.3 mg, 100 μ M) were prepared in deionized water. A solution of FA-PGG (10.5 mg, 0.88 mM) was prepared in 30 mL Tris•HCl/Trizma buffer (50 mM, pH= 8.2) that contained NaCl (0.53 g, 0.3 M). These stock solutions were used to prepare the reaction mixtures outlined in Table S8. Upon mixing of the components, the reaction mixtures were transferred to a Fisher quartz cuvette (1.0 mL) and the cuvette was lowered into a sand bath set to 37 °C. After heating for 5 min, the cuvette was removed and the UV-Vis spectrum was collected from 200-800 nm. The cuvette was then returned to the sand bath until 2 minutes had elapsed. At this time, the cuvette was removed and another UV-Vis spectrum from 200-800 nm was collected. This process was repeated until a total reaction time of 21 min was reached. The absorbance at 340 nm was recorded and plotted as a function of time (Figures S4.29-S4.38). The % inhibition was determined by the ratio of the slope when inhibitor is present by the slope when no inhibitor is present as summarized by equation (3).

$$(3) \quad \% \text{ ACE Inhibition} = \left[1 - \left(\frac{\rho A_{\text{Inhibitor}}}{\rho A_{\text{Control}}} \right) \right] \times 100$$

All entries and the corresponding % inhibition are summarized in Tables S4.14 and S4.15. All reactions were conducted in duplicate.

Entry	ACE Stock (αL)	Water (αL)	FA-PGG Stock (αL)	Peptide 2a (αL)	Peptide 2b (αL)
A	40.0	560.0	200.0	-	-
B	40.0	560.0	200.0	-	-
C	40.0	540.0	200.0	-	40.0
D	40.0	540.0	200.0	-	40.0
E	40.0	540.0	200.0	40.0	-
F	40.0	540.0	200.0	40.0	-
G	40.0	160.0	200.0	-	400.0
H	40.0	160.0	200.0	-	400.0
I	40.0	160.0	200.0	400.0	-
J	40.0	160.0	200.0	400.0	-

Table S4.14: Reaction mixtures used to assess the inhibition of peptides **8a** and **8b**.

Entry	Slope	% Inhibition	Average % Inhibition	Error
A	0.0141	0		
B	0.012	0	0	-
C	0.0112	14.2		
D	0.0104	20.3	17	4
E	0.0104	20.3		
F	0.0094	28.0	24	5
G	0.0061	53.3		
H	0.0064	51.0	52	1
I	0.0067	48.7		
J	0.0054	58.6	54	7

Table S4.15: The slope and % inhibition corresponding to each entry described by Table S4.10.

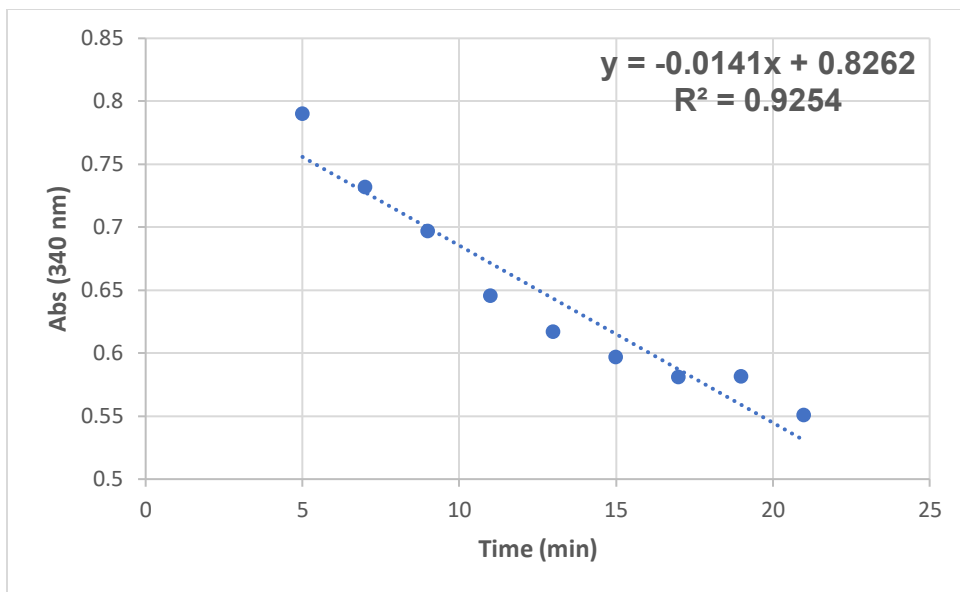


Figure S4.29: The absorbance of entry A detected across minutes 5-20.

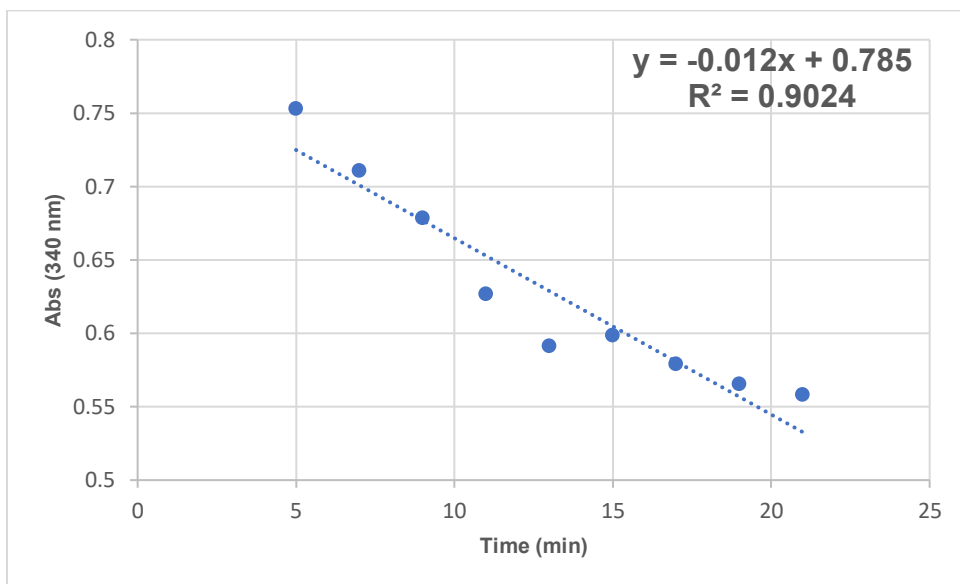


Figure S4.30: The absorbance of entry B detected across minutes 5-20.

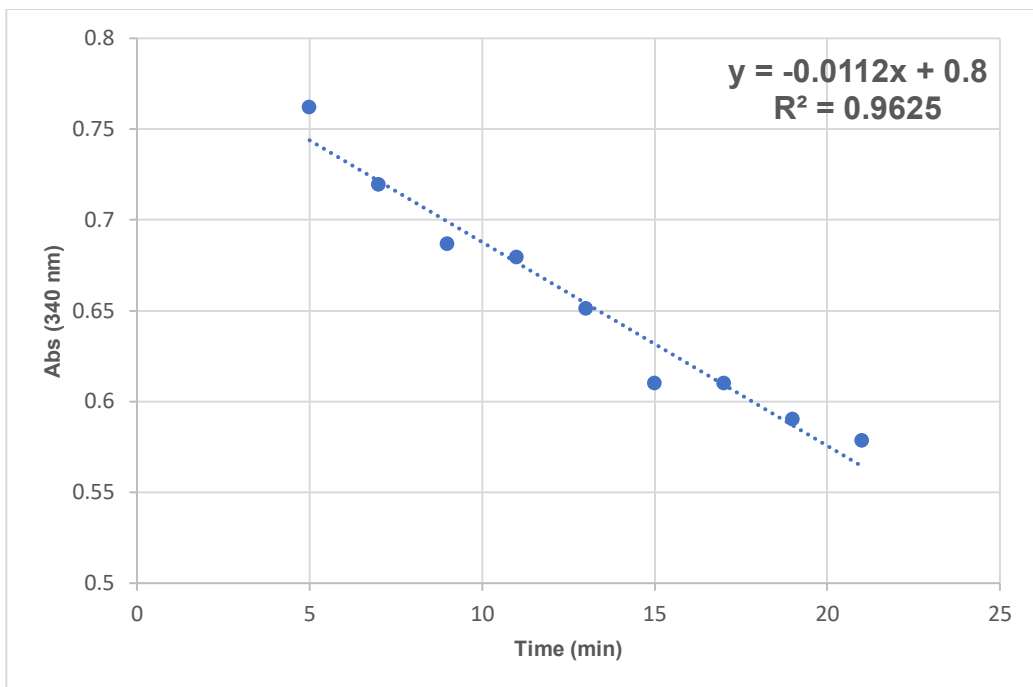


Figure S4.31: The absorbance of entry C detected across minutes 5-20.

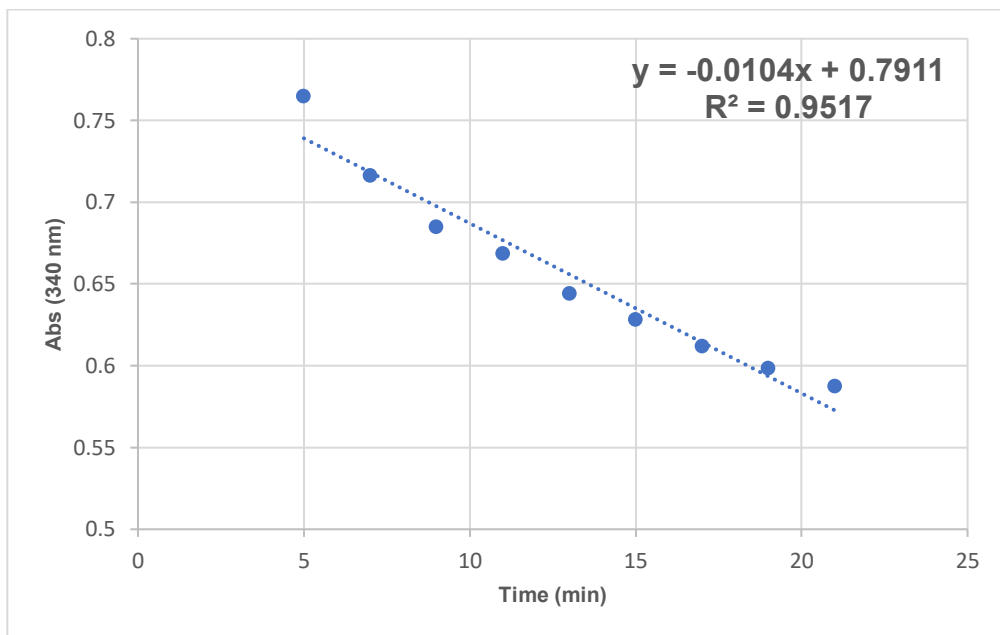


Figure S4.32: The absorbance of entry D detected across minutes 5-20.

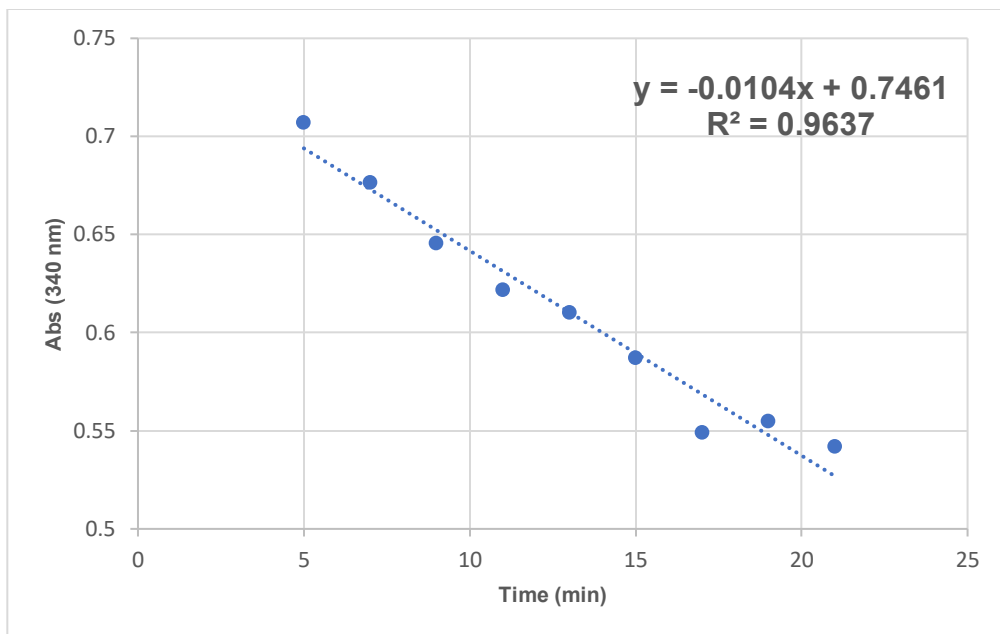


Figure S4.33: The absorbance of entry E detected across minutes 5-20.

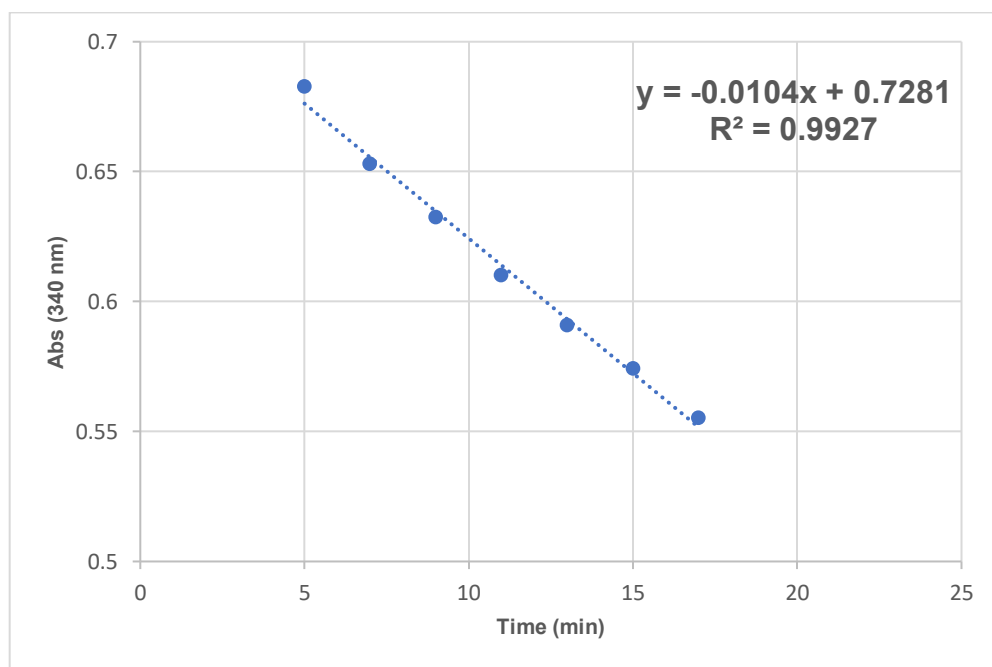


Figure S4.34: The absorbance of entry F detected across minutes 5-20.

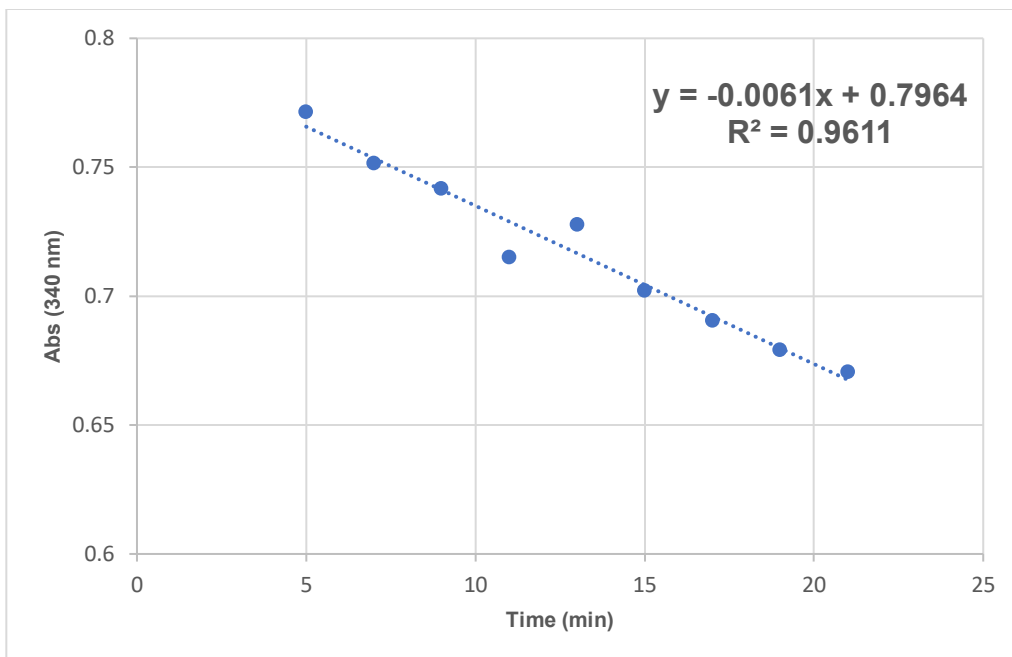


Figure S4.35: The absorbance of entry G detected across minutes 5-20.

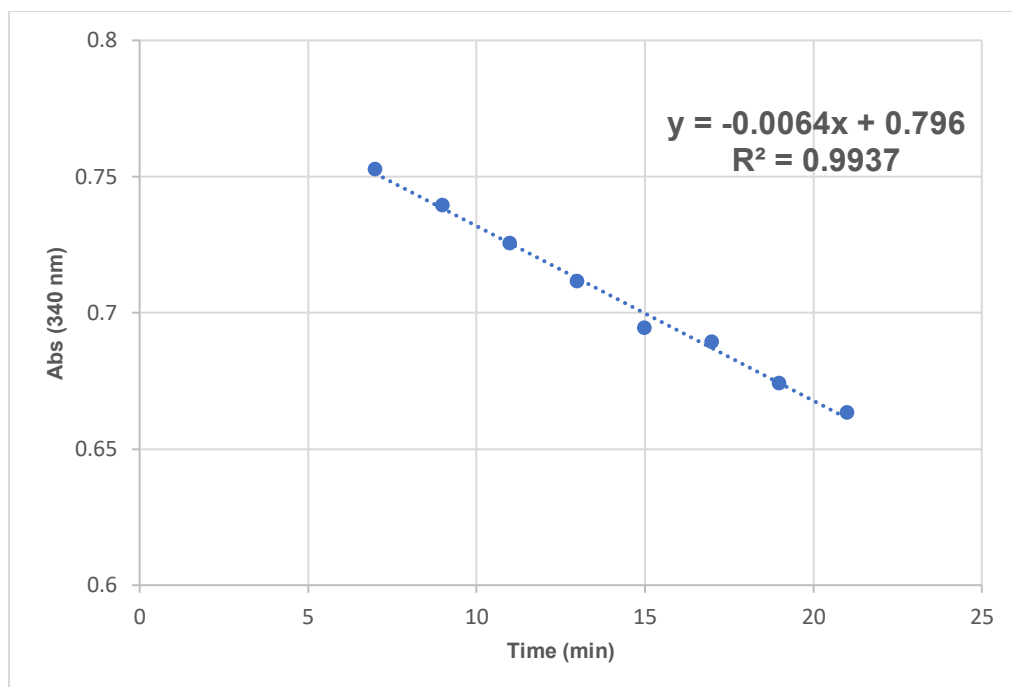


Figure S4.36: The absorbance of entry H detected across minutes 5-20.

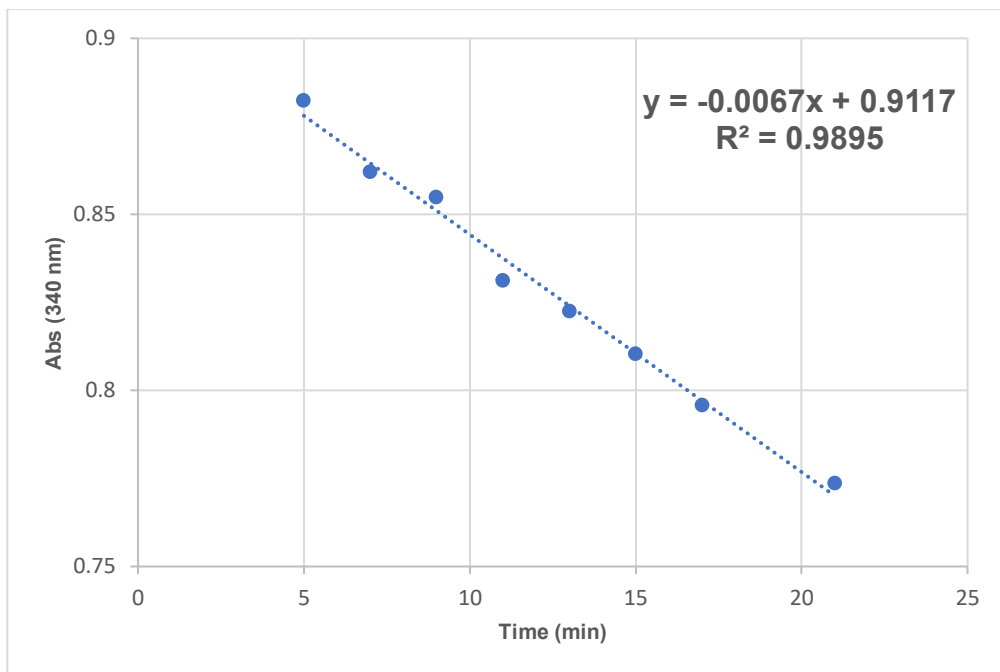


Figure S4.37: The absorbance of entry I detected across minutes 5-20.

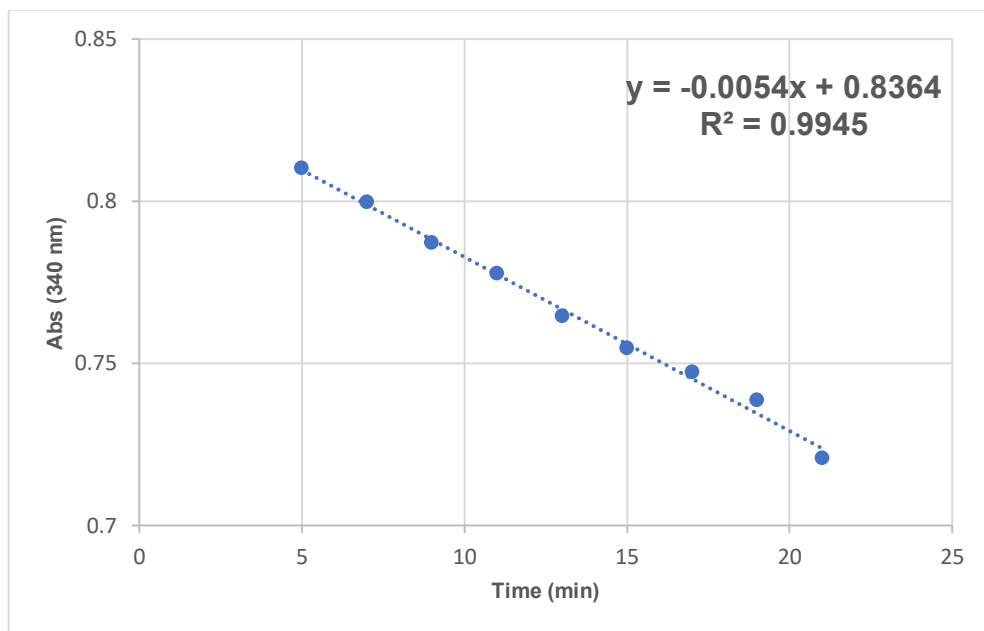


Figure S4.38: The absorbance of entry J detected across minutes 5-20.

VIII. Molecular Dynamics Simulations

Peptides **2a**, **2b** and **2c** were initially positioned in a similar way as transition state analog peptide inhibitors of proteinase K.^{9,19} According to previous studies, the substrate recognition site of proteinase K is formed by two segments, to Gly100 to Tyr104 and Ser132 to Gly136.⁹ The peptide substrate binds between these two segments as the center strand of a three-stranded antiparallel β -pleated sheet with the C-terminus of the peptide near the catalytic triad, Asp39-His69-Ser224.⁹ In each binding simulation, peptides **2a**, **2b** and **2c** are prepared in β -sheet geometry with Avogadro²⁰ and positioned between the two-segment substrate recognition site with the C-terminus facing the catalytic triad. The initial geometries and positions of the peptides relative to proteinase K for the three systems were aligned using the “measure fit” function in VMD.¹⁸ The three systems have all been equilibrated for 120 ns (Figures 4.5, S4.39). In the simulation of **2b** interacting with Proteinase K, the carborane cluster binds to a binding pocket within 5 ns of equilibration and binds to that pocket stably afterwards throughout the entire 120 ns of equilibration (Figures S4.40-S4.41).

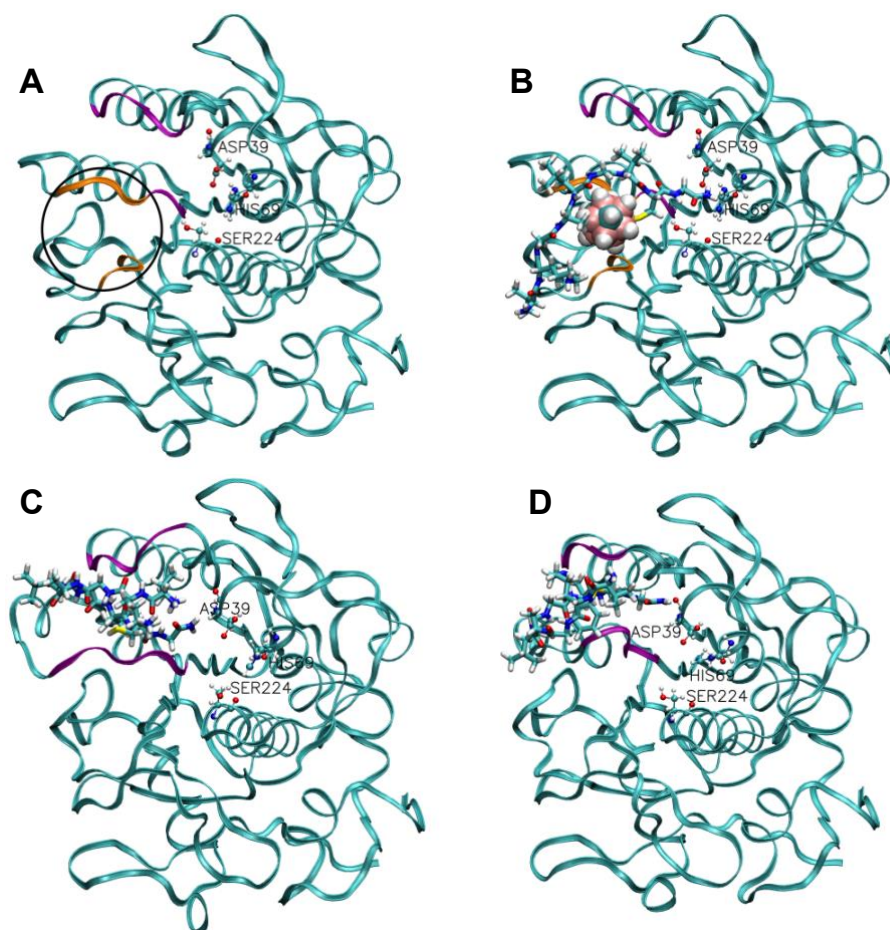


Figure S4.39: Molecular dynamics simulations rendered as stick and ribbon of **A:** the secondary binding pocket identified as an important docking site, **B:** **2b** binding with Proteinase K, **C:** **2a** binding with Proteinase K and **D:** **2c** binding with Proteinase K at 120 ns of equilibration. Proteinase K is represented using QuickSurf representation in VMD.

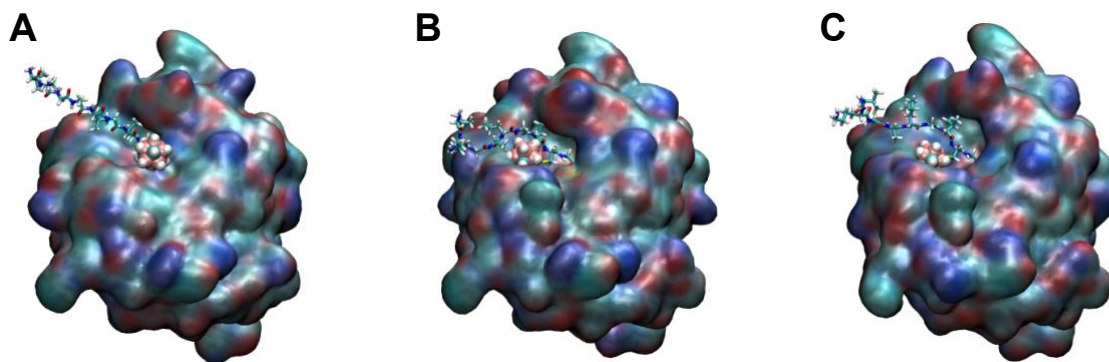


Figure S4.40: The binding of **2b** with proteinase K, at **A:** 0 ns, **B:** 5 ns and **C:** 120 ns of equilibration.

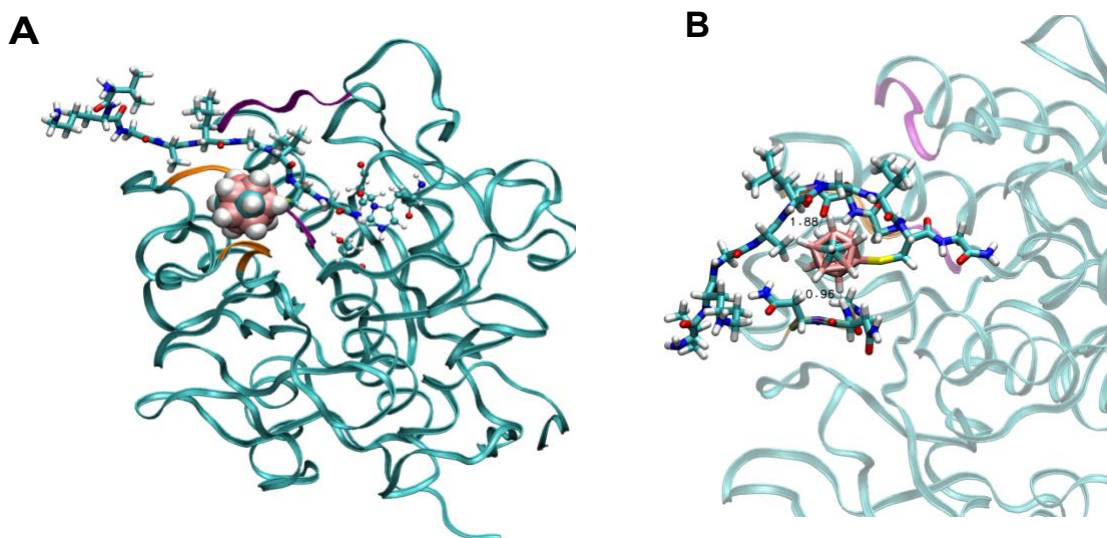


Figure S4.41 A: The binding of **2b** with proteinase K at 120 ns of equilibration; the proteinase K is shown in Ribbons representation with the substrate binding site in purple and carborane binding pocket in orange; the catalytic triad residues are shown in ball-and-stick model **B:** Detailed view of the carborane binding pocket with representative B-H \cdots H-N dihydrogen bonding (H to H distance of 0.96 Å) and C-H \cdots O hydrogen bonding (H to O distance of 1.88 Å)

The binding pocket of the carborane consists of two segments, one of which, Gly134-Gly135-Gly-136, is also part of the substrate recognition site and the other is Gly160-Asn161-Asn162. The residues that line the binding pocket contain only amide functional groups; therefore, binding through B-H \cdots H-N dihydrogen bonds is implicated (Figure S4.41B).^{21,22} The acidic C-H vertices of carborane may also form C-H \cdots O (Figure S4.41B) or C-H \cdots N hydrogen bonds.^{22,23} Comparatively, simulations of **2a** and **2c** binding to Proteinase K indicate only 3-4 residues from the C-terminus stay bound between the two segments of the substrate recognition site without apparent interactions with other parts of the protein (Figure S4.42).

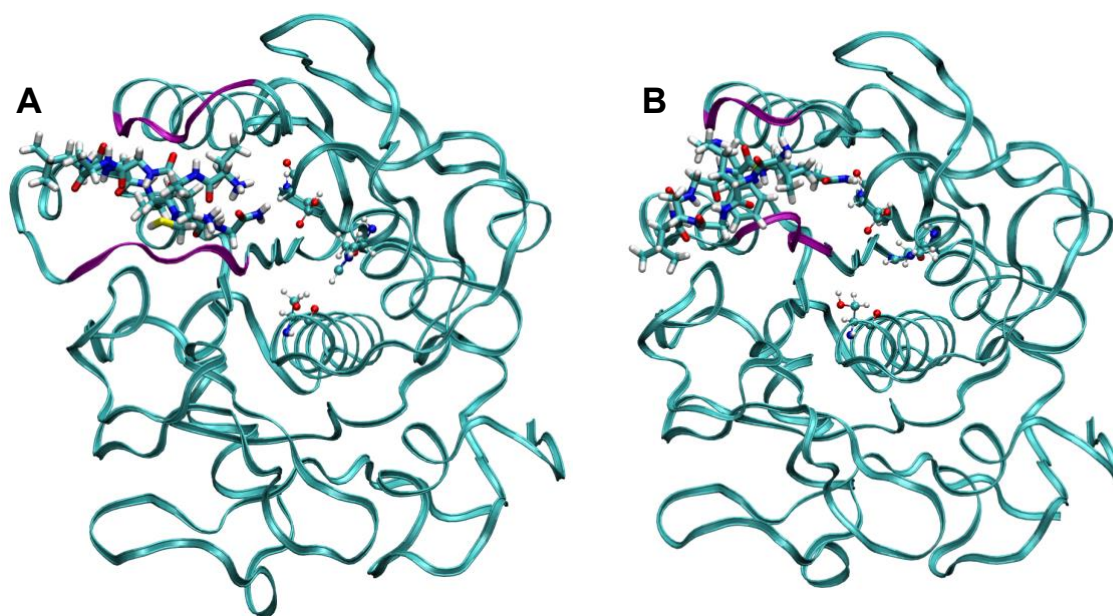


Figure S42 A: The unmodified and **B:** Cys-arylated nonapeptide binding with proteinase K at 120 ns of equilibration; the proteinase K is shown in Ribbons representation with the substrate binding site in purple.

The unique binding pocket for **2b** may pull the C-terminus of the peptide away from the catalytic triad, preventing nucleophilic attack by the hydroxyl oxygen atom of Ser224 on the

carbonyl carbon atom of the peptide bond,²⁴ thereby protecting **2b** from hydrolysis. Over the 120-ns trajectory (Figure S4.43), the average center-to-center distance between **2a** and the catalytic triad is 13.49 Å while that between **2b** and the catalytic triad is 15.60 Å. The binding of the carborane to the binding pocket and the consequent steering of the peptide away from peptidolytic residues may be another explanation for the protection afforded by the borylation beyond the steric hindrance that obviates the approach of bulkier **2b** to the substrate binding site and the nearby catalytic triad.

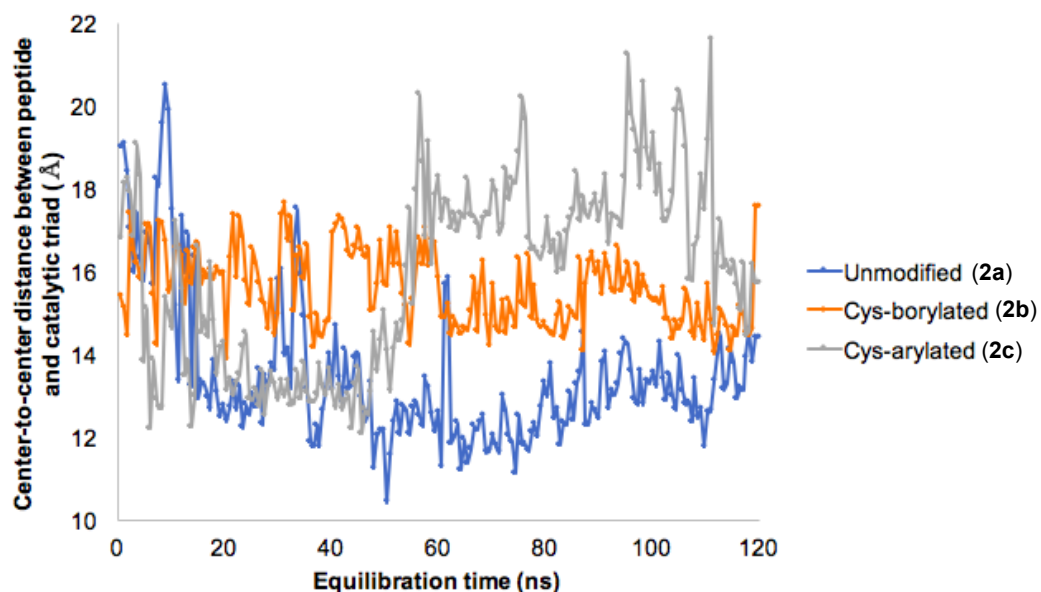


Figure S4.43: Center-to-center distance between the nonapeptide (unmodified, Cys-borylated or Cys-arylated) and the catalytic triad over 120 ns of equilibration.

IX. SI References

1. Vinogradova, E. V., Zhang, C., Spokoyny, A. M., Pentelute, B. L. & Buchwald, S. L. Organometallic Palladium Reagents for Cysteine Bioconjugation. *Nature* **2015**, *526*, 687-691.
2. Messina, M. S., Stauber, J. M., Waddington, M. A., Rheingold, A. L., Maynard, H. D. & Spokoyny, A. M. Organometallic Gold(III) Reagents for Cysteine Arylation. *J. Am. Chem. Soc.* **2018**, *140*, 7065-7069.
3. Saleh, L. M. A., Dziedzic, R. M., Khan, S. I. & Spokoyny, A. M. Forging Unsupported Metal-Boryl Bonds with Icosahedral Carboranes. *Chem. Eur. J.* **2016**, *22*, 8466-8470.
4. Jullian, M., Hernandez, A., Maurras, A., Puget, K., Amblard, M., Martinez, J. & Subra, G. N-Terminus FITC labeling of peptides on solid support: the truth behind the spacer. *Tet. Lett.* **2009**, *50*, 260-263.
5. Phillips, J. C., Braun, R., Wang, W., Gumbart, J., Tajkhorshid, E., Villa, E., Chipot, C., Skeel, R. D., Kale L. & Schulten, K. Scalable molecular dynamics with NAMD. *J. Comput. Chem.* **2005**, *26*, 1781-1802.
6. Jorgensen, W. L., Chandrasekhar, J., Madura, J. D., Impey, R. W. & Klein, M. L. Comparison of simple potential functions for simulating liquid water. *J. Chem. Phys.* **1983**, *79*, 926-935.
7. Vanommeslaeghe, K., Hatcher, E., Acharya, C., Kundu, S., Zhong, S., Shim, J., Darian, E. et al. CHARMM general force field: A force field for drug-like molecules compatible with the CHARMM all-atom additive biological force fields. *J. Comput. Chem.* **2010**, *31*, 671-690.

8. MacKerell Jr, A. D., Bashford, D., Bellott, M. L. D. R., Dunbrack Jr, R. L., Evanseck, J. D., Field, M. J., Fischer, S., Gao, J., Guo, H., Ha, S., Joseph-McCarthy, D., Kuchnir, L., Kuczera, K., Lau, F. T. K., Mattos, C., Michnick, S., Ngo, T., Nguyen, D., Prodhom, B., Reiher, W., Roux, B., Schlenkrich, M., Smith, J., Stote, R., Straub, J., Watanabe, M., Yin D. & Wiorkiewicz-Kuczera, J. All-atom empirical potential for molecular modeling and dynamics studies of proteins. *J. Phys. Chem. B* **1998**, *102*, 3586-3616.
9. Wolf, W. M., Bajorath, J., Muller, A., Raghunathan, S., Singh, T. P., Hinrichs, W. & Saenger, W. Inhibition of Proteinase K by methoxysuccinyl-Ala-Ala-Pro-Ala-chloromethyl ketone. An x-ray study at 2.2-Å resolution. *J. Biol. Chem.* **1991**, *266*, 17695-17699.
10. Frisch, M. J., Trucks, G. W., Schlegel, H. B., Scuseria, G. E., Robb, M. A., Cheeseman, J. R., Scalmani, G. et al. Gaussian 09, Revision A.02, Gaussian, Inc., Wallingford, CT, 2016.
11. Breneman, C. M. & Wiberg, K. B. Determining atom-centered monopoles from molecular electrostatic potentials. The need for high sampling density in formamide conformational analysis. *J. Comput. Chem.* **1990**, *11*, 361-373.
12. Mayne, C. G., Saam, J., Schulten, K., Tajkhorshid, E. & Gumbart, J. C. Rapid parameterization of small molecules using the force field toolkit. *J. Comput. Chem.* **2013**, *34*, 2757–2770.
13. Qian, E. A., Wixtrom, A. I., Axtell, J. C., Saebi, A., Jung, D., Rehak, P., Han, Y. Mouilly, E. H., Mosallaei, D., Chow, S., Messina, M., Wang, J.-Y., Royappa, A. T., Rheingold, A. L., Maynard, H. D., Kral, P. & Spokoyny, A. M.* “Atomically Precise Organomimetic Cluster Nanomolecules Assembled via Perfluoroaryl-Thiol S_NAr Chemistry”, *Nature Chem.* **2017**, *9*, 333-340.

14. Darden, T., York, D. & Pedersen, L. Particle mesh Ewald: An N log (N) method for Ewald sums in large systems. *J. Chem. Phys.* **1993**, *98*, 10089-10092.
15. Han, Y., Albericio, F. & Barany, G. Occurrence and Minimization of Cysteine Racemization during Stepwise Solid-Phase Peptide Synthesis^{1,2}. *J. Org. Chem.* **1997**, *62*, 4307-4312.
16. Fielding, Lee. NMR Methods for the Determination of Protein-Ligand Dissociation Constants. *Curr. Top. Med. Chem.* **2003**, *3*, 39-53.
17. Shalaby, S. M., Zakora, M. & Otte, J. Performance of two commonly used angiotensin-converting enzyme inhibition assays using FA-PGG and HHL as substrates. *J. Dairy Res.* **2006**, *73*, 178-186.
18. Humphrey, W., Dalke, A. & Schulten, K. VMD: visual molecular Dynamics. *J. Mol. Graph.* **1996**, *14*, 33-38.
19. Liu, S.-Q., Tao, Y., Meng, Z.-H., Fu, Y.-X. & Zhang, K.-Q. The effect of calciums on molecular motions of Proteinase K. *J. Mol. Model.* **2011**, *17*, 289-300.
20. Hanwell, M. D., Curtis, D. E., Lonie, D. C., Vandermeersch, T., Zurek, E. & Hutchison, G. R. Avogadro: An advanced semantic chemical editor, visualization, and analysis platform. *J. Cheminformatics* **2012**, *4*, 1-17.
21. Fanfrlík, J., Lepšík, M., Horinek, D., Havlas, Z. & Hobza, P. Interaction of carboranes with biomolecules: formation of dihydrogen bonds. *ChemPhysChem* **2006**, *7*, 1100-1105.
22. Sarosi, M-B., Neumann, W., Lybrand, T. P. & Hey-Hawkins, E. Molecular modeling of the interactions between carborane-containing analogs of indomethacin and cyclooxygenase-2. *J. Chem. Inf. Model.* **2017**, *57*, 2056-2067.

23. Scholz, M. & Hey-Hawkins, E. Carbaboranes as pharmacophores: properties, synthesis, and application strategies. *Chem. Rev.* **2011**, *111*, 7035-7062.
24. Liu, S.-Q., Liang, L.-M., Tao, Y., Yang, L.-Q., Ji, X.-L., Yang, J.-K., Fu, Y.-X. & Zhang, K.-Q. Structural and dynamic basis of serine proteases from nematophagous fungi for cuticle degradation. in *Pesticides in the Modern World—Pests Control and Pesticides Exposure and Toxicity Assessment* ed. Stoytcheva, M.; Intech, 2011.
25. Wingfield, P. T. N-terminal methionine processing. *Curr. Protoc. Protein Sci.* **2017**, *88*, 6.14.1–6.14.3.

CHAPTER 5

Narratives of Undergraduate Research, Mentorship, and Teaching at UCLA

This chapter is a version of Stevens, S. L.; Phung, A. C.; Gonzalez, A.; Shao, Y.; Moully, E. H.; Nguyen, V. T.; Martin, J. L.; Mao, C.; Saebi, A.; Mosallaei, A.; Kirolos, M.; Chong, P.; Umanzor, A.; Qian, K.; Marin, G.; Ebrahim, O. M.; Pathuri, R. S.; Hopp, M.; Ramachandran, R.; Waddington, M. A.; Spokoyny, A. M. "Narratives of Undergraduate Research, Mentorship, and Teaching at UCLA", *Pure & Appl. Chem.* **2021**, *93*, 207-221.

Abstract

This work describes select narratives pertaining to undergraduate teaching and mentorship at UCLA Chemistry and Biochemistry by Alex Spokoyny and his junior colleagues. Specifically, we discuss how individual undergraduate researchers contributed and jump-started multiple research themes since the conception of our research laboratory. This work also describes several recent innovations in the inorganic and general chemistry courses taught by Spokoyny at UCLA with a focus of nurturing appreciation for research and creative process in sciences including the use of social media platforms.

Introduction

The Spokoyny laboratory opened its doors at UCLA on August 1, 2014; through the past six years, we have been actively engaged in creating a world-class research environment and infrastructure to fully support our scientific and teaching needs.

As a UCLA alumnus and having conducted undergraduate research in chemistry, Spokoyny feels strongly about creating more of such opportunities for the next generation of UCLA undergraduates. As a result, in less than six years our group has mentored and graduated over 30 undergraduate students and we plan to continue to provide our laboratory as a safe and

interactive resource for those who are willing to commit and learn more about experimental chemistry. Furthermore, our policy in selecting undergraduates has always been GPA-blind as we are convinced that we simply cannot close the doors on those who are less fortunate in their academic achievements at such an early stage. We mentor and guide these students on an individual basis, where we discuss their career goals and objectives and how their research involvement can advance these specific goals as well as their general learning. We believe that no matter what these individuals decide to do in their future, their exposure to a true research environment will be able to open their eyes to the world of scientific enterprise, which simply cannot be adequately communicated in any traditional lecture course offered at the college level. This approach has already bred tremendous success: over 20 of our undergraduate researchers are co-authors on research manuscripts published or currently submitted for publication. These individuals represent a very diverse group consisting of first-generation college students, immigrants, athletes, and military veterans coming from many places across the United States and the World and covering various socio-economic backgrounds.

Importantly, our ultimate goal is not to create a future army of chemists, but rather to provide each individual a tailored experience of what hypothesis-driven laboratory research is all about. By doing so, we hope to contribute to educating future generations on the critical impact of academic science and fundamental research in our society, disproving the myth among some that we (academics) represent an elitist class of individuals fundamentally out of touch with the real world. It happens often that undergraduate researchers are the “unsung heroes” in academic laboratories and their contributions tend to be dismissed and overlooked. To combat this attitude, below are presented 18 short narrative profiles of undergraduate students who worked in our laboratory and contributed immensely to the science and human interactions in our laboratory. The

remainder of this work highlights some teaching innovations and philosophies that Spokoyny and his colleagues have implemented over the past several years.

Narratives of Undergraduate Researchers:



Figure 5.1: A cohort of undergraduate researchers in the Spokoyny laboratory who worked in the group circa 2014-2016. Top: Simone Stevens (left), Alice Phung (center), Alejandra (Ali) Gonzalez. Bottom: Yanwu Shao (left), Elamar Mouilly (center), Vinh Nguyen (right).

As a high school student, Simone Stevens (Figure 5.1) was convinced that architecture was her sole calling in life. It was not until she took her first chemistry class that she quickly realized the world was revolving largely around this fundamental subject. At first, she had a difficult time navigating the next steps in her education as she was a first-generation college student. Joining a research lab was an invaluable experience that helped translate theories from the classroom setting to hands-on work and its potential future applications. While a member of the Spokoyny Lab at UCLA, Stevens worked on the synthesis of B-bromo-carboranes that were subsequently used as a versatile electrophile-based platform for new Pd-catalyzed cross-coupling chemistry (Figure 5.2).¹

Not only did she learn useful laboratory techniques, but more importantly, how to begin the research process. This set of skills has helped Simone in every endeavor since, including working to develop food chemistry at Beyond Meat during her first job after graduating college. Stevens is currently finishing a Master's degree in Mechanical Engineering at San Diego State University with an emphasis in materials—perhaps a realistic blend of architecture and chemistry after all. She enjoys tuning chemical and structural components to achieve preferred properties and hopes to use this in the development of new smart materials in her future career.

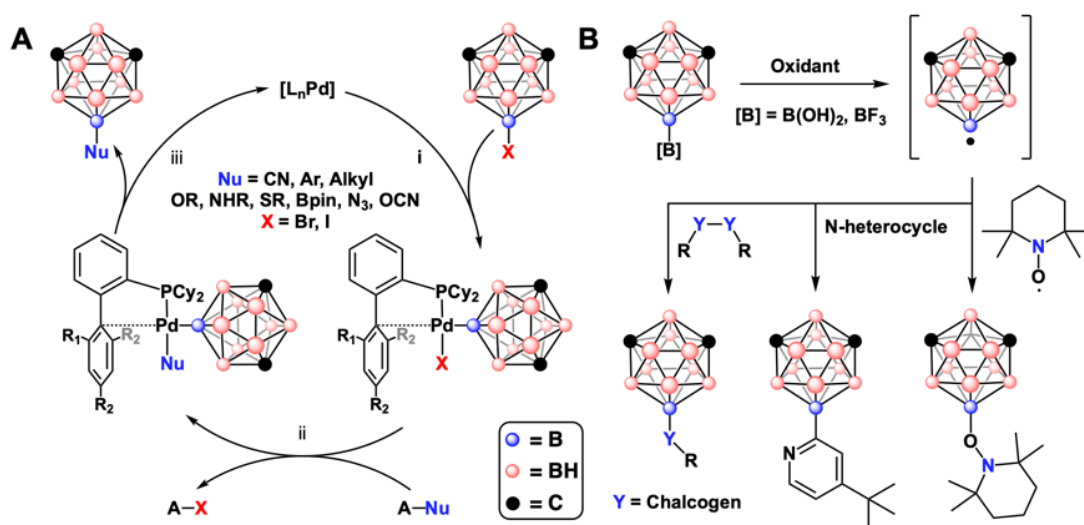


Figure 5.2: New carborane chemistry developed with a contribution of UCLA undergraduates. **A:** Pd-catalyzed cross-coupling chemistry and **B:** radical-based approach towards carborane functionalization at boron vertices. Steps i-iii represent oxidative addition, transmetalation and reductive elimination, respectively.

In her final year as an undergraduate at UCLA, Alice Phung (Figure 5.1) was on a pre-pharmacy path, working as a pharmacy technician at the nearby Veteran's Affairs (VA) facility. She wanted to explore other career paths open to a biochemistry major such as herself, so during her last term, she sought to join a laboratory in the Chemistry and Biochemistry Department. As a

senior who was one month away from graduation, laboratories were generally unwilling to allow her participation. Despite this, she was hired by the Spokoyny group as a lab assistant. Alice was the first undergraduate student to join Spokoyny's laboratory as she had enlisted on the first day of his arrival to UCLA in August of 2014. Needless to say, she has seen and experienced all aspects of setting up a brand-new chemistry laboratory and helped the group tremendously throughout the process. Emboldened by the sense of community and the dedicated work ethic the group instilled, and not discouraged by dealing with a multitude of chemistry vendor sales representatives, she chose to remain in research and continue to create new molecules that previously did not exist. Currently, Alice is a Ph.D. student in the Chemistry Department at UC Davis where she is studying organometallic synthesis in the laboratory of Prof. Philip Power. Recently, Alice and co-workers published a manuscript disclosing a new process featuring metathesis between metal-metal triple bonds.² She is also continuing to explore her multifaceted hobbies which include baking, soap making, and creative fiction writing.

Prior to attending college, Alejandra Gonzalez (Ali, Figure 5.1) was unsure of what she wanted to do as she did enjoy many academic subjects in both the arts and sciences. Upon enrolling at UCLA, Ali joined a professional Chemistry fraternity chapter (Alpha Chi Sigma), which allowed her to make many important connections and push to pursue her interests in chemistry. She enrolled in Spokoyny's inorganic chemistry course and after discovering her passion towards exotic molecules, joined his lab where she focused on developing the syntheses and exploring the materials properties of luminescent compounds. Under Spokoyny's mentorship, Gonzalez was a part of a UC LEADS program and gained skills in both materials research and organic chemistry. Ali worked as a part of a team (together with Alice Phung) that was able to successfully synthesize and characterize unique, blue phosphorescent d^8 metal complexes featuring photophysically

innocent boron cluster-based ligands (Figure 5.3A).³ Upon graduating from UCLA, Gonzalez continues to pursue her passion in materials chemistry at Brandeis University as a Ph.D. student in Prof. Grace Han's laboratory. She is currently conducting research on energy storage materials in the solid state and their applications in controlled heat release. Recently, Ali was a lead author on a review work describing solid-state photoswitching of molecules in a condensed phase.⁴ Aside from conducting research, Ali enjoys working as a teaching assistant for the organic chemistry laboratory and fine-tuning her already impeccable repertoire of puns and one-liner jokes.

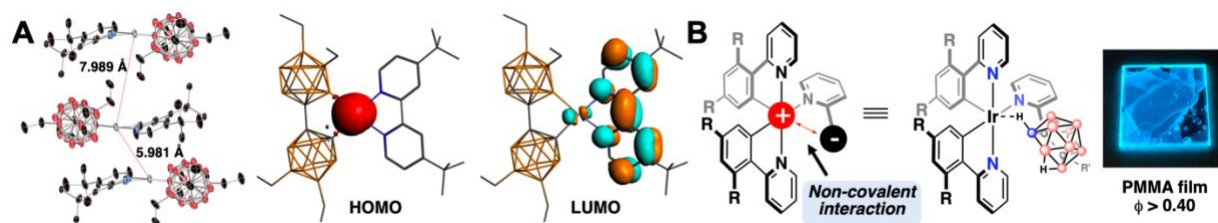


Figure 5.3: Development of photophysically innocent carborane-based scaffolds for metal-based phosphorescent materials. **Figure 5.3A** was partially reproduced from materials in with the permission from the Royal Society of Chemistry.³ **Figure 5.3B** was adapted with permission from Copyright (2016) American Chemical Society.⁹

Like most other high school students in Suzhou, China, Yanwu Shao (Figure 5.1) spent most of his time focusing on the subjects required by national college entrance examinations: Chinese, mathematics and English. He quickly realized that his college life at UCLA would be very different. After arriving in Los Angeles in 2012, Yanwu decided to dedicate his undergraduate studies towards chemistry. Yanwu's research experience began in 2015, where he joined the Spokoyny research group and pioneered synthetic methods for the preparation of $B_{12}(OR)_{12}$ clusters (Figure 5.4A, B).⁵ This effort was foundational to the development of several research thrusts in the laboratory including the generation of photooxidants, hybrid polymers and atomically

precise nanoclusters.^{6,7} With the guidance of senior group members, Yanwu was able to master numerous synthetic and analytical skills. This training became extremely useful for his subsequent studies as a Ph.D. researcher at Texas A&M where he has been studying the synthesis and characterization of bimetallic pincer complexes. During his time at UCLA, Yanwu also learned to appreciate other fields outside of the sciences such as linguistics, sociology and film studies. He plans to blend together his multifaceted interests in his future career upon graduating from Texas A&M this year.

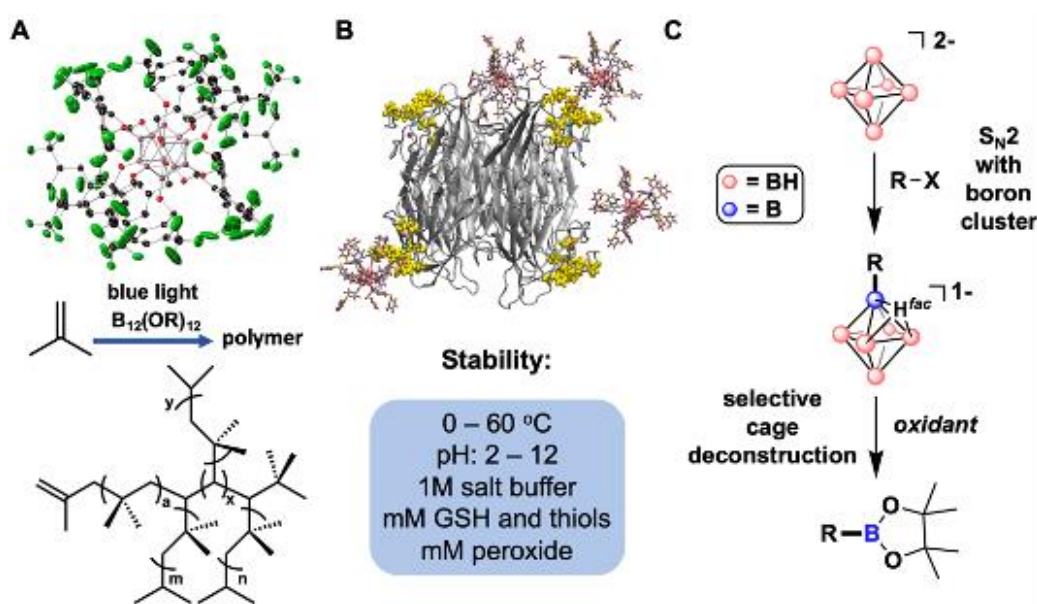


Figure 5.4: Recent developments in the area of polyhedral boron clusters in the Spokoyny group with contributions from the undergraduate researchers. **A:** Discovery of perfunctionalized $B_{12}(OR)_{12}$ cluster photooxidant and weakly coordinating proanions for polymerization. **B:** Development of cluster-based platform for multivalent protein binders. **C:** Umpolung approach towards nucleophilic borylation chemistry using $B_6H_6^{2-}$ cluster. **Figure 5.4A** was adapted with permission from Copyright (2016) American Chemical Society.⁶

Upon starting at UCLA, Elamar Mouilly (Figure 5.1) quickly identified her passion for chemistry and biology. While classes were often difficult (she still has nightmares about her last organic chemistry exam!), laboratory courses were her favorite—three hours of mixing chemicals, setting up impressive glassware, and feeling like a “real” scientist. She decided to dive deeper into the world of chemistry research and worked in the Spokoiny research group during her last two years. At first, as she admits, it was slightly terrifying. This was Elamar’s first time handling chemicals outside of a classroom setting, and she was constantly afraid of causing a catastrophic explosion. But with time, practice, and some guidance, Elamar found her footing. While in the group, Elamar was exposed to the marvelous world of boron cluster chemistry, and had the opportunity to initiate several thrusts pertaining to bioinorganic chemistry. One of these was her contribution to the development of atomically precise, organomimetic clusters capable of multivalent molecular recognition (Figure 5.4B).⁷ This work, which was published in 2016, was her first scientific contribution to the world. Additionally, Elamar pioneered some early discoveries from the group pertaining to a new bioconjugation strategy for biological molecules using organometallic boron clusters. Elamar is currently a Ph.D. student at Northwestern University working on the design of high-throughput biochemical assays for a variety of applications, such as single-cell analysis and metabolic pathway characterization. Elamar was recently a lead author on a manuscript describing her Ph.D. work generating assays to measure tyrosine phosphatase activity in single cells.⁸ She plans to graduate within the next year and pursue a career in science education and outreach. She hopes to work on STEM program development, both in and out of the classroom, to inspire the next generation of scientists.

Vinh Nguyen (Figure 5.1) was born and raised in Southern California. During his time as an undergraduate at UCLA, he entertained various career paths through various internships,

including those at St. Mary's Medical Center, CalTeach, and UCLA CityLab. However, it was research in the Spokoyny group that ultimately sparked his current interests in synthetic chemistry. Vinh cites an enthusiastic group dynamic and opportunity to study the light-emitting and material properties of carborane complexes (Figure 5.3B) as a major force that encouraged him to pursue a career in research.⁹ Following his graduation, Vinh was employed as an R&D analytical chemist at Catalent Pharma Solutions in San Diego, where he designed HPLC methods and supported manufacturing of Phase I/II pharmaceutical candidates. Currently, he is a chemistry Ph.D. student at Texas A&M University working in the laboratory of Prof. Oleg Ozerov. His projects revolve around developing catalysts that regioselectively functionalize pharmaceutically and agriculturally relevant compounds. In the future, Vinh plans on pursuing a research-oriented career with opportunities to pay forward his knowledge and received mentorship.



Figure 5.5: A cohort of undergraduate researchers in the Spokoyny laboratory who worked in the group circa 2016-2018. Top: Joshua Martin (left), Chantel Mao (center), Azin Saebi (right). Bottom: Daniel Mossalaei (left), Monica Kirollos (center), Paul Chong (right).

Joshua Martin (Josh, Figure 5.5) was born in Washington D.C. and grew up in Rome, Italy where his parents worked for the United Nations. He later moved to Southern California to pursue a B.S. in Biochemistry at UCLA. Josh spent nearly two years working in the Spokoyny Lab, where he focused on the palladium-catalyzed, boron-vertex functionalization of carboranes, culminating in several seminal contributions (Figure 5.1).^{10,11} During his time in the lab, he learned how to set up moisture and air-free reactions, analyze the results and interpret their significance. The most significant intangible skill that Josh learned during his undergraduate research experience was the importance of connecting disparate fields in a way that had previously been overlooked or underappreciated. Josh is currently a Ph.D. candidate at the University of Michigan, Ann Arbor where he works under the tutelage of Prof. John Montgomery. His work aims to develop novel methods for the construction of complex carbohydrates. Recently, Josh and co-workers reported a discovery of efficient and simple glycosylation via fluoride migration catalysis.¹² After completing his Ph.D., Josh hopes to pursue a career in the pharmaceutical industry which he hopes can be located in an area with an abundance of very spicy food, which he enjoys a lot.

After being intrigued with the prospects of what inorganic chemistry can offer while taking Spokoyny's undergraduate course, Chantel Mao (Figure 5.5) decided to join our laboratory and experience it firsthand. While Chantel originally wanted to get hands-on experience in the lab in order to prepare for a career in chemical industry, her plans slowly changed as she became immersed more in the world of synthetic inorganic chemistry. During her stint, Chantel learned how to conduct laboratory synthesis and contributed to the group's methodology in carborane chemistry. Research sounded intimidating to Chantel at first, but with the encouragement and support of her co-workers, she developed a solid foundation of functional knowledge. Chantel collaborated with senior group members on the development of new methodology for carborane cluster functionalization. This work culminated in a publication paper disclosing dramatically improved Pd-based cross-coupling reactions and nucleophilic aromatic substitution reactions with carboranes.¹³ She is currently pursuing her Ph.D. in chemistry at UC Davis in Marie Heffern's laboratory and is truly enjoying her time in graduate school despite being significantly farther

away from Universal Studios and Disneyland. While still interested in inorganic chemistry, Chantel has been expanding her expertise and moving towards the exploration of metals in medicine and biology. Back in high school, chemistry was Azin Saebi's (Figure 5.5) *least* favorite science course. There were always too many exceptions to the "rules" for her liking and electrons just didn't behave! This trend continued until she took chemistry in Saddleback Community College. Learning organic chemistry was especially fun. Upon transferring to UCLA, Azin took an inorganic chemistry course with Spokoyny and really enjoyed learning about inorganic elements and how they are used in our daily lives. In that class, Azin discovered her passion for boron clusters and shortly began her stint in the Spokoyny lab. Having had very limited experience in chemistry labs, everything was new to her: the Schlenk lines, glove boxes, rotor evaporators. Through her hard work and tireless mentorship of senior group members, things improved fast, and Azin found many amazing friends in the lab who would be support system for when her reactions didn't work as well as expected. During her first phase in the group, she collaborated with Elamar Mouly, Daniel Mossalaei and colleagues to generate atomically precise organomimetic clusters.⁷ She then started an independent project on development of histone deacetylase inhibitors, which would marry the two fields she was most excited about: neuroscience and chemistry. On her very last day in the laboratory, she synthesized the final target molecule, which was later shown to be biologically active.¹⁴ Azin's experience at UCLA helped her form a better understanding of her aspirations and shaped her current career path. Azin is now a Ph.D. student at the Massachusetts Institute of Technology working on the development of antimicrobial conjugates using palladium-mediated bioconjugation chemistry and chemical synthesis of proteins. Recently, she and her colleagues reported a significant breakthrough in chemistry showcasing an automated synthesis of large proteins.¹⁵ After graduation, Azin is hoping to use her expertise to contribute to making new therapeutics and treatments for infectious diseases.

Daniel Mosallaei (Figure 5.5) grew up in Orange County suburbia and spent most of his adolescence finding adventures and getting into trouble with his friends. As he admits, he was far from a good student. After attending a local community college Daniel was able to excel academically and found his passion for chemistry. Two years later, he transferred to UCLA and was inspired by an inorganic

chemistry course taught by Spokoyny. After joining the Spokoyny lab, Daniel struggled at first, but his fellow undergraduate and graduate students from the lab quickly showed him the ropes. Other than the plethora of hands-on chemistry and laboratory experience, Daniel found the weekly group meetings to be incredibly beneficial to his own learning. Daniel was ecstatic when his hard work in the laboratory paid off and he became a co-author on a publication.⁷ Daniel notes that the Spokoyny group became his second family, and he made lifelong connections during his time there. Daniel graduated Summa Cum Laude with highest departmental honors from UCLA in 2016, which was a stark contrast to his original academic performance in earlier life. He decided to pursue a medical degree and began attending USC Keck School of Medicine the next Fall. He has recently finished his 3rd year in the medical school and is currently continuing to conduct research in the laboratory of Mei Chen doing bench-to-bedside research in wound healing and *epidermolysis bullosa*. Daniel plans on applying to dermatology residencies in the 2021 cycle and continuing his career in medicine.

Monica Kirolos (Figure 5.5) was born in Cairo Egypt, and has lived in California since moving stateside. She joined the Spokoyny lab in October of 2015, working on the synthesis of tunable and atomically precise nanoparticles from stable boron clusters. Her work in the group was tremendously enjoyable, because not only did she learn air- and moisture-free techniques, handled expensive equipment, and mastered NMR software, but she also gained a family of coworkers and a mentor whose advice remains invaluable to her until today! Being a team player paid off, as Monica and her colleagues developed and recently published a new discovery and method showcasing how one can efficiently use small boron clusters for nucleophilic borylation of small molecule electrophiles (Figure 5.4C).¹⁶ Monica's lifelong passion has been medicine and the potential to help people. She has now started her second year at the Mayo Clinic Alix School of Medicine, and has continued to pursue her growing interest in research. Monica plans to incorporate evidence-based medicine into her practice by working in an academic setting and contributing to the scientific community with innovative and meaningful research.

Having failed chemistry in high school, Paul Chong (Figure 5.5) believed that he was simply not cut out for the sciences. He ended up dropping out during his junior year in favor of obtaining a GED. As

a nontraditional student returning to education and attending community college in his twenties, Paul was required to enroll into a general chemistry course, which seemed daunting at the time given his prior experience with the subject. However, his concerns were alleviated by a superb line up of instructors at his local community college. Upon completing the first course in organic chemistry, Paul began a search for research opportunities with no clue of where to start. He contacted about a dozen principal investigators and received a lone reply from Spokoyny who agreed to host and train him in his lab. Paul notes that his time in the Spokoyny lab turned out to be a transformative experience that finally convinced him that he belongs in the sciences. As a sophomore community college student, Paul has co-authored a manuscript from the lab disclosing the discovery of $B_{12}(OR)_{12}$ clusters as extremely strong photooxidants.⁶ Paul developed immense enthusiasm for research and eventually transferred to UCLA in order to complete his undergraduate degree while continuing research on polymer chemistry.¹⁷ Under the guidance of Paul's graduate mentor (Dr. Marco Messina), he learned essential laboratory skills that he uses to this day, but more importantly, he learned how to think critically in performing research. Paul's undergraduate research experience shaped his ultimate decision to pursue a graduate education in sciences. Over a decade after failing his first chemistry course in high school, he is now a Ph.D. candidate in chemistry at Stanford University, performing research at the interface of materials chemistry and neuroscience. Paul and his colleagues recently published a manuscript on the development of new tools for minimally invasive sono-optogenetics.¹⁸

Alex Umanzor (Figure 5.6) was born and raised in Long Island, New York to Salvadoran immigrants. His mother is a nurse practitioner, so growing up surrounded by her medical encyclopedias made him fall in love with science at a young age. His passion for chemistry, similarly to many others, began in high school. Alex initially struggled in his freshman chemistry class, but once he found the study method that worked best for him, he began to excel. He took his newfound interest and ran with it, enrolling in a summer class at Columbia University called Intensive Seminars in Modern Chemistry. Conducting experiments in a research lab and attending seminars from the likes of Ged Parkin and Ronald Breslow ignited his passion for the subject. Upon starting at UCLA as an undergraduate, Alex has struggled to stay

afloat in the cutthroat STEM classes. However, all of this changed when he joined the Spokoyny group. Mentored by several senior graduate students and post-docs, Alex worked as an undergraduate researcher for three formative years, focusing on boron cluster-based applications to organic synthesis.¹⁶ Doing hands-on chemistry fueled his determination to improve his academic performance as well as dedicate time to research. His work on sterically unprotected nucleophilic boron cluster reagents later resulted in his first co-authored publication, which Alex cites as one of the greatest accomplishments of his undergraduate career. After graduating from UCLA, Alex moved Minneapolis where he is currently a first year Ph.D. student at the University of Minnesota, Twin Cities. Now that Alex is on the “other side”, he is excited to pay forward the mentorship he received and mentor undergraduate students throughout his graduate career, and one day become a professor of organic chemistry at a predominantly undergraduate institution.



Figure 5.6: A cohort of undergraduate researchers in the Spokoyny laboratory who worked in the group circa 2017-2020. Top: Alex Umanzor (left), Kevin Qian (center), Gustavo Marin (right). Bottom: Omar Ebrahim (left), Ramya Pathuri (center), Morgan Hopp (right).

Kevin Qian (Figure 5.6) had a long-standing interest in chemistry, and his understanding and appreciation for the subject has grown substantially because of the mentorship he received over the last

several years. Kevin began his undergraduate studies in chemistry at Columbia University in 2016. Then in the summer of 2018, he was accepted into the Amgen Scholars program at UCLA, which provided him the opportunity to work in the Spokoyny laboratory for a few months. Although it was a relatively short stint, it was very productive. Working as a part of a team, Kevin and co-workers studied reactivity of the *closo*-B₆H₆²⁻ cluster as a sterically unprotected nucleophilic boron reagent. Kevin's involvement in this project was an incredibly informative and humbling experience as it presented him with a new world of questions and challenges. Furthermore, he found that his time spent in the Spokoyny group was particularly enriching because of his exposure to their interdisciplinary approach to science. Being in the presence of researchers who were exploring a great variety of problems has helped him better understand and contextualize his work within the broader scientific community. Kevin is currently pursuing a Ph.D. in Chemistry at the Massachusetts Institute of Technology, with a long-term goal of a career in academia.

Gustavo Marin (Figure 5.6) was born in Queens, New York, where he lived until the age of 14. Afterwards, he moved to his family's home country of Colombia to finish high school. Gustavo always dreamed about attending UCLA for his undergraduate studies and his dream eventually became reality. Once he moved to Los Angeles, he quickly realized that he was going to be challenged personally and mentally in order to become a successful scientist. Upon joining the Spokoyny research laboratory, Gustavo learned that an entire world of intelligent people exists around him outside of classes, and that he can tap into this collective knowledge to advance his learning. Gustavo worked on several projects that explored using boron clusters as cross-linkers in the synthesis of hybrid polymers (Figure 5.7).¹⁹ Importantly, he believes that this research experience allowed him to be exposed to invaluable materials characterization techniques and tools ranging from powder X-ray diffraction analysis (PXRD) to scanning electron microscopy (SEM) which he would not have experienced by simply taking courses. Upon graduating from UCLA this year, Gustavo returned back to Colombia and is currently living with his family, eagerly anticipating the end of the COVID-19 pandemic. He is currently enjoying spending time with his family and also pursuing mini projects like trying to learn a new language (French). Ultimately Gustavo is planning to continue his research endeavors as a Ph.D. student in materials chemistry.

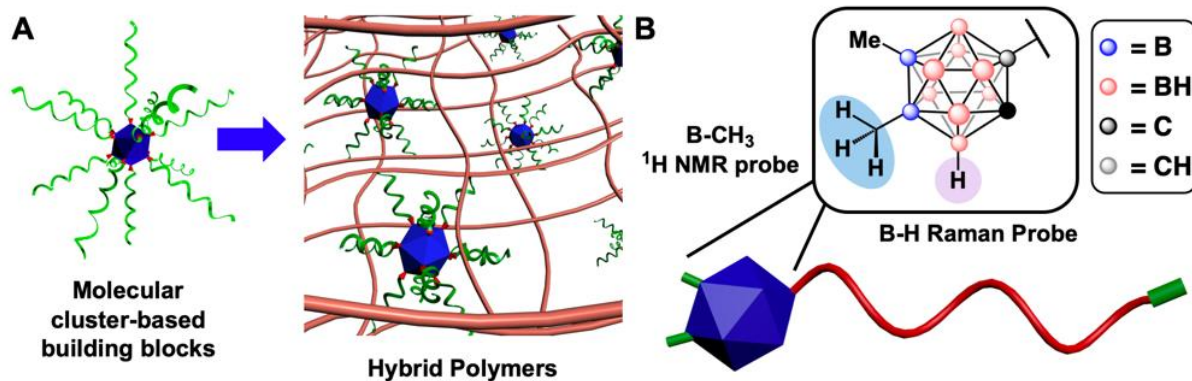


Figure 5.7: Recent utilization of boron-rich clusters as building blocks for polymer materials developed by UCLA undergraduates. **A:** Perfunctionalized boron clusters can be applied as cross-linkers for hybrid polymers. **B:** Carboranes can be employed as unique NMR and Raman spectroscopic handles for controlled polymerization.

Being diagnosed with diabetes as a child, Omar Ebrahim (Figure 5.6) did not understand the difference between insulin types, why mixing insulins creates crystals, or why glucagon pellets had to be dissolved in strong acid before administration. He originally planned to address this gap in understanding by pursuing a medical degree. But his experience working with in multiple laboratories at UCLA, allowed him to take an unconventional approach to human disease by developing synthetic chemical tools to probe or augment biomolecules. Working jointly in the Spokoyny and Maynard laboratories at UCLA, Omar was part of the team effort focused on the development of carborane containing chain transfer agents used to characterize polymeric materials grown via reverse addition fragmentation chain transfer polymerization. The carborane functions as a Raman probe, allowing us to characterize polymers in biological media.¹⁷ These fundamental techniques have carried over into his graduate career at Northwestern University where he is now developing peptide brush polymer displays of various incretins to not only protect the peptides from degradation, but engender new therapeutic properties not present in the individual free peptides. Eventually, he hopes that these new therapies will combat unaddressed comorbidities in patients with Type

2 Diabetes. Despite mounting evidence to suggest that the pathophysiology of diabetes is more complicated than previously thought, little information is translated to patients and patient care remains stagnant.

Ramya “Maya” Pathuri (Figure 5.6) was born in an immigrant family and grew up in a small town in north Georgia where her love of science was greatly encouraged by her high school chemistry teacher. Though she was initially interested in a pre-medical track, once at UCLA, Pathuri found that she was much more excited by basic research. In the spring of her second year, Pathuri joined the Spokoyny research group. Pathuri’s first project involved the design and implementation of carborane-based chain-transfer agents (CTAs) for radical addition-fragmentation chain-transfer (RAFT) polymerization.¹⁷ Her work contributed towards a paper, on which she was co-author, published in *Polymer Chemistry*. Pathuri’s second project involved the design, characterization, and application of anion-based room-temperature ionic liquids (RTILs) based on the tunable *closo*-B₁₂H₁₂ scaffold. Specifically, she developed ionic liquids that facilitate electrodeposition in high-vacuum environments, and this work was done in collaboration with the Air Force Research Laboratory (AFRL). Starting this Fall, Pathuri is pursuing a Ph.D. in chemistry at Northwestern University.

Morgan Hopp (Figure 5.6) learned the word “experiment” and its definition in preschool and could not wait to tell her mom that day. This passion was solidified by her amazing AP chemistry teacher who inspired Morgan to further explore chemistry. She decided to enroll at UCLA as a biochemistry major to prepare for a future career in medicine. Morgan joined the Spokoyny lab as an undergraduate researcher to explore further educational options, as she had never met someone who did chemistry research and wanted to push her boundaries. Given Morgan’s interests on the interface of biology and chemistry, she embarked on a collaborative project focused on developing carborane clusters as substitutes for adamantane in pharmacophores to target epigenetic regulation. Three years later, after much contemplation and exploration, Morgan still plans to be a medical doctor, but admits that she absolutely loves chemistry research. In fact, she decided to delay her UCLA graduation and pursue an advanced master’s degree to stay an extra year to do research through a department honors program. She recently co-authored a manuscript showcasing the synthesis of carborane clusters with appended N-based reactive functional

groups.²⁰ Morgan finds it extremely rewarding to have seen a project progress from theoretical concepts sketched on a piece of paper into the development of molecules that can be implemented in animal testing. Morgan is currently in the process of applying for admissions to medical schools across the country. She strongly believes that her work in the Spokoyny lab on understanding the implications of drug design will make her ultimately a better doctor.

Improving Chemistry Appreciation Among STEM and non-STEM Students

In addition to undergraduate mentorship, Spokoyny's long-term goal is also to improve undergraduate education in chemistry. A recent report from PCAST on STEM education²¹, for example, cited "uninspiring introductory courses" as a major reason for the low attrition rate among students in sciences. The same report recommends the "diversification of teaching methods" as a solution to this problem. Young and idealistic minds would be more cognizant to learn and rationalize chemical concepts by considering their historical and societal contexts. By incorporating these concepts in the form of case studies in the structure of the introductory inorganic course Spokoyny has taught, we attempted to engage students and help them establish connections between fundamental and applied chemical sciences and contemporary societal problems in the areas of environment, energy, and healthcare. Knowledge creation has been another focal point of our attempt to revive the excitement among students in the classes. For the inorganic chemistry courses Spokoyny taught, we have implemented two assignments which were designed to engage students in a collaborative effort to produce either a Wikipedia article on a non-existent area of research pertaining to inorganic chemistry or a short documentary video for Youtube featuring a site or a person within Southern California who is deeply impacted by inorganic chemistry.²² These assignments not only allow our students to apply their creativity that sometimes cannot be harnessed through traditional paper-based examinations, but also produce a potentially useful piece of digital and open-source information benefiting the public. Similarly, in the upper division/graduate chemistry course that was taught, we covered frontiers of the inorganic chemistry interfaced with biological systems. Importantly, during this course, students developed an original research idea and put together a formal research proposal, which was then evaluated by a student-based peer review panel (similar to a NIH study group). This

assignment was extremely popular with the students (especially undergraduates) and allowed us to mentor them throughout a 10-week period in identifying a suitable research topic and proper framing of scientific arguments.

Over the past several years, Spokoyny has also revamped an inorganic synthesis laboratory course to incorporate guided and open-inquiry pedagogical strategies. The main objective of this course was to introduce students to a collaborative project in inorganic chemistry, which tackles the unknown. This is in contrast to the traditional “cookbook” laboratory chemistry courses at UCLA, which make students work on projects that have been tested and validated and the answer to the problem being solved is already known. During the first time the class was offered in 2017, students quickly picked up on the techniques and were able to complete a significant body of work developing a new class of precatalysts for metal-catalyzed cross-coupling. Importantly, course lecture meetings were held in the format of a group meeting, where we discussed ongoing progress in the laboratory and theory behind methods and strategies to tackle and troubleshoot challenges one can encounter in the laboratory. The work that was performed by this class was disclosed in a peer-refereed journal in the field²³, and every undergraduate was included as a co-author. This is important since 90% of the students in the class did not perform formal undergraduate research at UCLA, although the majority of these individuals attempted (unsuccessfully) to find a suitable laboratory and mentor. The format of this class therefore helps to address the issue of poor scalability in our department (as well as many other departments across the nation) in terms of individual undergraduate mentorship, where given the large number of students it is nearly impossible for everyone to be hosted in a single PI’s research laboratory. Conceptually, this course can be thought of as a short-term undergraduate thesis project, which is a common model for independent research at liberal arts colleges. Importantly, the original success of our effort was recognized by the community and the class saw a dramatic increase in enrollment.^{24,25}

Lastly, we have been working on development of a new course (Chemistry 3) at UCLA targeting non-STEM majors that covers essentials of modern chemistry and materials science. This is important, since the fundamental mission of our teaching is to educate the future electorate and enable these individuals

to make well-informed decisions. While chemistry surrounds essentially every aspect of our life from vaccines to plastics, we tend to overlook explaining fundamental importance of our field to the general non-science audience. We've all heard that familiar groan, a subtle shifting of eyes when you announce your STEM class will involve a writing-based project. As educators we share the burden of addressing more than the course materials prescribed by the title of the class. We attempt to develop a multitude of facets of scientific literacy: enhanced written communication skills, an appreciation for the historical context of a discovery, ways of critically evaluating new information and so many more. This can be especially challenging considering the time restrictions of university courses.

In 2018, we developed the first general education chemistry course at UCLA (Figure 5.8). Previously, students from non-science majors would satisfy this requirement by enrolling in the introductory chemistry courses also taken by students in the major. While these courses represent a fundamentally important survey of the underlying concepts of basic chemistry, the highly mathematical nature of the course alienates many from appreciating the broader impacts of a chemical education. Furthermore, many non-STEM students at UCLA feel a lack of belonging in a science classroom which figuratively solidifies the physical divide between the sections of campus where non-STEM and STEM students are taught (historically referred to at UCLA as “north campus” versus “south campus”). We observed these events and developed the class, Material World, to showcase key materials throughout history and how the properties of these materials have shaped our society. From the smelting of metals to the advent of various plastics to the generation of medicines and biological warfare, a survey of approachable topics conveys underlying principles ranging from density to nuclear fission.

The pilot course was administered in 2018 and was well-received. One point of improvement was the quarter-long project, which required students to write a mock press release of a recently published research journal article. While educational, the assignment felt antiquated with little tangible outcome. Through the assignment, we hoped students would visualize how warped information can become through media interpretation. But was there a better way to achieve this goal incorporating, perhaps, a modern and accessible platform? We taught the class again in 2019 but with a new project in mind. We envisaged how

social media, primarily Twitter, could be utilized as a tool for identifying the spread of scientific misinformation. Given the restrictions of social media, students would have to be brief in articulating counterarguments, a valuable writing skill. We also saw the opportunity for both creativity and interactivity which we hoped would make researching new topics more rewarding to our students.

To achieve these learning outcomes, we allocated the mandatory discussion section time attached to the regular lectures in the course as an evolving forum for the Twitter project. The class was broken into two discussion sections, each meeting once a week. We split the sections into groups of 2-3 students and each group made a new Twitter account, specifically for the course. Each group was asked to find one false scientific claim recently posted on Twitter and to respond to it, politely, articulately and with cited sources. The students were then assigned due dates at which time they presented the transcript of the communication to their respective discussion section and explained the concepts underlying the misinformation. Because social media updates in real time, they were free to engage with Twitter whenever and wherever they chose, lending flexibility to the assignment. The platform is free and easily accessible. After tutorials on how to navigate Twitter as well as examples of effective communication, the students got started. They were graded on how thorough and well referenced each response was, how well they presented the topic and timely completion. The groups with the top three presentations were asked to present to the entire class and were awarded extra credit. This gave a chance for everyone to hear the most thorough, yet succinct responses as a template for future Twitter communication while also providing incentive for students to be fully invested in the assignment.



Figure 5.8: Key contributors to the development of Chemistry 3 course at UCLA: (left) Mary Waddington (teaching assistant), (center) Roshini Ramachandran (science education expert and instructor during Fall 2020) and (right) Alex Spokoyny (course originator and instructor during Fall 2017-2019).

The results of this exercise were very promising. Students who had never read a scientific journal before were analyzing article findings to present in their maximum 280-character responses. Due to the nature of social media, students were forced to be concise, organized and brief, choosing every word extremely carefully. While some original posters responded to the students with negativity upon being corrected, a significant fraction did not. We found an exchange with a medical doctor from Florida to be particularly interesting. The original tweet states “A popular workout supplement is #Creatine. Unfortunately, it may accelerate male pattern #hairloss by increasing DHT.” The tweet then provided a link to an article in the *Clinical Journal of Sports Medicine*. The students read the article and realized that while correlations between DHT (dihydrotestosterone) and creatine were reported, hair loss was not included or even commented on. Further, the small sample size ($n= 20$) limits widespread applicability. The students provided links to other published studies as well as a popular podcast explaining that baldness is more complicated than correlation to DHT levels. Through this exercise, the students evaluated research

conclusions while crafting a counter argument within the space of a couple tweets, exemplifying the goal of interfacing social media and education.

In anonymous reviews of the class, one student wrote “I’ve learned a lot about different materials that are highly relevant to my everyday life and critical perspectives of viewing our society!” We believe this exercise produced new tools by which our students can engage with the media and critically assess the information provided. With the recent transition we’ve all made towards remote learning, projects that force students to engage with one another while developing essential writing, communication and research skills are increasingly important. We implemented this project to fit a classroom setting, but the structure could easily be extended to a virtual setting, providing a free, accessible and engaging learning tool. We coined the project the “Twitter Throwdown” and hope our experience encourages more educators to employ social media as a tool for preparing students to practice scientific inquiry and make well-informed decisions in their daily lives by dissecting the real from the fake scientific news.

Importantly, we believe that these assignments help to improve a general science appreciation among the students and increase their performance towards achieving anticipated learning outcomes in the course (Figure 5.9). Further evaluation of this course and its impact on student’s science appreciation is currently underway. Nevertheless, it is already apparent that this course is a very successful test bed for developing clear explanations and analogies necessary to make the material interesting to a broad audience of social scientists and humanists. Furthermore, during our evaluation in 2019, we observed a significant improvement in student’s post-survey when asked whether learning science will affect how they vote in the elections. We are currently working on developing a laboratory module for Chemistry 3, which we believe will further improve chemistry appreciation and scientific literacy among students.

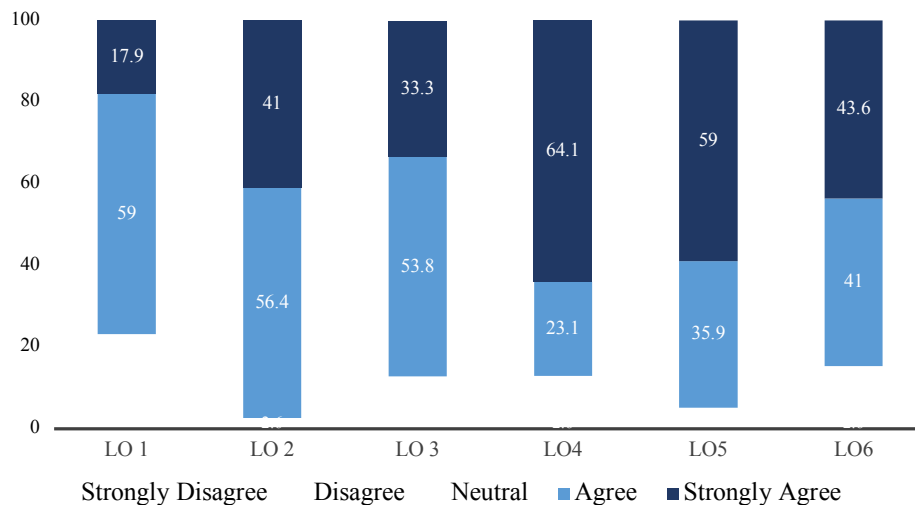


Figure 5.9: Summary of student post-course responses in a Chemistry 3 course taught in 2019.

The question asked whether students agree that the course helped them to achieve key learning outcomes: LO1. Estimate the size and relative dimensions of the microscopic world; LO2. Explain complexities associated with the toxicity of materials; LO3. Gain a qualitative understanding of light/matter interactions; LO4. Make connections between historical and technological events; LO5. Connect technologies with societal areas of need; LO6. Predict outcomes of emerging technologies.

References:

1. Dziejcz, R. M.; Saleh, L. M. A.; Stevens, S. L.; Martin, J. L.; Royappa, A. T.; Rheingold, A. L.; Spokoyny, A. M. B-N, B-O and B-CN Bond Formation via Palladium Catalyzed Cross-Coupling of B-Bromo-Carboranes. *J. Am. Chem. Soc.* **2016**, *138*, 9081-9084.
2. Queen, J. D.; Phung, A. C.; Caputo, C. A.; Fettingner, J. C.; Power, P. P. Metathetical Exchange between Metal–Metal Triple Bonds. *J. Am. Chem. Soc.* **2020**, *142*, 2233-2237.
3. Kirlikovali, K. O.; Axtell, J. C.; Gonzalez, A.; Phung, A. C.; Khan, S. I.; Spokoyny, A. M. Luminescent Metal Complexes Featuring Photophysically Innocent Strong-Field Chelating Boron Cluster Ligands. *Chem. Sci.* **2016**, *7*, 5132-5138.

4. Gonzalez, A.; Kengmana, E. S.; Fonseca, M. V.; Han, G. G. D. Solid-state Photoswitching Molecules: Structural Design for Isomerization in Condensed Phase. *Mater. Today Adv.* **2020**, *6*, 100058.
5. Wixtrom, A. I.; Shao, Y.; Jung, D.; Machan, C. W.; Kevork, S. N.; Qian, E. A.; Khan, S. I.; Kubiak, C. P.; Spokoyny, A. M. Rapid Synthesis of Redox-Active Dodecaborane B₁₂(OR)₁₂ Clusters Under Ambient Conditions. *Inorg. Chem. Front.* **2016**, *3*, 711-717.
6. Messina, M. S.; Axtell, J. C.; Wang, Y.; Chong, P.; Wixtrom, A. I.; Kirlikovali, K. O.; Upton, B. M.; Hunter, B. M.; Shafaat, O. S.; Khan, S. I.; Winkler, J. R.; Gray, H. B.; Alexandrova, A. N.; Maynard, H. D.; Spokoyny, A. M. Visible-Light Induced Olefin Activation using 3D Aromatic Boron-Rich Cluster Photooxidants. *J. Am. Chem. Soc.* **2016**, *138*, 6952-6955.
7. Qian, E. Q.; Wixtrom, A. I.; Axtell, J. C.; Saebi, A.; Rehak, P.; Han, Y.; Mouly, E. H.; Mosallaei, D.; Chow, S.; Messina, M.; Wang, J.-Y.; Royappa, A. T.; Rheingold, A. L.; Maynard, H. D.; Kral, P.; Spokoyny, A. M. Atomically Precise Organomimetic Cluster Nanomolecules Assembled via Perfluoroaryl-Thiol S_NAr Chemistry. *Nature Chem.* **2017**, *9*, 333-340.
8. Mouly, E. H.; Berns, E. J.; Mrksich, M. Label-Free Assay of Protein Tyrosine Phosphatase Activity in Single Cells. *Anal. Chem.* **2019**, *91*, 13206-13212.
9. Axtell, J. C.; Kirlikovali, K. O.; Djurovich, P. I.; Jung, D.; Nguyen, V. T.; Munekiyo, B.; Royappa, A. T.; Rheingold, A. L.; Spokoyny, A. M. Blue Phosphorescent Zwitterionic Iridium(III) Complexes Featuring Weakly Coordinating Carborane-based Ligands. *J. Am. Chem. Soc.* **2016**, *138*, 15758-15765.

10. Dzedzic, R. M.; Martin, J. L.; Axtell, J. C.; Saleh, L. M. A.; Yang, Y.; Messina, M.; Houk, K. N.; Spokoyny, A. M. Cage-Walking: Vertex Differentiation by Palladium-Catalyzed Isomerization of B(9)-Bromo-*meta*-Carborane. *J. Am. Chem. Soc.* **2017**, *139*, 7729-7732.
11. Mills, H. A.; Martin, J. L.; Rheingold, A. L.; Spokoyny, A. M. Oxidative Generation of Boron-Centered Radicals in Carboranes. *J. Am. Chem. Soc.* **2020**, *142*, 4586-4591.
12. Sati, G. C.; Martin, J. L.; Xu, Y.; Malakar, T.; Zimmerman, P. M.; Montgomery, J. Fluoride Migration Catalysis Enables Simple, Stereoselective, and Iterative Glycosylation. *J. Am. Chem. Soc.* **2020**, *142*, 7235-7242.
13. Anderson, K. P.; Mills, H. A.; Mao, C.; Kirlikovali, K. O.; Axtell, J. C.; Rheingold, A. L.; Spokoyny, A. M. Improved Synthesis of Icosahedral Carboranes Containing Exohedral B-C and C-C Bonds. *Tetrahedron* **2019**, *75*, 187-191.
14. A. Saebi, "Three-Dimensional Boron Cluster Pharmacophores". UCLA Thesis (2017).
15. Hartrampf, N.; Saebi, A.; Poskus, M.; Gates, Z. P.; Callahan, A. J.; Cowfer, A. E.; Hanna, S.; Antilla, S.; Schissel, C. K.; Quartararo, A. J.; Ye, X.; Mijalis, A. J.; Simon, M. D.; Loas, A.; Liu, S.; Jessen, C.; Nielsen, T. E.; Pentelute, B. L. Synthesis of Proteins by Automated Flow Chemistry. *Science* **2020**, *368*, 980-987.
16. Mu, X.; Axtell, J. C.; Bernier, N. A.; Kirlikovali, K. O.; Jung, D.; Umanzor, A.; Chen, X.; Bay, K. L.; Kirolos, M.; Rheingold, A. L.; Houk, K. N.; Spokoyny, A. M. Sterically Unprotected Nucleophilic Boron Cluster Reagents. *Chem* **2019**, *5*, 2461-2469.
17. Messina, M. S.; Graefe, C. T.; Chong, P.; Ebrahim, O. M.; Pathuri, R. S.; Bernier, N. A.; Mills, H. A.; Rheingold, A. L.; Frontiera, R. R.; Maynard, H. D.; Spokoyny, A. M. Carborane RAFT Agents as Tunable and Functional Molecular Probes for Polymer Materials. *Polym. Chem.* **2019**, *10*, 1660-1667.

18. Wu, X.; Zhu, X.; Chong, P.; Liu, J.; Andre, L. N.; Ong, K. S.; Brinson Jr., K.; Mahdi, A. I.; Li, J.; Fenno, L. E.; Wang, H.; Hong, G. Sono-optogenetics Facilitated by a Circulation-delivered Rechargeable Light Source for Minimally Invasive Optogenetics. *Proc. Natl. Acad. Sci (USA)* **2019**, *116*, 26332-26342.
19. Jung, D.; Raffan-Montoya, F.; Ramachandran, R.; Zhang, Y.; Islamoglu, T.; Marin, G.; Dziedzic, R.; Farha, O. K.; Stoliarov, S. I.; Spokoyny, A. M. Cross-Linked Polyurethane Materials Featuring Dodecaborate Clusters as Inorganic Polyol Equivalents. *Chem. Commun.* **2019**, *55*, 8852-8855.
20. Mu, X.; Hopp, M.; Dziedzic, R. M.; Rheingold, A. L.; Sletten, E. M.; Axtell, J. C.; Spokoyny, A. M. Expanding the Scope of Pd-Catalyzed B-N Cross-Coupling Chemistry in Carborane. *Organometallics* **2020**, *39*, 4380–4386.
21. <https://obamawhitehouse.archives.gov/sites/default/files/microsites/ostp/pcast-stem-ed-final.pdf>
22. <http://www.organomimetic.com/teaching.html>.
23. Kirlikovali, K. O.; Cho, E.; Downard, T. J.; Grigoryan, L.; Han, Z.; Hong, S.; Jung, D.; Quintana, J. C.; Reynoso, V.; Ro, S.; Shen, Y.; Swartz, K.; Ter Sahakyan, E.; Wixtrom, A. I.; Yoshida, B.; Rheingold, A. L.; Spokoyny, A. M. Buchwald-Hartwig Amination Using Pd(I) Dimer Precatalysts Supported by Biaryl Phosphine Ligands. *Dalton Trans.* **2018**, *47*, 3684-3688.
24. Ely, R.; Richardson, P.; Ziota, A.; Steven, A.; Kargbo, R.; Nawrat, C. C.; Day, D. P.; Knight, J. Some Items of Interest to Process R&D Chemists and Engineers. *Org. Process Res. Dev.* **2018**, *22*, 1-12.

25. <https://dailybruin.com/2018/02/20/remodeled-chemistry-course-allows-for-student-research-publishing>.